Muscle Impairment in Cerebral Palsy

Does the current "standard" method of simulating muscle activations during human walking produce valid results?

Lewis, Andrew Peter

Awarding institution:
King's College London

Muscle Impairment in Cerebral Palsy

Does the current "standard" method of simulating muscle activations during human walking produce valid results?

A thesis submitted in partial fulfilment of the requirements for the degree of

Doctor of Philosophy

Division of Imaging Sciences & Biomedical Engineering
King's College London
2015

Andrew Peter Lewis

Supervisors:
Dr. Adam Shortland & Prof. Stephen Keevil

Abstract

It has been proposed that musculo-skeletal modelling techniques may provide new tools for use in clinical gait analysis to help our understanding of the role of muscles and tendons in movement dysfunction. Sensitivity and validity analyses are necessary and important steps in achieving this goal.

The aim of this investigation was to evaluate SimTrack, a workflow for generating muscle driven simulations of movement embedded within the 3D musculo-skeletal modelling software package OpenSim (Delp et al., 2007). Walking in both pathological (cerebral palsy) and typically developing subjects was analysed. If muscle activations can be accurately determined using such techniques, advanced simulation methods may be used to determine the mechanical potential of muscles in these groups and therefore help identify muscles in subjects with cerebral palsy that cannot make significant contribution to support and progression in walking. Ten typically developing adolescents and ten independently ambulant adolescents with cerebral palsy were recruited and the following data collected: MRI of the lower-limbs; 2D-ultrasound of a number of lower limb muscles; 3D motion, electromyography and ground-reaction-force data of the subjects' walking patterns.

The muscle morphology of subjects in the two groups were assessed and this data was used to inform 3D musculo-skeletal models. Each model's muscle activations were allowed to vary to track the subject's recorded walking pattern and the sensitivities of these simulated activations to changes in model muscle strength were tested over a normative range. The validity of the simulated activations were then determined by comparison with experimental electromyographic data.

In the case group, muscle volumes were found to be smaller (principally in the distal musculature) and physiological cross-sectional areas were found to be larger in the thigh and smaller in the shank than the control group. The musculo-skeletal model was insensitive to changes in muscle strength. All simulated activations were found to be invalid. The results suggest that the application of SimTrack to the understanding of normal and pathological gait may be compromised by an inability to generate valid muscle activations.

Acknowledgments

I would like to express my great appreciation for all the help, guidance and encouragement that my two supervisors, Dr. Adam Shortland and Prof. Stephen Keevil, have given me throughout this project with additional thanks to Adam for his assistance in the collection of ultrasound data.

A big thank you must also go to the Jonathan Noble for his help designing and testing the MRI sequences used in this project as well as his tireless efforts extracting muscle volumes from the subsequent data.

Thank you also to the Guy's Hospital Gait Laboratory team for their support and to Dr. Julie Stebbins and the staff at the Oxford Gait Laboratory for their patience and understanding during the writing-up period.

I would also like to thank Dr. Caroline Stewart for first introducing me to the world of gait analysis and for her help and encouragement in pursuing a career in this field.

And finally I wish to give heartfelt thanks to my wife Erica for her unlimited patience, support and encouragement, without which this thesis would never have been finished.

This research was funded by Guy's and St. Thomas' Charity and supported by the National Institute for Health Research (NIHR) Biomedical Research Centre at Guy's and St Thomas' NHS Foundation Trust and King's College London. The views expressed are those of the author and not necessarily those of the NHS, the NIHR or the Department of Health.

Table of Contents

List of Figures

List of Tables

Nomenclature

2D	two dimensional
3D	three dimensional
Abd	abduction
Add	adduction
ADDS	hip adductor muscle group
AFO	ankle-foot orthosis
Ant	anterior
ASCII	American Standard Code for Information Interchange
ASIS	anterior superior iliac spine
BFLH	biceps femoris long head
BFSH	biceps femoris short head
BMI	body mass index
Cases	subjects with cerebral palsy
CMC	computed muscle control
CoM	centre of mass
Controls	typically developing subjects
CP	cerebral palsy (case group)
DF	dorsiflexion or the ankle dorsiflexor muscle group
DoF	degrees of freedom
Dors	dorsiflexion
EMG	electromyography
Ext	extension or external
Flex	flexion
GlutMax	gluteus maximus
GlutMed	gluteus medius
GlutMin	gluteus minimus
GRA	gracilis
HJC	hip joint centre
IAA	induced acceleration analysis
Int	internal
IK	inverse kinematics
IQR	inter-quartile range
KJC	knee joint centre
LED	light emitting diode
LG	lateral gastrocnemius
MG	medial gastrocnemius
MTP	metatarsal-phalangeal joint
MVC	maximum voluntary contraction
NRMSE	normalised RMSE
MRI	magnetic resonance imaging
OpenSim	Musculo-skeletal modelling software (Delp et al., 2007)
PCSA	physiological cross-sectional area
PMD	percentage muscle deficit
PF	plantarflexion or the ankle plantarflexor muscle group
Plan	plantarflexion
Post	posterior
PSIS	posterior superior iliac spine
RRA	residual reduction algorithm
RF	rectus femoris
RMS	root mean square
RMSE	root mean square error
SAR	sartorius
SD	standard deviation
SE	standard error
sEMG	surface electromyography
SimTrack	OpenSim workflow for generating muscle driven simulations of movement
SM	semimembranosus
ST	semitendinosus
SO	static optimisation
SOL	soleus
TA	tibialis anterior DEEP – deep compartment SUP – superficial compartment
TD	typically developing (control group)
TP	tibialis posterior
Var	varus
Val	valgus
VCM	Vicon Clinical Manager
VI	vastus intermedius
VL	vastus lateralis
VM	vastus medialis

Additional detail of abbreviations used in this thesis can be found in the following figures:

1 Background

"That's one small step for man…

one giant leap for mankind"

1.1. Introduction

When Neil Armstrong spoke these words on 20th July 1969 he was making reference to the leap in technological and scientific achievement that had enabled him to become the first person to set foot on the moon. Human language has always made use of walking terminology to describe the concepts of advancement and progression. We refer to the *steps* of a process, we like to *run* with an idea, and we make *leaps* of understanding. Expressions such as these are commonplace and universally understood because of our innate fascination with the human ability to move.

Armstrong's analogy between walking and technology is very apt if we examine the development of our understanding of human walking. In his history of early gait analysis, Baker (2007) tells us that the earliest known work on the subject comes from Aristotle (384-322 BC), who amongst many observations recognised that we do not walk purely horizontally but rather our body rises and falls with each step. However, it was not until the advent of photography in the 19th Century that some of the complexities of walking began to be unravelled and as technology developed so instrumented gait analysis was born. Jules Etienne Marey (1830–1904) invented the first high-speed camera "gun" that could record images from the same position at 12 frames per second and the 3D motion

capture systems found in most modern gait analysis laboratories are still based on photographic techniques.

Walking is an ability that many of us take for granted but an injury or disorder to the neural or musculo-skeletal system, such as with cerebral palsy, can make walking difficult or impossible. The resulting immobility may be a barrier to physical and social activity and consequently lead to a reduced quality of life (Jaspers et al., 2013). Modern clinical gait analysis centres use a variety of data such as 3D joint angles/torques and recordings of muscle activity combined with medical understanding of patient groups to make treatment recommendations in an attempt to improve an individual's gait and mobility. However, despite such sophisticated measurement tools, the subsequent analysis of movement patterns is in the most part limited to simple descriptions of the deviations of the data from a normal pattern and it is left to clinicians to interpret the data to find clinical meaning.

There is a need therefore for new tools in clinical gait analysis (Baker, 2006) and musculo-skeletal modelling and simulation techniques may provide a solution (Delp, 1990). However, there is still a requirement for evaluation and validation of such methods and this thesis attempts to make one small step towards achieving this goal.

This introductory chapter provides some background to the disabling condition of cerebral palsy and briefly describes how musculo-skeletal modelling may both help our understanding of this condition and be used to aid treatment decision making.

1.2. Cerebral Palsy (CP)

Cerebral Palsy is:

"*an umbrella term covering a group of non-progressive, but often changing, motor impairment syndromes secondary to lesions or anomalies of the brain arising in the early stages of development*." (Mutch et al. 1992, p.549)

Cerebral palsy is a static perinatal encephalopathy and was originally known as Little's Disease after William Little linked it to difficult labours and perinatal hypoxia in 1862 (Jones et al., 2007). Since then, advances in the understanding of early life brain injury mechanisms have led to more specific ideas of cerebral palsy aetiology which, as du Plessis (2009) explains, include hypoxic, ischemic, haemorrhagic and inflammatory brain lesions to the ante-, peri- and post-natal child. Other proposed pre-natal causes of cerebral palsy include genetic abnormalities, congenital brain malformation and in utero infections.

Whatever the cause, this non-progressive neuropathy leads to a complex variety of primary abnormalities dependent on both the location of the brain lesion(s) and the stage of brain development in which it occurred. Primary abnormalities can include both sensory and motor elements such as cognitive difficulties, epilepsy, behavioural disorders and dysarthria (motor speech disorder) as well as balance difficulties, the loss of selective motor control, and abnormal muscle tone (Fowler & Goldberg, 2009; Gormley, 2001; Jones et al., 2007; Stackhouse et al., 2005). As individuals with cerebral palsy grow they will also develop progressive secondary abnormalities such as anomalies of muscle and bone growth due to the influence of loading and activation patterns on the development of the musculo-skeletal system (Gage & Schwartz, 2009a).

Muscles can become short and stiff (a muscle contracture) which limits the range of movement of the joint (Barber et al., 2011), and a number of studies (Brown et al., 1991; Wiley & Damiano, 1998) have shown that the muscles of children with spastic cerebral

palsy are weak. The term *cerebral palsy* means weakness originating from the brain (Damiano et al., 2002). There are a number of recognised causes for this weakness: subjects with spastic cerebral palsy have smaller muscle volumes (Barber et al., 2011; Fry et al., 2007; Malaiya et al., 2007; Oberhofer et al., 2010), they have incomplete muscle activation and/or increased co-activation (Elder et al., 2003; Stackhouse et al., 2005; Tammik et al., 2008) and there are myopathic changes in muscle microstructure including increased fat and connective tissue content (Booth et al., 2001; Castle et al., 1979; Johnson et al., 2009), and changes in muscle fibre stiffness (Lieber et al., 2003; Smith et al., 2011). These changes have a direct effect on the active and passive mechanics of muscle and so, if measured, it should be possible to incorporate them into a musculo-skeletal model and so analyse their influence on a walking pattern.

Bone abnormalities that often occur in the lower limbs of children and adults with cerebral palsy include torsion of the long bones (tibial torsion, femoral anteversion), hip dislocation and a number of foot deformities (Gage & Schwartz, 2009a). Many of these abnormalities lead to the problem of lever-arm dysfunction where the change in skeletal geometry affects the line of action of the muscles and hence alters their rotational action on the related joint. For someone with cerebral palsy, the progressive nature of these secondary abnormalities typically leads to a decline in mobility during adulthood (Strauss et al., 2004).

Various classifications of cerebral palsy have been proposed (SCPE, 2000) including a topographical classification:

- *diplegia* – legs more affected than arms
- *hemiplegia* – one side only (usually arm more than leg)
- *quadriplegia* – all four limbs affected (legs more than arms)
- *double hemiplegia* – all four limbs affected (arms more than legs)

and a motor classification:

- *dyskinetic/choreo-athetoid* – loss of postural control with unwanted movements
- *ataxic* – poor balance and coordination, often with shaky hand movements
- *spastic* – hyper-excitability of the muscle/tendon stretch reflex

The different types of cerebral palsy can be explained in terms of the location of the brain lesion. As explained by Peacock (2009) and Albright (2009a) human movement begins with a thought in the cerebral cortex and, after interaction with various other motor control centres, a nerve impulse is passed via the brainstem and down the spinal cord through the corticospinal tract (also known as the pyramidal tract) to synapse with a lower motor neuron and hence onto the appropriate muscle. Originally it was thought that damage to the pyramidal tract was the principal cause of spasticity and hence the terms pyramidal and extrapyramidal were commonly used to describe lesion location. However, this is incorrect and it is now accepted that it is disruption to the inhibitory influence of the neighbouring reticulospinal and vestibulospinal tracts which is important and therefore any lesions affecting the reticular and vestibular midbrain nuclei or their cortical/spinal connections can result in spasticity. Non-spastic cerebral palsy is caused by damage to the basal ganglia, cerebellum or their cortical connections. However, due to the variation in the extent and severity of these injuries, it is often difficult to fit a patient with cerebral palsy into a particular classification. A collaboration of cerebral palsy surveys and registers in Europe (SCPE, 2000) revealed that between two and three children per 1000 live births were diagnosed as having cerebral palsy with spastic cerebral palsy being the most common type.

Cerebral palsy cannot, at present, be cured and so the principal aims of intervention are to prolong functional mobility and reduce pain. There are a number of current techniques used by clinicians to achieve these goals including physiotherapy, pharmacological treatments, the use of orthoses and orthopaedic surgery (Gage et al., 2009). Physiotherapy is typically used to try and maintain joint range of motion, to improve

strength and to facilitate mobility (Damiano et al., 2002, 1995; Darrah et al., 1997; Haney, 1998; Murr & Walt, 2009).

There are many pharmacological treatments used in the management of cerebral palsy, all principally dealing with the reduction of abnormal muscle tone. The mechanisms of each drug are different and these complexities are outside the scope of this thesis. However, two of the more commonly used treatments are the systemic action of intrathecal Baclofen (Krach, 2009) which reduces both dystonia and spasticity, and the action of Botulinum toxin type A injections (Molenaers & Desloovere, 2009) which can reduce local spasticity. Two operative treatments are also used to address the problem of abnormal muscle tone. Selective dorsal rhizotomy is a technique to reduce spasticity that involves the selective cutting of dorsal spine (sensory) nerve rootlets between the levels of the sacral and first lumbar vertebrae with selection based on a rootlet's abnormal response to electrode stimulation (Trost et al., 2009). Deep brain stimulation is a technique in which electric pulses are delivered via electrodes placed in the basal ganglia to reduce dystonia (Albright, 2009b).

Orthoses can include a variety of foot splints (e.g. supra-malleolar orthosis - SMO), foot and ankle splints (e.g. ankle-foot orthosis - AFO), and less commonly, foot, ankle and knee splints, all of which are typically manufactured from moulded plastic and worn to compensate for neuro-motor deficiencies. The stiffness and contact region(s) can be varied in order to achieve the required support and they can be used to address both structural and functional impairments. Some common requirements of an orthosis include the prevention of drop-foot, the reduction of crouch gait or the elimination of the excessive knee stresses caused by recurvatum (Novacheck et al., 2009).

There are too many orthopaedic procedures used in the treatment of cerebral palsy to be described here but they can be summarised into a number of groups. Soft tissue surgery can be used to reduce muscle contracture via lengthening techniques, or to transfer tendons to change a muscle's line of action in order to regain function, and bony surgery

can be carried out to reduce torsion of the long bones or to correct specific deformities of the foot (Gage et al., 2009).

It is important to be able to measure the functional changes that occur as a result of these interventions in order to inform and improve treatment. The International Classification of Functioning, Disability and Health (ICF; WHO, 2001) provide a framework and common language for the discussion of health issues (Figure 1.1). The ICF terminology defines an individual with two medical domains, *body functions* (physiology) and *body structures* (anatomy), and two social domains, *activity* (day-to-day tasks) and *participation* (social involvement), which are measured in terms of *performance* (current ability) and *capacity* (possible ability with aid). The framework also includes additional contextual influences such as *personal* or *environmental factors* that can act as barriers or facilitators to any of the four domains.

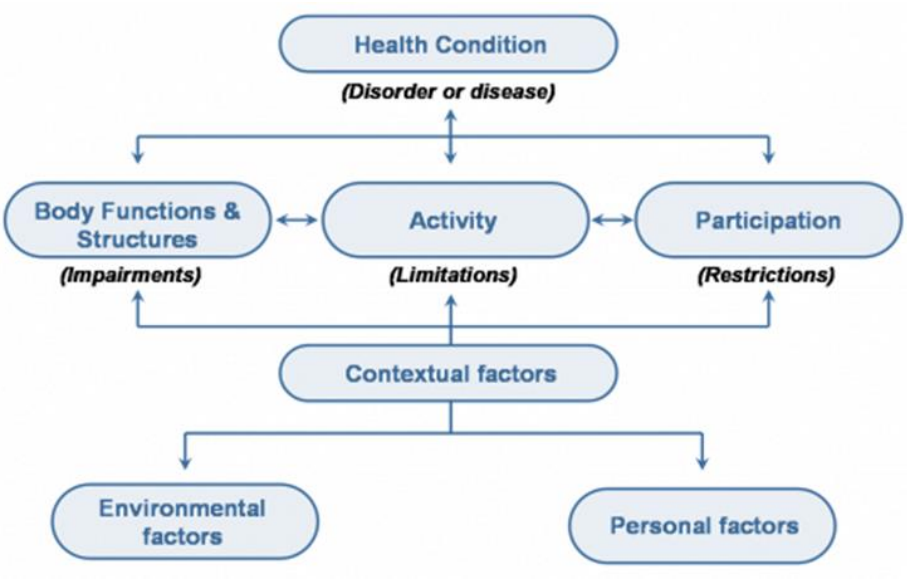

Figure 1.1 – The International Classification of Functioning, Disability and Health framework for measuring health and disability (ICF; WHO, 2001)

It is important to consider this framework in healthcare provision (Rauch et al., 2008) as it promotes a more global assessment of the individual and in this context, as regards cerebral palsy, tools such as the Gross Motor Function Classification System (GMFCS; Palisano et al., 1997), the Gillette Functional Assessment Questionnaire (GFAQ; Novacheck et al., 2000) and the Gross Motor Function Measure-66 (GMFM-66; (Russell et al., 2002)

have been shown to be good predictors of mobility and functionality in daily life, measures that can be used to monitor the efficacy of treatment.

1.3. Cerebral Palsy Assessment

An individual with cerebral palsy will experience a combination of the primary and secondary abnormalities described above which is likely to have a detrimental effect on their ability to carry out motor tasks, and specifically within the context of this work, on their ability to walk. For example, bony deformities and short/stiff muscles may lead to limitations in the range of movement at the joints, and the lack of selective motor control, muscle weakness and/or abnormal muscle tone including co-contraction and spasticity may make balance and coordination of the lower limbs more difficult. These factors will inevitably result in a walking pattern that is different to that of typically developing individuals. Such deviations from normal walking are known as pathological gait and the prevalence study of Wren et al. (2005) describes typical gait pathologies seen in subjects with cerebral palsy:

- *equinus gait* – increased ankle plantarflexion in the stance phase
- *crouch gait* – increased knee flexion in the stance phase
- *recurvatum* – hyperextension of the knee in the stance phase
- *stiff knee gait* – decreased range of knee motion

A subject's walking pattern can be defined by their kinematics (joint angles), kinetics (joint torques) and/or other gait data such as spatio-temporal parameters (walking speed, step length etc.) which can be measured using gait analysis techniques (section 2.3.2). Distinctions between normal and pathological gait are then limited to the comparison of a patient's gait data, such as joint angle and joint torque graphs, with previously collected normal data from unaffected individuals. This can be done visually using the graphical data or by using a number of quantitative measures of gait deviation such as the Gillette Gait Index (GGI) by Schutte et al. (2000), the Gait Deviation Index (GDI) by Schwartz & Rozumalski (2008), or the more recent Gait Profile Score (GPS) from Baker et al. (2009) but

it is ultimately left to clinicians to interpret the data to find clinical meaning. The quality of treatment decision making is therefore heavily dependent upon the experience of the interpreting clinician(s) and the gait impairments identified by these techniques do not explain much of the variance in functional *capacity* or *performance* in children with cerebral palsy (Ostensjø et al., 2004). In addition, the use of clinical gait analysis in the evaluation of treatment efficacy is usually restricted to the same global measures of gait deviation gathered from retrospective pre/post-intervention studies.

There is a clear need therefore for new tools in the field of clinical gait analysis (Baker, 2006); tools which it is hoped will better identify the underlying pathology and true functional limitations of the individual and hence have a more direct input to treatment decision making and the improved efficacy of intervention. Musculo-skeletal modelling and simulation techniques may provide a solution (Delp, 1990) and access to sophisticated musculo-skeletal modelling software packages has become more available in recent years (Delp et al., 2007) leading to a number of cerebral palsy studies in the literature based on simulated data. Some of these studies evaluate the contribution of individual muscles to supporting the body against gravity and to progressing the body forwards. Subject-specific identification of individual muscle contributions and potential deficits in this way may help our understanding of a condition and be used to aid treatment decision making. These techniques have already been used to analyse muscle contributions in gait pathologies such as crouch gait (Arnold & Delp, 2005; Arnold et al., 2007; Hicks et al., 2008), stiff-knee gait (Anderson & Pandy, 2003) and equinus foot posture (Higginson et al., 2006), as well as in investigations into the effects of bony deformities on muscle capacity (Hicks et al., 2007).

However, there are currently a number of limitations to these techniques which have prevented their adoption into standard gait analysis protocols. Firstly, these studies made use of generic musculo-skeletal models that were scaled to match subject size. Arnold et al. (2001) and Scheys et al. (2008a, 2008b) however have shown that using models with bespoke musculo-skeletal geometry (usually obtained from MRI) result in significant differences in muscle moment-arm lengths and muscle-tendon lengths. It is likely

therefore that subject-specific models will be necessary if such techniques are to provide effective targeting of an individual's treatment or give reliable predictions of intervention outcomes. Current methods of creating subject-specific models however are too expensive and time-consuming to be carried out in routine clinical practice. Secondly, these techniques usually involve optimisation algorithms (to minimise a cost function) to overcome the static indeterminacy problem (section 2.1.3) when calculating muscle activations from experimental joint torques. Various cost functions have been proposed, often focusing on a global measure of muscle activation. These cost functions may well prove valid in the simulation of muscle activation in typically developing subjects but they lack any element of neurological control which is likely to have a strong influence on the walking patterns of subjects with neurological conditions such as cerebral palsy.

1.4. Problem Statement

Musculo-skeletal modelling techniques may provide a useful tool in the analysis and treatment of individuals with cerebral palsy but there is still a need for evaluation and validation of such methods (Baker, 2006).

1.5. Project Scope

This work includes a validity analysis of simulated muscle activations generated using SimTrack (section 2.2.3) which is a workflow for generating muscle driven simulations of movement embedded within the 3D musculo-skeletal modelling software package OpenSim (Delp et al., 2007). This method is fast becoming accepted as an industry standard approach due to interest from leading international centres and an increasing number of OpenSim human simulation studies appearing in the literature (as detailed in section 1.3).

The sensitivity of the simulated muscle activations to changes in muscle strength is assessed for typically developing adolescents and the validity of the activations compared

to experimental electromyographic data is assessed for both typically developing adolescents and for ambulant adolescents with cerebral palsy.

1.6. Thesis Overview

- Chapter 2: description of current musculo-skeletal modelling methods and research including the algorithms utilised in this work - SimTrack. Later sections provide an overview of gait analysis methods and our current understanding of human gait followed by an outline of the equipment and methodology used in the principal data collection.

- Chapter 3: description of the differences in muscle size and morphology between the two subject cohorts using data collected from both magnetic resonance and ultrasound imaging and comparison to the literature.

- Chapter 4: evaluation of the sensitivity of simulated muscle activations in the control group to changes in muscle strength.

- Chapter 5: calculation of the validity of the simulated muscle activations in both subject groups by comparison to electromyographic data.

- Chapter 6: summary of findings and suggested further work.

2 Methods

This chapter begins with in-depth description of current musculo-skeletal modelling methods and research with specific focus on SimTrack – the OpenSim workflow for generating muscle driven simulations of movement. Later sections provide an overview of gait analysis methods and our current understanding of human gait. The final sections outline the equipment and methodology used in the principal data collection of this work.

2.1. Musculo-skeletal Modelling

2.1.1. Introduction to musculo-skeletal modelling

The term *model* in the context of computer modelling refers to a mathematical construct used to represent a system of interest – in this case the human musculo-skeletal system. This system is a complex, three dimensional, mechanical linkage of interconnected bodies including bones, muscles, tendons and ligaments. It is logical therefore for a model of this system also to be based around a mechanical linkage of segments. However, the level of complexity of such a model should be chosen as appropriate for the parameters under investigation. For example, for the analysis of a single joint torque and ground-foot interaction forces (ground-reaction-forces), a simple 2D, two segment model (Figure 2.1a) may suffice, whereas using a more complex 3D, multi-segment model enables the calculation of multiple joint torques and bone-on-bone forces. Typically segments are modelled as rigid bodies with appropriate joint constraints chosen for inter-segment connections, e.g. ball, hinge joints. The contribution of active elements can also be added into the system (Figure 2.1b) using appropriate muscle models to allow calculation of individual muscle forces and tendon lengths.

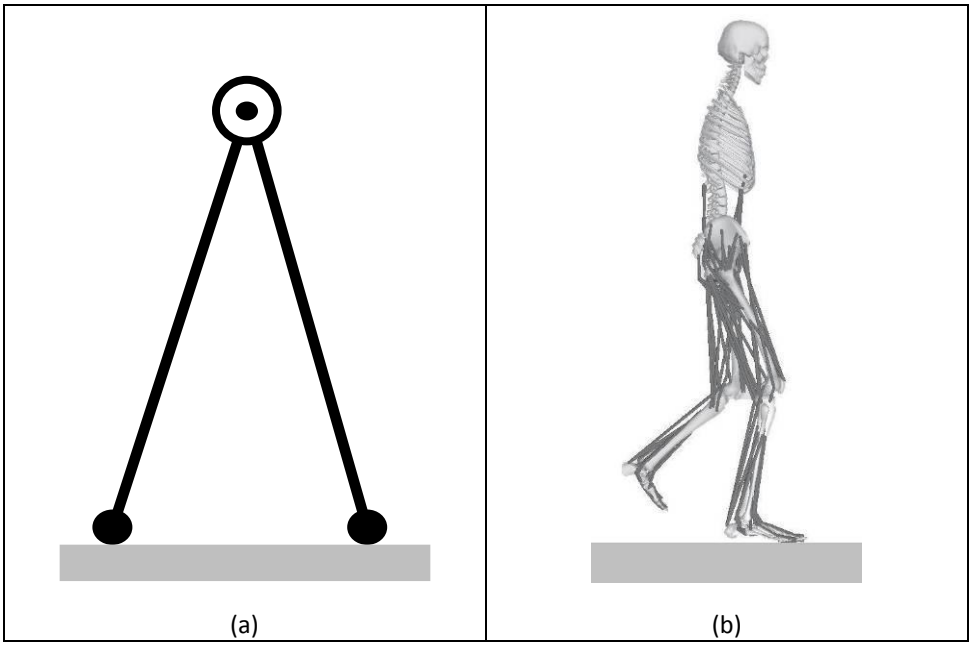

Figure 2.1– (a) 2D, two segment reciprocating model (b) 3D multi-segment model

However, despite their difference in complexity, the techniques and equations of motion used to analyse these types of models are based on the same geometric and mechanical principles. Rigid body translation and rotation mathematics can track segment movement and the subsequent accelerations can be linked to forces by the appropriate inertial parameters (e.g. mass). The Newton-Euler equations (Equation 2.1 & Equation 2.2) provide an intuitive understanding of the method but techniques such as Lagrangian mechanics, which make use of energy calculations to simplify and reduce the number of necessary equations, and matrix algebra are more efficient and are typically used in modern modelling packages.

Equation 2.1 $$F = m \cdot a$$ Newton's 2nd Law

where: *F* is the net force on an object (N)

m is the mass of the object (kg)

a is the resulting acceleration of the object (ms^{-2})

Equation 2.2 $$T = I \cdot \alpha$$ Euler equation

where: T is the net torque on an object (Nm)

I is the moment of inertia of an object (kgm^2)

α is the resulting angular acceleration of the object ($rads^{-2}$)

This provides the mathematical link between the model *kinematics* (position, velocity, acceleration) and the model *kinetics* (forces and resultant energetics) and gives rise to the two main approaches of dynamic model analysis.

- *Forward dynamics* – the kinetics are known and used to calculate the kinematics
- *Inverse dynamics* – the kinematics are known and used to calculate the kinetics

Direct measurement of muscle force is possible via surgically implanted transducers but the invasive nature of such techniques prohibits their use in human studies. A workflow to achieve a full forward dynamic simulation of human gait (Figure 2.2) would therefore typically involve the following steps:

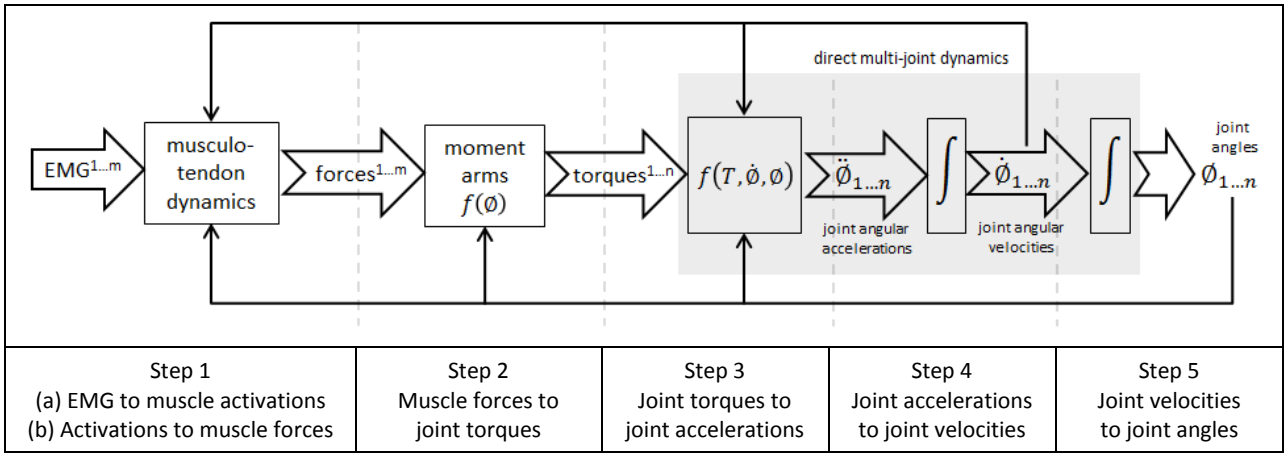

Figure 2.2 – Forward dynamic workflow from EMG signals to model joint angles.
EMG = electromyogram, m = muscles, n =joints, T = torques

- Step 1 – (a) Muscle activation states are determined from electromyographic (EMG) recordings of the muscle action during the motion of interest. (b) Musculo-tendon dynamics defined by the chosen muscle model (e.g. a spring/damper complex) are used to convert the muscle activations into muscle forces.
- Step 2 – Muscle forces and external forces (e.g. ground-reaction-forces) are combined with joint geometry (force moment-arms) to convert the forces into joint torques.
- Step 3 – The Newton-Euler equations or Lagrangian mechanics are employed to convert joint torques into joint angular accelerations and resultant forces into linear accelerations.
- Step 4 – Accelerations are integrated to give joint angular velocities and the global translational velocities of the model.
- Step 5 – Velocities are integrated to give joint angles and the global translational position of the model.

This workflow requires feedback elements as can be seen in Figure 2.2. The musculo-tendon dynamics has dependencies on both joint angles and velocities, the joint geometry is a function of joint angle and the centripetal effects from angular velocities must be included in step three when calculating accelerations. An inverse dynamics analysis would run the steps in reverse beginning with joint angle data (e.g. from a motion capture system). An estimation procedure will be necessary however to calculate individual muscle forces from joint torques due to the problem of static indeterminacy (section 2.1.3).

The implementation of steps 2-5 is straightforward using standard mechanics and equations of motion and is often summarised using a matrix equation similar to Equation 2.3.

Equation 2.3 $$M(q)\ddot{q} + C(q,\dot{q}) + G(q) + R(q)F_{MT} + E = 0$$

where:
- q is the coordinate positions (e.g. joint angles, global position) in a system of *n* kinematic degrees of freedom
- $\dot{q}$ is the coordinate velocities
- $\ddot{q}$ is the coordinate accelerations
- *M* is the system mass matrix (*n* x *n*)
- *C* is the centripetal and Coriolis effects *(n* x *1)*
- *G* is the gravitation effects *(n* x *1)*
- *R* is a matrix of muscular moment-arms *(n x m)* where m is the number of muscles
- F_{MT} is the forces of the muscles *(m* x *1)*
- *E* is the external forces applied to the system

However, the relationships between muscle excitation and activation (activation dynamics) and between activation and the resulting force (contraction dynamics), Figure 2.2 step 1(a) and (b) respectively, are more complex. Activation dynamics is discussed in more detail in section 5.2.2. To parameterise contraction dynamics the construction of a muscle model is necessary.

2.1.2. Muscle Modelling

Skeletal muscles are responsible for the generation of active musculo-skeletal movement in the human body. These muscles are complex structures able to produce powerful and sustained contractions that work on the mechanical levers of the skeleton to induce rotational movement of the joints. The physiology and detailed structure of muscle tissue is beyond the scope of this thesis but some of the elements of structure and function that are pertinent to the construction of a muscle model are described below.

Each muscle is a separate organ composed of hundreds to thousands of long, cylindrical cells known as muscle fibres held together with a series of layers of connective tissue that join together at the ends of the muscle to produce the tendons that attach on to bone (Purslow, 2008). There are a number of subunits within a muscle fibre including parallel protein filament elements and it is here, driven by a chemical mechanism involving

calcium ions and adenosine triphosphate, that the sliding filament mechanism takes place that is the source of muscle contraction force. A variety of fibre types exist, dependent on the way that adenosine triphosphate is generated, which can be crudely classified as slow or fast in relation to their contraction speed and speed to fatigue. Typical skeletal muscles contain a combination of fibre types but this can change depending on disease, genetic factors or by following specific exercise regimes (Tortora & Derrickson, 2007).

Groups of muscle fibres, known as a motor unit, are innervated by a single motor neuron. The resultant electrical signal, known as a motor unit action potential, travels along the membranes of all the corresponding muscle fibres simultaneously triggering the contraction mechanism (Winter, 2005). Muscles that control large, powerful movements of the body therefore contain motor units made up of thousands of fibres and muscles that control small, precise movements will contain motor units of tens of fibres. It is the combined electrical signal from many neighbouring motor unit action potentials that can be detected in EMG.

In addition, different muscles in the human body adopt different muscle fibre alignments determined by the muscle pennation angle: the angle between the line of the muscle fibres and the line of force that the muscle exerts upon contraction. At this stage it becomes convenient to use the term fascicle (bundles of fibres), rather than fibre, as the base unit of contraction in the muscle model. This is for two reasons: firstly, fascicle lengths are more typically reported in the literature as they are more easily identifiable using conventional imaging techniques; and secondly, muscle fibres do not run the full width of the muscle to connect internal tendon to internal tendon but a number of fibres may be joined end to end along the length of a fascicle. However, for the purposes of large scale muscle models, the terms fibre and fascicle are used interchangeably and refer to the contractile element that extends across the width of the muscle belly (Figure 2.3).

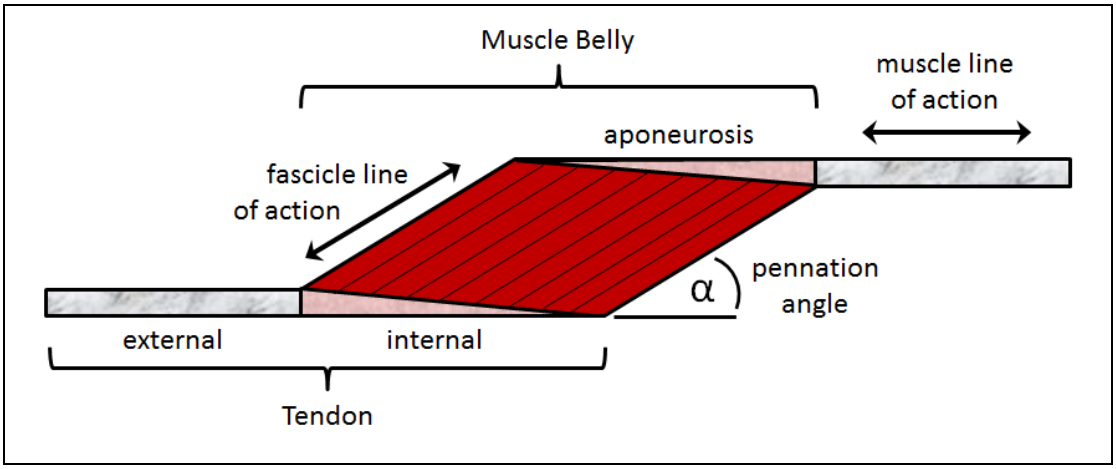

Figure 2.3 – Simplified muscle morphology. The muscle originates and inserts at the ends of the external tendons giving a horizontal muscle line of action. Muscle fascicles run in parallel between the two internal tendons (aponeuroses) at a pennation angle α to the muscle line of action.

Each alignment gives a different contraction characteristic to the muscle. Typically, the smaller the pennation angle, the longer the fascicles and hence the greater number of fibres that are in series which increases both the maximum possible change in length of a muscle belly (the excursion) and the contractile velocity of the muscle. Due to volumetric constraint, muscles with large pennation angles have short fibres but have space to pack more side by side. This gives a reduced excursion range but with more fibres able to contract in parallel the muscle is able to exert a much greater force. The physiological cross-sectional area of a muscle, a combination of muscle size with architectural alignment (Equation 2.4), is therefore the only muscle parameter that is directly proportional to the maximum tension that can be generated by a muscle (Lieber & Fridén, 2000).

Equation 2.4

$$PCSA = \frac{V_m \cdot \cos(\theta)}{L_f}$$

where:

PCSA is physiological cross-sectional area

V_m is muscle volume

θ is pennation

L_f is fascicle length

Finally, it is necessary to consider the passive stretch of the tendons to which the muscles are connected in series. These are usually modelled as a series spring-type element in a muscle model. The resultant mechanical behaviour of human muscle is therefore driven by the sliding filament contraction mechanism and influenced by a combination of muscle architecture, fibre type and the passive mechanical response of the tendons. In order to analyse and simulate models of the musculo-skeletal system it is therefore necessary to construct a mathematical representation of this muscular-tendinous contraction unit which, as the name suggests, is made up of two constituent parts: the muscle belly is solely responsible for the active component of muscle action as well as contributing to the passive stretch; and the tendon is only a passive structure.

Most modern muscle models are variations on the classic Hill-type model first proposed in a number of publications by Hill, Wilkie and Ritchie in the 1930-50s and conveniently reviewed by Felix Zajac (Zajac, 1989). A typical Hill-type muscle model is shown in Figure 2.4.

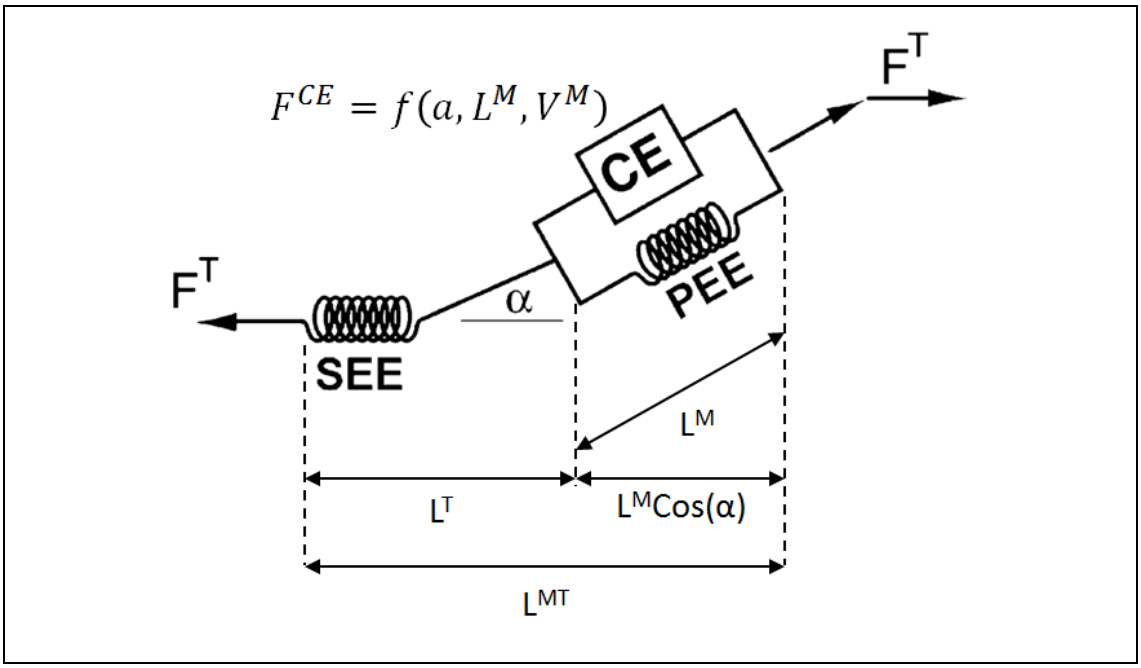

Figure 2.4 – Hill-type muscle model. L^{MT} is the musculo-tendinous unit length. The muscle belly is represented by a contractile element (CE) that is a function of activation (a), fibre length (L^M) and fibre contraction velocity (V^M), and a passive elastic element (PEE). The tendon is represented by a series elastic element (SEE) of length L^T. α is the pennation angle, the angle between the contractile element of the muscle and the line of action of the musculo-tendinous unit. F^T is tendon force which is equal to the net force of the musculo-tendinous unit.

The muscle belly is modelled by two elements in parallel. The contractile element (CE) represents the active component of the musculo-tendinous unit and the passive elastic element (PEE) represents the muscle belly's resistance to passive stretch. These elements both act at an angle α (the pennation angle) to the line of action of the whole musculo-tendinous unit. The series elastic element (SEE) represents the tendon's resistance to passive stretch and this acts in parallel to the line of action of the whole musculo-tendinous unit. As the force generated by the contractile component is a function of fascicle contraction velocity (as well as activation and fascicle length), the passive component of the CE/PEE complex is sometimes represented by a spring/damper mechanism. Figure 2.5 shows a typical parameterisation method often used to represent this model (Erdemir et al., 2007).

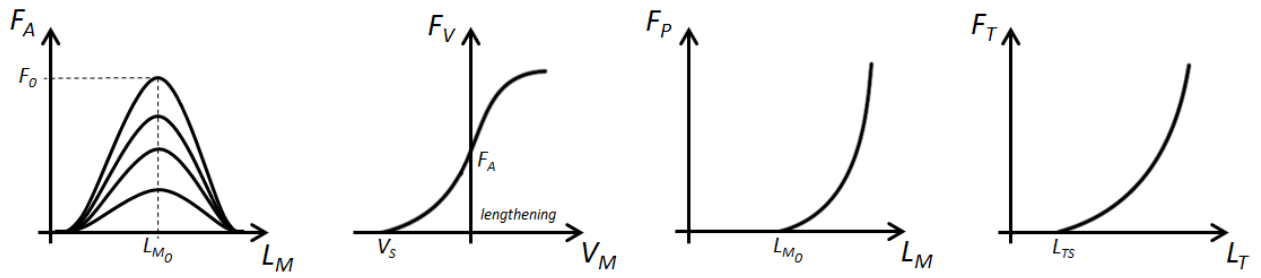

(a) Contractile Element (CE) Force-Length Curve	(b) Contractile Element (CE) Force-Velocity Curve	(c) Passive Elastic Element (PEE) Force-Length Curve	(d) Series Elastic Element (SEE) Force Length Curve
A series of isometric force curves (F_A) for each activation over a range of muscle lengths (L_M)	A force curve (F_V) for a single muscle activation (F_A) over a range of muscle contraction velocities (V_M)	Muscle belly passive stretch force curve (F_P) over a range of muscle lengths (L_M)	Tendon passive stretch force curve (F_T) over a range of tendon lengths (L_T)

Figure 2.5 – Hill-type muscle model curves.

Parameters:
F_0 maximum isometric force of the muscle
L_{Mo} optimal (resting) muscle length
V_s maximum muscle shortening velocity
L_{TS} tendon slack length (Hoy et al., 1990)

The parameters and shape factors chosen to represent these curves determine the contraction dynamics of the muscle model. A detailed example is described below in section 2.2.2.

2.1.3. Calculating Muscle Forces

If reliable measures of muscle activations can be obtained and muscle morphology is known then isometric muscle forces at optimal fibre length can be calculated using Equation 2.5:

Equation 2.5 $$F = a \cdot PCSA \cdot T$$

where: *F* is muscle force (N)

a is muscle activation

PCSA is muscle physiological cross-sectional area

T is specific muscle tension of human skeletal muscle tissue (typically 22.5N/cm^2 – Lieber & Fridén, 2000)

However, there are two principal obstacles that prevent the calculation of muscle activations from EMG (step 1, Figure 2.2). Firstly, for a complex model such as that shown in Figure 2.1(b) it is not possible to obtain EMG from all the muscles. This is because there are too many muscles for this to be a practical task and the electrical signals of some muscles can only be detected with needle electrodes which are undesirable in movement studies. Secondly, even if it were possible to obtain EMG from all the muscles there is also a problem of processing these signals to give a quantitative value of muscle activation (zero = no activation, 1 = maximum activation) or force. This is often achieved by normalising the signal amplitude to previously collected maximum voluntary contraction levels (Lloyd & Besier, 2003; Potvin & Brown, 2004) but such methods can be unreliable for subjects with upper motor neurone problems, such as cerebral palsy, for whom a maximum voluntary contraction may produce sub-maximal muscle contractions and/or force measurements may be confounded by co-contraction of neighbouring muscles (Stackhouse et al., 2005).

In reality, even if muscle forces are calculated accurately from EMG signals, the model kinematics produced from a forward dynamic simulation are unlikely to match the original

movement due to the cumulative errors generated from measurement inaccuracies, signal processing errors, rounding effects and the difficulty of double integration of potentially noisy data. For this reason full forward dynamic simulations are rarely carried out, but instead elements of forward dynamics, inverse dynamics and additional techniques are employed to calculate the parameters of interest. For example, as gait pathology in subjects with cerebral palsy can be caused by weak muscles and malformation of joint geometry, it is of interest to calculate and analyse the muscle forces and moments arms of this population.

Joint angles and ground-reaction-forces can be measured using the motion capture and force-plate equipment of a gait laboratory (sections 2.4.1, 2.4.2), and inverse dynamics carried out to calculate the joint torques necessary for the movement of interest (steps 3, 4, 5 in reverse, Figure 2.2, p.25). Working step 2 backwards to calculate muscle forces from joint torques however introduces the problem of static indeterminacy. The multiple muscles spanning each joint give rise to a large number of different muscle-force combinations that can produce the same overall joint torque and hence there can be more than one numerical solution. This can be overcome by employing iterative optimisation algorithms that converge to a single solution by maximising or minimising a specified cost function. One such algorithm, since termed *Static Optimisation,* was developed by Hardt (1978) – the name denoting the fact that each time frame is considered separately and so the movement is treated as a series of consecutive static poses (and hence musculo-tendon dynamics are ignored). One cost function (*J*) proposed by Crowninshield & Brand (1981) is based on the minimisation of muscle stress and is shown below in Equation 2.6:

Equation 2.6

$$J = \left[\sum_{m=1}^{M} \left(f_m / A_m \right)^3 \right]^{1/3}$$

where:

J is the cost function to be minimised

M is the total number of muscles

f_m is the force of muscle m

A_m is the cross-sectional area of muscle m

Davy & Audu (1987) proposed another algorithm called *Dynamic Optimisation*. Here the cost function to be minimised combines both a kinematic tracking error (the difference between the recorded motion and the motion generated by model muscle action) and the energy expenditure over the whole motion. Muscle energy expenditure is calculated by including a muscle model (a spring/damper complex) and hence musculo-tendon dynamics are included within the algorithm which has the advantage of ensuring that rates of change of muscle activation and hence force are limited to physiologically realistic levels. The disadvantage of the Dynamic Optimisation algorithm however is that, as each iteration is carried out over the entire motion rather than a single time frame, the computation time is significantly increased. Thelen et al. (2003) compared their computed muscle control algorithm (based on Static Optimisation) against Dynamic Optimisation for a three degree of freedom pedalling model and found the respective computation times were 10 minutes verses 120 hours.

Static and dynamic optimisation algorithms may overcome the problem of static indeterminacy but they are only as good as the cost functions that they use. Davy & Audu (1987) described the cost function of Crowninshield & Brand (1981), shown in

Equation 2.6, as having one of the more realistic physiological justifications. Minimising energy expenditure is a likely analogue of the way a typically developing person may activate their muscles to coordinate complex movements. However, confidence in how appropriate these functions are for determining human muscle forces is lacking and validations for both typically developing and pathological individuals are needed. Modenese et al. (2011) investigated the change in muscle activation that resulted from a cost function (Equation 2.7) similar to Equation 2.6.

Equation 2.7

$$J = \sum_{m=1}^{M} \left(f_m / f_{m,\max} \right)^p$$

where:

J is the cost function to be minimised

M is the total number of muscles

f_m is the force of muscle m

$f_{m,max}$ is the maximum potential force of muscle m

p is the user defined power of the cost function

Within this mathematical construct, the parameter p can be considered as a synergism factor, for higher values of p will penalise high muscle activations and hence promote sharing of activation across all muscles. Modenese et al. (2011) carried out a series of musculo-skeletal simulations using a six segment, 3D, single lower limb model using the open source modelling software OpenSim (Delp et al., 2007). The simulation was driven by published kinematics and ground-reaction-forces during walking from a study of four arthroplasty patients with instrumented prostheses. A number of muscle force sets were calculated using Equation 2.7, varying the power p from 1 to 15. The hip contact forces that resulted from each force set were calculated and compared to the published experimental hip contact forces measured from the instrumented prostheses. Muscle forces were also compared to published EMG. Their results showed the best agreement between simulated hip contact forces and experimental data was found using linear optimisation (p=1) but the best qualitative agreement between simulated muscle force

and EMG required a quadratic synergism factor (p=2). Higher values of p produced over-estimates of the hip contact forces due to increased antagonistic action promoted by higher muscle activation synergy.

An alternative technique proposed by Kepple et al. (1997) allows some degree of muscle analysis without the need for individual muscle force data. *Induced acceleration analysis* involves calculating the instantaneous acceleration of model segments for a unit force input to a single muscle (Figure 2.6).

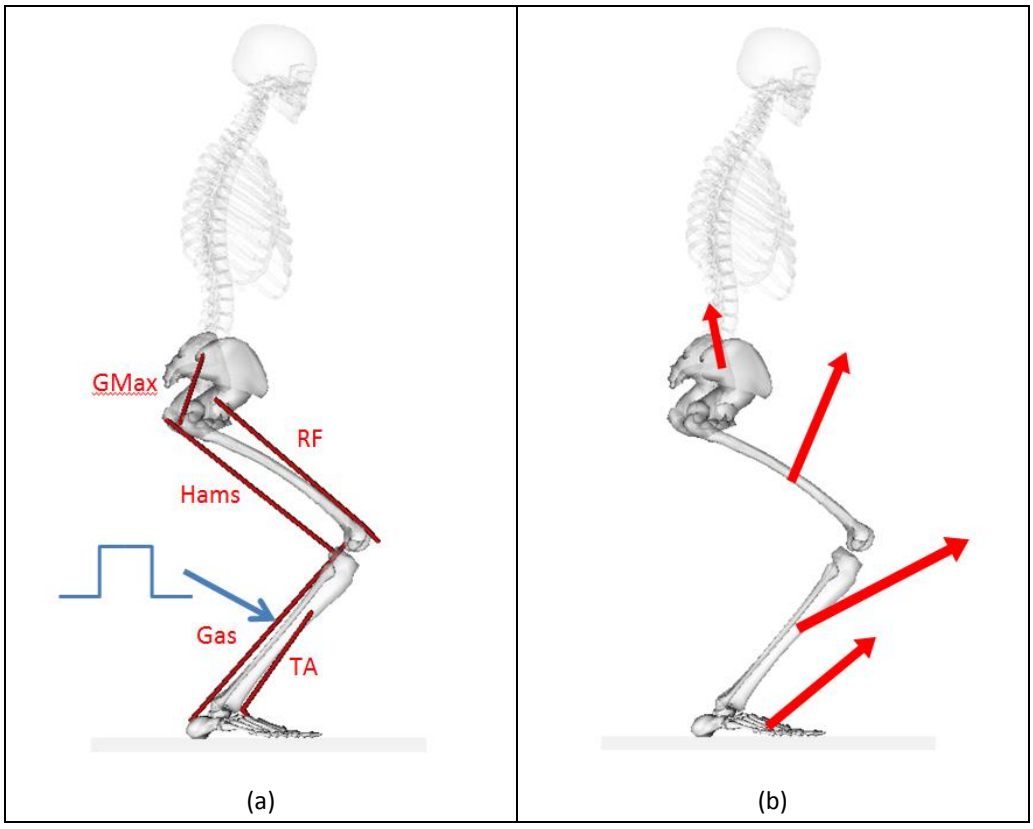

Figure 2.6 – Induced acceleration analysis: (a) a unit force input to the gastrocnemius muscle of a 2D, four segment model: (b) typical instantaneous accelerations induced in the four segments of foot, shank, thigh, pelvis.

Gmax = gluteus maximus, Hams = hamstrings, RF = rectus femoris
Gas = gastrocnemius, TA = tibialis anterior

The magnitudes of the resulting accelerations are arbitrary as the input is an arbitrary unit force rather than a proportionate value of a known muscle force and the body's mechanical impedances to movement (e.g. other active/passive structures) are ignored.

However, it is the relative directions of the accelerations that are of interest as they can provide information about the contributions of each muscle for support and progression of the model. If the input forces are scaled to muscle physiological cross-sectional area then the relative magnitudes of the induced accelerations can also be compared. This process can be repeated for different muscles and for various times (different model poses) during the movement of interest. Many such analyses have been carried out which include investigations into normal walking (Hof & Otten, 2005; Kepple et al., 1997), cerebral palsy crouch gait (Arnold & Delp, 2005; Hicks et al., 2008) and tibial torsion (Hicks et al., 2007). Chen (2006) however showed that induced acceleration analysis can produce a variety of results depending on the degrees of freedom used in the model and hence called for the re-evaluation of this method in the analysis of muscle function in locomotion. However, this argument also implies that such an analysis will produce meaningful results if used on a model that matches the degrees of freedom of the real system under investigation.

If the muscle forces necessary for a specific motion have been calculated by one of the optimisation methods described above then a technique known as *perturbation analysis* (Liu et al., 2006) can be used, like induced acceleration analysis, to determine the muscle contributions to support and progression. A unit force perturbation is applied to a single muscle and the forward dynamics simulation progressed for a small time period to calculate the accelerations on the body segments. This technique has the advantage over induced acceleration analysis that, as external and other muscle forces (both active and passive) are included in the simulation, the magnitudes of the accelerations actually describe the true accelerations of the model. However, this process is still reliant on the validity of the muscle forces used as input to the forward dynamic simulation. If the effects of muscle action on a specific kinematic parameter are of interest then an alternative perturbation analysis can be carried out where the force of a specific muscle is changed over a more prolonged time period during a forward dynamic simulation and the system response observed. Goldberg et al. (2004) used this technique to investigate stiff-knee gait. They looked at the change in knee flexion velocity after each muscle of the

lower limb was given incremental strengthening and weakening perturbations during the double support phase of the gait cycle.

There are currently a number of commercially available musculo-skeletal software packages – these include: the LifeMOD™ system from The Biomechanics Research Group Inc., California; the AnyBody Modeling System™ from AnyBody Technology, Denmark; and SIMM (Software for Interactive Musculo-skeletal Modelling) from Musculographics Inc., California (Delp & Loan, 1995). However, in 2007, Simbios, the National Institutes of Health Centre for Biomedical Computation at Stanford University, released the open-source software package OpenSim (Delp et al., 2007) which uses SIMM models for the analysis of dynamic simulations of movement. Simbios also hosts a web-based file exchange and discussion forum known as SimTK (tool kit) that allows the sharing of models, analyses and code.

Due to the free, open-source nature of OpenSim its use has become widespread across the globe with interest from a number of leading international centres. For this reason there have been an increasing number of OpenSim human simulation studies appearing in the literature (as detailed in section 1.3) and SimTrack, the OpenSim workflow for generating muscle driven simulations of movement, is fast becoming accepted as an industry standard approach. However, there is little or no validation of the muscle activations generated by this workflow and this is the work that this thesis attempts to undertake.

2.2. OpenSim

2.2.1. OpenSim Introduction

OpenSim is a freely available, user extensible software system that lets users develop 3D models of musculo-skeletal structures and create dynamic simulations of movement (Delp et al., 2007). The software is written in C++ with a graphical user interface written in Java (Figure 2.7).

OpenSim uses a plug-in architecture that allows open-source third party tools to be used for some functionality and computational components such as dynamics engines, integrators, and optimisers to be updated as appropriate without extensive restructuring. The plug-in capability also allows users to extend the functionality by developing their own musculo-skeletal models, contact models, controllers, and analyses.

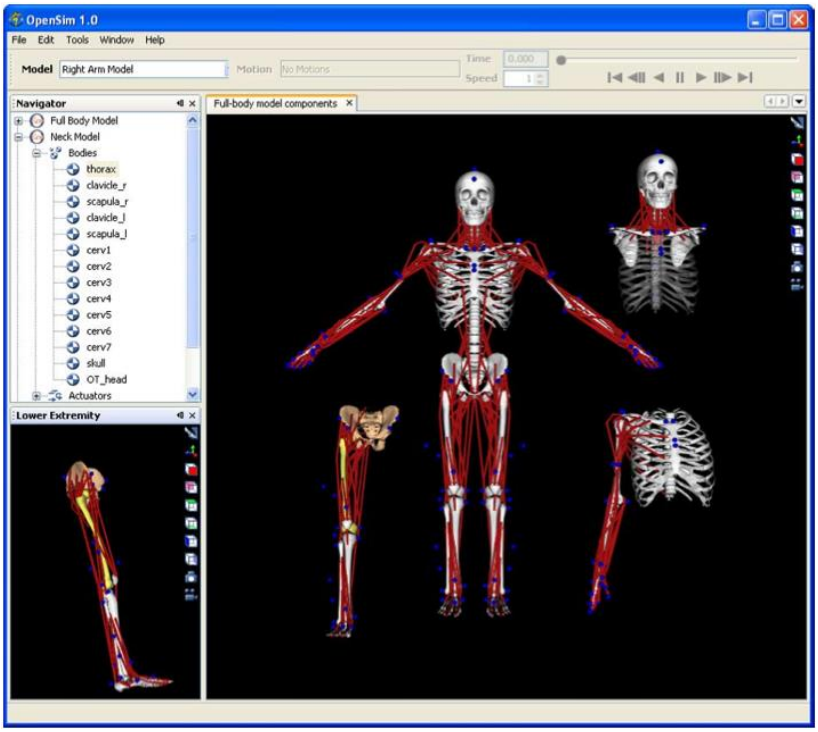

Figure 2.7 – OpenSim graphical user interface. A number of musculo-skeletal models are shown: lower extremity, full body, neck, and upper extremity.

OpenSim musculo-skeletal models are coded in Extensible Markup Language (XML). The models are built up from a number of rigid skeletal bodies, each assigned with appropriate inertial properties and degrees of freedom (DoFs) of movement to mimic the system under investigation (in this case, the human musculo-skeletal system). The inter-body joint constraints are therefore set by the degrees of freedom and each degree of freedom gives rise to a model *coordinate* parameter. Some joints can be highly constrained with only a single coordinate, for example a simple hinge ankle joint limited solely to flexion/extension, whilst others can be less constrained and therefore capable of more complex movements, such as a ball and socket hip joint being allowed to rotate around all three orthogonal axes giving flexion/extension, abduction/adduction and long axis

rotation. Usually, there are no translational degrees of freedom between body segments but one body (typically the pelvis) is given universal freedom relative to the ground to control the model's global position and orientation. Muscles are then represented by *actuator* elements attached to specified points on the body elements and controlled by appropriate muscle models.

A number of models have been published and are shared on the SimTK forum, four of which were suitable for use in this work as they were designed for the analysis of gait (Figure 2.8).

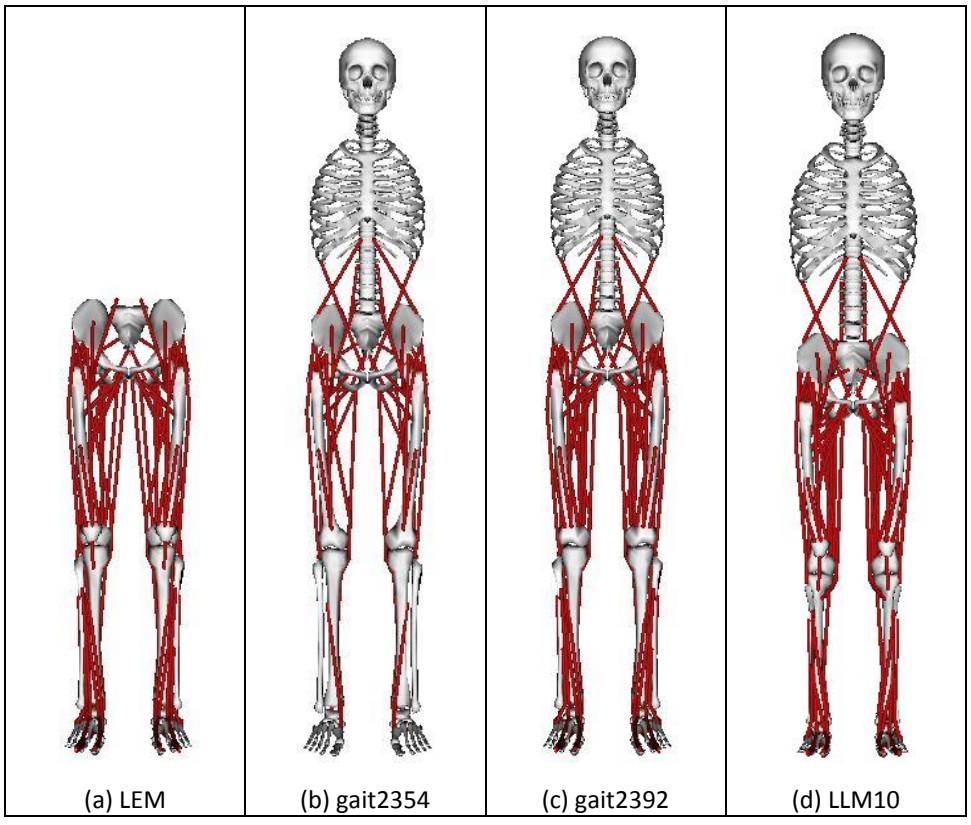

Figure 2.8 – Four OpenSim, lower extremity, human musculo-skeletal models.
(a) LEM = lower extremity model - 20 DoFs, 88 Schutte actuators
(b) gait2354 - 23 DoFs, 54 Thelen actuators
(c) gait2392 - 23 DoFs, 92 Thelen actuators
(d) LLM10 = lower limb model 2010
23 DoFs, 90 Schutte actuators and 6 Thelen actuators

DoFs = degrees of freedom
Schutte actuator = muscle model from Schutte et al. (1993)
Thelen actuator = muscle model from Thelen (2003)
(a-c) Delp et al. (1990), (d) (Arnold et al., 2010)

The lower extremity model, gait2354 and gait2392 were created by Darryl Thelen (University of Wisconsin-Madison) and Ajay Seth, Frank Anderson, and Scott Delp (Stanford University). The models feature lower extremity joint definitions taken from Delp (1990), low back joint and anthropometry from Anderson & Pandy (1999), and a planar knee model taken from Yamaguchi & Zajac (1989). The muscle models were parameterised using data collected from five cadaveric specimens from two studies (Friederich & Brand, 1990; Wickiewicz et al., 1983). These studies are described in more detail in section 3.2. Muscle strengths were determined using physiological cross-sectional area measurements from these studies but they were found to be weak when compared to the experimental data of Anderson & Pandy (1999). An inflated value of specific tension ($61N/cm^2$) compared to the commonly accepted value for mammalian muscle ($23N/cm^2$; Spector et al., 1980) was therefore used to compensate. However, this does raise questions over the validity of the other muscle data. More recently, in recognition of the limited sample size of these older studies, the Lower Limb Model (Arnold et al., 2010) was created to update the gait2392 model using anatomical data from the newer, 21 cadaver study of Ward et al. (2009). All four models have the same rigid body segments and degrees of freedom listed in Table 2.1 except the lower extremity model which has no torso body.

It was necessary to choose one of these models for use in this work. The lower extremity model was not chosen because it lacked a torso segment and the inertial properties of a segment of high mass would have significant influence on the ground-reaction-force.

The gait2354 model was not chosen as it was designed as a simpler version on the gait2392 model to reduce simulation time for teaching and presentation purposes and, with fewer muscle actuators than either the gait2392 or LLM10 models, the origins, insertions and moment-arms of true human musculature would be less closely matched.

12 Bodies	12 Joints		23 Degrees of Freedom	23 Coordinates
torso	back	ball & socket joint with pelvis	3 orthogonal rotations	trunk flexion, abduction, rotation
pelvis	ground-pelvis	universal joint with external environment	3 orthogonal translations 3 orthogonal rotations	model global position X, Y, Z, pelvic tilt, obliquity, rotation
femur (L&R)	hip	ball & socket joint with pelvis (L&R)	3 orthogonal rotations (L) 3 orthogonal rotations (R)	hip flexion, abduction, rotation (L&R)
tibia/fibula (L&R)	knee	complex hinge type joint with femur (L&R)	1 rotation/translation (L) 1 rotation/translation (R)	knee flexion (L&R)
talus (L&R)	ankle	hinge joint with tibia/fibula (L&R)	1 rotation (L) 1 rotation (R)	ankle flexion (L&R)
calcaneum (L&R)	subtalar	*hinge joint with talus (L&R)	*1 rotation (L) *1 rotation (R)	*subtalar in/eversion (L&R)
toes (L&R)	MTP	*hinge joint with calcaneum (L&R)	*1 rotation (L) *1 rotation (R)	*toe flexion (L&R)

Table 2.1 – OpenSim model degrees of freedom. Bodies, joints, degrees of freedom and corresponding coordinates for the OpenSim gait models listed in Figure 2.8. The complex hinge joint of the knee consists of both rotational and translational elements and is defined by Yamaguchi & Zajac (1989). L&R = exists for both left and right legs. MTP = metatarsal-phalangeal joint.

* the OpenSim User Guide recommends that these joints are locked at neutral for simulations involving the Computed Muscle Control tool as there is not enough musculature in the model to adequately control their movement. This reduces the number of joints from 12 to 9 and the number of DoFs/coordinates from 23 to 19.

It would have been preferable to use the LLM10 model over gait2392 as it was based on newer anatomical data from a larger study of cadavers, but LLM10 performed poorly in initial tests of computational time for calculating muscle forces over a single gait cycle. Using the same machine, the LLM10 simulation took 4.7 hours to run, whereas the gait2392 simulation took only 30 minutes. The difference in simulation time between these two similar models is likely to have been caused by the different muscle models that each one incorporated (as detailed in Figure 2.8). Longer processing time made the LLM10 model impractical to use for multiple simulations and so the gait2392 model was selected for use in this work.

2.2.2. The Gait2392 Model

The gait2392 model has a mass of 75.16kg and a height of 1.8m. In addition to the 12 body segment and 23 degrees of freedom listed in Table 2.1 the model also contained 92 muscle actuators based on the Thelen (2003) model. Six actuators control torso

movement relative to the pelvis, and the remaining 86 are assigned to the lower limbs (43 each side). The muscle actuators are string elements and typically a single actuator is used to represent each anatomical muscle; however, multiple actuators are used for the glutei and adductor magnus muscles to more accurately characterise their broad origins. Actuators for the right lower limb are listed below in Table 2.2 and a matching set also exists for the left side.

muscle actuator	corresponding muscle
glut_max1_r	
glut_max2_r	gluteus maximus
glut_max3_r	
glut_med1_r	
glut_med2_r	gluteus medius
glut_med3_r	
glut_min1_r	
glut_min2_r	gluteus minimus
glut_min3_r	
semimem_r	semimembranosus
semiten_r	semitendinosus
bifemlh_r	biceps femoris long head
bifemsh_r	biceps femoris short head
sar_r	sartorius
add_long_r	adductor longus
add_brev_r	adductor brevis
add_mag1_r	
add_mag2_r	adductor magnus
add_mag3_r	
tfl_r	tensor fasciae latae
pect_r	pectineus
grac_r	gracilis

muscle actuator	corresponding muscle
iliacus_r	iliacus
psoas_r	psoas
quad_fem_r	quadratus femoris
gem_r	sup/inferior gemellus
peri_r	piriformis
rect_fem_r	rectus femoris
vas_med_r	vastus medialis
vas_int_r	vastus intermedius
vas_lat_r	vastus lateralis
med_gas_r	medial gastrocnemius
lat_gas_r	lateral gastrocnemius
soleus_r	soleus
tib_post_r	tibialis posterior
flex_dig_r	flexor digitorum longus
flex_hal_r	flexor hallucis longus
tib_ant_r	tibialis anterior
per_brev_r	peroneus brevis
per_long_r	peroneus longus
per_tert_r	peroneus tertius
ext_dig_r	extensor digitorum brevis/longus
ext_hal_r	extensor hallucis longus

Table 2.2 – 43 muscle actuators for the right lower limb in the gait2393 model

The Thelen (2003) muscle model characterises the muscle response curves outlined in section 2.1.2 using the following equations.

Activation dynamics are driven by a non-linear, first order differential equation (Equation 2.8a,b).

Equation 2.8a

$$\frac{da}{dt} = \frac{u - a}{\tau_a(a,u)}$$

Equation 2.8b

$$\tau_a(a,u) = \begin{cases} \tau_{act}(0.5 + 1.5a); & u > a \\ \tau_{deact} / (0.5 + 1.5a); & u \le a \end{cases}$$

where:

a is muscle activation
t is time
u is the idealised muscle excitation (ranging from 0-1)
$\tau_a(a,u)$ is an activation time constant that varies with activation
τ_{act} is the activation time constant
τ_{deact} is the deactivation time constant

Three equations are used to characterize the muscle and tendon properties. The passive component of the muscle belly force-length relationship (the parallel elastic element) is represented by the exponential function Equation 2.9.

Equation 2.9

$$\overline{F}^{PE} = \frac{e^{\left(k^{PE}(\overline{L}^{M} - 1) / \varepsilon_0^{M}\right)} - 1}{e^{k^{PE}} - 1}$$

where:

$\overline{F}^{PE}$ is the normalised passive muscle force
k^{PE} is the exponential shape factor
$\overline{L}^{M}$ is the normalised muscle fibre length
ε_0^{M} is the passive muscle strain at maximum isometric force

The active component of the muscle belly force-length relationship (the contractile element) is represented by the Gaussian function Equation 2.10.

Equation 2.10
$$f_l = e^{\frac{-\left(\overline{L}^M - 1\right)^2}{\gamma}}$$

where:

f_l is the active force-length scale factor
$\overline{L}^M$ is the normalised muscle fibre length
γ is a shape factor

The force-length relationship of the tendon (the series elastic element) is characterised by an exponential function for an initial non-linear toe region and a linear function at higher strains (Equation 2.11).

Equation 2.11
$$\overline{F}^T = \begin{cases} \dfrac{\overline{F}^T_{toe}}{e^{k_{toe}} - 1}\left(e^{\frac{k_{toe}\cdot\varepsilon^T}{\varepsilon^T_{toe}}} - 1\right); & \varepsilon^T \le \varepsilon^T_{toe} \\ k_{lin}\left(\varepsilon^T - \varepsilon^T_{toe}\right) + \overline{F}^T_{toe}; & \varepsilon^T > \varepsilon^T_{toe} \end{cases}$$

where:

$\overline{F}^T$ is the tendon force normalised to maximum isometric force
$\overline{F}^T_{toe}$ is the transition tendon force between toe and linear regions = 0.33
k_{toe} is an exponential shape factor = 3
ε^T is the tendon strain
ε^T_{toe} is the minimum tendon strain for linear behaviour
k_{lin} is a linear shape factor

And for continuity of slopes between the two regions

ε^T_{toe} = 0.609 ε^T_0 ε^T_0 is passive tendon strain at maximum isometric force
k_{lin} = 1.712/ ε^T_0

The muscle-tendon contraction dynamics are characterised by the force-velocity curve defined by Equation 2.12a,b. Parameter *b* varies dependent on whether the active muscle is shortening (concentric action) or lengthening (eccentric action).

Equation 2.12a

$$V^M = (0.25 + 0.75a) \cdot V^M_{\max} \frac{\overline{F}^M - af_l}{b}$$

Equation 2.12b

$$b = \begin{cases} af_l + \overline{F}^M / A_f & \overline{F}^M \le af_l \ \text{(concentric)} \\ \dfrac{\left(2 + 2/A_f\right)\left(af_l \cdot \overline{F}^M_{len} - \overline{F}^M\right)}{\overline{F}^M_{len} - 1} & \overline{F}^M > af_l \ \text{(eccentric)} \end{cases}$$

where:

V^M is the muscle fibre contraction velocity
$V^M_{\max}$ is the maximum muscle fibre contraction velocity
a is activation
$\overline{F}^M$ is the active muscle force
f_l is the active force-length scale factor
A_f is the force-velocity shape factor
$\overline{F}^M_{len}$ is the maximum normalised muscle force for eccentric action

During a simulation, these equations are numerically integrated alongside the equations of motion to calculate time varying actuator activations and fibre lengths.

Finally, the pennation angle of the fibres in each muscle are incorporated within the model by linking musculo-tendinous lengths to muscle fibre and tendon lengths (Equation 2.13).

Equation 2.13 $$\overline{L}^{T} = \overline{L}^{MT} - \overline{L}^{M}\cos(\alpha^{M})$$

where:

$\overline{L}^{T}$ is the normalised tendon length

$\overline{L}^{MT}$ is the normalised musculo-tendinous unit length

$\overline{L}^{M}$ is the normalised muscle fibre length

α^{M} is the muscle fibre pennation angle

A graphical representation of these equations is shown in Figure 2.9.

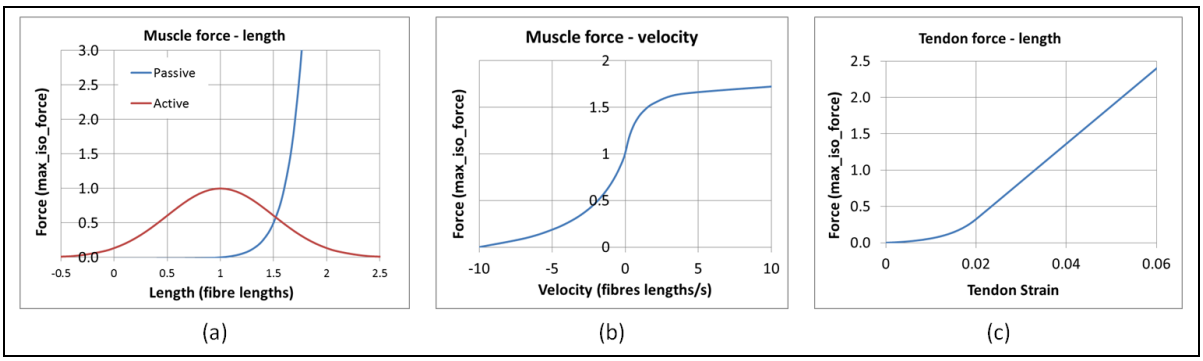

Figure 2.9 – Example Thelen (2003) muscle model curves

(a) The active (contractile element) and passive (parallel elastic element) forces-length relationship of the muscle belly component of the muscle model. The active curve represents the response for a single level of activation. Total muscle belly force is given by combination of both the active and passive components. max_iso_force is the maximum isometric force of the muscle

(b) The muscle belly force-velocity relationship for a single level of muscle activation. Shortening velocities (concentric action) are negative.

(c) The passive (series elastic element) force-length relationship of the tendon component of the muscle model. The non-linear, toe region extends to a strain of 0.02 and a linear relationship continues at higher strains

16 muscle parameters are used to fully characterise the Thelen (2003) muscle model in the gait2392 model. 12 of these parameters are common to all 92 actuators and four parameters are muscle specific (Table 2.3).

gait2392 model parameter	Description	Value	Thelen Model
max_isometric_force	max. isometric muscle force used for normalisation	m.s.	n/a
optimal_fiber_length	resting fibre length used for normalisation	m.s.	n/a
tendon_slack_length	resting tendon length used for normalisation	m.s.	n/a
pennation_angle	muscle fibre pennation angle	m.s.	α^M
activation_time_constant	activation time constant	0.01	τ_{act}
deactivation_time_constant	deactivation time constant	0.04	τ_{deact}
max_contraction_velocity	max. muscle fibre contraction velocity	10	$V^M_{\max}$
Vmax	max. muscle fibre contraction velocity at full activation	10	n/a
Vmax0	max. muscle fibre contraction velocity at low activation	5	n/a
FmaxTendonStrain	passive tendon strain at max. isometric force	0.033	ε^T_0
FmaxMuscleStrain	passive muscle strain at max. isometric force	0.6	ε^M_0
KshapeActive	active muscle belly shape factor	0.5	γ
KshapePassive	passive muscle belly exponential shape factor	4	k^{PE}
damping	passive damping in the force-velocity relationship	0.05	n/a
Af	force-velocity shape factor	0.3	A_f
Flen	max. normalised muscle force for eccentric action	1.8	$\overline{F}^M_{len}$

Table 2.3 – Gait2392 muscle actuator parameter names, descriptions, values and their Thelen (2003) muscle model equivalents. m.s. = muscle specific

2.2.3. SimTrack - Calculating Muscle Activations in OpenSim

SimTrack (Delp et al., 2007) is the OpenSim tool for generating muscle driven simulations of movement. It is a four step process (Figure 2.10) that requires a musculo-skeletal model (e.g. gait2392), experimental kinematics and experimental ground-reaction-force data as inputs. These datasets are usually obtained from a motion capture system following a protocol similar to that described in section 2.4.

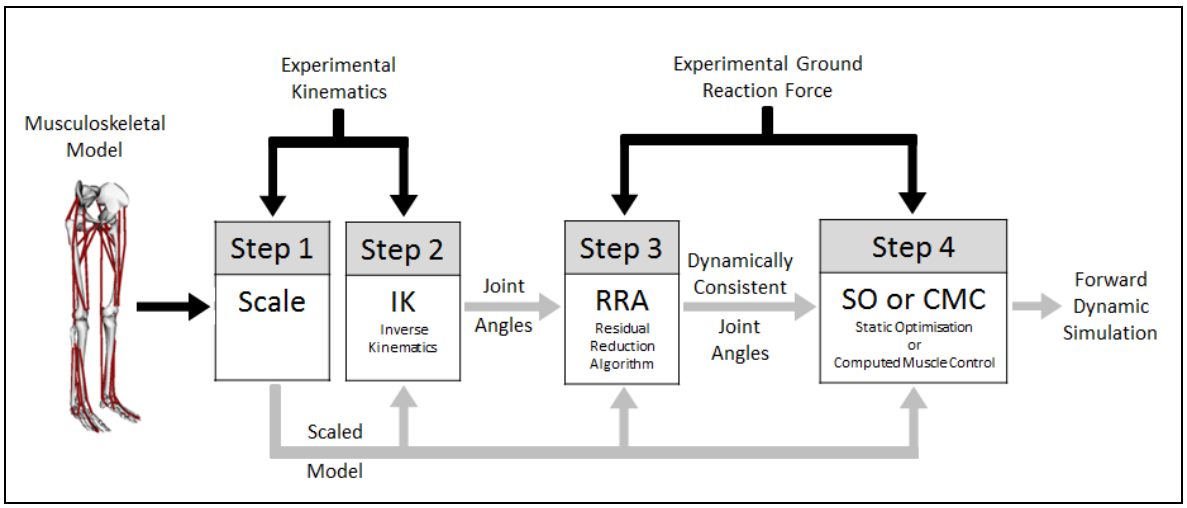

Figure 2.10 – SimTrack: the four step process in OpenSim for generating a muscle driven simulation from motion capture data.

There are two ways in which movement data from a motion capture system can be imported into OpenSim. Firstly the joint coordinate data for each time frame can be supplied directly as an input to the model. However, as these joint coordinates are calculated from biomechanical models run within third party software, incompatibilities may exist between these models and the model being used within OpenSim, resulting in an incomplete or erroneous set of coordinates.

The second method requires the OpenSim Inverse Kinematics tool to calculate the necessary joint coordinates using the trajectories of the motion capture markers. For clarity, the markers used in motion capture will be referred to as *experimental* markers and the markers attached to the OpenSim model will be referred to as *virtual* markers. This technique avoids the problem of incompatibility of models but it is reliant on a carefully chosen marker set and weightings to ensure that the Inverse Kinematics tool is able to accurately reconstruct the original movement. For this project, motion capture was performed using a combination of the standard gait2392 marker set and the Vicon Plug-in-Gait marker set, as described in section 2.4.1. This allowed the experimental marker trajectories to be directly compatible with the virtual markers attached to the gait2392 model and also allowed kinematics and kinetics to be calculated independently by running the standard Plug-in-Gait model in the motion capture software. The

kinematics generated by the OpenSim Inverse Kinematics tool could then be checked by comparison.

OpenSim is not able to read the binary C3D data file format output by the motion capture system and so file conversion was necessary before running SimTrack. A number of Matlab scripts (The Mathworks^{TM}, MA, USA) are available for download from the online SimTK resources depository for this purpose. Three sets of scripts were evaluated for their suitability to the Guy's Hospital Gait Laboratory setup and the Gait Extraction Toolbox (Dorn, 2008) was selected for use. The following binary to ASCII file conversions were carried out:

Standing trial C3D file converted to:
**.trc* file – 3D trajectory data for the experimental markers (120Hz)
**coordinates.mot* file – Vicon model joint angles and ground-reaction-force (120Hz)

Walking trial C3D file converted to:
**.trc* file – 3D trajectory data for the experimental markers (120Hz)
**coordinates.mot* file – Vicon model joint angles and ground-reaction-force (120Hz)
**kinetics.mot* file – ground-reaction-force data (1080Hz)
**EMGSet.mot* file – EMG data channels 1-16, raw and processed (1080Hz)

SimTrack Step 1 – Scaling

The Scale tool resizes the generic model to match the size of the subject. There are three phases in the scaling process. The first stage scales the size of each of the model's body elements based on either manual scaling factors or scaling factors calculated from the ratio of the distances between experimental and virtual marker pairs from the static trial. For example, the torso body can be scaled in all three orthogonal axes by the ratio of the experimental sacrum-to-head marker distance to the virtual sacrum-to-head marker distance. The model's mass distribution will also be scaled to the subject's weight. In the second stage the Inverse Kinematics tool is run to place the scaled model in the standing pose (Figure 2.11) to match experimental marker positions (with user defined weightings)

and/or directly input coordinates. In the final stage selected virtual markers are then moved to match the positions of the experimental markers. This allows the position of the virtual markers to be corrected to the positions actually used during motion capture which should allow better motion tracking in the subsequent dynamic inverse kinematics.

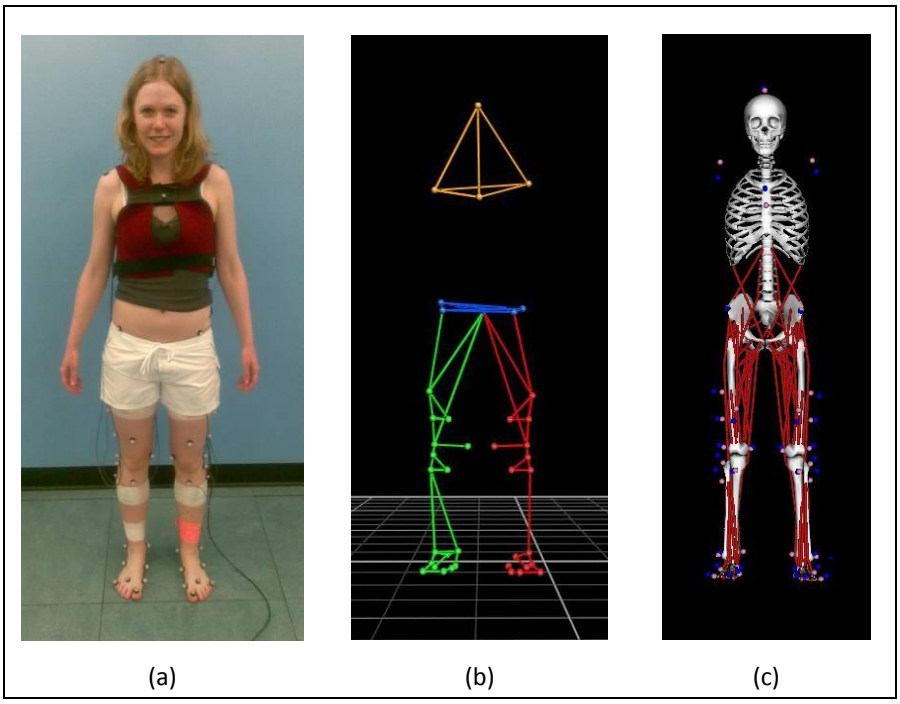

Figure 2.11 – OpenSim SimTrack Step 1 - Scaling
(a) markers on the subject in the standing pose
(b) marker trajectories in motion capture software
(c) OpenSim model standing pose after scaling but before marker adjustment (experimental markers blue, virtual markers pink)

SimTrack Step 2 – Inverse Kinematics (IK)

The Inverse Kinematics tool determines a set of coordinates to position the model in a specific pose for each time frame (Figure 2.12). The coordinates are calculated using weighted least squares optimisation (Equation 2.14) to minimise marker error (the distance between virtual and experimental markers) and/or coordinate error (difference between OpenSim coordinates and input coordinates) to track a set of marker trajectories and/or input coordinates from motion capture. The final motion can be very sensitive to the set of marker and/or coordinate weightings chosen.

Equation 2.14

$$E_{sq} = \sum_{i=1}^{\text{markers}} w_i \left(\vec{x}_i^{\text{subject}} - \vec{x}_i^{\text{model}} \right)^2 + \sum_{j=1}^{\text{coordinates}} \omega_j \left(\theta_j^{\text{subject}} - \theta_j^{\text{model}} \right)^2$$

where:

E_{sq} is the squared error

w_i is the weighting factor for the i^{th} marker

$\vec{x}_i^{\text{subject}}$ is the 3D position of the i^{th} experimental marker

$\vec{x}_i^{\text{model}}$ is the 3D position of the i^{th} virtual marker

ω_j is the weighting factor for the j^{th} coordinate

$\theta_j^{\text{subject}}$ is the 3D position of the j^{th} input coordinate

θ_j^{model} is the 3D position of the j^{th} OpenSim coordinate

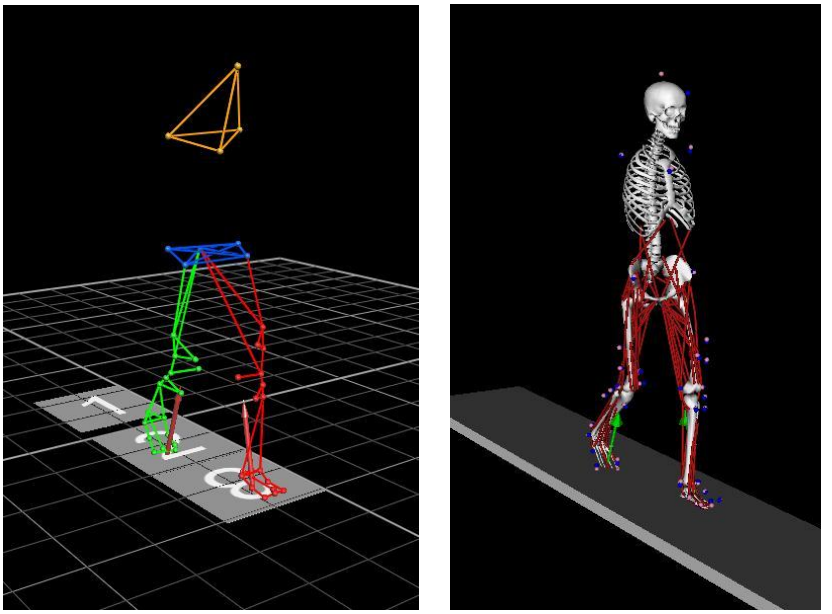

(a) (b)

Figure 2.12 – OpenSim SimTrack Step 2 – Inverse Kinematics
(a) marker trajectories in the motion capture software
(b) OpenSim model movement after running the Inverse Kinematics tool

SimTrack Step 3 – Residual Reduction Algorithm (RRA)

The Residual Reduction Algorithm is used to reduce the dynamic inconsistencies that result from the imperfect matching of the experimental kinematics and kinetics. These arise from inaccuracies in the measurement of size and weight of the subject, as well as inaccuracies and noise that arise in motion and ground-reaction-force data collection and processing. The dynamic inconsistency exists in the form of a mismatch (the residual force in Equation 2.15) between the ground-reaction force and the model inertia. An analogous equation exists for the residual moment necessary to balance rotational inertia with the ground-reaction-moment.

Equation 2.15

$$\vec{F}_{\text{grf}} = m_T\vec{g} + \sum_{i=1}^{\text{bodies}}\left(\text{m}_\text{i}\vec{\text{a}}_\text{i}\right) + \vec{F}_{\text{residual}}$$

where:

$\vec{F}_{\text{grf}}$ is the measured ground-reaction-force
m_T is the total mass of the subject
$\vec{g}$ is the acceleration due to gravity
m_i is the mass of the i^{th} body segment
$\vec{a}_i$ is the linear acceleration of the i^{th} body segment
$\vec{F}_{\text{residual}}$ is the residual force necessary to balance the equation

The Residual Reduction Algorithm is a form of forward dynamic simulation which calculates the joint torques necessary for the model to propel itself to track the motion determined by Inverse Kinematics. All the muscle actuators are replaced by ideal joint actuators (known as *reserves*), one for each coordinate, and six *residual* actuators for the three global orthogonal forces and three global orthogonal moments (Fx, Fy, Fz, Mx, My, Mz). The forward simulation is run frame by frame optimising the *reserves* to produce the desired motion. Magnitudes of the *residual* actuators are then calculated to compensate for the difference between the inertial terms and the ground-reaction-force. After the first run of the algorithm the Mx and Mz *residuals* (anterior/posterior, medial/lateral leaning) are minimised by creating a new model with an adjusted torso centre of mass and the Fy

residual (vertical) is minimised by altering the model total mass. The algorithm can then be run for a second time using the new model and with limits on the magnitude of the *residual* actuators. This allows the dynamic inconsistencies to be reduced further but this time by forcing the kinematics to change. The limits imposed on the *residuals* therefore need to be chosen with care to ensure that kinematics do not change too severely. Recommended thresholds for *residuals* and kinematic tracking deviations to determine an "acceptable" walking or running simulation are provided by the OpenSim software developers (Table 2.4).

Thresholds:	Good	OK	Bad
Max. residual force (N)	0-10	10-25	>25
RMS residual force (N)	0-5	5-10	>10
Max. residual moment (Nm)	0-50	50-75	>75
RMS residual moment (Nm)	0-30	30-50	>50
Max. translation error (cm)	0-2	2-5	>5
RMS translation error (cm)	0-2	2-4	>4
Max. rotation error (°)	0-2	2-5	>5
RMS rotation error (°)	0-2	2-5	>5

Table 2.4 – Acceptability thresholds after running the Residual Reduction Algorithm for residuals and kinematic tracking position errors. Data taken from the OpenSim 2012 User Guide

However, from the perspective of clinical gait analysis, some of these thresholds are arguably too high (too lenient). Let us examine the maximum thresholds of the "*Good*" category. The peak vertical/anterior/medial ground reaction forces in normal gait for a typical adult (70kg) would be approximately 750N/170N/35N (1.1/0.25/0.05 x body weight – Wearing et al., 2000) and so a maximum residual force of 10N is small (1.3%) in comparison to the vertical component, but starts to become proportionally larger (5.9% and 28.6%) if applied in the anterior and medial directions. A maximum residual moment of 50Nm however is a very large turning force to be applied globally to the model. It is equivalent to holding a 10kg weight at arm's length (0.5m) away from our body – a task few people could physically achieve. Allowing such a large correction to a simulation would call into question the validity of any subsequent kinetic analysis.

Maximum translation errors of the model are given an acceptability threshold of 2cm in the *"Good"* category. Again this limit is high compared to the acceptance limits of marker position error typically used for quality assurance testing of motion capture equipment in clinical gait laboratories (c.2mm). If the maximum joint rotation error is maintained below 2° as advised however, then the changes in model joint kinematics that result from these errors may be acceptable. Error propagation into the calculation of kinetics may be more problematic however as a translational shift of the model will alter the point of application of the ground reaction force (as there will be a relative movement between the model and the experimental ground reaction force's centre of pressure). There is little published research on the necessary accuracy of force-plate data in clinical gait analysis but some unpublished work by the author examined the changes to kinetic data as a result of artificially imposed force-plate errors. An acceptable change in kinetics was classified as a RMS difference less than 0.5 standard deviations of the gait laboratory's control dataset. Following this criteria the limit of a force-plate's centre of pressure error was calculated to be 20mm. It would appear therefore that the OpenSim User Guide recommended 2cm threshold for maximum translational error is appropriate, but certainly the thresholds for both the "*OK*" and "*Bad*" categories are likely to allow significant errors in the calculation of joint torques.

SimTrack Step 4 – Static Optimisation or Computed Muscle Control

As discussed in section 2.1.3 various techniques have been proposed to overcome the problem of static indeterminacy when calculating muscle forces from joint moments and OpenSim offers two alternative methods.

Static Optimisation

First proposed by Hardt (1978), Static Optimisation is a technique for resolving net joint moments into muscle forces by considering each time frame individually. A movement is therefore treated as a series of consecutive static poses and hence activation dynamics and most elements of musculo-tendon dynamics are ignored. The Static Optimisation tool within OpenSim first carries out an inverse dynamics step to calculate net joint torques from experimental kinematics and ground-reaction-forces. A set of muscle activations, dependent on the muscle-activation-to-force condition, are then calculated which will generate these joint torques. The static indeterminacy of this calculation is overcome by use of a cost function (Equation 2.16) that finds a solution to minimise the sum of all muscle activations raised to a user defined power.

Equation 2.16

$$J = \sum_{m=1}^{n} \left(a_m\right)^p$$

where:

J is the cost function

n is the total number of muscle actuators

a_m is the activation of the m^{th} muscle actuator

p is the user defined power (typically p=2)

The Static Optimisation tool within OpenSim offers two alternative muscle-activation-to-force conditions. The first condition (the “non-physiological” case: Equation 2.17) replaces the muscle model with unconstrained ideal force generators and so all elements of musculo-tendon dynamics are ignored. The second condition (the “physiological” case: Equation 2.18) imposes a simplified version of the muscle model (described in section 2.2.2) by only considering the active component of this model (the tendon is made inextensible and the parallel elastic element is ignored). The muscle actuators are therefore only constrained to follow the appropriate active force-length-velocity curves.

Equation 2.17

$$\sum_{m=1}^{n} \left(a_m \cdot F_m^0\right) \cdot r_{m,j} = \tau_j$$

Equation 2.18

$$\sum_{m=1}^{n}\left[a_m \cdot f\left(F_m^0, l_m, v_m\right)\right] \cdot r_{m,j} = \tau_j$$

where: n is the total number of muscle actuators

a_m is the activation of the m^{th} muscle actuator at a discrete time step

F_m^0 is the maximum isometric force of the m^{th} muscle actuator

l_m is the length of the m^{th} muscle actuator

v_m is the shortening velocity of the m^{th} muscle actuator

$f\left(F_m^0, l_m, v_m\right)$ is the force-length-velocity surface of the m^{th} muscle actuator

$r_{m,j}$ is the moment arm of the m^{th} muscle actuator about the j^{th} joint axis

τ_j is the generalised moment acting about the j^{th} joint axis

In the muscle model of this second condition the pennation angles of the muscles are constant and the tendon is fixed at the tendon slack length. Therefore, as can be seen from Equation 2.13, the muscle fibre length can be directly calculated from the musculo-tendinous length, and hence from the angle(s) of the joint(s) that the muscle crosses – the input kinematics. No reference is made in the OpenSim user-guide however on how the Static Optimisation tool determines muscle fibre velocity and so it can only be assumed that it is calculated from the current and previous frame muscle fibre lengths. If this is correct then it is not truly a static process. It also follows therefore that if the Static Optimisation tool is run on a single frame of data alone, the fibre velocity has to be assumed to be zero.

The suitability of such a cost function (Equation 2.16) for the predication of human muscle activity during gait is discussed in a number of papers. Crowninshield & Brand (1981) describe how early cost functions were chosen more for ease of implementation rather than for their physiological validity and justified their choice of cost function (similar to Equation 2.16) by describing it as an analogue to maximum muscle endurance.

A number of criticisms however, summarised succinctly by Anderson & Pandy (2001), have been made against the use of static optimisation algorithms for the estimation of in-vivo muscle forces during gait – these include: the reliance on potentially inaccurate experimental kinematics and, due to the time-independent nature of the technique, the difficulty of incorporating muscle physiological properties or muscle coordination principles into the algorithm. However, as the title of their article suggests, they go on to show that for normal gait, static and dynamic optimisation solutions are practically equivalent.

The review article of Erdemir et al. (2007) points out that despite the use of static optimisation techniques in research for a number of decades, none of these methods have been successfully translated into clinical practice due to the ever present difficulty of validating these simulated muscle forces, especially in pathological populations.

Computed Muscle Control

An alternative method for calculating muscle forces from joint moments is the Computed Muscle Control algorithm first proposed by Thelen et al. (2003) and subsequently updated (Thelen & Anderson, 2006). This also makes use of the Static Optimisation algorithm to determine muscle activations but added into the optimisation loop is a proportional derivative feedback control to track experimental kinematics and a forward dynamics step to enable activation and contraction dynamics to be included in the calculations (Figure 2.13 and Equation 2.19).

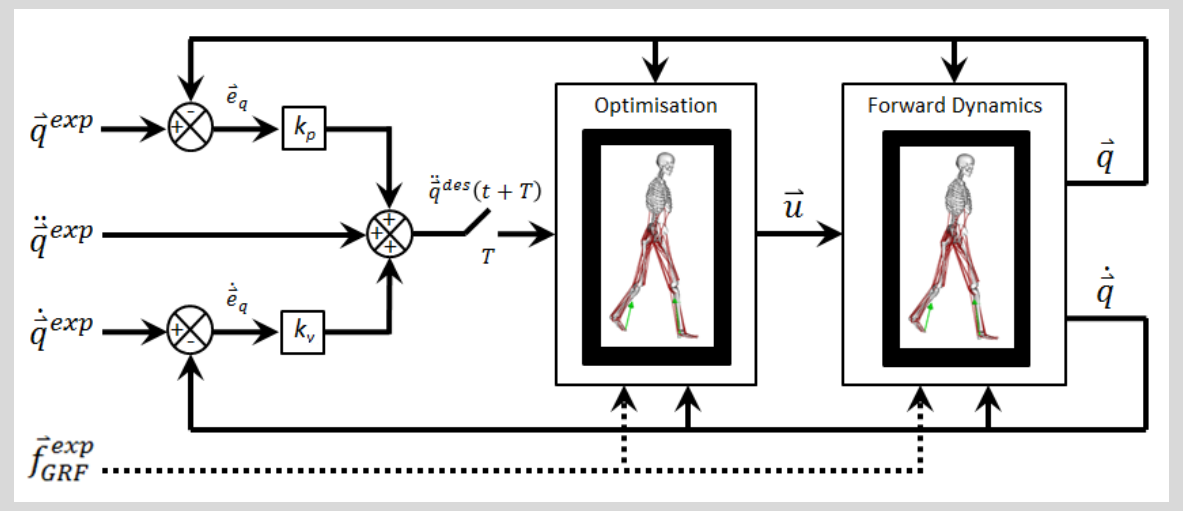

Figure 2.13 – OpenSim SimTrack Step 4 – a schematic showing the Computed Muscle Control algorithm applied to gait. Errors between simulated and experimental joint angles and joint angle velocities are used in a feedback loop in the calculation of the desired joint accelerations necessary to track the experimental kinematics. Nomenclature defined in Equation 2.19.

$\vec{f}_{GRF}^{\,\exp}$ = ground-reaction-force, $\vec{e}_q$ = position error, $\dot{\vec{e}}_q$ = velocity error, $\vec{u}$ = actuator excitations

Equation 2.19 $$\ddot{\vec{q}}_j^{des}(t+T) = \ddot{\vec{q}}_j^{\exp}(t+T) + k_v\left[\dot{\vec{q}}_j^{\exp}(t) - \dot{\vec{q}}_j(t)\right] + k_p\left[\vec{q}_j^{\exp}(t) - \vec{q}_j(t)\right]$$

where:

$\ddot{\vec{q}}_j^{des}$ is the desired j^{th} coordinate acceleration

t is the time

T is the integration time step (typically T = 0.01s)

$\ddot{\vec{q}}_j^{\exp}$ is the experimental j^{th} coordinate acceleration

k_v is the velocity feedback gain (typically k_v = 20)

$\dot{\vec{q}}_j^{\exp}$ is the experimental j^{th} coordinate velocity

$\dot{\vec{q}}_j$ is the simulated j^{th} coordinate velocity

k_p is the position feedback gain (typically k_p = 100)

$\vec{q}_j^{\exp}$ is the experimental j^{th} coordinate position (e.g. joint angle)

$\vec{q}_j$ is the simulated j^{th} coordinate position

There are a number of distinct stages within the Computed Muscle Control optimisation loop that are described below:

The initial states of the model (joint angles, velocities, accelerations) are set to the experimental kinematics. The desired accelerations are then calculated from the experimental accelerations modified by previous frame (t - T) simulated position and velocity errors (Equation 2.19). Clearly, it is not possible to calculate previous frame simulated data for the first frame (t = 0) and so no feedback is used for the initial state. For this reason, muscle states (activations and fibre-lengths) are typically out of equilibrium and simulated muscle forces can change dramatically during this initial time interval. It is therefore recommended that the Computed Muscle Control algorithm is started at least 0.03 seconds (3 time steps) before the interval of interest.

The modification of experimental accelerations to give desired accelerations is carried out with a proportional derivative control (Equation 2.19), so called because the feedback is in proportion to the position error and the velocity error (the derivative of position). Values of the feedback gains are chosen to drive the errors to zero in a critically damped fashion.

Static optimisation is used to overcome static indeterminacy (section 2.1.3) and to compute a set of muscle excitations and hence the forces that will drive the body segments to produce these desired accelerations. Two formulations of the static optimisation cost function are offered in the Computed Muscle Control tool, both similar to Equation 2.16. The first formulation, the "*slow target*" (Equation 2.20), contains two terms: the first is the sum of squared muscle excitations, and the second is a weighted sum of squared joint acceleration errors. When the cost function is minimised therefore the first term will minimise and distribute excitations across the muscles, and the second term will drive the model towards the desired accelerations.

Equation 2.20 - the slow target

$$J = \sum_{i=1}^{n} x_i^{\,2} + \sum_{j=1}^{m} w_j \left(\ddot{q}_j^{des} - \ddot{q}_j \right)^2$$

where:

J is the cost function

n is the total number of muscle actuators

x_i is the excitation of the i^{th} muscle actuator

m is the total number of coordinates

w_j is *p* is the user defined power (typically *p*=2)

$\ddot{q}_j^{des}$ is the desired j^{th} coordinate acceleration

$\ddot{q}_j$ is the simulated j^{th} coordinate acceleration

The second formulation of the cost function, the "*fast target*" (Equation 2.21), replaces the tracking term of the slow target with a set of equality constraints that require the desired accelerations to be achieved within a set tolerance.

Equation 2.21 - the fast target

$$J = \sum_{i=1}^{n} x_i^{\,2} \qquad C_j = \ddot{q}_j^{*} - \ddot{q}_j$$

where:

J is the cost function

n is the total number of muscle actuators

x_i is the excitation of the i^{th} muscle actuator

C_j is the equality constraint for the j^{th} coordinate

The main difference between these two formulations therefore is that the fast target is faster (computationally) and will ensure good tracking except where muscles are not strong enough to generate an appropriate acceleration, in which case the algorithm will fail. The slow target on the other hand is slower, but muscle "weakness" will manifest as a tracking error rather than causing the algorithm to fail.

The OpenSim user-guide does not explicitly define the muscle-model used in the static optimisation stage of Computed Muscle Control. It can only be assumed therefore that it is the same simplified version of the muscle model as described for the Static Optimisation tool – with an inextensible tendon and ignoring the parallel elastic element. It is important to note however that the output variable in both of these formulations of static optimisation cost functions is muscle actuator excitation, rather than activation as used in the Static Optimisation tool. Inverse muscle activation dynamics (Equation 2.8) must therefore be included in the static optimisation stage of Computed Muscle Control.

Finally, in the last stage of Computed Muscle Control, the muscle excitations calculated from static optimisation are used in a standard forward dynamics simulation (see section 2.1.1). Again it is not explicitly stated in the OpenSim user-guide but it is assumed that the full muscle model (described in section 2.2.2) is used for this process. Once the coordinate accelerations are calculated from the muscle model, the equations of motion are integrated over a user-defined time step (typically 0.01s) using a 5th-order Runge-Kutta-Fehlberg integrator to calculate coordinate velocities and positions. These are then used in the proportional derivative feedback loop to various stages within the Computed Muscle Control workflow. Foot-floor forces during this forward simulation are set to the experimental values of the ground-reaction-force.

During Computed Muscle Control the same residual and reserve actuators used during the Residual Reduction Algorithm are added to the model in addition to the muscle actuators. These extra actuators enable the simulation to maintain kinematic tracking in case the muscle actuators have insufficient strength to generate the necessary accelerations. If the limits placed on the maximum magnitude of these residual/reserve actuators are too tight, they may not be able to make up any force/moment deficit caused by muscle actuator weakness and the simulation may fail to track the experimental kinematics. However, if the residuals/reserves are allowed to become too large then their action may dominate and the validity of the muscle actuator action may be reduced.

Once again the OpenSim software developers provide a rule of thumb guide to residual/reserve acceptability thresholds (Table 2.5) during walking and running simulations.

Thresholds:	Good	OK	Bad
Max. residual force (N)	0-10	10-25	>25
RMS residual force (N)	0-10	10-25	>25
Max. residual moment (Nm)	0-50	50-75	>75
RMS residual moment (Nm)	0-30	30-50	>50
Max. translation error (cm)	0-1	1-2	>2
RMS translation error (cm)	0-1	1-2	>2
Max. rotation error (°)	0-2	2-5	>5
RMS rotation error (°)	0-2	2-5	>5
Max. reserve (Nm)	0-25	25-50	>50
RMS reserve (Nm)	0-10	10-25	>25

Table 2.5 – Acceptability thresholds after running the Computed Muscle Control algorithm.for residuals/reserves and kinematic tracking position errors. Data taken from the OpenSim 2012 User Guide

Examining the maximum values in the "*Good*" category, many of the thresholds are the same as those discussed above for the Residual Reduction Algorithm tool. The maximum allowed translational error however has reduced from 2cm to 1cm which may be more appropriate when considering that a 20mm shift in the ground reaction force's centre of pressure can begin to produce significant changes in joint kinetics. An additional parameter that requires discussion here however is the maximum threshold for a reserve joint actuator – a joint torque that can be applied to any model degree of freedom to ensure kinematic tracking. The threshold of 25Nm is a large torque to be applied to any joint (equivalent to holding a 5kg weight at an arm's distance of 0.5m) and so, rather contradictorily, the OpenSim User Guide also recommends that peak reserve actuator torques should be kept below 10% of the expected peak joint torque. Example 10% thresholds for a 70kg adult are shown in Table 2.6 calculated from peak joint torques during walking for typically developing adult male subjects (Winter, 2005; p.200). These thresholds give a much tighter limit on acceptable peak reserve actuator torques compared to the 25Nm limit in Table 2.5.

Joint	Torque (Nm/kg)	Torque (Nm)	10% Torque (Nm)
hip extension	1	70	7
hip abduction	1	70	7
hip rotation	0.2	14	1.4
knee extension	0.6	42	4.2
ankle plantar-flexion	1.9	133	13.3

Table 2.6 – Peak joint torques (normalised to body weight) during walking for typically developing adult males (Winter, 2005) and the corresponding peak joint torques for a 70kg adult with 10% CMC reserve actuator thresholds.

Judging whether or not a Computed Muscle Control simulation was "successful" (i.e. having confidence in the simulated muscle activations) must therefore involve a check of both the kinematic tracking and the magnitude of the residuals/reserves. Kinematic and kinetic tracking is regularly reported in the literature for studies using the Computed Muscle Control algorithm but there is often a lack of information regarding the associated residuals/reserves values. This makes it difficult for a researcher to evaluate the quality of published musculo-skeletal simulation data.

A number of limitations in the use of the Computed Muscle Control algorithm are described by Thelen et al. (2003). Firstly, the authors highlight the fact that CMC can only optimise to performance criteria that can be evaluated in an instant of time, and not global measures such as metabolic energy expended over the whole task which may be more appropriate for investigations into pathological movement. Secondly, the authors acknowledge that, as Computed Muscle Control is a tracking algorithm rather than a performance-based dynamic optimisation, it is heavily reliant on the quality of the input kinematic data.

2.3. Gait Analysis

Gait analysis is the systematic study of animal locomotion and generally focuses on the walking of humans. The review articles of Sutherland (2001) and Baker (2007) detail the progression of gait analysis from the early methods (based purely on human observation through various ingenious photographic techniques) to the modern gait analysis laboratory, which typically combines digital cameras, motion capture systems, force-plates and electromyography to record a great many different movement parameters, including body segment motion, joint forces and muscle activity.

2.3.1. Gait Cycle

Walking is the repetitive action of placing one foot in front of the other in order to achieve forward motion (and to support against gravity) and as a cyclical process analysis usually focuses on the gait cycle – the repeating unit within the action of walking. The gait cycle was first described by Gaston Carlet in 1872 (Baker, 2007) and is defined as the events that occur between successive contacts of the same foot with the ground (Figure 2.14).

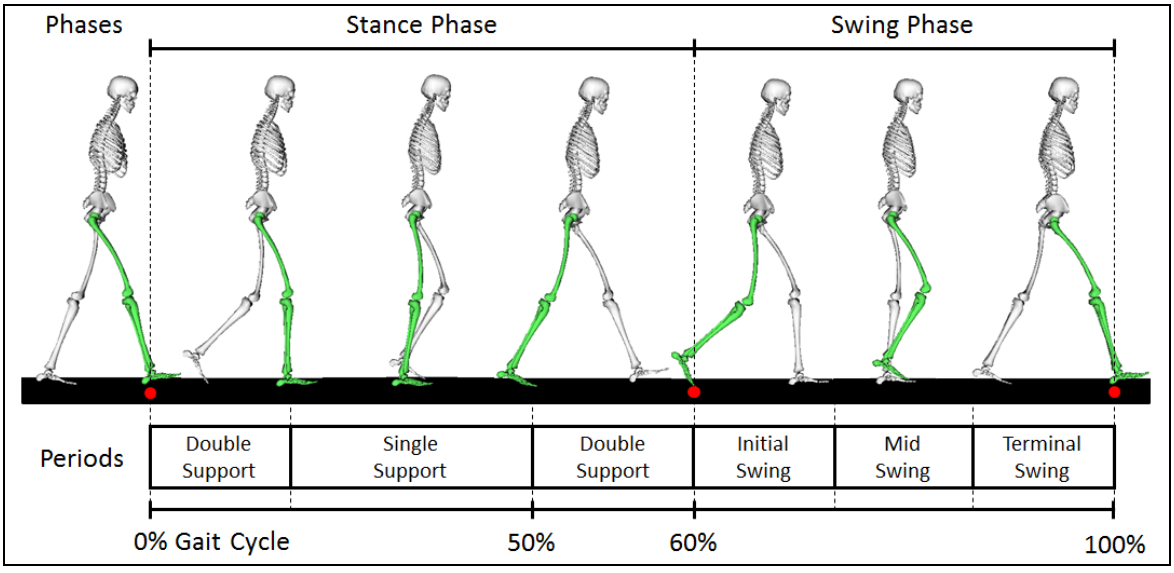

Figure 2.14 – Gait cycle for the right lower limb. Red dots mark initial contact, foot off and second initial contact

Specific events that occur at instantaneous points during walking are used to define the gait cycle. It begins at 0% with *initial contact* of the foot with the ground and ends at 100% after two steps (one stride) when the same foot makes *initial contact* again. The period of time during which the limb of interest (ipsilateral limb) is in contact with the ground is termed the *stance* phase and off the ground is the *swing* phase. The event that divides these two phases is known as *foot off* which typically occurs at approximately 60% of the gait cycle. *Initial contact* and *foot off* are alternatively known as *heel strike* and *toe off* but these terms can be misleading when describing a non-standard gait pattern. The gait cycle for the other (contralateral) limb is identical but shifted in time by 50%. This gives two periods of *double support* (both limbs in contact with the ground) in the gait cycle at 0-10% and 50-60%. The middle 40% of the *stance* phase is therefore the *single support* period that corresponds to the *swing* phase of the contralateral limb. During the *stance* phase of normal walking, the movement of the foot relative to the ground is analogous to a wheel-like rolling motion which Perry (1992) described in terms of three *rockers*. Additionally, Perry coined a number of more descriptive time periods that she related to specific changes in muscle activity. These time periods are described below in terms of the joint kinematics (position, velocity, acceleration) along with what is generally believed to be the corresponding muscle actions (Gage & Schwartz, 2009b).

Loading Response (first period of double support)

This period begins with the 1st foot rocker (the heel rocker), the motion of the foot immediately after initial contact when only the heel is in contact with the ground. The ground-reaction-force, lying posterior to the ankle, drives the mid/forefoot flat to the floor, controlled by the eccentric (activation whilst lengthening) action of the dorsiflexor muscles. During this time, body weight is transferred onto the ipsilateral limb. The knee is controlled by eccentric action of the vasti group and glutei/abductors are active to control the hip and pelvis.

Mid-Stance (first half of single support)

This period corresponds to the 2nd foot rocker (the ankle rocker) when the tibia hinges forward over the stationary foot controlled by eccentric action of the plantarflexors.

During this time the origin of the ground-reaction-force moves forwards at the foot and the line of action moves in front of the knee and behind the hip, stabilising both joints and allowing both sets of extensor muscles to relax.

Terminal Stance (2nd half of single support)

This period corresponds to the 3rd foot rocker (the forefoot rocker) when the combined action of the plantarflexor muscles stop the dorsiflexion movement of the tibia as it hinges forward over the foot and instead begins to raise the heel off the floor in concentric (activation whilst shortening) plantarflexion action. Tibialis posterior, peroneal and toe flexor action all contribute to stabilising the foot. The ground-reaction-force vector still runs in front of the knee and behind the hip, continuing its stabilising action on both of these joints. This calf muscle action in terminal stance provides a significant amount of the propulsive force necessary for walking (Neptune et al., 2001).

Pre-Swing (2nd period of double support)

During this period the ipsilateral limb is prepared for swing and correspondingly the contralateral limb responds to loading. The ground-reaction-force has moved to the forefoot and the vector now runs behind the knee leading to a strong external flexing moment. The gastrocnemius muscle now also begins to contribute to knee flexion as do the hip flexors through their action of flexing the hip. The knee therefore begins its rapid acceleration into flexion, and tibialis anterior action begins to lift the toes, both necessary for foot clearance in the swing phase.

Initial Swing

This period spans the time between foot off and when the ipsilateral limb has swung forward to pass the contralateral stance limb. At normal walking speed this pendulum-like movement occurs largely passively being driven by inertial forces and gravity. Tibialis anterior action dorsiflexes the ankle and prevents the toes catching the ground.

Mid Swing

Muscle activity remains the same in this period and the ipsilateral limb swings forward past the contralateral stance limb. Tibialis anterior is still active but now is responsible for maintaining a neutral ankle posture against the external plantarflexion moment of gravity.

Terminal Swing

During this period the swinging limb is slowed down in preparation for initial contact. This is achieved principally by eccentric hamstring action which decelerates both hip flexion and knee extension. Tibialis anterior action maintains a neutral ankle posture in readiness for its eccentric action during loading response to prevent foot slap.

However, this conventional understanding of lower-limb muscle action in normal gait has come under scrutiny from work using more advanced musculo-skeletal modelling techniques such as induced acceleration analysis. Many of these studies are summarised in the review article by Zajac et al. (2003). Neptune et al. (2001) recognised that conflicting conclusions on the role of the plantarflexors during gait were reported in the literature and identified three main theories: the plantarflexors (1) provide a controlled *roll-off*; (2) actively provide forward progression or *push-off*; and/or (3) accelerate the leg into swing. The authors suggested that the lack of consensus may have arisen from the monoarticular/biarticular mix of the triceps surae group which had not been delineated in these early studies as they were based on joint torques rather than individual muscle contributions. They therefore carried out a forward dynamics analysis using a 2D model with 30 muscle actuators developed in SIMM (MusculoGraphics, Inc., Illinois, USA) based on experimental kinematic data from five healthy male adult subjects. Their results showed that both the gastrocnemius and soleus support the trunk during the single-support/pre-swing periods but contributions to forward progression were more complex. In early single-support the soleus and gastrocnemius both decelerate trunk progression; in middle single-support they have opposite effects with the soleus decelerating the leg and accelerating trunk progression (with the gastrocnemius opposing both); and in late single-support/pre-swing the soleus accelerates trunk progression and the gastrocnemius accelerates leg progression (hence contributing to swing initiation).

Anderson & Pandy (2003) were interested in identifying other muscles that contributed to support during walking, particularly during early stance, and also to calculate the passive contribution made by the skeleton. Using a 3D model similar to the gait2354 model outlined in section 2.2.1, with additional ligament action to prevent anatomically unfeasible joint angles, they carried out a dynamic optimisation over a gait cycle using a cost function based on total metabolic energy divided by forward displacement of the centre of mass, and derived initial conditions from mean experimental data from five healthy adult male subjects. Contributions to support were then determined via decomposition of the resultant vertical ground-reaction-force. Muscles and ligaments of the ipsilateral limb were found to make the largest contribution to support accounting for 50-95% of the vertical ground-reaction-force (with less than 15% from the contralateral limb). The passive transmission of force through the joints and bones in resistance to gravity accounted for 20-50% of support when the foot was flat on the ground but much less before *foot flat* or after *heel off*. A much smaller contribution to support came from inertial or centrifugal effects.

At initial contact, support was generated by the contralateral plantarflexors and ipsilateral dorsiflexors but the contribution of the dorsiflexors stopped abruptly when the foot became flat to the floor. The first peak of the vertical ground-reaction-force was then principally generated by action of the gluteus maximus, the vasti, and the posterior gluteus medius/minimus. The force was maintained by the posterior gluteus medius/minimus, passive action of the skeleton and an increasing contribution from the anterior gluteus medius/minimus through mid-stance. This action diminished in late stance when support was taken over by action of the soleus and gastrocnemius to produce the second peak in the vertical ground-reaction-force, with the soleus action producing twice the support of gastrocnemius. Little contribution to support was provided by the hamstrings or rectus femoris. The authors acknowledge however that these results are only as good as the muscle forces generated by the simulation and they describe the simulated muscle excitation patterns as similar to those measured from the subjects (although no detail of EMG methodology is given).

Since the review article of Zajac et al. (2003), there have been many more studies in the literature looking at muscle coordination during walking in typically developing human subjects (Anderson et al., 2004; Arnold et al., 2005; Arnold et al., 2007; Hof & Otten, 2005; John et al., 2012; Jonkers et al., 2003; Liu et al., 2006, 2008; Neptune et al., 2004a, 2004b; Siegel et al., 2006; Xiao & Higginson, 2008). Other papers have focused on the muscle coordination involved in specific pathological gait patterns such as stiff knee gait (Goldberg et al., 2004), crouch gait (Correa et al., 2012; Hicks et al., 2008; Steele et al., 2010) or jump knee gait (Correa et al., 2012). There is some agreement between the papers investigating muscle coordination of walking in typically developing human subjects (similar to the results of Anderson & Pandy, 2003) and discrepancies between them are a likely result of differences in modelling of the foot-ground interactions (Dorn et al., 2012). In terms of contributions to support, these discrepancies typically involve changes in the timing and relative magnitude of muscle contributions but not changes to the muscle function. The plantarflexor contribution to support in early stance is a good example: Neptune et al. (2001) showed that the soleus and gastrocnemius were the principal contributors to support for the whole of the single-support period and into pre-swing, but Anderson & Pandy (2003) found that their contribution was limited to pre-swing. Discrepancies between studies in terms of contributions to progression and medial/lateral accelerations can be more conflicting, with the same muscles shown to have opposite function in different studies. However, care must be taken in the interpretation of data from these techniques because, at present, few model predictions of muscle function have been validated as it is difficult to measure a single muscle's contribution to the ground-reaction-force experimentally. Although some pioneering work in this area has been carried out by Stewart et al. (2007, 2008).

2.3.2. Gait Analysis Methods

Many different types of gait analyses are possible. An experienced clinician may be able to identify gait deviations simply by watching the subject as they walk up and down – an observational gait analysis.

This technique may be improved through the use of video which can then be slowed down and recorded from specific positions to give views of the motion in the anatomical planes. Quantitative scoring methods have also been developed for observational gait analysis such as the Physician's Rating Score (Koman et al., 1993) and the Edinburgh Visual Gait Score (Read et al., 2003).

A gait analysis will become *instrumented* if measurements are taken during walking. For example, a basic instrumented gait analysis might make use of a ruler and stop-watch to allow calculation of a few simple spatio-temporal parameters of the gait cycle such as cadence (number of steps per minute) and walking speed.

Finally, with the use of more sophisticated equipment, such as force-plates, 3D motion tracking systems and electromyography, more advanced instrumented gait analyses are possible in which ground-reaction-forces, 3D joint kinematics (position, velocity, acceleration), 3D joint kinetics (turning moments and bone-on-bone forces) and the electrical activity of surface muscles can be measured. It is this type of gait data that has been used to inform and test the musculo-skeletal simulations performed in later chapters. The data was collected at the Guy's Hospital Gait Laboratory, London. The data collection methodologies and equipment are described below.

2.4. Data Collection Methods

Ten adolescents with spastic diplegic cerebral palsy and ten typically developing control subjects were recruited following approval from the local Research Ethics Committee and the NHS Research & Development Office (Appendix A). The case subjects were selected from referrals to the Guy's Hospital Gait Laboratory in London. Control subjects were

recruited from siblings of the case subjects or volunteers known to the research team. Example patient information sheets can be seen in Appendix B.

Inclusion criteria for selection were:

- all subjects aged between 10 and 22 years of age
- all subjects to demonstrate an understanding of what they would be asked to do if they agreed to participate in the study
- case subjects to have a diagnosis of spastic diplegic cerebral palsy
- case subjects to be independently ambulant

Exclusion criteria for selection were:

- any subject unable to comply with the safety requirements of MRI (e.g. previous abdominal surgery without a post-operative x-ray or having cerebral aneurysm clips in place)
- any case subject who has undergone any orthopaedic intervention to their lower limbs in the previous year
- any control subject who has any known neurological condition or has had any previous orthopaedic intervention to their lower limbs

A number of different datasets were collected in order to inform the musculo-skeletal models used in later chapters (Figure 2.15).

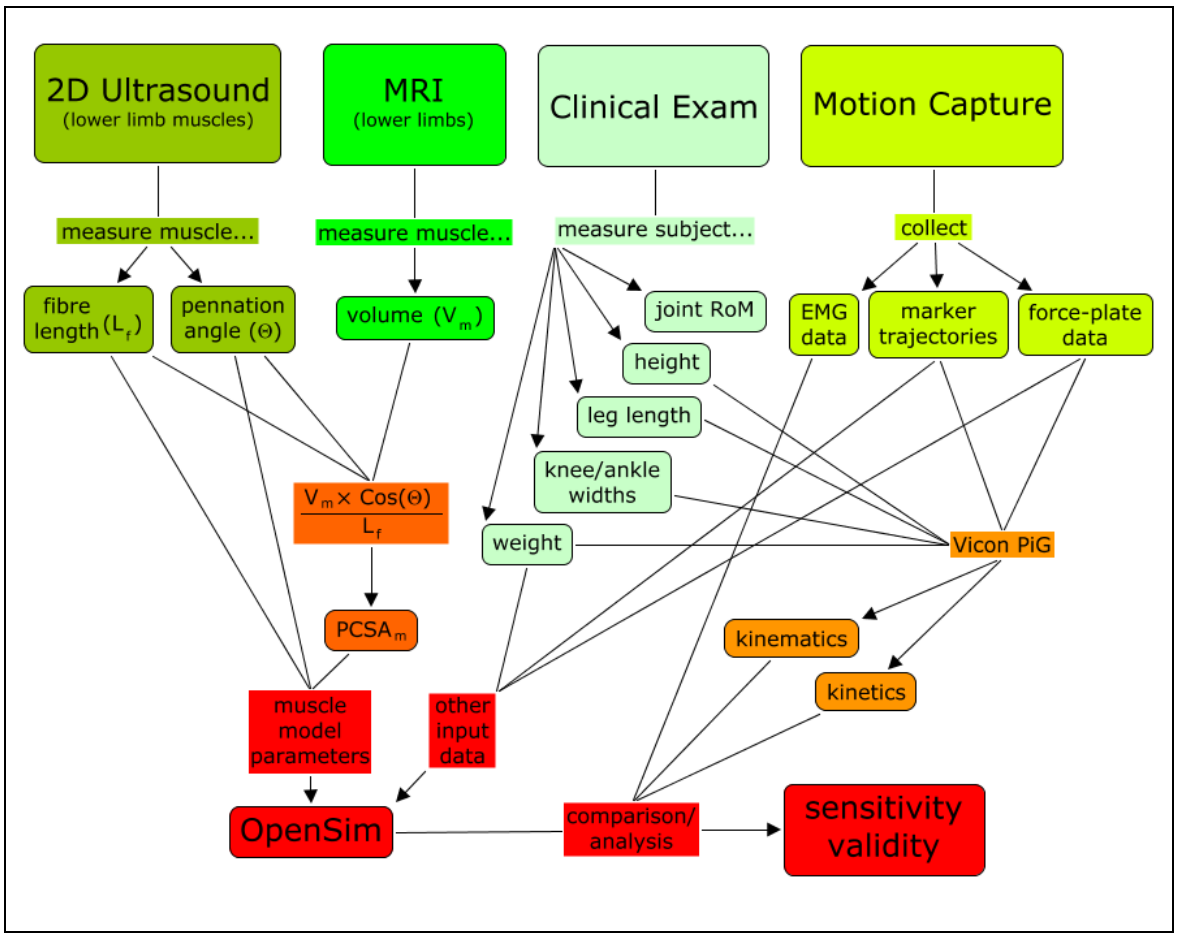

Figure 2.15 – Summary of data collected in this project including dependencies between data sources. MRI = magnetic resonance imagery, EMG = electromyography

Details of ultrasound and magnetic resonance imaging methods are described in section 3.3. The clinical examination protocol can be seen in Appendix C. Height, knee/ankle widths and weight were measured using a wall-mounted stadiometer, joint callipers and a set of chair-scales respectively. Leg lengths were measured from the anterior superior iliac spine to the medial ankle malleolus using a tape measure.

An overview of the motion capture methodology is described here and further detail is given in sections 2.4.1 - 2.4.4 below. The principal pieces of equipment used during data collection in the gait laboratory were a 3D motion capture system, three force-plates embedded in the floor of a 10m walkway and a surface electromyography system.

- Subjects dressed in shorts and t-shirt and were barefoot
- Surface electromyography sensors were placed on nine muscles (Table 2.8) of one randomly selected leg
- Motion capture markers were placed on the lower limbs, torso and head using a combined OpenSim and Helen Hayes maker set (Figure 2.19)
- Motion capture was performed using a Vicon Nexus opto-electronic motion capture system (section 2.4.1)
- A single static trail was recorded with the subjects standing stationary with both feet within the borders of one force-plate and with arms out-stretched to avoid obscuring markers
- A number of dynamic walking trials were then collected with the subject walking the length of the 10m walkway. Walking was carried out at a self-selected walking speed and repeated until five trials with three sequential force-plate hits were obtained with the selected limb on the second plate. This provided full ground-reaction-force data for an entire gait cycle for the selected limb. Joint kinematics and kinetics were calculated from marker trajectories using the Conventional Gait Model (section 2.4.1)
- Synchronous collection of force-plate data (section 2.4.2) and electromyography data (section 2.4.3) was carried out during walking
- Electromyography data was also collected during maximum voluntary contractions for appropriate muscles (section 2.4.4)

2.4.1. 3D Motion Capture

Motion capture was carried out using a Vicon Nexus motion capture system (Oxford Metrics Group, Oxford, UK) with seven T-series cameras arranged around the 10m walk-way (Figure 2.16). Vicon Nexus is an opto-electronic motion capture system that tracks the movement of passive retro-reflective markers (plastic balls surrounded with reflective tape).

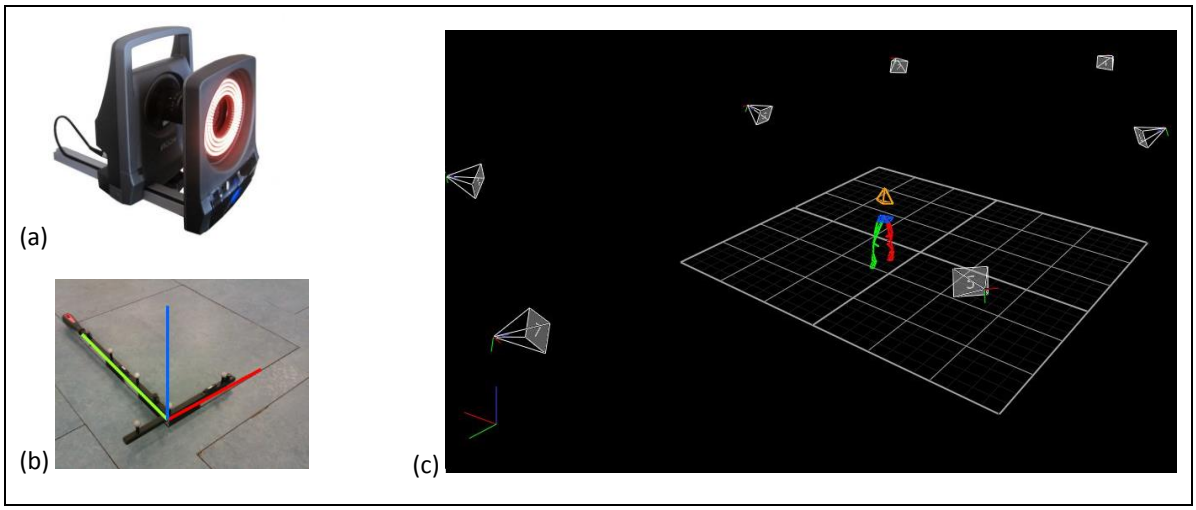

Figure 2.16 – Vicon Motion Capture System

(a) Vicon T-series motion capture camera

(b) Calibration L-frame – five markers define two horizontal orthogonal axes (red and green) and the origin of the capture volume axis system. The third, vertical, axis (blue) is created orthogonal to the first two axes

(c) The capture volume, as displayed in the Vicon Nexus software, showing the position of the seven T-series cameras. The global axis system is marked in the lower left corner and the combined Helen Hayes and OpenSim lower limb & torso marker set can be seen in the centre (torso orange, pelvis blue, left leg red, right leg green)

A ring of near-infra-red LEDs around each camera lens strobe synchronously at 120Hz and the resulting marker reflections are recorded from each camera view at this frequency. A calibration object (L-frame) is used to calibrate the 3D capture volume, to calculate the relative position and orientation of each camera, and to set the Cartesian coordinate origin and axis system used to describe the capture volume. With the position and orientation of each camera known, the location of any marker visible by a camera must lie on the ray projected out normal to the camera field of view. Therefore, if a marker can be seen by two cameras, its 3D position will be located at the intersection of the two rays. A marker must therefore be seen by a minimum of two, non-parallel cameras to be

reconstructed in three dimensions. The camera resolution, size of the capture volume (distance of the cameras to the markers), marker diameter and centroid identification algorithm combine to give approximately 1mm accuracy in marker location.

Markers are attached to the surface of an object and the motion of interest is performed in the capture volume whilst collecting camera data. The 2D image data from all cameras is then combined to reconstruct 3D marker trajectories. Appropriate transformations, dependent on the marker set used, are then necessary to calculate the object motion from the trajectories of the attached markers. For this project, the Vicon Plug-in-Gait lower limb model and Helen Hayes marker set (Kadaba et al., 1989, 1990; Sutherland, 2002) were used to capture the gait pattern of human walking.

SACR	SACRUM: placed mid-way between the posterior superior iliac spines
LASI & RASI	Placed directly over the left or right anterior superior iliac spine (ASIS)
LTHI & RTHI	Placed on the lateral surface of the THIGH at approximately 2/3 the distance from hip to knee
LKNE & RKNE	Placed over the lateral epicondyle of the left or right KNEE
LTIB & RTIB	TIBIA: placed on the lateral surface of the shank at approximately 2/3 the distance from knee to ankle
LANK & RANK	ANKLE: placed over the lateral malleolus along an imaginary line passing through the transmalleolar axis
LTOE & RTOE	TOE: placed between the 2nd & 3rd metatarsal heads
LHEE & RHEE	HEEL: placed over the calcaneus at the same height above the plantar surface of the foot as the toe marker

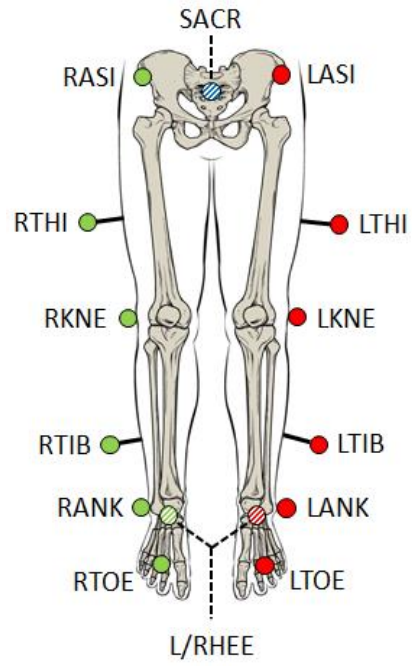

Figure 2.17 – Skin surface marker positions for the Helen Hayes lower body marker set. Left side markers are shown in red and right side markers in green. SACR and L/RHEE have alternate shading to indicate that these markers would not be visible in an anterior coronal view.

The Conventional Gait Model is also known as the Newington, Gage, Davis, Helen Hayes, Kadaba or Vicon Clinical Manager (VCM) model (Baker, 2006). For the lower limbs this is a seven segment model (pelvis, 2 x thigh, 2 x shank, 2 x foot) with three degrees of freedom at both the hip and knee and two at the ankle. It is typically implemented using the Helen Hayes marker set which, for the lower limbs, consists of 15 skin surface markers placed on bony landmarks, three around the pelvis and six on each lower limb (Figure 2.17).

Surface marker positions and a number of anatomical measurements (leg length, knee width, ankle width) are then used to calculate joint centres and segment axes systems. The hip joint centres (HJC) are defined using the regression equations of Davis et al. (1991). The chord function (Figure 2.18) is used to define: the knee joint centres (KJC) using the KNE marker, HJC, THI marker and knee width; and ankle joint centres using the ANK marker, KJC, TIB marker and ankle width for points i, j, k and length A respectively.

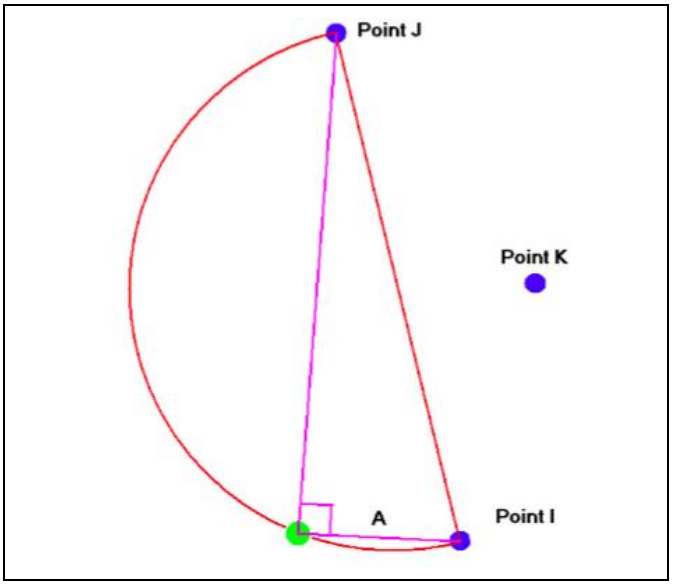

Figure 2.18 – The chord function
This function uses three points, i, j, k (blue dots), to define a plane. A circle, diameter point i to point j, is drawn within the plane. A chord, length A, is drawn from point i in the direction of the required joint centre. The joint centre (green dot) then lies at the other end of the chord.

Surface marker and joint centre positions are then used to define local Cartesian coordinate systems for each segment using an angle sequence that attempts to match anatomical flexion, abduction and rotation. Joint angles can then be calculated from rotations between the local coordinate systems of adjoining segments.

In this study, the Helen Hayes lower limb marker set was combined with a full body marker set recommended for use with the OpenSim gait2392 lower limb and torso model (Delp, 1990) to produce a 40 marker set (Figure 2.19). This enabled kinematic modelling using the Conventional Gait Model as well as providing marker trajectory data that could be imported into OpenSim.

1 = Top.Head	22 = L.Shank.Front
2 = Sternum	23 = LTIB
3 = R.Acromium	24 = RANK
4 = L.Acromium	25 = R.Ankle.Med
5 = SACR	26 = LANK
6 = RASIS	27 = L.Ankle.Med
7 = LASIS	28 = RHEE
8 = R.Thigh.Upper	29 = R.Toe.Med
9 = R.Thigh.Front	30 = R.Midfoot.Lat
10 = RTHI	31 = R.Midfoot.Med
11 = L.Thigh.Upper	32 = R.Toe.Lat
12 = LThigh.Front	33 = R.Toe.Tip
13 = LTHI	34 = LHEE
14 = RKNE	35 = L.Toe.Med
15 = R.Knee.Med	36 = L.Midfoot.Lat
16 = LKNE	37 = L.Midfoot.Med
17 = L.Knee.Med	38 = L.Toe.Lat
18 = R.Shank.Upper	39 = L.Toe.Tip
19 = R.Shank.Front	40 = RTOE
20 = RTIB	41 = LTOE
21 = L.Shank.Upper	

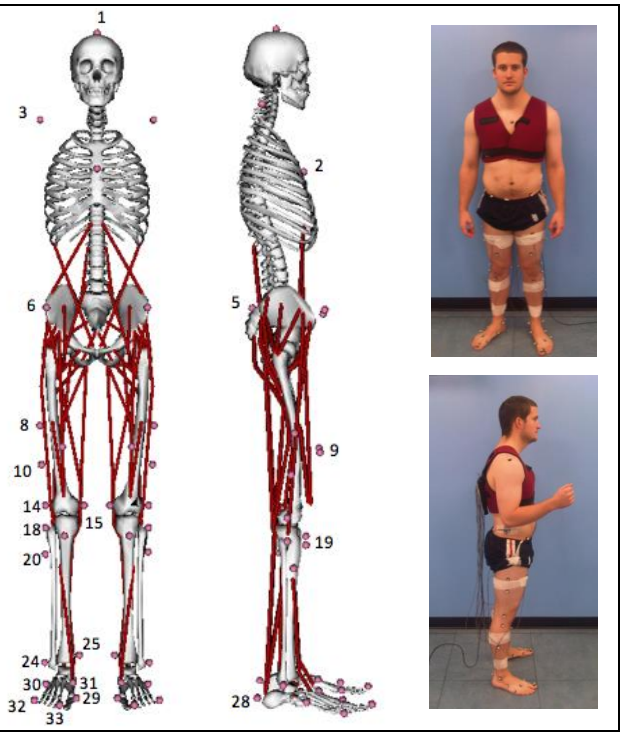

Figure 2.19 - OpenSim lower limb and torso marker set combined with the Helen Hayes marker set. For clarity, only right side markers have been labelled. Two additional lateral pelvic markers were used in case the standard pelvic markers were obscured. Surface EMG sensors can also be seen on the subject secured with white, self-adhesive bandage (vastus lateralis sensors omitted for clarity).

2.4.2. Force-Plates

Three AMTI OR6 force-plates (AMTI Inc., MA, USA) were embedded to lie flush with the floor in the centre of the gait laboratory walkway. The contact surface of the force-plate is supported at each corner by a tri-axial, strain-gauge force transducer, the signals of which are combined to give a six channel device output representing the three orthogonal forces (Fx, Fy, Fz) and three orthogonal moments (Mx, My, Mz) applied to the plate (Figure 2.20).

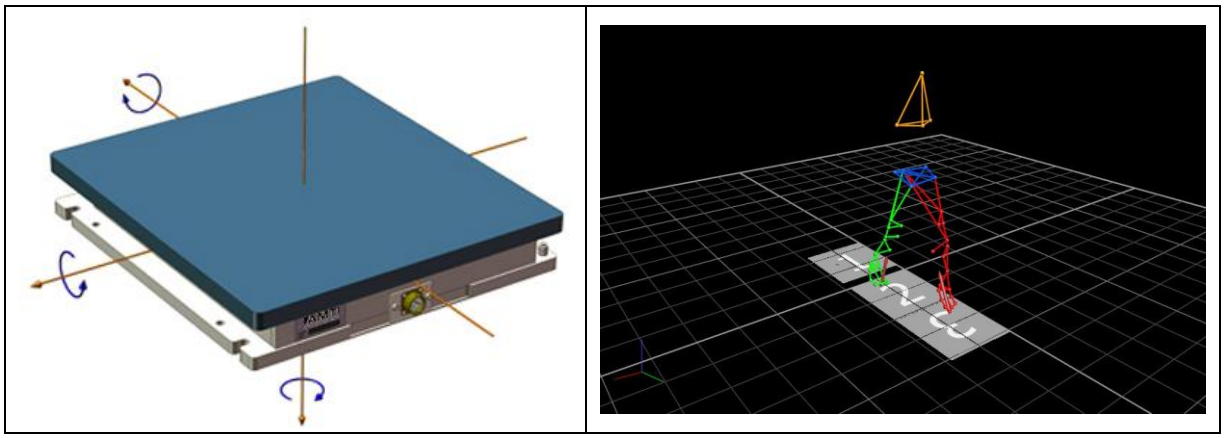

Figure 2.20 – Force Plates (a) AMTI OR6 force-plate(b) Position of the 3 force-plates in the capture volume

The force-plates were orientated in the laboratory such that the X-axes were aligned across the walkway, the Y-axes along the walkway and the Z-axes in the vertical direction. The Fz channel therefore provided the principal component of the ground-reaction force, with Fx and Fy representing the shear forces applied to the plate. The Mx and Mz moments represented the offset of the centre-of-pressure of the ground-reaction-force from the plate's centre and the Mz moment represented the *free moment* applied by any twisting contact force. Assuming contact with the plate is made at the surface, simple processing of the six channels can provide the three components of the ground-reaction-force vector, the two surface coordinates of the centre-of-pressure and any free moment Mz. The force-plate specifications are shown in Table 2.7.

Parameters	Values
Fx, Fy, Capacity (N)	2224
Fz, Capacity (N)	4448
Mx, My, Capacity (Nm)	1129
Mz, Capacity (Nm)	565
Fx, Fy, Natural Frequency, Hz	400
Fz, Natural Frequency, Hz	1000
Fx, Fy, Sensitivity (μV/N)	0.674
Fz, Sensitivity (μV/N)	0.169
Mx, My, Sensitivity (μV/Nm)	1.59
Mz, Sensitivity (μV/Nm])	3.37

Table 2.7 – AMTI OR6-6 force-plate specification

2.4.3. Surface Electromyography

Motion capture systems and force-plates enable the measurement of spatio-temporal parameters, kinematics and kinetics of motion – useful information for the task of identifying underlying causes of motor disability. However, as many conditions will include an element of neurological involvement it is important to get an understanding of the excitatory signals that are being sent to the muscle fibres. This is done with electromyography (EMG).

Surface EMG (sEMG) was collected using a Delsys Bagnoli-16 EMG system (Delsys Inc., MA, USA) (Figure 2.21). Bipolar electrodes were taped to the skin over each muscle of interest and secured using self-adhesive bandage (Figure 2.19). During muscle activity the combination of local motor unit action potentials travelling along the muscle fibres set up a potential difference at the skin's surface, and hence between the two electrodes. Typical sEMG signals tend to be in the region of μV and have a frequency in the low hundreds of hertz range. The signals are amplified by a differential amplifier (gain 1000), filtered using a 450Hz low pass analogue filter to avoid aliasing and then sampled at 1080Hz for digital storage. A digital band-pass filter (20-400Hz) was then applied using Matlab (The Mathworks^{TM} Inc., MA, USA) to remove DC offsets and low frequency artefacts.

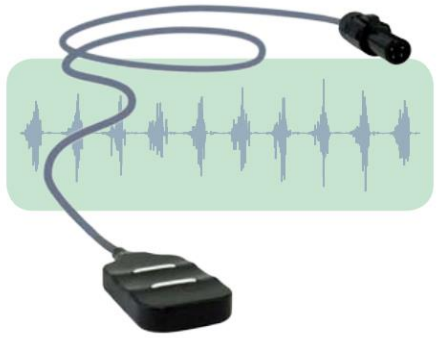

Parameters	Values
Differential Amplification	1000
Analogue Filter	450Hz low pass
Bandwidth Roll-Off	80 dB/decade
Overall Noise	≤1.2uV
Saturation Error Threshold	± 4.8V (output)
Medical Device Conformity	IEC 60601-1, CE mark
Classification	Class I (93/42/EEC), Type BF

Figure 2.21 – Delsys Bagnoli-16 bipolar surface EMG electrode and system specifications

2.4.4. Maximum Voluntary Contractions

sEMG signals are a recording of the electrical activity of motor unit action potentials as they manifest at the skin surface. As such, they provide an almost direct indication of the timing of muscle activity (ignoring the electro-mechanical delay of muscle tissue – typically 0.1s; Buchanan et al., 2004) but not of the muscle activation level. As a muscle becomes more active, a larger proportion of its total motor units are recruited via action potentials and hence the magnitude of the sEMG signal increases. However, the absolute voltage "seen" by the sEMG sensor is dependent on many factors including the number and distribution of motor units within the muscle, the muscle size, the depth of the muscle beneath the skin, the subcutaneous fat thickness and the electrical impedance of the sensor-skin contact.

Prediction of sEMG amplitudes is therefore an extremely complex task and rarely undertaken. Instead, the amplitude of sEMG signals are often normalised to the peak amplitude obtained during a maximum voluntary contraction (MVC) to give an indication of muscle activation levels. The MVC methodology used in this study is outlined below. A major limitation to this technique however is that some subjects (especially those with cerebral palsy) are unable to achieve maximal contraction of their muscles voluntarily (Stackhouse, 2005) and the pain associated with a maximal contraction obtained via external electrical stimulation is often prohibitive. This will need to be considered when comparing simulated muscle activations to normalised EMG signals.

Specific isometric tasks were performed to illicit the appropriate muscle activations (Table 2.8). For some muscles, the contractions were carried out at two different joint positions to better represent joint ranges during walking. Tasks were carried out with the subject either sitting on the edge of a couch with legs hanging freely or standing. Joint movement was manually constrained by the examiner to ensure isometric contraction. Subjects were given one practice trial of each task before the task was repeated three times with verbal encouragement to obtain maximal contraction. The MVC for each muscle was then calculated from the mean peak voltage from all associated trials.

	Muscle	Isometric Tasks
Sitting	Rectus Femoris	knee extension at 90° knee extension at 30°
	Vastus Lateralis	knee extension at 90° knee extension at 30°
	Tibialis Anterior	ankle dorsiflexion at 0° (knee 90°)
	Semimembranosus	knee flexion at 30°
	Semitendinosus	knee flexion at 30°
	Biceps Femoris Long Head	knee flexion at 30°
Standing	Medial Gastrocnemius	ankle plantarflexion at 0° (knee 0°)
	Lateral Gastrocnemius	ankle plantarflexion at 0° (knee 0°)
	Soleus	ankle plantarflexion at 0° (knee 0°) ankle plantarflexion at 0° (knee 30°)

Table 2.8 – Maximum voluntary contraction tasks. Isometric tasks performed to collect maximum voluntary contraction electromyography data. Each task was repeated three times and the maximum voluntary contraction for each muscle calculated from the mean peak amplitude from all associated trials.

Peak EMG amplitude for each task was calculated using a four step process carried out in Matlab (The Mathworks™ Inc., MA, USA):

1. standard EMG filtering was carried out as described above in section 2.4.3
2. the signals were rectified by taking the absolute value of the signal
3. the signal envelope was calculated using a low-pass Butterworth filter with zero phase shift (2nd order, cut-off 6Hz)
4. peak signal amplitude (V) was selected

2.5. Summary

Clinical gait analysis (section 2.3.2) provides a useful tool in treatment decision making for subjects with cerebral palsy and as an outcome measurement but its clinical power is limited (Baker, 2006). It is able to describe the movement of an individual but it cannot describe the functional contributions of individual muscles during that movement. Such information would be useful as pathological changes in skeletal morphology may alter the function of particular muscles, and changes in muscle and tendon material properties may alter the timing of the development of muscular force.

It is hoped that more advanced techniques, such as the SimTrack method of musculo-skeletal simulation, may be able to provide more specific information on muscle function. However, to date, quantitative validation of muscle activations generated by such techniques has been lacking despite many publications using SimTrack or similar methods appearing in the literature. As a result the clinical utility of this technique for typically developing subjects or for subjects with cerebral palsy remains in doubt.

The aim of this study therefore is to validate the simulated muscle activations generated using the models and analysis techniques of SimTrack. This will be carried out by comparison to experimentally recorded electromyographic data in both typically developing subjects and subjects with cerebral palsy. If found valid, simulated muscle activations could be used in further techniques such as induced acceleration analysis to identify and quantify specific functional muscle contributions. For children with cerebral palsy this may help our understanding of the movement dysfunction associated with this disorder and it has the potential to provide a new tool in clinical gait analysis to assess how interventions alter the contributions of muscles and observe whether the reconfiguration of the skeletal posture results in improved muscle action.

3 Muscle volumes & architecture in typically developing adolescents & in adolescents with cerebral palsy

Muscle morphological data (volume, fibre length, pennation angle) was collected using 2D ultrasound and magnetic resonance imaging for a number of lower limb muscles from ten typically developing adolescents and ten adolescents with cerebral palsy. Muscle physiological cross-sectional area was also calculated from these three parameters. Muscle volumes and fibre lengths were found to be smaller in the case group with smaller volumes more prominent in the distal musculature. Physiological cross-sectional area was found to be larger in the thigh and smaller in the shank for the case group and no difference between groups was found in pennation angle. A high variation in reported muscle pennation was noted from the literature.

3.1 Introduction

The mathematical models used to represent muscle action in musculo-skeletal simulations have been described in Chapter 2. The Thelen (2003) muscle model used in the gait2392 OpenSim model uses a number of parameters (Table 2.3) to characterise muscle action. Muscle morphological data was collected from typically developing subjects and subjects with cerebral palsy in order to inform the appropriate model parameters indicated in Table 3.1. This data was used to examine differences between the groups and to create bespoke musculo-skeletal models for both a sensitivity and validity analysis described in Chapters 4 & 5 respectively.

Morphological Data		Model Parameter
1. muscle pennation angle	used to inform	pennation_angle
2. muscle fascicle length	used to inform	optimal_fiber_length
3. muscle length 4. tendon length	used to inform	tendon_slack_length
5. muscle volume	used with 1 & 2 to calculate PCSA to inform	max_isometric_force

Table 3.1 – Informing the muscle model with morphological data

3.2 Altered Muscle Morphology in Cerebral Palsy

Typically developing muscle morphology has been described in Chapter 2 and an outline of musculo-skeletal abnormalities found in subjects with cerebral palsy was given in Chapter 1. There have also been a number of studies looking in more detail at human muscle morphology both in typically developing subjects and in subjects with cerebral palsy. Wickiewicz et al. (1983) measured the muscle mass, length and physiological cross-sectional area, the fibre length and pennation and the number of sarcomeres per fibre in 27 lower limb muscles of three cadavers. The age and sex of the specimens are unfortunately not reported. They found similar fibre to muscle length ratios across the three subjects and generally consistent pennation angles throughout each muscle.

Friederich & Brand (1990) carried out a similar study on two cadavers (37 year old male & 63 year old female) measuring muscle length, volume, fibre length and pennation, and calculated physiological cross-sectional area on all the lower limb muscles. They found consistent fibre length within each muscle but found variation between muscles. They compared their data to Wickiewicz et al. (1983) and found consistency in fibre to muscle length ratio data. It is principally the data from these two papers that are used to inform the muscle model parameters in the OpenSim gait2392 model.

Many musculo-skeletal simulations use the data from these two early studies to parameterise their muscle models but this is based on a limited sample of five cadaveric specimens for which the age and sex of three cadavers is unknown. With the current increased interest in musculo-skeletal modelling, Ward et al. (2008) recognised the need

for a larger cadaveric study of human muscle morphology to parameterise these muscle models. They therefore disassembled 27 lower limb muscles from one side of 21 cadaveric specimens (9 male, mean age 83 years) and measured muscle mass (and hence volume), muscle length, fibre length, sarcomere length, pennation angle and physiological cross sectional area (PCSA). The authors conceded that the mean age of their subjects, and the associated muscle shrinkage through sarcopenia (Dutta et al., 1997; Shortland, 2009) were likely to make PCSA comparisons to in vivo data problematic, but they also found large differences in fibre length and PCSA when comparing to the cadaveric data of Wickiewicz et al. (1983) and Friederich & Brand (1990). Newer musculo-skeletal models are now using the Ward et al. (2008) data for muscle model parameterisation as it is based on a larger cadaveric sample.

With the advance of imaging techniques a number of more recent papers have begun to look at muscle morphology in vivo. Fukunaga et al. (1992) measured muscle length and volume in human leg muscles from T1-weighted magnetic resonance images from 12 healthy subjects (20-49 years old, mean age 32.6) and compared the results to Wickiewicz et al. (1983), Friederich & Brand (1990) and a number of other papers. It is unfortunate however that individual fascicles cannot be delineated from magnetic resonance images and so it should be highlighted that the fibre lengths and physiological cross-sectional area data reported here were calculated using the appropriate fibre length/muscle length ratios and pennation angles of Wickiewicz et al. (1983). The authors justify this by stating that measurements of fibre length/muscle length ratios appear consistent between subjects and across studies. They do not comment on the consistency of pennation angles.

Lampe et al. (2006) used a similar magnetic resonance technique to compare the lower limb muscle volumes between the paretic and non-paretic sides of 16 hemiplegic cerebral palsy subjects (aged 16-25). They found a mean reduction of thigh muscle volumes to 83% and a statistically significant mean reduction of the lower leg muscle volumes to 74% with the calf muscles being particularly affected.

Fry (2008) used T1-weighted magnetic resonance images to measure the volumes of eleven lower-limb muscles in nine young adults with spastic cerebral palsy (14-22 years) compared with nine age and sex-matched control subjects. All muscles were found to be smaller in the case group with an average 42% volume reduction and with the distal muscles more affected. Larger volume deficits were also found in biarticular compared to monoarticular muscles.

Malaiya et al. (2007) used 3D ultrasound to compare gastrocnemius muscle morphology between 16 children with spastic hemiplegic cerebral palsy (mean age: 7.8 years; range: 4-12) and 15 typically developing children (mean age: 9.5 years; range: 4-13). They measured muscle volume, muscle length, fascicle length and pennation angle and normalised volume and lengths by controlling for body mass and fibular length respectively. They found that the muscle was smaller and shorter in the paretic limb when compared to both the non-paretic limb and to the typically developing group. However, the altered morphology was not due to a decrease in fascicle length and so the authors suggested that the medial gastrocnemius deformity in spastic hemiplegic cerebral palsy is caused by lack of cross-sectional growth. Barber et al. (2011) used similar techniques to compare the medial gastrocnemius volume, fascicle length and pennation angle between younger typically developing children and children with spastic cerebral palsy (2-5 years) and found similar results.

Oberhofer et al. (2010) used magnetic resonance imaging to compare the volumes and lengths of six lower limb muscles between five typically developing children (mean age 10.2 years) and six children with cerebral palsy (four with spastic diplegia and two with hemiplegia; mean age 9.6 years). Volumes were normalised to body mass and lengths to the thigh or shank segment length (hip to knee joint centre or knee to ankle joint centre respectively). Muscle volumes in the case group were all smaller but significant reductions were only found in the biceps femoris, the combined vasti group, and the rectus femoris. All muscles in the case group were shorter with significance found in all muscles except the soleus and biceps femoris.

At this time, to the author's knowledge, there are no studies in the literature that directly compare muscle fibre lengths or muscle pennation angles between typically developing subjects and subjects with cerebral palsy for multiple muscles of the lower limb.

3.3 Methodology

Ten adolescents with spastic diplegic cerebral palsy and ten typically developing control subjects were recruited for the study following the methods and selection criteria described in section 2.4.

3.3.1 Ultrasound

All subjects underwent an ultrasound scan of the lower limb muscles to record images of the fascicular architecture. The subject changed into shorts and lay prone on the examination couch. 2D, B-mode images were obtained bilaterally for the lower limb muscles listed in Table 3.2 using a Philips HD11 Scanner and L12-5 linear array probe (Philips Healthcare, Best, The Netherlands). Muscles were identified with the probe orientated in the transverse plane, the probe was then rotated to optimise viewing of the muscle fascicles and the image recorded. Image depths varied from 4-6cm as appropriate for each muscle.

soleus	(SOL)	semimembranosus	(SM)
medial gastrocnemius	(MG)	biceps femoris long-head	(BFLH)
lateral gastrocnemius	(LG)	biceps femoris short-head	(BFSH)
tibialis posterior	(TP)	rectus femoris	(RF)
tibialis anterior – superficial compartment	(TA-sup)	vastus medialis	(VM)
tibialis anterior – deep compartment	(TA-deep)	vastus lateralis	(VL)
semitendinosus	(ST)	vastus intermedius	(VI)

Table 3.2 – Lower limb muscles examined with 2D, B-mode ultrasound

Images were exported to a personal computer in bitmap format with a resolution of 800x564 pixels. Measurement of fascicle length and pennation angle for each muscle was then carried out in Matlab (The Mathworks™ Inc., MA, USA) (code in Appendix D). Pixel locations (x, y) were output for the ends of four lines manually drawn on the image (Figure 3.1).

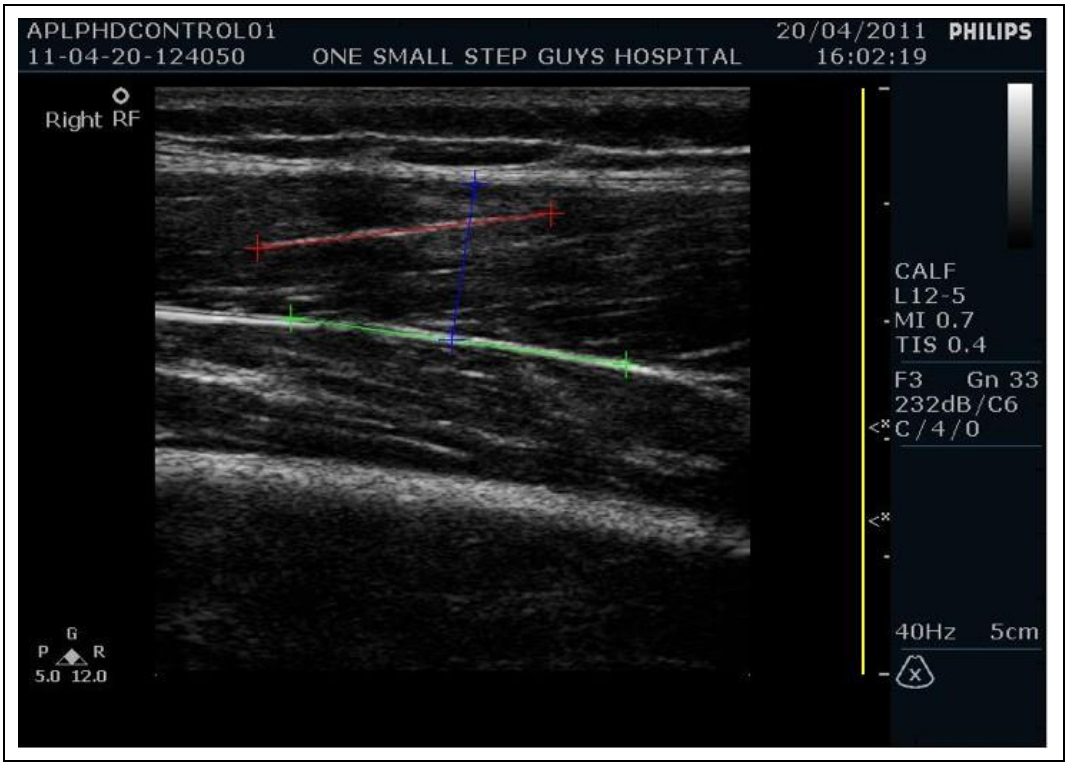

Figure 3.1 – Example ultrasound image showing the rectus femoris of Control01. Four lines were drawn to allow calculation of fascicle length and pennation angle:

Line 1: yellow line drawn along the vertical scale of the image
Line 2: green line drawn along the line of the muscle aponeurosis
Line 3: red line drawn along the line of a muscle fibre
Line 4: blue line drawn from the superficial to the deep aponeurosis and perpendicular to line 2

Pixel size was calculated by dividing the image depth by the pixel length of line 1. Pennation angle was calculated using the dot product of line vectors 2 and 3. Muscle thickness was determined by calculating the length of line 4. Muscle fascicle length was then calculated by dividing muscle thickness by the sine of the pennation angle. Similar to the methodology of Shortland et al. (2002), muscle fascicle length was then normalised to leg length to minimise the non-clinical variation of this parameter and allow comparison between subjects.

3.3.2 Magnetic Resonance Imaging

All subjects also underwent an MRI investigation of the pelvis and lower limbs to measure muscle volume. After completing the MRI safety questionnaire (Appendix E), data was collected using a 1.5T Philips Achieva MR system (Philips Healthcare, Best, The Netherlands) with the subject lying supine and feet first in the scanner. Image data was collected from the iliac crest to the distal calcaneum with a quadrature body coil using a three point Dixon sequence (TE/TR=4.6/13ms, echo time shift=1.53ms, 120^{o} echo phase shift, 20^{o} flip angle, 0.9x0.9mm in-plane voxel size, number of averages=2, 5mm slice thickness). Each scan took approximately 30 minutes. A Dixon sequence was chosen over the more conventional T1 weighted sequence to enable simultaneous collection of both volume data and fat content data which could be used as a measure of muscle quality if subsequently required.

Volume measurements were performed using Osirix (v3.7.1; Rosset et al., 2004). The proximal and distal endpoints of each muscle belly were identified visually and regions of interest were outlined on every image slice manually using a tablet and stylus (Figure 3.2). The total volume was calculated as the sum of the outlined cross sectional areas multiplied by slice thickness. Volumes were collected for the muscles listed in Table 3.2 and additionally from the adductor group (ADDS), gluteus maximus (GlutMax), gluteus medius (GlutMed), gluteus minimus (GlutMin), sartorius (SAR) and gracilis (GRA). A strong correlation between muscle volume and body mass has been reported in the literature (Malaiya et al., 2007; Fry et al., 2007; Noble et al., 2013) and so muscle volumes were normalised to body mass to allow comparison between subjects and across groups.

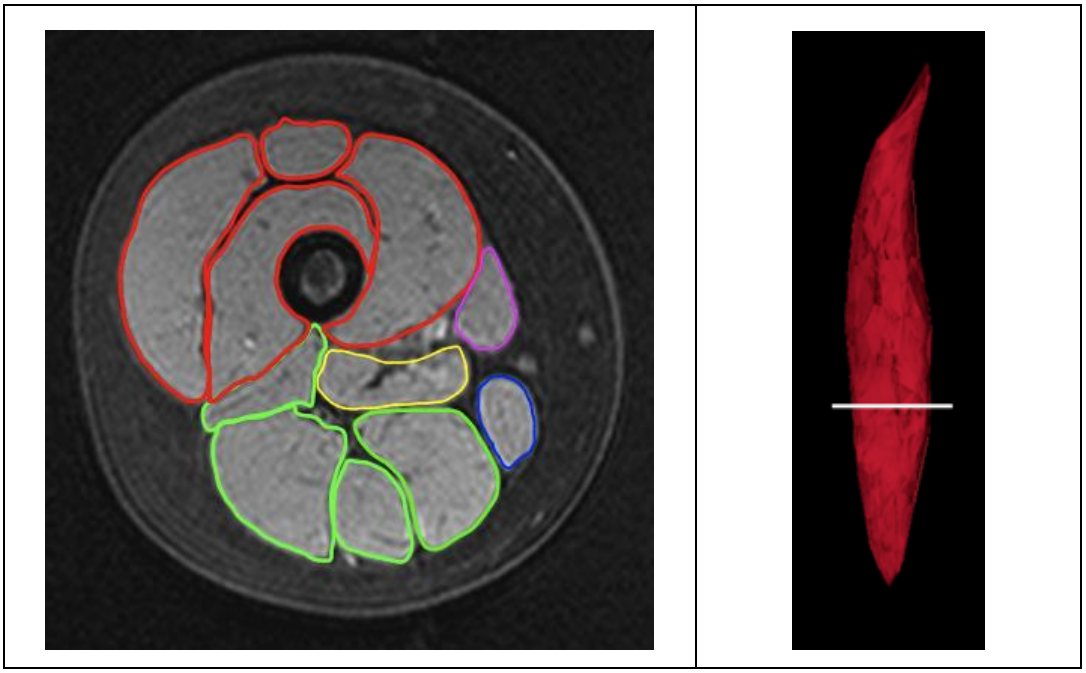

Figure 3.2 – Example MRI image

(a) Muscle delineation of the right thigh of a control subject

red = quadriceps, green = hamstrings, yellow = adductors, blue = gracilis, purple = sartorius

(b) Volume render of right BFLH

(white line indicates location of slice shown in (a))

Percentage muscle deficit (PMD) of the case subject muscles were then calculated using Equation 3.1.

Equation 3.1

$$PMD_{m,c} = \left(\frac{\overline{V}_m - V_{m,c}}{\overline{V}_m} \right) \times 100$$

where: $PMD_{m,c}$ is percentage muscle deficit for muscle *m* for case subject *c*

$\overline{V}_m$ is mean normalised muscle volume for muscle *m* from the typically developing group

$V_{m,c}$ is normalised muscle volume for muscle *m* for case subject *c*

Normalised muscle physiological cross-sectional area (PCSA) was then calculated using Equation 3.2:

Equation 3.2

$$PCSA_m = \frac{V_m \cdot \cos(\theta_m)}{L_{f,m}}$$

where:

V_m is normalised muscle volume for muscle *m*

θ_m is muscle pennation angle for muscle *m*

$L_{f,m}$ is the fascicle length for muscle *m*

Data was tested for normality using the Shapiro-Wilk test with a significance threshold of 0.05. Group differences were then compared with either independent samples T-Test or a non-parametric median test for two samples as appropriate with a significance threshold of 0.05. Control of type I errors was carried out using the Benjamini correction for multiple tests (Benjamini et al., 2001). All statistical analyses were performed using IBM SPSS Statistics v.20 (SPSS Inc., IL, USA).

3.3.3 Hypothesis

It is hypothesised that the lower limb muscles of subjects with cerebral palsy will be smaller in volume than their typically developing peers. It is also expected that the two groups will have similar fascicle lengths and pennation angles leading to smaller physiological cross-sectional areas in the cerebral palsy group. Distal (shank) and bi-articulate (RF, BFLH, SM, ST, MG, LG) muscles are likely to be especially affected.

3.4 Results

Full magnetic resonance datasets were successfully collected from all of the typically developing subjects but only from 6/10 subjects with cerebral palsy. One subject became nauseous halfway through the scan and so only thigh images were obtained; one subject moved their left leg during the scan and so motion artefact rendered the images for this leg unusable; one subject had extensive metal bone plates in both lower limbs causing distortion in all the images; and one subject had a metal bone plate in their right thigh causing distortion in the thigh muscles of this leg. A reduced muscle volume dataset was therefore obtained from these subjects.

Full ultrasound datasets were successfully collected from all of the typically developing subjects but only from 9/10 subjects with cerebral palsy due to time constraints after delays in gaining access to the hospital MRI scanner. A list of all previous surgery for the case subjects is given in Appendix F.

3.4.1 Subject Data

Subject data for age, height, mass and BMI can be seen in Figure 3.3 and Table 3.3. All data sets were found to be normally distributed using the Shapiro-Wilk Test with a threshold of 0.05. However, this test is less reliable for small sample sizes (such as those used here) and the appearance of skewedness on the box-plots for some variables gives a strong indication of non-normality. For this reason both parametric and non-parametric tests were performed to test for group differences. The outlier for age in the case group was not excluded as there is little change in musculo-skeletal maturation after 19 years of age (Tanner & Whitehouse, 1976). Outliers for height and body mass index were not excluded as muscle fibre lengths and muscle volumes were normalised to leg lengths and mass respectively. Both parametric and non-parametric tests showed there was no difference in age but the CP group were found to have significantly lower height, mass and BMI than the typically developing control group (Table 3.3).

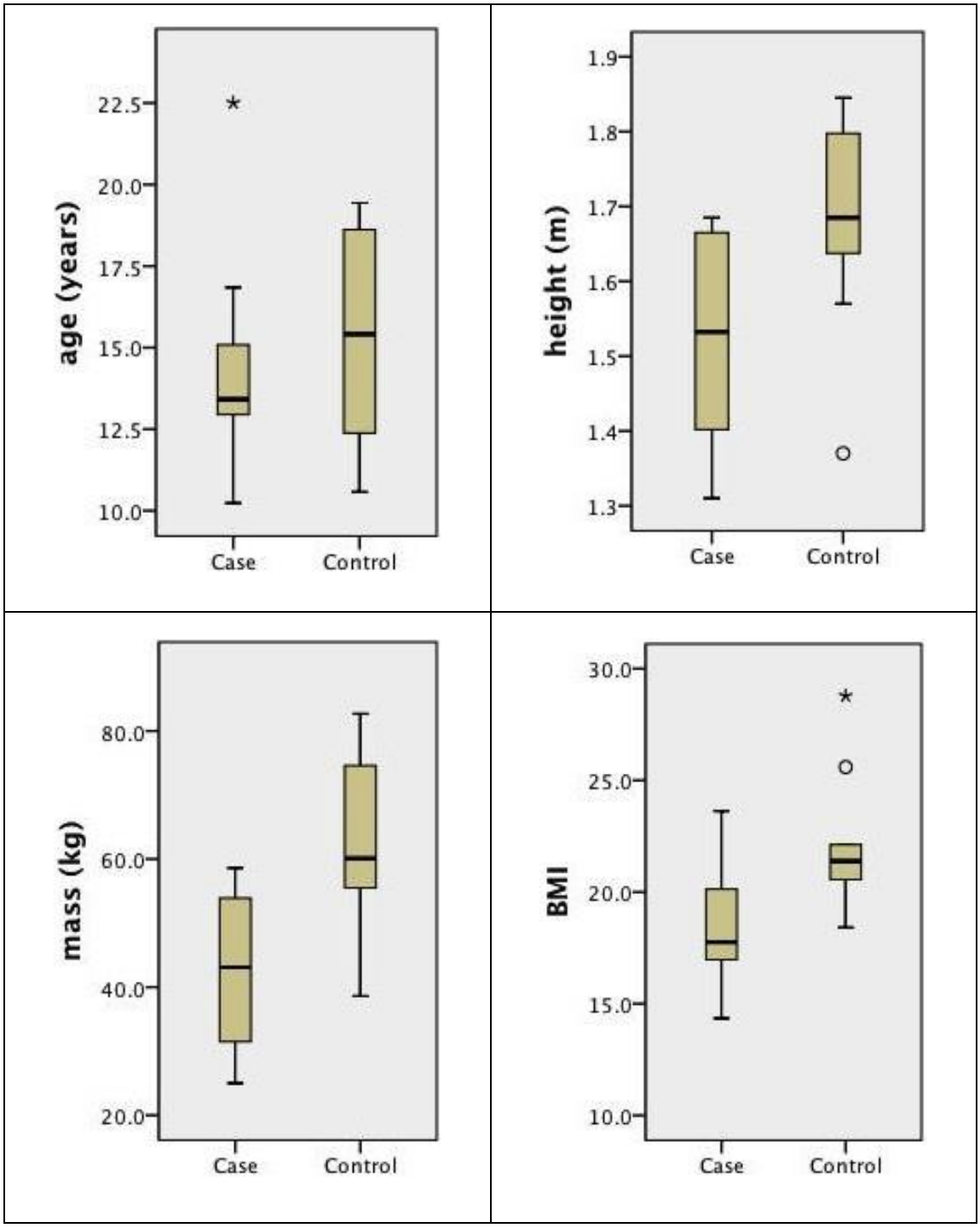

Figure 3.3 – Box-plot group comparisons for age, height, mass and BMI.

Box = inter-quartile range (IQR), horizontal line = median, whiskers = data range
o = outlier (1.5-3xIQR from box), * = extreme (>3xIQR from box)

	n	male/female	age (years)	height (m)	mass (kg)	BMI
Controls	10	5/5	15.4 (3.2)	1.7 (0.1)	62.8 (14.4)	22.0 (3.1)
Cases	10	6/4	14.3 (3.5)	1.5 (0.1)	43.1 (12.5)	18.3 (2.8)
T-Test p-value			0.47	0.02*	0.01*	0.01*
Mann-Whitney U Test p-value			0.44	0.03*	0.01*	0.01*

Table 3.3 – Subject Group Data - mean (SD). * indicates significance

Correlation analysis was carried out to test the suitability of the normalisation schemes adopted in the methodology. Data from the control and case subjects was analysed separately. The relationships of muscle volume with body mass, physiological cross-sectional area with body mass, and fascicle length with leg length were tested with simple linear regression for each muscle. The mean R^2 values are shown in Table 3.4.

	Muscle Volume	Muscle PCSA	Fascicle Length
Controls	0.55 (0.16)	0.32 (0.23)	0.18 (0.14)
Cases	0.68 (0.21)	0.45 (0.22)	0.05 (0.06)

Table 3.4 – Regression analysis. The mean R^2 (SD) value from simple linear regression of muscle volume with body mass, physiological cross-sectional area (PCSA) with body mass, and fascicle length with leg length.

3.4.2 Pennation Angle

Muscle pennation data can be seen in Figure 3.4. No significant differences were found between the two groups. Data from the semitendinosus (ST) and vastus medialis (VM) are omitted as these muscles were typically found to have parallel fibre structures (very small or zero pennation angle) and so measurement of fascicle length was prone to high error using the ultrasound image methodology described above.

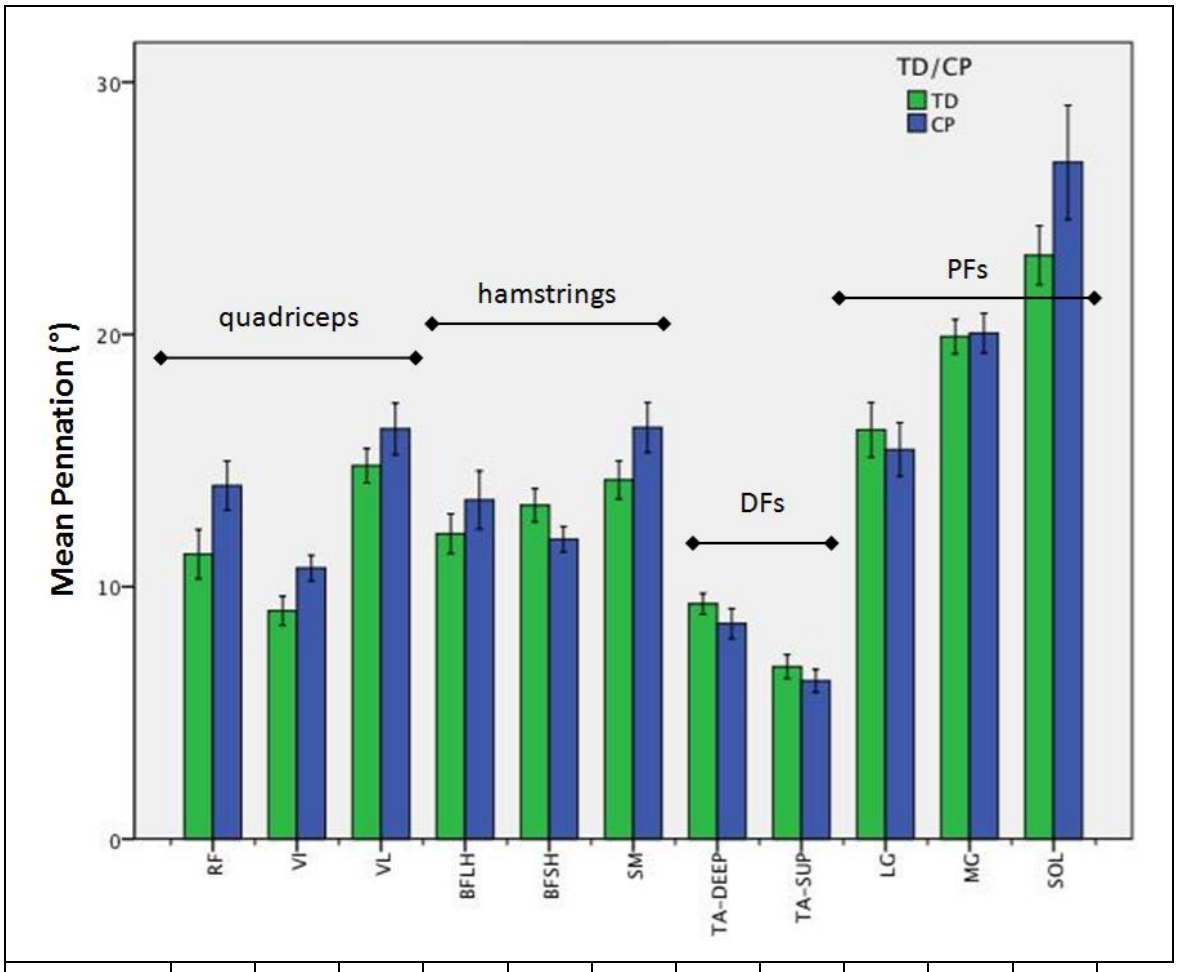

TD n	20	20	20	19	15	20	20	20	20	20	20
CP n	17	16	18	17	14	17	17	17	18	17	14
p-value	0.84	0.04	0.24	0.34	0.12	0.10	0.28	0.40	0.61	0.90	0.13

Figure 3.4 – Group differences in mean pennation between TD subjects and CP subjects. Underlining shows data was not normally distributed , error bars show ±1SE, DFs = dorsiflexors, PFs = plantarflexors

3.4.3 Fascicle Length

Muscle fascicle data can be seen in Figure 3.5. Data was normalised to leg length to allow comparison across subjects (Fry et al., 2007). Data from the semitendinosus (ST) and vastus medialis (VM) are omitted as described above. There was a universal trend for shorter fascicle lengths in the case group especially for the rectus femoris (RF), vastus intermedius (VI) and semimembranosus (SM) muscles but only the difference in semimembranosus was found to be significant after applying the post-hoc correction for multiple tests (Benjamini et al., 2001).

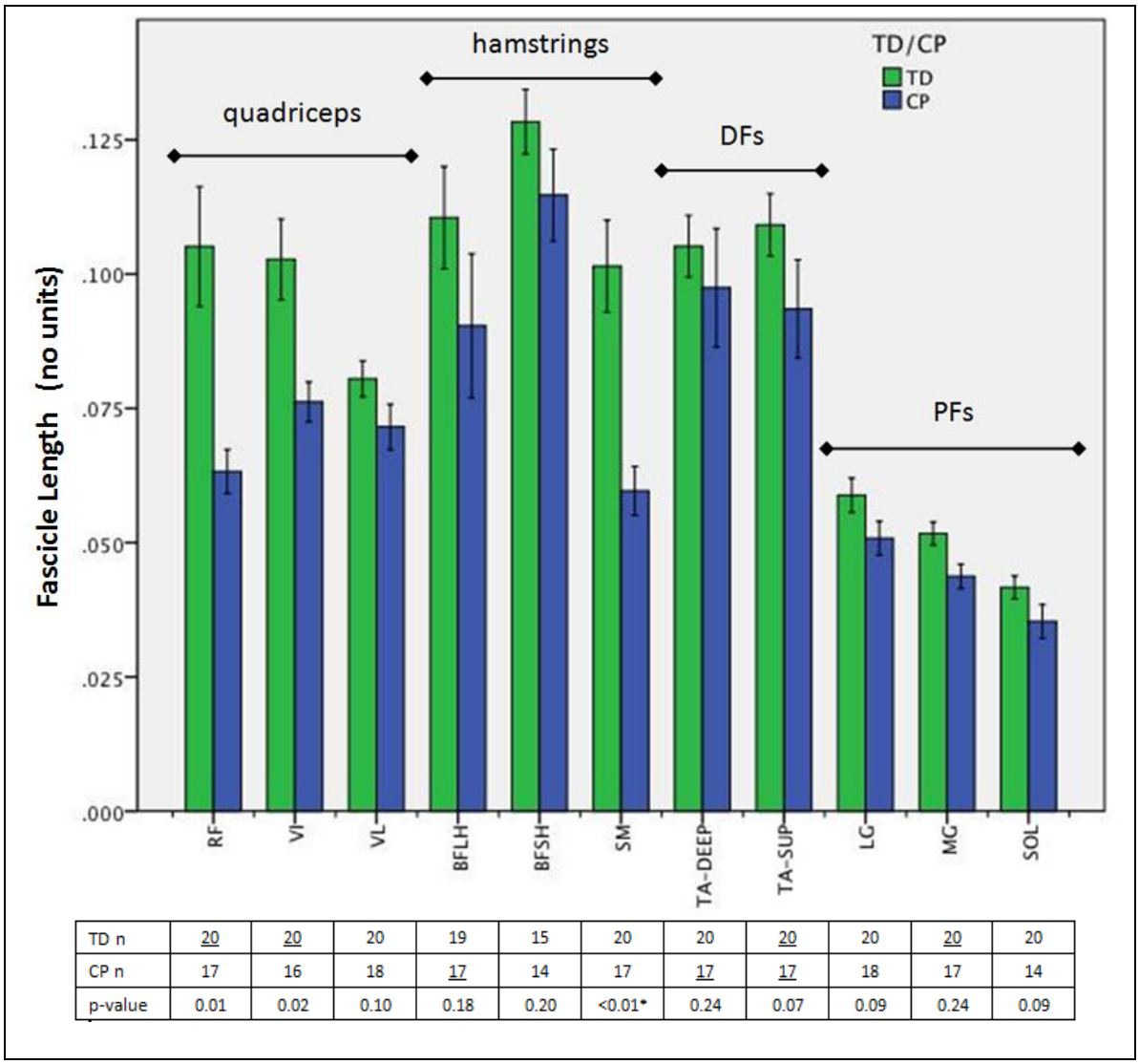

TD n	20	20	20	19	15	20	20	20	20	20	20
CP n	17	16	18	17	14	17	17	17	18	17	14
p-value	0.01	0.02	0.10	0.18	0.20	<0.01*	0.24	0.07	0.09	0.24	0.09

Figure 3.5 – Group differences in normalised mean fascicle length between TD & CP subjects. Fascicle lengths were normalised to leg length. Error bars show ±1SE. Underlining shows data was not normally distributed, * indicates significance, DFs = dorsiflexors, PFs = plantarflexors

3.4.4 Muscle Volume

Normalised muscle volume data is shown in Figure 3.6. There was a trend for all measured muscles to be smaller in the cerebral palsy group compared to their typically developing peers except for the tibialis posterior.

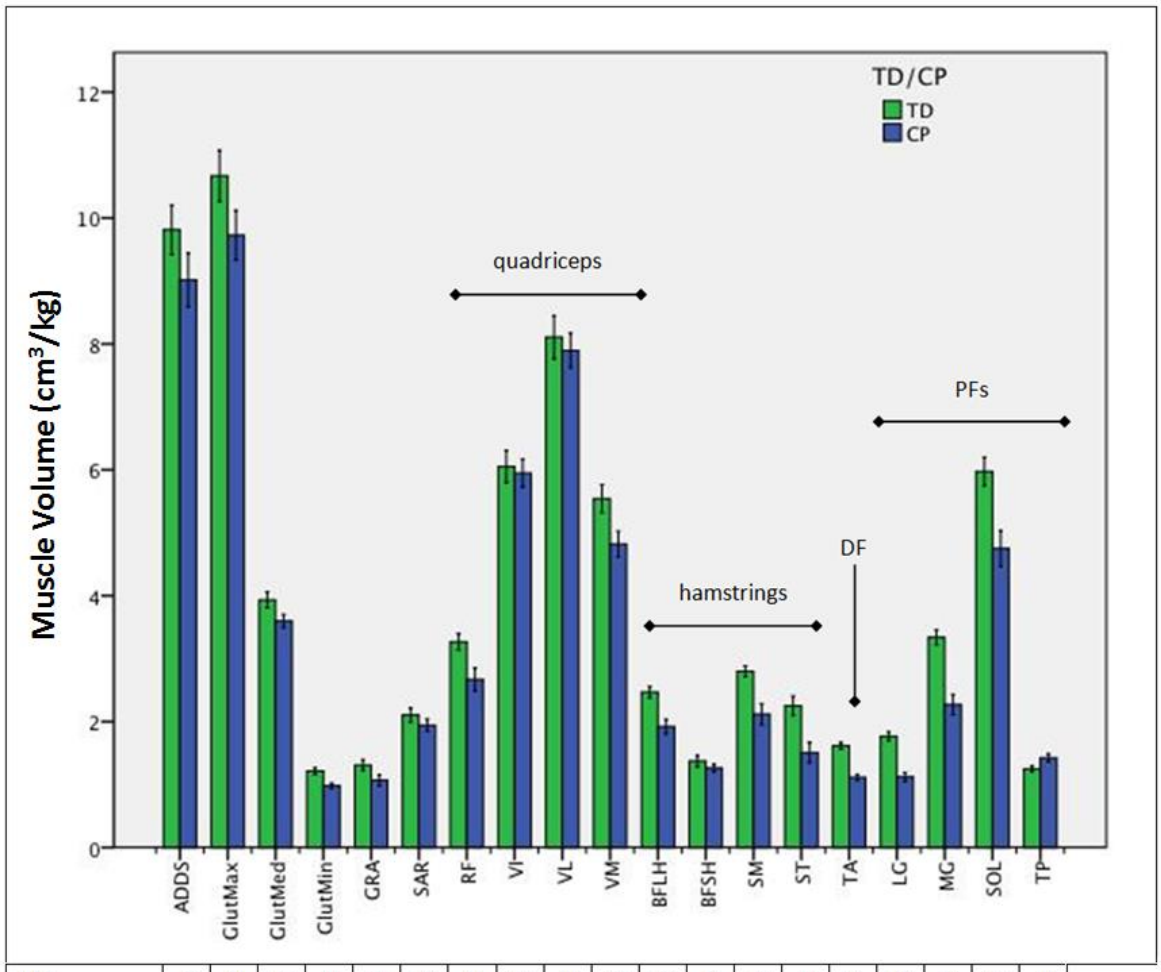

TD n	20	20	20	20	20	20	20	20	20	20	20	20	20	20	20	20	20	20	20
CP n	14	16	14	14	15	15	15	14	14	14	16	17	17	17	18	17	18	18	17
p-value	0.19		0.08		0.06		0.01*		0.73		<.01*		<.01*		<.01*		<.01*		0.03
p-value		0.11		<.01*		0.31		0.73		0.03		0.34		0.07		<.01*		<.01*	

Figure 3.6 – Group differences in normalised mean muscle volume between TD & CP subjects. Muscle volumes were normalised to body mass. Error bars show ±1SE. Underlining shows data was not normally distributed, * indicates significance, DF = dorsiflexor, PFs = plantarflexors

Significant volume reductions were found in the gluteus minimus (GlutMin), rectus femoris (RF), biceps femoris long head (BFLH), semimembranosus (SM), tibialis anterior (TA) and all three calf muscles (LG, MG, SOL). Percentage muscle deficits for the muscles reduced in volume can be seen Figure 3.7. The mean deficit of the distal muscles was 32% (or 23% if including the tibialis posterior) compared to 16% for the proximal muscles. With the exception of sartorius (SAR) there was a trend for larger volume deficits in the biarticular muscles compared to their monoarticular neighbours.

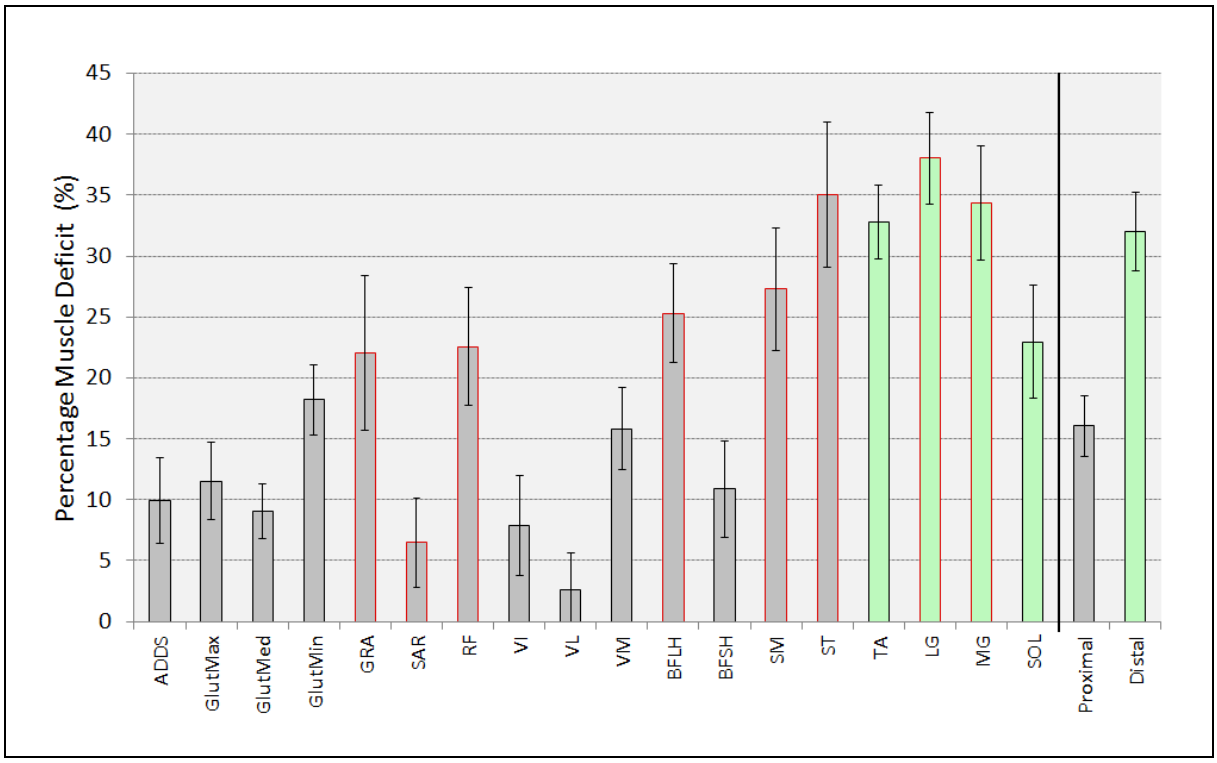

Figure 3.7 – Percentage muscle volume deficits for muscles found to be smaller in the cerebral palsy group. Proximal muscles are shown in grey and distal muscles in green. Biarticular muscles are marked with red borders. Mean deficits for proximal and distal muscle groups are also shown. Error bars show ±1SE.

3.4.5 Muscle Physiological Cross-Sectional Area

Normalised muscle PCSA data can be seen in Figure 3.8. The mean pennation angle and fascicle length from the two compartments of the tibialis anterior (TA) muscle were used to calculate tibialis anterior PCSA. There was a trend for increased PCSAs in all the thigh muscles and decreased PCSAs in all the shank muscles of the case group but after post-hoc correction for multiple tests (Benjamini et al., 2001), significant differences were only found in one thigh muscle, vastus intermedius (VI), and one shank muscle, medial gastrocnemius (MG).

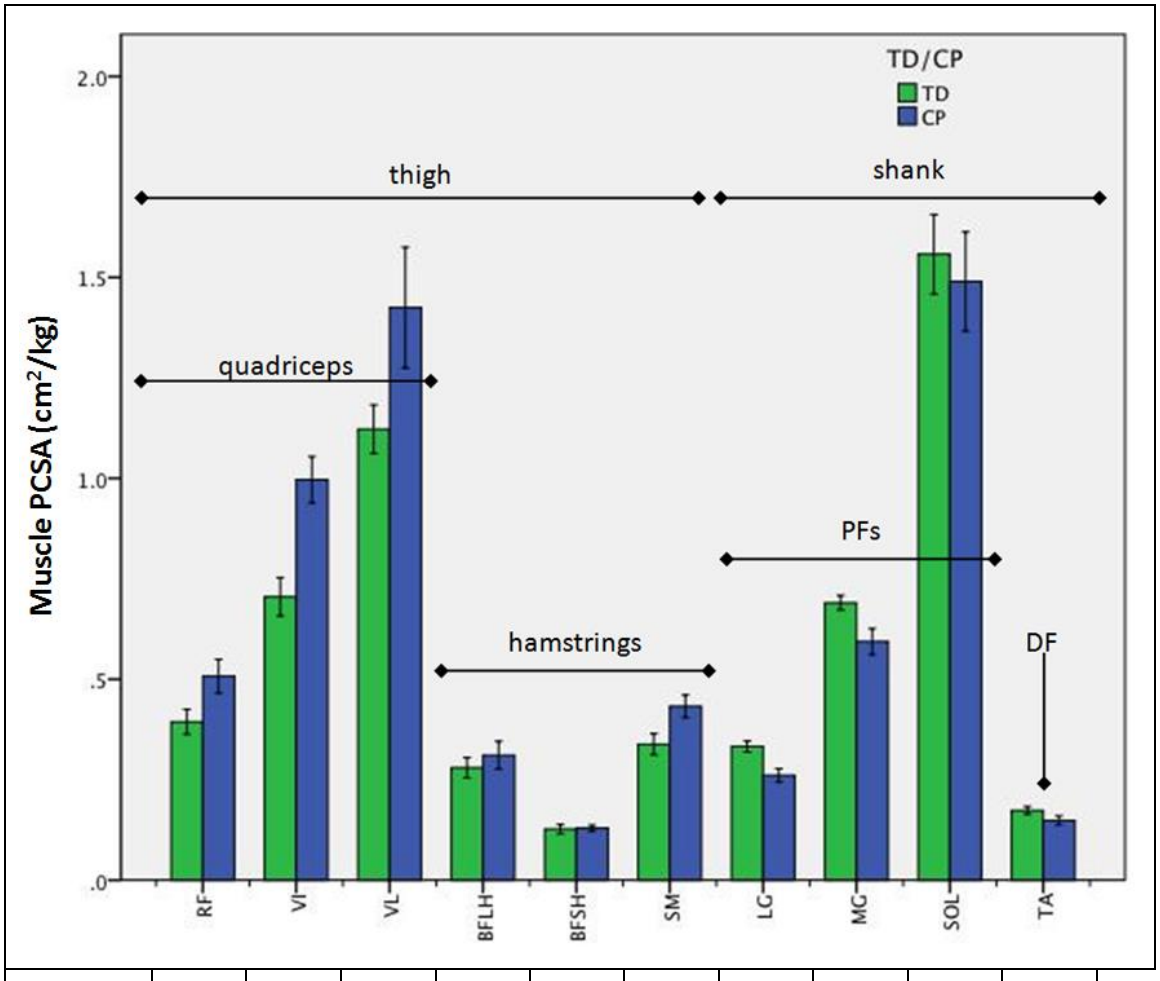

TD n	19	15	20	20	20	20	20	20	20	20
CP n	12	10	12	13	11	14	16	15	13	15
p-value	0.04	<0.01*	0.07	0.47	1.00	0.02	0.02	0.01*	0.67	0.10

Figure 3.8 – Group differences in normalised mean muscle PCSA between TD & CP subjects. PCSAs were normalised to body mass. Error bars show ±1SE. Underlining shows data was not normally distributed, * indicates significance, DF = dorsiflexor, PFs = plantarflexors

3.5 Discussion

By design, there was no difference between the mean ages of the case and control groups but the mean height, mass and BMI of the case subjects were significantly reduced compared to their typically developing peers. This is an unexpected result as the large study of Day et al. (2007) found little difference between independently ambulant subjects with cerebral palsy when compared to growth charts of the general population, although they did find a reduction in growth for the more severely affected and hence non-ambulant individuals with cerebral palsy. However, reasonable relationships were found between body mass and both muscle volume and physiological cross-sectional area (Table 3.4) and so the normalisation schemes adopted for this data should enable fair comparisons between groups.

3.5.1 Muscle Physiological Cross-Sectional Area

Muscle PCSAs in the cerebral palsy group were found to be larger in the thigh and smaller in the calf than their typically developing peers. Statistically significant differences were only found in 2 of the 10 muscles tested however, but this is likely to be an effect of the small sample size and multiple test correction.

As described in section 1.3, individuals with cerebral palsy often have weak muscles and so it was hypothesised that all muscle PCSAs would be smaller in the cerebral palsy group with larger deficits in the shank. A typical explanation for this is that as development of the long tracts of the spinal cord take place in utero and during the early years of life, and because the motor neurons of distal musculature connect to the cord in distal locations, the altered muscle development that occurs as a consequence of cerebral palsy neuropathy is more severe for the distal muscles (Gough & Shortland, 2012). The imbalance of PCSA reduction only being found in the shank muscles of the cerebral palsy group in this study supports this supposition. However, the increased PCSA of the thigh muscles is a surprising result, especially considering the volumes were found to be smaller. It is worth remembering that PCSA is the only muscle parameter that is directly proportional to the maximum tension that can be generated by a muscle (Lieber & Fridén,

2000). This result therefore implies that the subjects with cerebral palsy recruited for this study have, on average, stronger thigh muscles than their typically developing peers. This is contrary to the study of Wiley & Damiano (1998) who carried out a case/control comparison of lower limb muscle strength using a hand-held dynamometer for a group of ambulant children with diplegic or hemiplegic cerebral palsy, and found all muscles were weaker in the case group. However, the PCSA of a muscle gives a measurement of the maximum potential force that a muscle can develop, and the ability of the subjects with cerebral palsy to voluntarily recruit these muscles is likely to be compromised by other factors of the condition, as described in section 1.2, including incomplete muscle activation and spasticity.

Based on the formula for calculating PCSA (Equation 3.2) it is clear that an increase in PCSA can be driven by an increase in muscle volume and/or a decrease in pennation angle and/or a decrease in fascicle length. Looking at the results of these three muscle parameters it should therefore be possible to determine which provides the principal contribution to this increase in PCSA at the thigh.

3.5.2 Muscle Volume

Muscle volumes were found to be smaller in subjects with cerebral palsy when compared to their typically developing peers and a greater reduction was found in the distal muscles. This is in agreement with the hypothesis and a number of studies in the literature (Malaiya et al., 2007; Fry, 2008; Oberhofer et al., 2010). Out of the 18 muscles measured only the tibialis posterior was found to be larger in the cerebral palsy group and so it was excluded from the analysis of mean muscle deficit in the distal muscles. As muscle volumes are smaller in the cerebral palsy group at both the thigh and shank level, the muscle volume parameter does not directly contribute to the increase in PCSA found in the thigh muscles but it does contribute to the imbalance of PCSA reduction between the proximal and distal segments.

3.5.3 Muscle Pennation Angle

No differences in muscle pennation angle were found between the two groups. This is in agreement with the hypothesis and with the findings of Malaiya et al, (2007) who found no difference in pennation angle of the medial gastrocnemius (at resting ankle angle) between a typically developing group and in the paretic limb of a group of subjects with spastic hemiplegic cerebral palsy. There is also good agreement with Malaiya et al. (2007) on the magnitude of the medial gastrocnemius pennation angle (Figure 3.9), a likely result as both methods utilised ultrasound imaging techniques on similarly aged child/adolescent populations.

	n (TD,CP)	mean age (years)	TD Pennation degrees (SD)	CP Pennation degrees (SD)
This study (imaging)	20,17	14	20 (3)	20 (3)
Malaiya et al., 2007 (imaging)	15,16	9	17 (2)	16 (3)
Ward et al., 2008 (cadaveric)	21	83	10 (4)	-
Friederich & Brand, 1990 (cadaveric)	1	50	7	-
Wickiewicz, 1983 (cadaveric)	3	?	17 (8)	-
Martin et al., 2001 (cadaveric)	5	73	33 (5)	-
Martin et al., 2001 (imaging)	9	76	19 (4)	-

Figure 3.9 – Mean pennation angles for the medial gastrocnemius from this study and other studies in the literature.

However, there is a wide variation in this pennation angle when compared to the cadaveric studies discussed in section 3.2. This is likely to be due to a combination of effects including differences in methodology, changes in muscle morphology associated with age (Shortland, 2009) and the complications of muscle shrinkage linked with cadaveric techniques (Martin et al., 2001). Comparing the pennation angles for other muscles, this variation between studies is most striking (Figure 3.10) with a consistent measurement only obtained for the semimembranosus (SM).

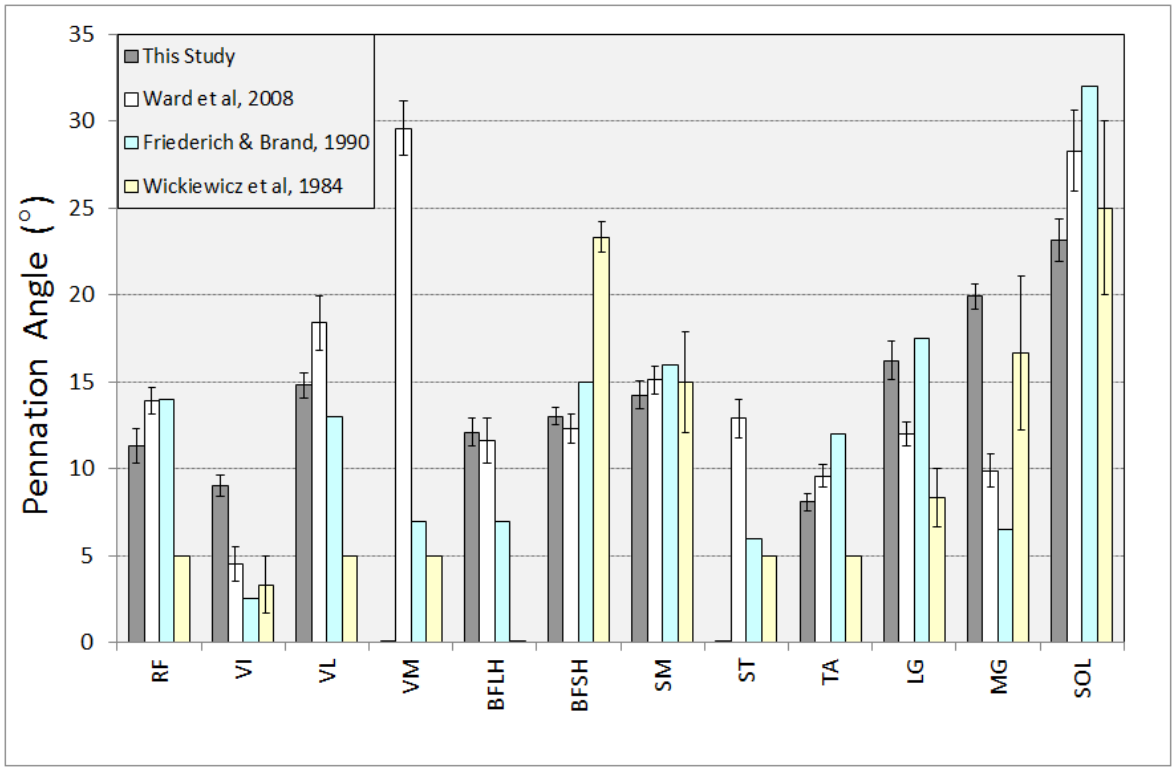

Figure 3.10 – Pennation angles for ten lower limb muscles in typically developing human subjects measured in vivo using ultrasound (this study) and from cadaveric data of three previous studies. Tibialis anterior (TA) angle from this study is the mean value obtained from both the superficial and deep compartments. Error bars show ±1SE. No variance data was provided in Friederich & Brand (1990).

There is currently no gold standard method for the measurement of human muscle pennation angle and these results highlight the difficulty in obtaining such data. All measurements must therefore be treated with caution and it is still not clear if the abnormalities of muscle growth associated with cerebral palsy affect this morphological parameter as any systematic changes in pennation angle may be masked by measurement variation. Despite finding no statistically significant changes in pennation angle between the groups, there was a general trend (5 out of 6) of higher pennation angles in the thigh muscles but not in the shank. This would lead to a slight decrease in PCSA and so for the results of this study, pennation angle opposes an increase in PCSA at the thigh.

3.5.4 Muscle Fascicle Length

By a process of elimination, the driving factor behind the increase in PCSA found in the thigh muscles of the subjects with cerebral palsy must therefore come from the differences in fascicle length. This would appear to agree with the data as there was a

universal trend for shorter fascicle lengths in the case group, especially at the thigh. For the data collected in this study, therefore, the stronger muscles found at the thigh in the cerebral palsy subjects are a result of the combination of decreased fascicle length and a limited volume reduction leading overall to an increase in PCSA. At the shank, the volume reduction dominates the calculation of PCSA leading to an overall reduction in PCSA.

The trend of reduced fascicle lengths in the cerebral palsy group does not support the original hypothesis and it is also contrary to the results of Malaiya et al. (2007) who found no difference between their groups, despite the use of a similar normalisation scheme (leg length vs. fibular length). The regression analysis of Malaiya et al. (2007) however showed a weak relationship between fascicle length and fibular length for their typically developing data and an even poorer relationship for their cerebral palsy data. In this study, no relationship was found between leg length and fascicle length in either group (Table 3.4). In the literature there is a lack of consensus on the difference in fascicle lengths between typically developing controls and individuals with cerebral palsy. This calls into question the appropriateness of using a leg length or fibula length based normalisation scheme. However, the study of Mohagheghi et al. (2008) examined exactly this problem by comparing muscle fascicle lengths between typically developing controls and subjects with diplegic cerebral palsy. They used statistical methods to control for the confounding effect of the normalisation scheme and showed that the pathological group had shorter fascicles both with and without normalisation. Indeed, the same conclusion can be drawn from the data in this study by comparing absolute fascicle lengths (Figure 3.11) and the normalised lengths shown above (Figure 3.5). Other than the difference in units, these two figures look remarkably similar, and the same result (shorter fascicles in the cerebral palsy group) remains.

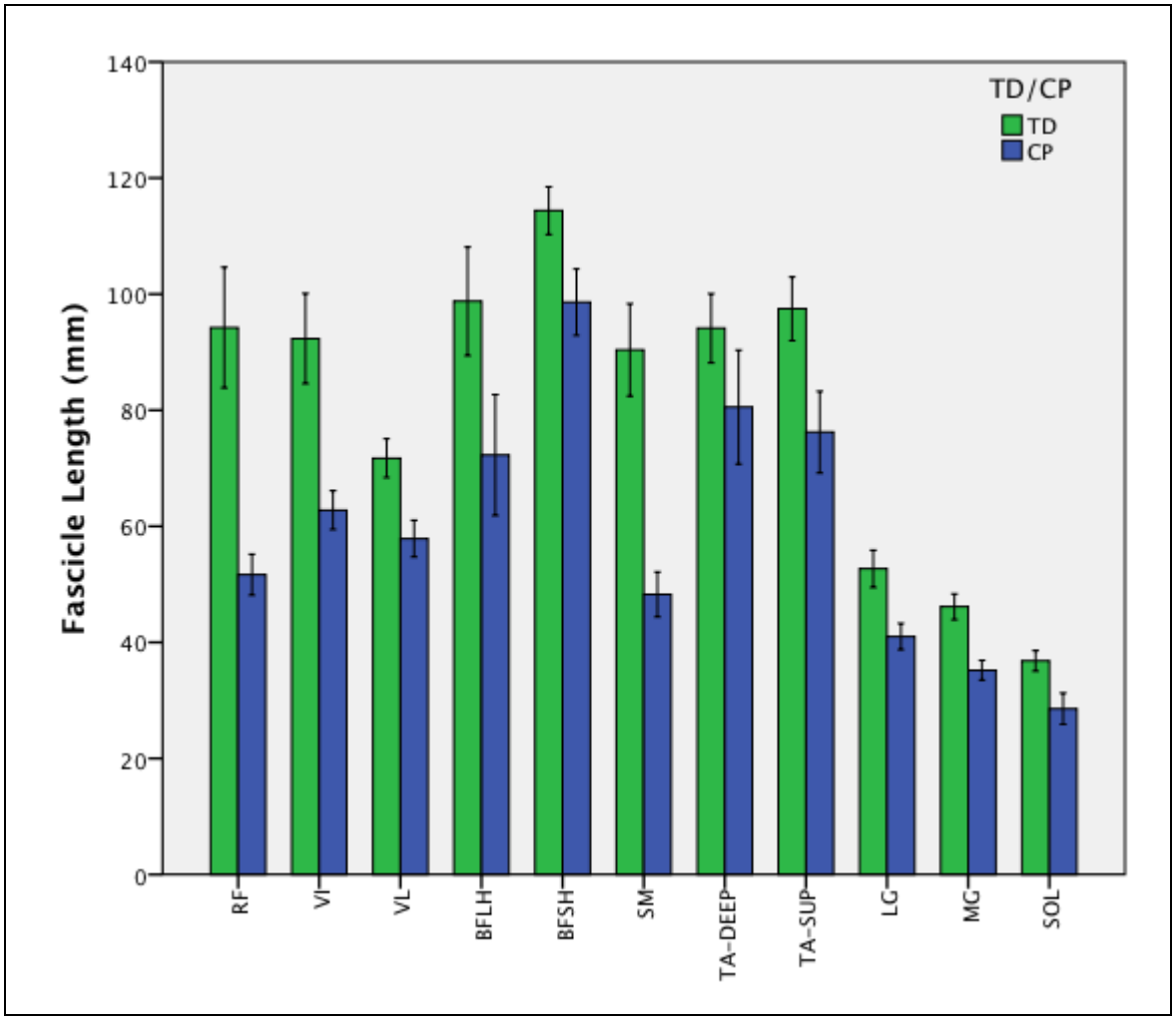

Figure 3.11 – Mean fascicle lengths in the TD and CP groups. Error bars show ±1SE.

3.5.5 Conclusions and Limitations

Muscle morphological data (volume, fibre length, pennation angle) was collected using 2D ultrasound and magnetic resonance imaging for a number of lower limb muscles from ten typically developing adolescents and ten adolescents with cerebral palsy. Muscle volumes and fascicle lengths were found to be smaller in the case group with smaller volumes more prominent in the distal musculature. Physiological cross-sectional area was therefore found to be larger in the thigh and smaller in the shank for the case group. No difference between groups was found in pennation angle.

There are a number of limitations in this study of muscle morphological data. Firstly, due to the time consuming nature of the data collection and processing it was only possible to

recruit a limited number of subjects and this reduces the statistical power of the subsequent analyses. General trends were seen in the data but after correction for multiple tests, many of the differences failed to reach statistical significance. Additionally, measurements were made on both lower limbs of each subject and the results analysed separately. This had the effect of increasing numbers but there will be a dependency between each limb pair that will not have been taken into account - a problem recently discussed by Sangeux et al. (2013).

The first purpose of collecting this morphological data was to investigate the differences between typically developing individuals and individuals with cerebral palsy. The increase in thigh muscle physiological cross-sectional area between these cohorts was contrary to the accepted premise that cerebral palsy subjects have weaker muscles. If this is a genuine finding it is possible that, due to distal weakness and poorer motor control, individuals with cerebral palsy make more use of their proximal musculature for tasks such as walking and hence alter the morphology of these muscles to make them stronger (they are still smaller). The increase in thigh muscle PCSA in the case group appears to be driven by more marked shortening of the fascicle lengths in the thigh muscles.

There is very little agreement between the pennation angles of resting muscles reported within the literature or between the literature and the values measured in this study. Plus, in individuals with abnormal muscle tone and spasticity as is common in cerebral palsy, it is arguable whether some muscles can ever be considered to be in a resting state. High variation, based on the standard error values, was also found in the measurement of muscle fascicle lengths in this study. As both of these parameters were calculated using the ultrasound technique described in section 3.3 their values and hence any errors are trigonometrically linked. There is low confidence therefore in the validity of these two parameters and subsequently to the derived PCSA data. Muscle volumes however were derived from MRI data and hence calculated independently from pennation and fascicle length. The muscle volumes measured in this study have now been published in combination with another magnetic resonance data set (Noble et al., 2013).

The second purpose of collecting these morphological parameters was to generate data for the parameterisation of musculo-skeletal models, as outlined in Table 3.1, for simulation analyses documented in later chapters. However, due to the uncertain validity of the pennation angle and fascicle length (and hence PCSA) data it was decided only to carry the muscle volume measurements forward. These will be used to generate normative ranges of maximum isometric muscle force for each cohort for use in sensitivity and validity analyses of simulated muscle activations.

4 The sensitivity of simulated muscle activations in the OpenSim model to changes in lower limb muscle volume in typically developing adolescents during walking

Muscle volumes calculated from the MRI data collected in Chapter 3 were used to generate a normative range of lower limb muscle volumes in typically developing adolescents. These volumes were used to scale the strength of the gait2392 OpenSim generic musculo-skeletal model to create a number of models to represent this normative range. Muscle activations were simulated for each model over a single gait cycle to examine the sensitivity of simulated muscle activation to changes in muscle strength. In general, small increases in muscle activation were seen for decreases in muscle strength confirming that the model is insensitive to changes in muscle strength over a normative range. However, large increases in activation occurred in synergist and compensatory muscles when any muscle approached maximum activation.

4.1. Introduction

Static Optimisation and the Computed Muscle Control (as described in Chapter 2) are two alternative methods for the calculation of simulated muscle activations from a prescribed set of kinematics and kinetics. Such information, if insensitive to small changes in model parameters, would be valuable in the study of biomechanics, human movement and specifically gait analysis.

Examples of human gait models available for and commonly used in OpenSim simulations are described in section 2.2.1. Many of these models are based on the work by Scott Delp (Delp, 1990) and use anatomical data from the cadaveric studies of Wickiewicz et al. (1983) and Friederich & Brand (1990) or more recently Ward et al. (2008) for muscle

parameterisation. Inevitably however, due to the availability of cadavers, all of these datasets are based on elderly adult subjects which results in models with a prescribed set of muscle parameters that may be unsuitable for use in simulations of movement of child/adolescent subjects – the typical population of interest in the treatment of cerebral palsy. When these models are scaled in size to match the stature of a specific subject, the only two muscle parameters which are also scaled are *tendon slack length* and *optimal fibre length*. The muscle parameter *maximum isometric force* is not scaled and as this is proportional to muscle physiological cross-sectional area and hence to muscle volume (Lieber & Fridén, 2000), it is likely that simulations of walking in non-adult populations that use these models will generate muscle activations that are unrepresentative for their group.

It is unlikely that data on muscle morphology from cadavers of children or adolescents will ever become available in sufficient quantity and so parameterisation of these muscle models must rely on measurements from alternative techniques such as imaging. There are few complete imaging studies of the muscles of the lower limbs in children (Oberhofer et al., 2010). Certainly more work could be done to elucidate muscle growth in the lower limb during childhood, though there are significant challenges to delineating the architecture (fascicle length and pennation angle) of muscles due to the length of many of the fascicles in the lower limb (Noorkoiv et al., 2010) and of the variation in fascicle length with position in some muscles (Blazevich et al., 2006). Therefore, if the outputs of current models and techniques in musculo-skeletal simulation can be shown to be insensitive to small changes in muscle morphology then researchers can have confidence in using them in further investigations of younger populations and for research into cerebral palsy.

A number of studies have investigated bespoke musculo-skeletal models based on MRI data (Correa et al., 2011; Scheys et al., 2005, 2008a, 2008b, 2008c). Focusing specifically on skeletal measures they found differences between the generic versus bespoke muscle moment-arms, muscle insertions, muscle-tendon lengths and hip joint centres which were shown to have significant effects on the output of simulations (Scheys et al., 2011). Although, based on potential induced accelerations, Correa et al. (2011) found no

difference in the prediction of muscle function between the two model types. It would appear therefore that these models require some bespoke skeletal elements if they are to provide the simulation fidelity necessary to be adopted into more routine use in orthopaedic/biomechanical research and clinical gait analysis. Whether this is also true for the muscle models however is still uncertain.

To date, there have been few studies in the literature that examine the sensitivity of such simulations to changes in muscle model parameters. In his original work on the development of SIMM (Delp, 1990) Delp carried out some initial sensitivity tests of the muscle models he employed. To investigate the sensitivity of muscle actuator force to changes in *tendon slack length* and *optimal fibre length* he varied these two parameters and calculated the change in the joint angle at which each of four actuators (Gastroc - gastrocnemius, RF – rectus femoris, ST - semitendinosus, GRA - gracilis) developed peak force. Maximum and minimum joint angle changes for a 5% change in *tendon slack length* (he does not specify if lengthened or shortened) were 38° (Gastroc) and 6° (GRA) and for a 5% change in *optimal fibre length* were 18° (ST) and 2° (Gastroc). Delp concluded that the angle of peak force was more sensitive to changes in *tendon slack length* for muscles with high ratios of tendon slack length to moment-arm length, and was more sensitive to changes in *optimal fibre length* for muscles with high ratios of fibre length to moment-arm length. Delp also carried out a series of isometric muscle model tests to look at the factors that affect the sensitivity of muscle force to changes in tendon length. The force of the baseline muscle (5cm fibres, 0° pennation, 30cm stiff tendon) was reduced by 48% following a decrease in tendon length by 2cm. He then repeated this tendon shortening in combination with other changes to the muscle model: decreasing the *optimal fibre length* by 1cm; increasing the tendon compliance to a nominal value; and increasing the pennation angle to 30°. For each of these changes, the corresponding muscle force reductions were 80%, 29% and 30% respectively. Delp therefore concluded that *optimal fibre length* was the most important parameter as regards muscle force sensitivity to changes in tendon length and that increases in tendon compliance and pennation angle reduced this sensitivity.

Correa & Pandy (2011) investigated a method of scaling the strength of the generic (adult) OpenSim gait model for use in children (7-13 years). For ten subjects they compared muscle forces simulated during normal walking from two models: a generic model with muscle strengths scaled by their own *mass-strength scaling law*, and a bespoke model with muscle strengths based on subject-specific MRI data. No differences were found between the muscle forces generated by the models and so they concluded that the use of mass-length scaling in the development of subject-specific musculo-skeletal models of children was appropriate. However, no comparison was made to the un-scaled generic model and so it was not clear that such scaling was necessary.

More recently Van der Krogt et al., (2012) used a similar OpenSim model driven by experimental gait data and investigated its response to progressive muscle weakness. They decreased the *maximum isometric force* of the muscle actuators in increments of 20% until the model was no longer able to follow the prescribed kinematics and examined the change in muscle force. They tested weakening all of the muscles together and also weakening selected muscle groups alone. Using this method they identified muscle groups that were robust (in terms of the maintenance of normal gait) to muscle weakness (hip and knee extensors) and muscle groups that were more sensitive to weakness (plantarflexors, hip abductors and hip flexors). They also observed that the weakening of a muscle not only resulted in its increased activation, as would be expected, but also an increase in the activation of synergist muscles as well as other muscles needed to compensate for these changes in synergist force. Compensatory strategies were therefore quite complex. However, there are two elements in this methodology that require comment. Firstly, the study used the gait2392 OpenSim lower limb and torso model scaled to six adolescent subjects (mean(SD) age: 15(1) years) but, as described above, this model is based on adult cadaver data and *maximum isometric force* is not scaled when the model is resized. The models used in this study therefore had muscle-tendon lengths, fibre lengths and segment masses of adolescent subjects but the muscle strengths of adults. Secondly, the arbitrary nature of weakening all muscles or functional muscle groups by 20% is unlikely to be representative of actual muscle weakness that occurs in humans.

In the work described in this Chapter, an investigation was undertaken into the sensitivity of simulated muscle activations to changes in lower limb muscle volume in a model of human walking. A normative range of muscle volumes were calculated using the data collected from ten typically developing adolescent subjects, as described in the previous chapter. This data was used to alter the muscle strengths of the gait2392 OpenSim generic human walking model. Seven models were created to represent this range and muscle activations computed for each one to drive them to produce the same set of experimental kinematics and kinetics over a single gait cycle. Differences in the resulting simulated muscle activations were then compared and hence the sensitivity of the model to changes in muscle strength was demonstrated.

4.2. Methodology

4.2.1. Capturing Human Walking Data

Ten adolescents with spastic diplegic cerebral palsy and ten typically developing control subjects were recruited for the study following the methods and selection criteria described in section 2.4. In addition to the muscle morphology data collected from the case and control groups, as described in Chapter 3, walking kinematic and kinetic data was also collected from all subjects using an opto-electrical motion capture system (Vicon MX system, T-series cameras, Oxford Metrics Group, Oxford, UK) and three strain-gauge AMTI OR6 force-plates (AMTI, MA, USA), following the methods described in Chapter 2.

4.2.2. Setting up the Models

As physiological cross-sectional area is directly proportional to the maximum tension that can be generated by a muscle (Lieber & Fridén, 2000) this parameter was to be used to scale the strength of the musculo-skeletal model for use in the sensitivity analysis. However, due to difficulties collecting architectural data (fascicle lengths and angles) as described in Chapter 3, and because muscle volume data was successfully collected on many more lower-limb muscles than was possible for PCSA due to the different imaging

modalities used, it was decided that muscle volume data would be used to scale the models as this made the most comprehensive use of the collected data. The normative range of muscle volume for each muscle was represented by seven data points calculated from the normalised muscle volume range of the control group data (Table 4.1).

Data Point	1	2	3	4	5	6	7
	min	LIQR	mid LIQR-med	median	mid UIQR-med	UIQR	max
Percentile	0%	25%	33%	50%	67%	75%	100%
ADDS	7.22	8.49	9.03	9.58	10.45	11.32	12.77
BFLH	1.96	2.16	2.30	2.43	2.54	2.65	3.12
BFSH	0.84	1.13	1.22	1.31	1.47	1.62	2.05
GlutMax	8.41	9.19	9.89	10.59	11.31	12.02	13.63
GlutMed	2.95	3.57	3.83	4.09	4.22	4.34	4.59
GlutMin	0.93	1.00	1.11	1.22	1.29	1.36	1.61
GRA	0.85	1.00	1.12	1.24	1.37	1.50	2.00
LG	1.24	1.65	1.71	1.77	1.88	1.99	2.17
MG	2.68	2.94	3.11	3.28	3.43	3.58	4.19
RF	2.39	2.69	3.08	3.46	3.60	3.74	3.81
SAR	1.41	1.73	1.86	1.99	2.26	2.54	2.97
SM	2.26	2.51	2.62	2.72	2.84	2.97	3.51
SOL	4.26	5.48	5.78	6.08	6.40	6.73	7.46
ST	1.42	1.77	1.96	2.14	2.26	2.38	3.55
TA	1.34	1.37	1.50	1.62	1.71	1.80	2.02
TP	0.98	1.13	1.19	1.26	1.28	1.31	1.64
VI	4.55	4.96	5.51	6.06	6.53	7.00	7.67
VL	6.20	6.91	7.29	7.67	8.63	9.60	10.29
VM	3.73	4.86	5.22	5.58	6.01	6.45	6.77

Table 4.1 – Normative range of muscle volumes. Seven normalised muscle volume data points to represent the normative range of muscle volumes collected from the control group (cm^3/kg)
min = minimum, LIQR = lower limit of inter-quartile range, mid LIQR-med = mean value of LIQR and median, mid UIQR-med = mean value of UIQR and median, UIQR = upper limit of inter-quartile range, max = maximum, muscle codes as defined in Chapter 3.

However, muscle volume is not one of the variables that can be proportionately scaled to a single OpenSim muscle actuator parameter, as shown in Table 3.1, and so a parameter conversion was necessary in order to enable appropriate scaling. This was carried out in two steps: firstly, the muscle actuator strength parameter, *max_isometric_force*, was converted to physiological cross-sectional area using the specific tension of $61N/cm^2$, used to create the original models (Delp, 1990); secondly, physiological cross-sectional area was

converted to volume using Equation 4.1, a rearranged version of Equation 3.2. Fascicle length and pennation values were taken from the muscle actuator parameters *optimal_fiber_length* and *pennation* respectively. The muscle volumes were then normalised to model body mass.

Equation 4.1

$$V_m = \frac{PCSA_m \cdot L_{f,m}}{\cos(\theta_m)}$$

Rearranged from Equation 3.2

$$PCSA_m = \frac{V_m \cdot \cos(\theta_m)}{L_{f,m}}$$

where:

V_m	is normalised muscle volume for muscle *m*
$PCSA_m$	is normalised muscle volume for muscle *m*
θ_m	is muscle pennation angle for muscle *m*
$L_{f,m}$	is the fascicle length for muscle *m*

Next it was necessary to select a baseline model from which to generate the range of sensitivity models. The gait2392 model was chosen and underwent scaling and marker adjustment (as described in Chapter 2) based on the control subject with mass closest to the control group median mass to avoid extremes of body size. Finally, seven versions of the baseline model were created with varied muscle strengths as determined by multiplying the *max_isometric_force* of each muscle actuator by the appropriate volume ratios (Equation 4.2).

Equation 4.2

$$R_{m,i} = \frac{N_{m,i}}{B_m}$$

where:

$R_{m,i}$	is volume Ratio for the m_{th} muscle for the i_{th} sensitivity model
$N_{m,i}$	is Normative muscle volume for the m_{th} muscle for the i_{th} sensitivity model
B_m	is Baseline model muscle actuator volume for the m_{th} muscle

For muscle actuators for which there were no experimental data, the mean volume ratio of all measured muscles was used. The resulting seven models (Table 4.2) therefore represented a range of muscle strengths from weak to strong as defined by the control muscle volume data measured in Chapter 3.

Percentile	0%	25%	38%	50%	63%	75%	100%
Model code	5b	5	6	7	8	9	10
R (vol. ratio)	0.82	0.96	1.03	1.11	1.18	1.26	1.44
Description	min	v. weak	weak	median	strong	v. strong	max

Table 4.2 – Mean volume ratios (R) and descriptions of the seven sensitivity models

An additional number of models were created to investigate the sensitivity of the simulations to the variation in hamstring, gastrocnemius or soleus muscle strength specifically. These models were copies of the median strength model (Model07 - Table 4.2) with additional modification of the appropriate muscles as outlined in Table 4.3.

	hamstrings				medial & lateral gastrocnemius				soleus			
Percentile	25%	38%	63%	75%	25%	38%	63%	75%	25%	38%	63%	75%
Model code	11	12	13	14	15	16	17	18	19	20	21	22
R (vol. ratio)	0.74	0.79	0.88	0.93	1.22	1.27	1.40	1.48	1.01	1.07	1.18	1.24
Description	very weak	weak	strong	very strong	very weak	weak	strong	very strong	very weak	weak	strong	very strong

Table 4.3 – Mean volume ratios (R) and descriptions of the additional sensitivity models

4.2.3. Simulations and Analysis

Using the gait data collected from the control subject chosen to create the baseline model, one walking trial was selected that contained three successive force-plate hits to ensure kinetic data was available over a whole gait cycle. Following the SimTrack method described in Chapter 2, marker trajectories and ground-reaction-force data from this gait cycle were input into OpenSim, and Inverse Kinematics, Residual Reduction and both Static Optimisation and Computed Muscle Control tools were run over this data range to calculate joint kinematics and two sets of muscle actuator activations for comparison. This was carried out for the baseline model and all eighteen sensitivity models (Table 4.2 and Table 4.3).

Analysis was carried out using Matlab (The Mathworks™ Inc., MA, USA). Sensitivity of the simulated muscle actuator activations to changes in muscle strength were then calculated using the following normalised root mean square error (RMSE) method (Equation 4.3).

- Activation data for each muscle actuator was re-sampled to 201 data-points over the gait cycle.
- RMSE between each instance of the model and the baseline model was calculated over the whole gait cycle for each muscle actuator for all muscle actuators in the lower limb on the side of the gait cycle selected (e.g. left or right).
- RMSE values for each muscle actuator were then normalised by dividing by the mean activation of that muscle of the baseline model. Results were then reported as percentages.

Equation 4.3

$$NRMSE_{s,m} = \frac{\sqrt{\sum_1^n \left[\left(A_{n,s,m} - A_{n,bl,m}\right)^2\right]}}{\overline{A}_{bl,m}} \times 100$$

where: *NRMSE* is normalised root mean square error (%)

A is simulated muscle actuator activation

subscripts:

s = s^{th} sensitivity model (18 sensitivity models)

m = m^{th} muscle actuator (43 muscle actuators)

n = n^{th} data-point (201 data-points)

bl = baseline sensitivity model

4.3. Results

The age, height, mass and mean muscle volume ratio (R) for all ten control subjects used to collate the normative muscle volume range for adolescents is shown in Table 4.4. The subject chosen to create the baseline model was Control08 as the mass (59.2kg) was closest to the control group median mass (60.1kg). Coincidentally, the height of Control08 was equal to the control group median height indicating that Control08 was a suitable mid-range subject for both height and mass. Motion capture data of a right leg gait cycle with continuous force-plate data from this subject was chosen for the sensitivity analysis.

Control	01	02	03	04	05	06	07	08	09	10	Gait2392
Age (years)	12.4	10.6	18.6	14.3	18.6	11.9	14.0	16.5	17.4	12.4	-
Height (m)	1.57	1.37	1.75	1.70	1.64	1.64	1.82	1.68	1.80	1.57	1.8
Mass (kg)	47	39	68	83	58	56	61	59	83	75	75
R (vol. ratio)	1.0	0.6	1.1	1.2	0.9	1.2	1.3	1.1	1.7	1.7	-

Table 4.4 – Mean volume ratios (R) for all ten control subjects

4.3.1. Scaling and Inverse Kinematics (IK)

Scaling and Inverse Kinematics tools were run successfully to create the input joint angles for the subsequent simulations. A comparison between the kinematics created using the Vicon Plug-in-Gait model and the kinematics resulting from the OpenSim Inverse Kinematics tool can be seen in Figure 4.1. The two kinematic datasets are not expected to be identical due to the differences between the two models (Table 4.5: in particular Plug-in-Gait ankle rotation and OpenSim subtalar_angle are not directly equivalent, however, this problem is overcome by locking the subtalar_angle at neutral, as explained in Chapter 2). However, as a rough comparison it shows that appropriate joint angles have been input to the simulations for this walk. Some deviation can be seen between the two kinematic datasets in hip rotation which is likely to have been caused by skin movement under the thigh marker (THI). A portion of this movement will be interpreted by the Plug-in-Gait model as thigh rotation but as the OpenSim Inverse Kinematics tool calculates rotations based on all the markers fixed to the thigh segment, erratic movement of one single marker will be smoothed out. Typically developing adult kinematics, as collected by

the Guy's Hospital Gait Laboratory, is also shown in Figure 4.1. The kinematics can be seen to broadly lie within these normal limits.

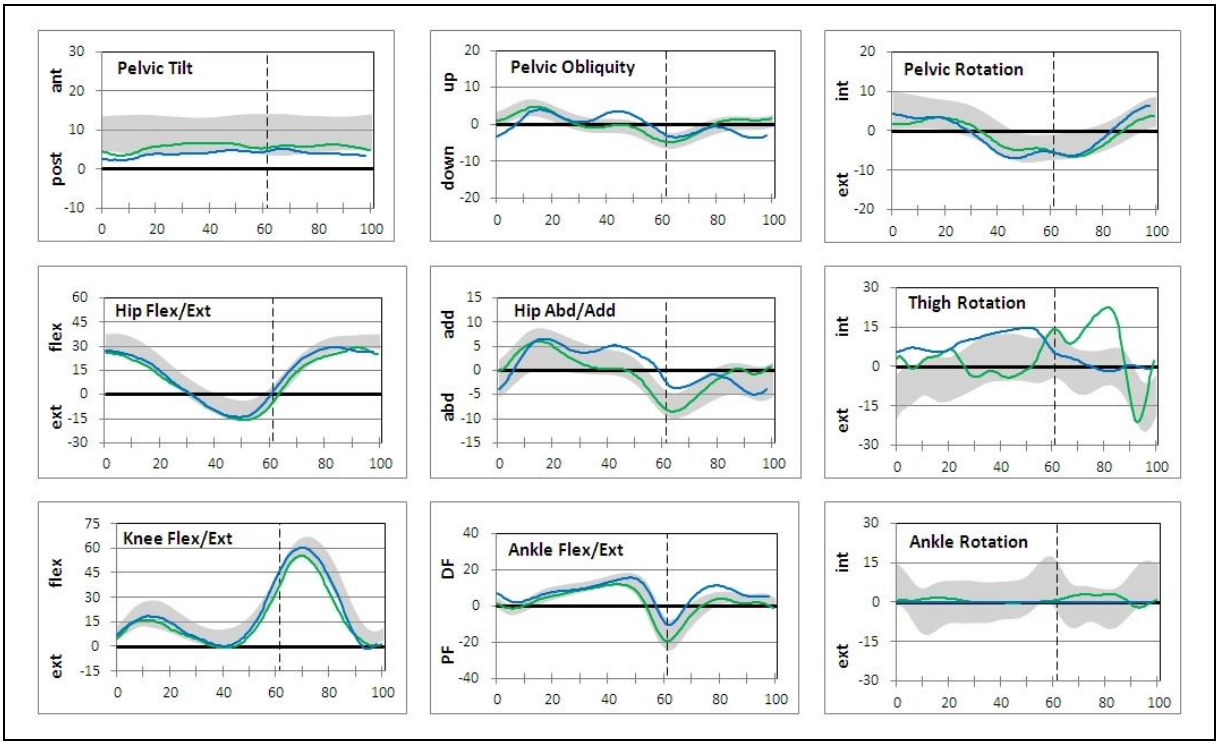

Figure 4.1 – Kinematic comparison between Vicon Plug-in-Gait and OpenSim. A comparison between the kinematics created using the Vicon Plug-in-Gait model (green curves) and the kinematics resulting from the OpenSim Inverse Kinematics tool (blue curves). The grey band shows the control limits for typically developing adults (Guy's Hospital Gait Laboratory).
Vertical axis shows joint angles measured in degrees, horizontal axis shows % gait cycle. Flex/Ext = flexion/extension, Abd/Add = abduction/adduction, post = posterior, ant = anterior, ext = external, int = internal, PF = plantarflexion, DF = dorsiflexion

Vicon Plug-in-Gait Joint Angle	OpenSim Coordinate
pelvis1 (tilt)	pelvis_tilt
pelvis2 (obliquity)	pelvis_list
pelvis3 (rotation)	pelvis_rotation
hip1 (flexion)	hip_flexion
hip2 (abduction)	hip_adduction
hip3 (rotation)	hip_rotation
knee1 (flexion)	knee_angle
ankle1 (dorsiflexion)	ankle_angle
ankle3 (rotation)	subtalar_angle

Table 4.5 – Comparison joint angles between the Vicon Plug-in-Gait and OpenSim gait2392 models

4.3.2. Residual Reduction Algorithm (RRA)

The Residual Reduction Algorithm tool was run twice on the simulation data to minimise mismatches between the recorded kinematics and kinetics and hence reduce the residual actuator forces that are necessary to ensure the simulation follows the prescribed kinematics. The magnitude of these six residual forces and moments over the gait cycle before and after running the Residual Reduction Algorithm tool are shown in Figure 4.2 Model changes and mean residual reductions can be seen in Figure 4.3.

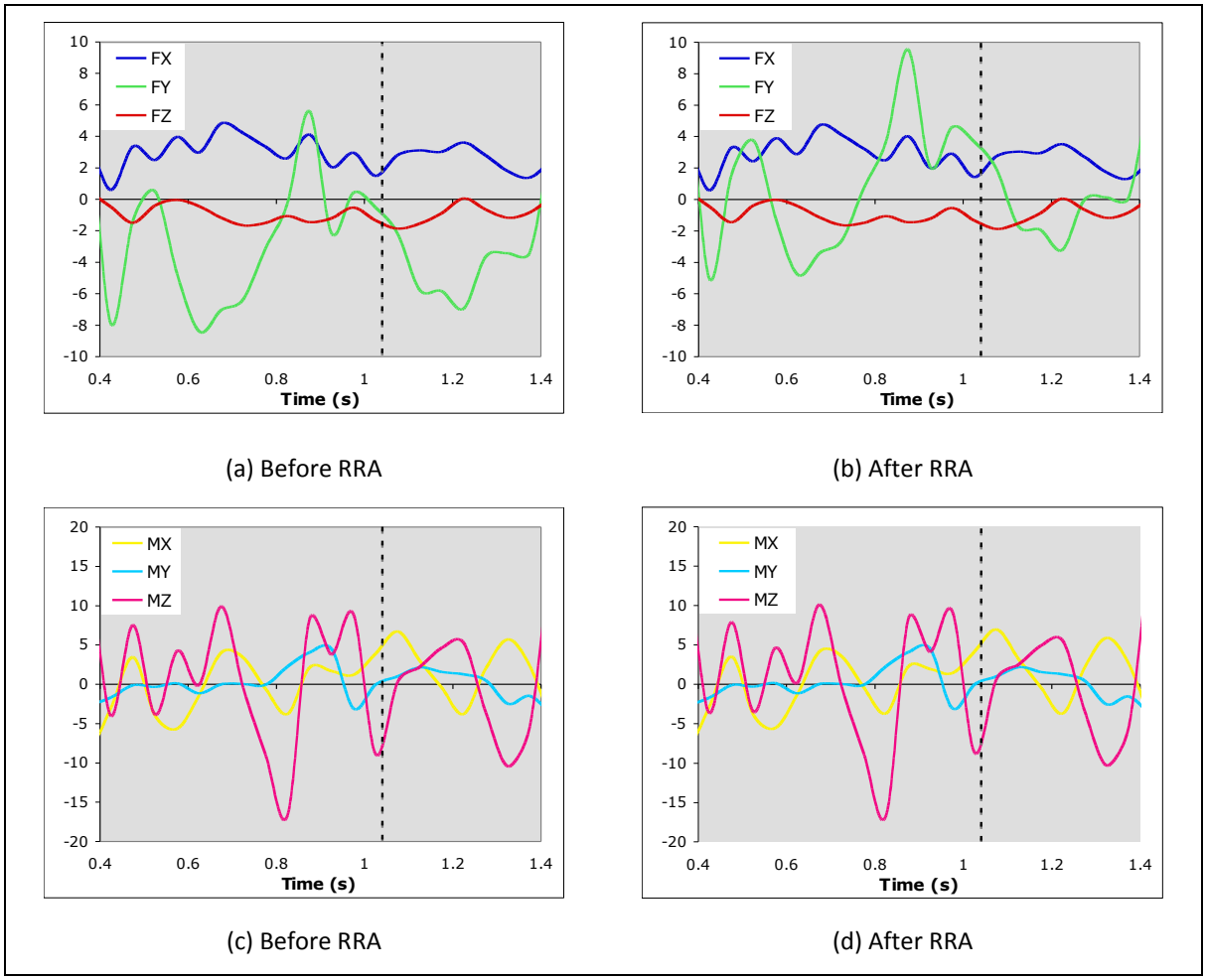

Figure 4.2 – Residual actuator forces and moments applied over the gait cycle to the model pelvis segment to minimise mismatch between the kinematics as calculated from the OpenSim Inverse Kinematics tool and the recorded ground-reaction-force. (a) and (b) show the residual forces (N) before and after running the Residual Reduction Algorithm (RRA). (c) and (d) show the residual moments (Nm) before and after RRA. X, Y. Z represent anterior/posterior, vertical and medial/lateral axes respectively.

It is difficult to see any changes in the residual actuators from Figure 4.2, except the mean shift of Fy closer to zero, but the magnitudes of these residuals give us an insight into the likelihood that a biomechanical walking simulation will successfully run using this model and the kinematic/kinetic input datasets.

The residual forces necessary to keep the kinematics and kinetics matched in the X (anterior/posterior) and Z (medial/lateral) directions are less than 5N and reasonably stable. The residual force in the Y (vertical) direction is more variable and larger, peaking at c.10N (2% bodyweight). The maximum residual moment is found around the Z (medial-lateral) axis and peaks at c.17Nm. The residual acceptability thresholds recommended by the OpenSim developers were residual forces and moments below 10N and 50Nm respectively (Table 2.4). It is difficult to compare these values to typical gait kinetics as these residuals are global moments applied to the whole model at the pelvis segment rather than individual joint moments. The appropriateness of these thresholds was discussed in section 2.2.3 and 50Nm was considered too high. However, the purpose of this sensitivity analysis was to test the SimTrack method of movement simulation and therefore, irrespective of this concern, both these residual acceptability thresholds were adopted and hence all residuals were deemed acceptable.

As described in section 2.2.3, outputs from the first run of the Residual Reduction Algorithm include suggested changes to the model mass (to reduce the Fy residual) and suggested changes to the position of the torso centre of mass (to reduce the Mx and Mz residuals). These changes were implemented before the second run of the residual reduction tool. However, the OpenSim software summarises each of these residuals using an arithmetic mean and, due to the cancellation of positive and negative values, this can give an overly generous and misleading impression of the success of residual reduction. This problem can be simply avoided by using the mean of the absolute residuals but this has to be calculated independently from the software.

The difference between these two methods of summarising residuals can be seen in Figure 4.3. The visual inspection of Figure 4.2 described above showed only the Fy residual successfully reduced. This is more clearly represented by mean absolute calculation.

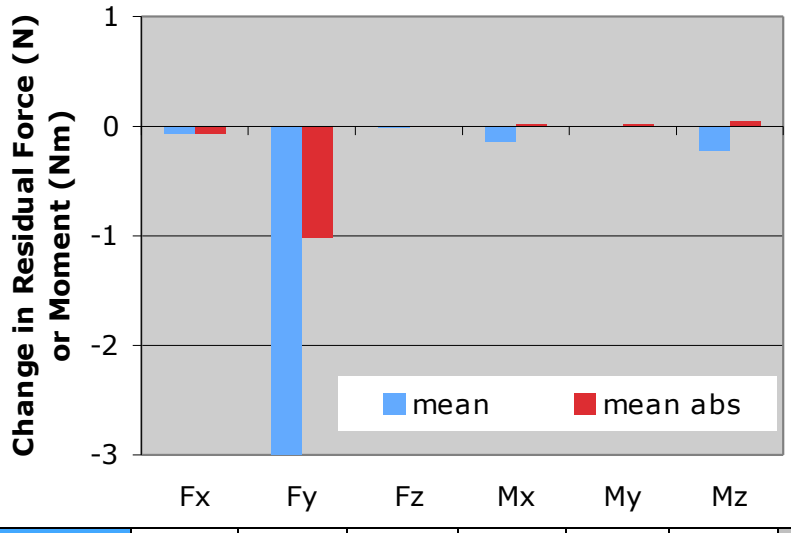

	Fx	Fy	Fz	Mx	My	Mz	Δmass (kg)	ΔCoMx (mm)	ΔCoMz (mm)
Before RRA	2.66	-3.50	-0.67	-0.17	0.09	-0.36	0.3	4	-2
After RRA	2.59	-0.46	-0.66	-0.03	0.08	-0.13	0.0	1	1
Before RRA	2.70	4.83	0.85	3.78	3.39	7.77			
After RRA	2.63	3.81	0.84	3.80	3.41	7.82			

Figure 4.3 – Mean changes in residual actuator forces and moments after running the Residual Reduction Algorithm. The table shows the mean residual actuator forces and moments for the sensitivity analysis walking trial before and after running the Residual Reduction Algorithm (RRA) twice. Suggested model mass changes (Δmass) and torso centre of mass position changes in the anterior/posterior direction (ΔCoMx) and medial/lateral direction (ΔCoMz) for each run are also shown. The figure shows the change (increase positive, reduction negative) for each of the six residual actuators as calculated by OpenSim using a arithmetic mean over the gait cycle or as calculated using the arithmetic mean of the absolute value (mean abs) over the gait cycle.

4.3.3. Static Optimisation (SO) and Computed Muscle Control (CMC)

Experimental kinematics and force-plate data during a right leg gait cycle from the baseline subject were used as input to both the Static Optimisation and the Computed Muscle Control tools in OpenSim to obtain simulated muscle actuator activations for each of the sensitivity models. Output kinematics from the Computed Muscle Control tool showed successful tracking of the input kinematics to within 1°. Output kinematics are not provided by the Static Optimisation tool.

The reserve forces/moments and residuals moments shown in Figure 4.4 are generally within acceptable limits as outlined in section 2.2.3 – again these limits have been adopted despite concerns of their appropriateness in order to test the SimTrack methodology. Residuals for the other sensitivity models were similar except for the weakest model (5b) which had larger residuals and a second ankle_angle_r spike at 0.85s (but still within acceptable limits) and the strongest model (10) which had lower residual actuator magnitudes.

Individual muscle actuator activations over the gait cycle for models 5b-10 from both Static Optimisation and Computed Muscle Control tools are shown in Figure 4.5. In the Computed Muscle Control data some unstable behaviour of the tibialis anterior actuator can be seen which appears to be propagating into other actuators, specifically toe flexors and plantarflexors. In addition, there are some unexpected peaks of high activity/saturation (even for the strong model) which suggests some form of problem has occurred running the Computed Muscle Control algorithm. This will be discussed in more detail in Chapter 5, where more than one set of input kinematics/ground-reaction-forces is available to allow a more detailed investigation into possible causes of the problem. For the rest of this chapter therefore, only actuator activations as calculated using the Static Optimisation tool will be discussed.

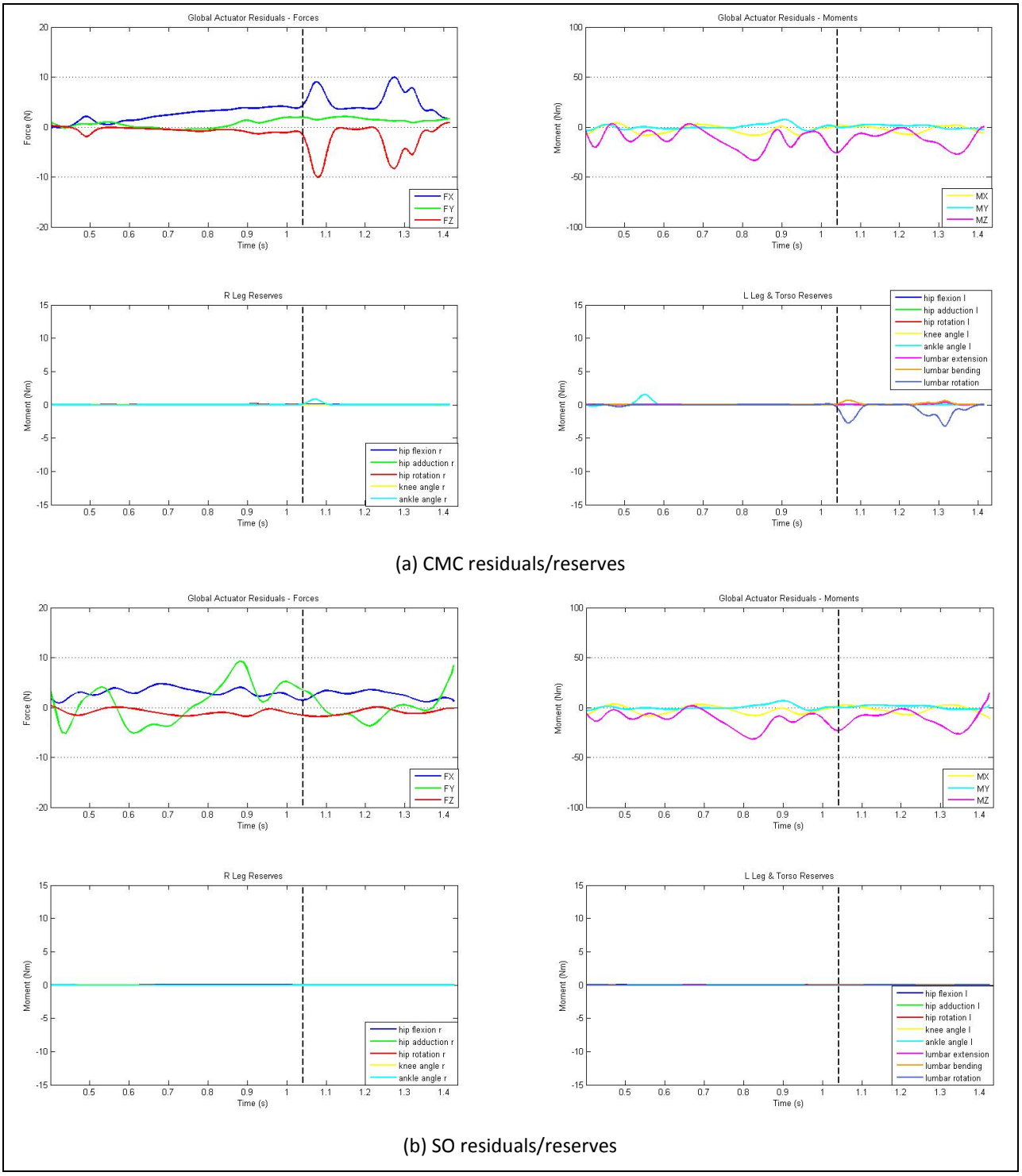

Figure 4.4 – (a) CMC & (b) SO residual forces/moments & reserve moments for the baseline model (Model07) . Acceptable limits: reserve forces ±10N, reserve moments ±50Nm, residual hip flexion/adduction ±5.9 Nm, hip rotation 1.2Nm, knee flexion 3.6Nm, ankle flexion 11.3Nm. X ,Y. Z represent anterior/posterior, vertical and medial/lateral axes respectively.

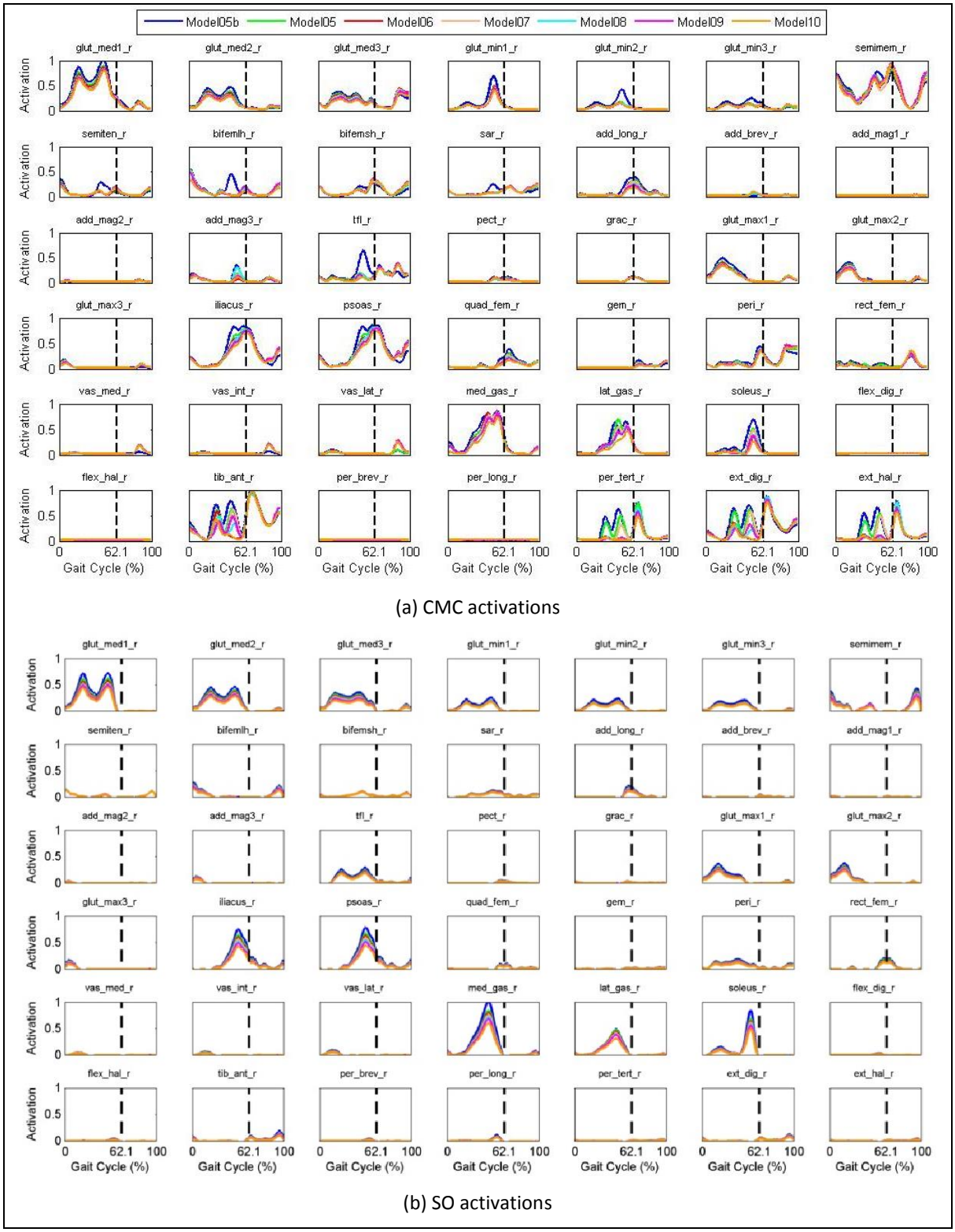

(a) CMC activations

(b) SO activations

Figure 4.5 – Muscle actuator sensitivity. (a) CMC and (b) SO simulated activations for 42 of the models' right lower limb muscle actuators for each of the seven principal sensitivity models.

In the Static Optimisation data all actuators show an increase in activation with decreasing model strength. This is confirmed by Figure 4.6 which shows the mean normalised RMSE values calculated from all 43 right lower limb actuators for the six globally altered models (5b-10). A normalised RMSE value of 100% would indicate that the RMS difference between the new activation and the baseline activation was equivalent to the magnitude of the mean baseline activation. As would be expected, there is a general increase in muscle actuator activation for the weakened models and a general decrease in activation for the strengthened models.

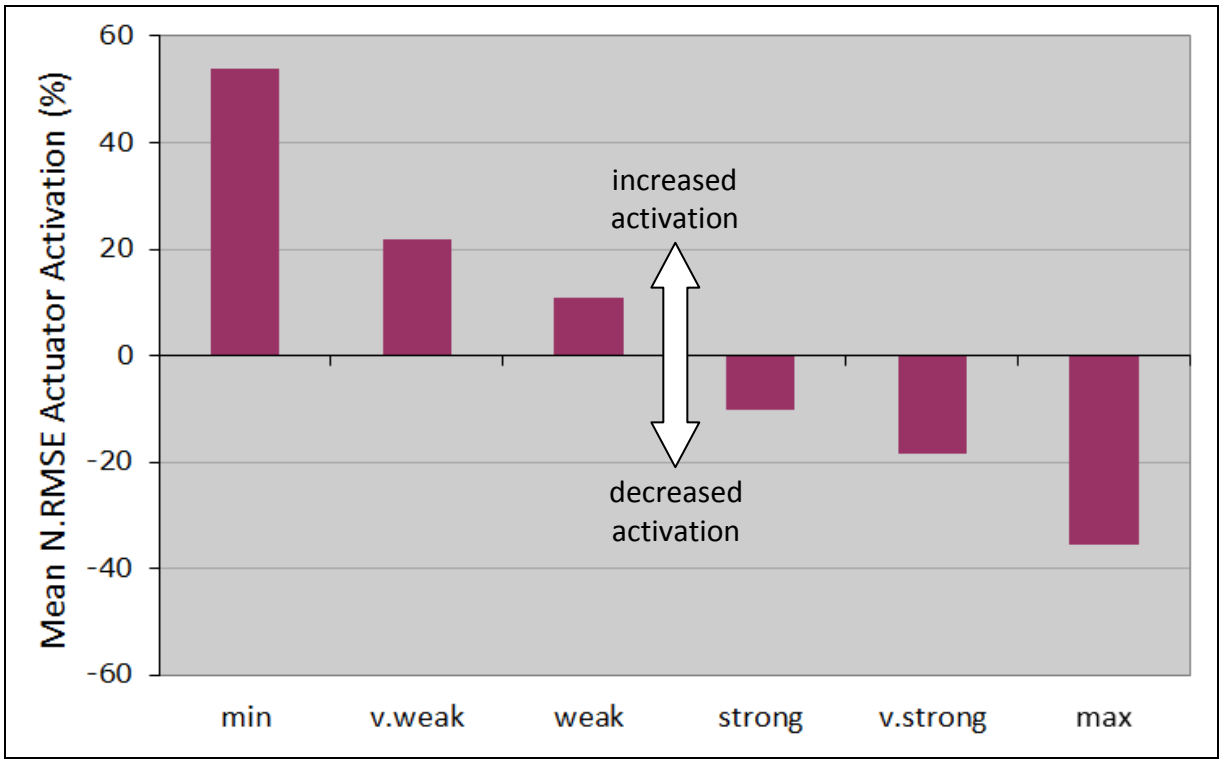

Figure 4.6 – Change in SO activations: mean normalised root mean square errors (NRMSE) for each of the six globally altered models (Models 5b-10) calculated from the mean NRMSE over all 43 right lower limb actuators. A positive value was assigned to models with a general increase in activation and negative to models with a general decrease in activation compared to the baseline model

Changes in muscle actuator activation over the gait cycle for variation in the strength of the hamstrings (Models 11-14), gastrocnemius (Models 15-18), and soleus (Models 19-22) are shown in Figure 4.7, Figure 4.8 and Figure 4.9 respectively.

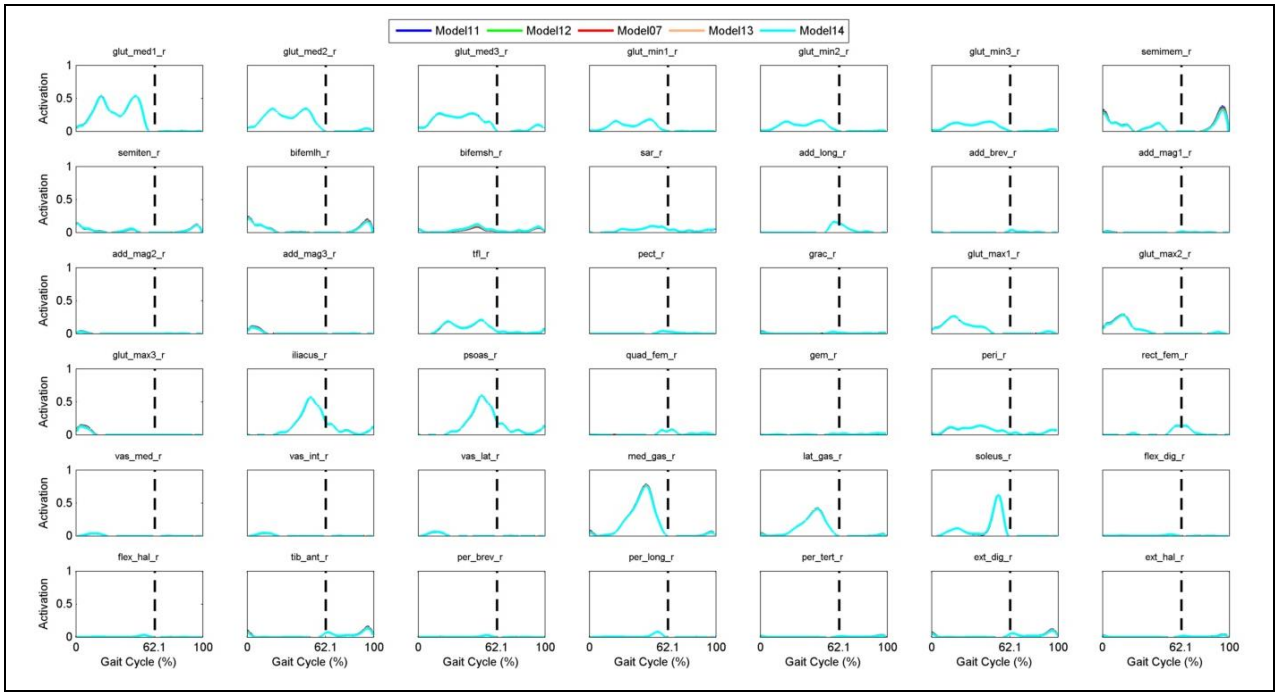

Figure 4.7 – Hamstring strength sensitivity. SO simulated muscle actuator activations for 42 of the models' right lower limb muscle actuators for each of the four sensitivity models 11-14 compared to the baseline Model07

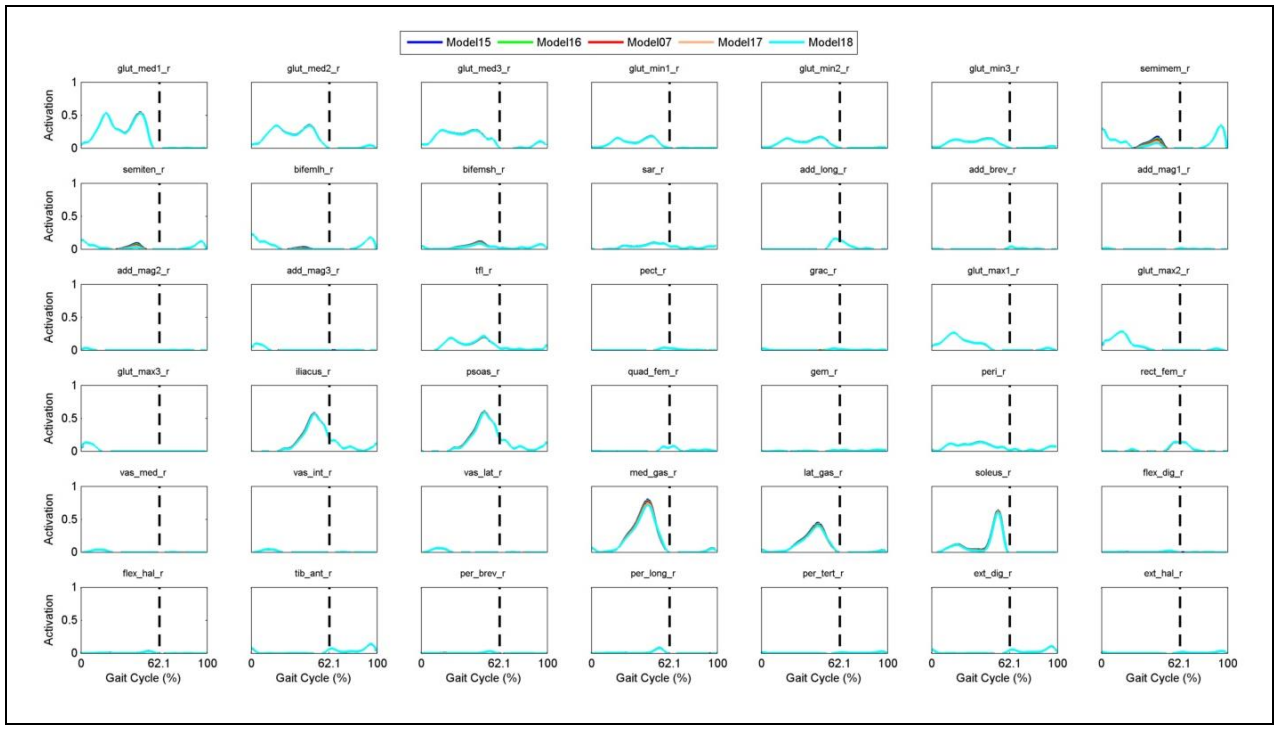

Figure 4.8 – Gastrocnemius strength sensitivity. SO simulated muscle actuator activations for 42 of the models' right lower limb muscle actuators for each of the four sensitivity models 15-18 compared to the baseline Model07

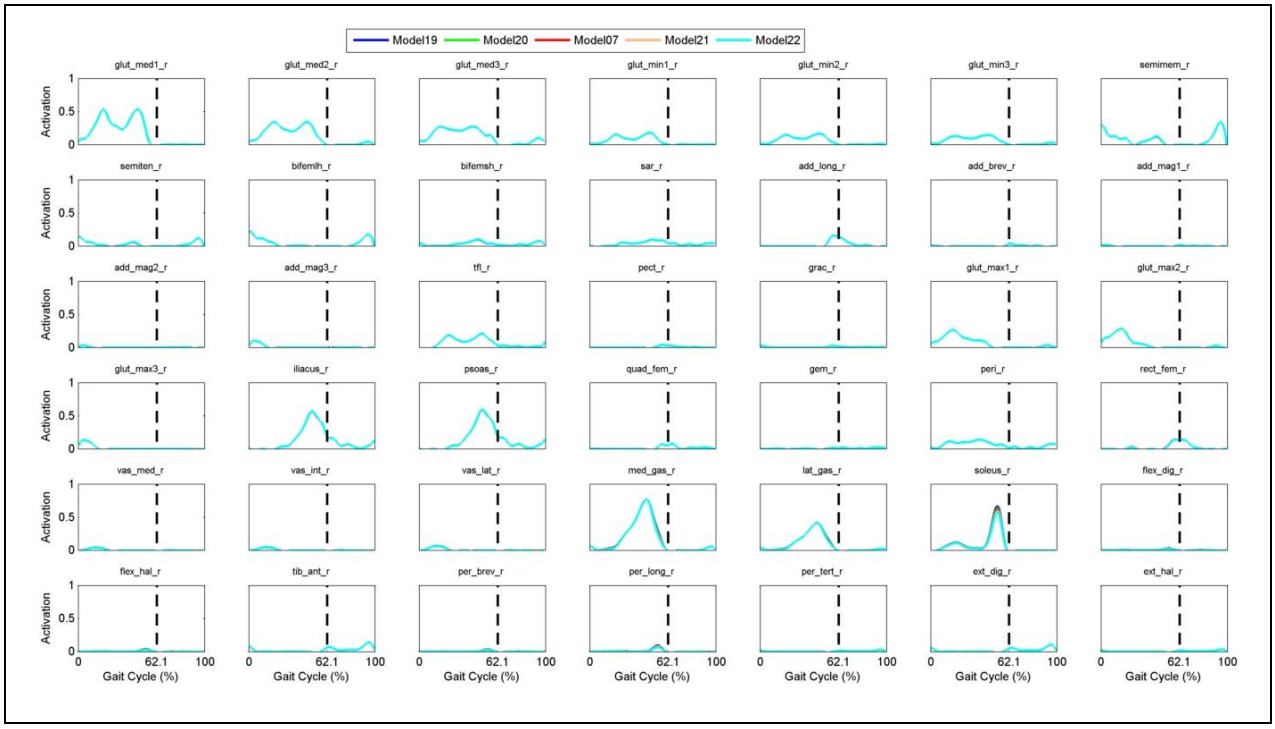

Figure 4.9 – Soleus strength sensitivity. SO simulated muscle actuator activations for 42 of the models' right lower limb muscle actuators for each of the four sensitivity models 19-22 compared to the baseline Model07

4.4. Discussion

The gait2392 model was created using adult cadaveric data with modified muscle strengths to match experimental data of adult joint torques and is based on a subject of height 1.8m and mass 75kg. As muscle strengths are not altered when this generic model is scaled to match the stature of smaller subjects, muscle strengths in these scaled models were expected to be inappropriate (too large) for child or adolescent populations. Muscle volumes were collected from ten typically developing child/adolescent subjects (mean(SD): age 15.4(3.2)years, height 1.7(0.1)m, mass 62.8(14.4)kg) and compared to the volumes of the gait2392 model using a muscle volume ratio (Equation 4.2) in order to test this supposition.

A mean volume ratio of less than one would imply that on average the subject has smaller muscle volumes than the generic gait2392 model. The mean and standard deviation of the mean muscle volume ratios for the control subjects (Table 4.4) were 1.18(0.34). Muscle

volumes in the child/adolescent group were therefore not generally smaller than the generic model.

An inspection of the relationships between muscle volume and potential predictors was carried out using simple linear regression (Figure 4.10). The deviation in muscle volume (and hence strength) from the generic gait2392 model appears to be most correlated to differences in body mass, and to a smaller degree, to differences in height or BMI, with little correlation found with age. Due to the small sample size there was not enough data to perform a fuller analysis to develop a predictive equation for muscle volume based on anthropometric parameters. It is likely therefore that the muscle strengths of the gait2392 model would be appropriate for child populations of typically developing subjects of similar weight to those used in this study, but maybe inappropriate for lighter children. It would also be useful for the OpenSim scaling tool to alter the *max_isometric_force* muscle parameters by the ratio of the subject mass/generic model mass.

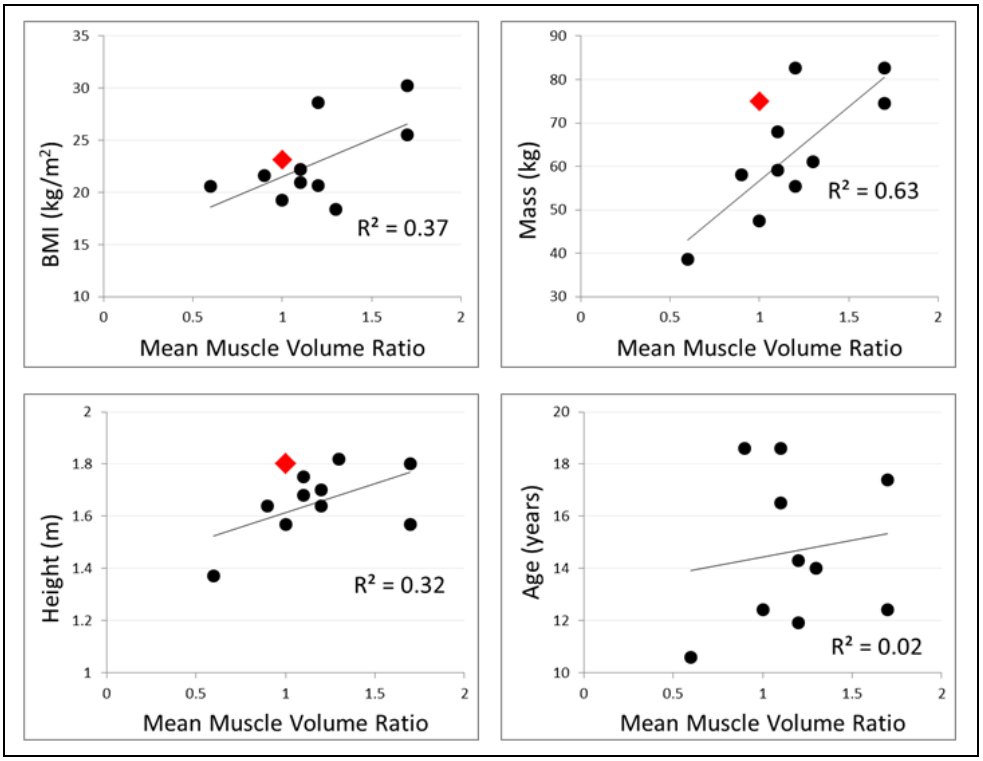

Figure 4.10 – Correlation of control group parameters against muscle volume. Correlation via linear regression of BMI, mass, height and age against the mean muscle volume ratio for each of the ten control subjects. BMI, height and mass of the un-scaled gait2392 model are shown in red.

The mean muscle volume ratios for the seven principal sensitivity models (Table 4.2) were calculated from this normative range of adolescent data using muscle volumes normalised to body mass. As the baseline model, Control08, had a similar mass (59.2kg) to that of the gait2392 model (75kg) the mean volume ratios for the sensitivity models were closer to unity than for the individual control subjects. The strengths of the sensitivity models were therefore more similar in magnitude to the gait2392 model than they would have been by using other control subjects.

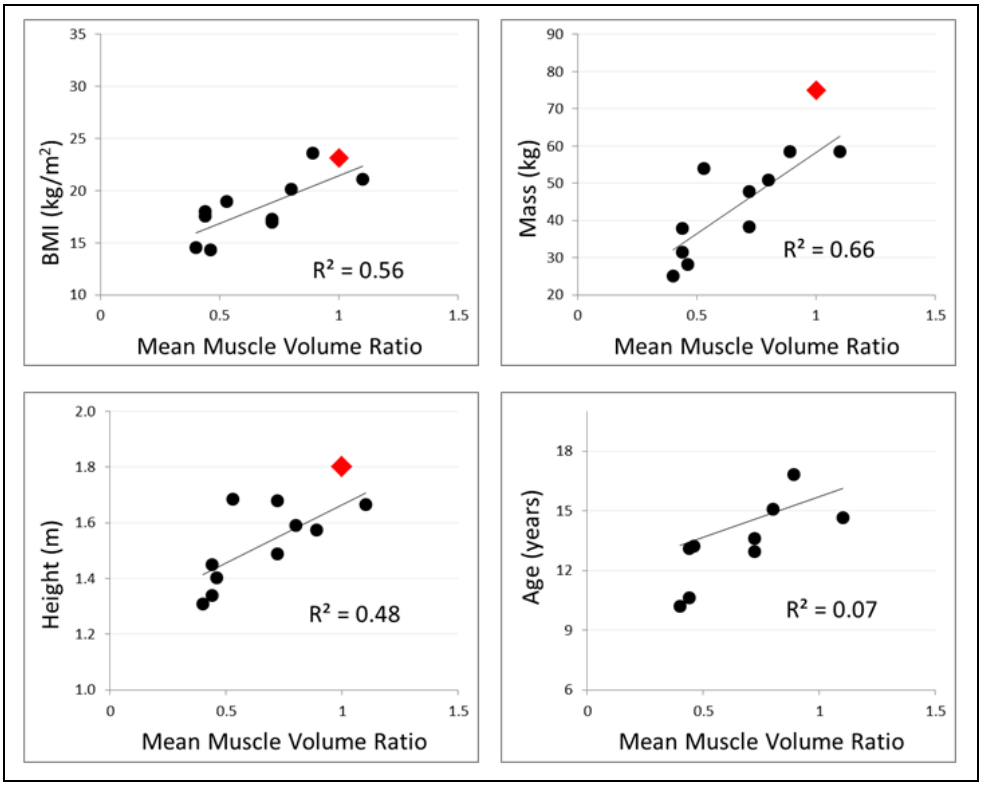

Figure 4.11 – Correlation of case group parameters against muscle volume. Correlation via linear regression of BMI, mass, height and age against the mean muscle volume ratio for each of the ten case subjects. BMI, height and mass of the un-scaled gait2392 model are shown in red.

Although not normally the case for the more ambulant individuals, subjects with cerebral palsy are often smaller and lighter than their typically developing peers (Day et al., 2007). This was shown to be true in the case and control data analysed in Chapter 3. The mean and standard deviation of mean muscle volume ratios for the case subjects were 0.7(0.2) with a range from 0.4 to 1.1. This shows that muscle volumes in this group are generally smaller than the generic model and so it would be ill advised to use this model in

simulations of cerebral palsy subjects without appropriate scaling of muscle strength. The simple linear regression analysis (Figure 4.11) shows the deviation in muscle volume from the generic gait2392 model appears to be most correlated to differences in body mass. Once again therefore it is suggested that the OpenSim scaling tool should alter the *max_isometric_force* muscle parameters by the ratio of the subject mass/generic model mass.

4.4.1. Activation changes following global alterations of muscle strength

Figure 4.5 shows the individual changes in muscle activation for each of the seven principal sensitivity models in which all muscle strengths were altered, and Figure 4.6 summarises the changes for each model. As expected, both show a clear trend of higher activations for weaker models. In particular, high sensitivity is seen in medial gastrocnemius, soleus, gluteus medius, iliacus and psoas. In addition, there are a number of individual activations which require further comment.

In the weakest model (Model05b) one muscle actuator, medial gastrocnemius, saturates into maximal activation. This can be seen to coincide with a slight increase in activation of the lateral gastrocnemius and a larger increase in activation of the slightly later acting soleus, both of which presumably have been recruited to compensate for the resulting plantarflexion insufficiency. There is also high activation and sensitivity in both the hip flexor actuators iliacus and psoas during pre-swing. High activity is not unexpected in this part of the gait cycle as this is a region of peak hip flexion but the reason for the increased sensitivity is less clear as these actuators were not disproportionately weakened compared to others. It is possible that the optimisation is complicated by muscle actuators operating outside of their optimum lengths but as the Static Optimisation tool does not output muscle fibre lengths this could not be verified.

4.4.2. Activation changes following localised alterations of muscle strength

Changes in activation following alterations to hamstrings, gastrocnemius, and soleus strength are shown in Figure 4.7, Figure 4.8 and Figure 4.9 respectively. The changes in activations are much smaller and more localised to the specific muscle actuators that have been weakened when compared to Figure 4.5 and again, as would be expected, there is a clear trend for increased activation in the weaker models.

Only the soleus is affected during soleus weakening (Figure 4.9). During hamstring weakening the most sensitive muscle actuator appears to be the semimembranosus (Figure 4.7) and during gastrocnemius weakening it is the medial side that appears slightly more sensitive (Figure 4.8). This is likely due to the cost function giving preference to the stronger muscles – in Model07 the semimembranosus is almost as strong as all the other hamstrings combined and the medial head of the gastrocnemius has twice the strength of the lateral head. Muscle weakness can therefore be resolved more "cheaply" by a small increase in activation of the larger muscle rather than a larger increase in activation of smaller ones.

4.4.3. Sensitivity of muscle activation to changes in muscle strength

To assess the sensitivity of the different muscle actuators in these simulations it is necessary to examine the individual root mean square activation differences from the baseline model. The ten most sensitive (largest RMSE) right lower limb actuators were counted from each of the eighteen simulations and the results are displayed below (Figure 4.12).

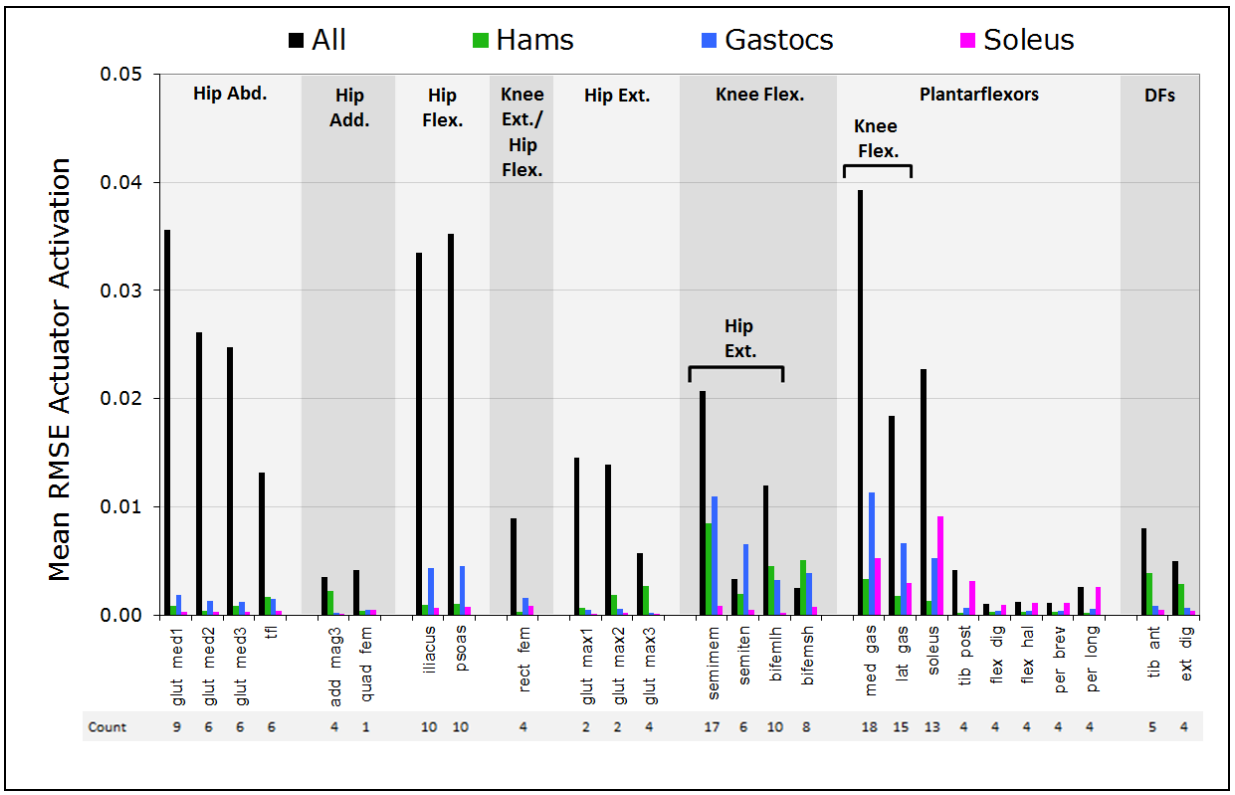

Figure 4.12 – Sensitivity Analysis. Mean root mean square errors (RMSE) for the most sensitive muscle actuators from all eighteen sensitivity simulations. The ten most sensitive actuators were selected from each simulation and compiled. The count number is the number of times an actuator appeared in the top ten (i.e. count = 18, one of the top 10 most sensitive actuators in all 18 simulations).

All = models 05b-10, Hams = models 11-14, Gastrocs = models 15-18, Soleus = models 19-22.

It can be seen that muscle activation sensitivity to global changes in muscle strength is dominated by the plantarflexors (principally the medial gastrocnemius), the hip adductor gluteus medius, and the hip flexors iliacus and psoas. Predictably, muscle activation sensitivity to local changes in muscle strength are localised to the weakened areas. The semimembranosus was most affected during hamstring weakening, and the medial head was more affected during gastrocnemius weakening. A link in sensitivity between the plantarflexors and the hamstrings can also be seen with both muscle actuator groups being affected by weakness at either location, and again with the semimembranosus and medial gastrocnemius being most affected. It is likely that both of these muscle groups are linked via a knee flexion weakness compensatory mechanism. It is the change in activation of the medial hamstrings at late stance during gastrocnemius weakening that is most striking however, as they are more sensitive to this than when they are weakened directly. It is possible that this is a result of the Static Optimisation criterion. As the gastrocnemius

is already very active and the hamstrings quiet during this period of the gait cycle, minimising total muscle activation squared means it “costs” far less to compensate for gastrocnemius knee flexion weakness with an increase in hamstring activity than it does to increase gastrocnemius activity.

4.5. Conclusions and Limitations

A normative range of lower limb muscle volumes in typically developing adolescents were used to scale the strength of the gait2392 OpenSim generic musculo-skeletal model and muscle activations were simulated over a single gait cycle to examine the sensitivity of simulated muscle activation to changes in muscle strength.

In general, small increases in muscle activation were seen for weakened muscles as well as in their synergists confirming that the model is insensitive to muscle strength changes over a normative range. However, larger increases in activation occurred in muscle actuators that approached maximum activation as well as in their synergist and compensatory muscles. This can be seen in Figure 4.5 where the medial gastrocnemius saturates into maximum activation in the weakest model. In such cases the model is very sensitive to changes in muscle strength and so simulated activations must be treated with caution.

As the muscle models in the gait2392 model have been parameterised using data from cadaveric studies of elderly subjects, and because muscle strength is not scaled when the model is resized to match the stature of a new subject, it was expected that the muscle strengths of the gait2392 model would not be appropriate for use in simulations of gait in child/adolescent subjects. However, muscle volumes from an adolescent group of typically developing subjects were found to be similar (as determined by the muscle volume ratio R) to muscle volumes calculated from the model. However, a strong correlation was found between the muscle volume ratio (R) and body mass, implying that the muscle strength of the generic model will become less appropriate for use in simulations of lighter subjects (of any age). It is therefore recommended that the subject/gait2392model mass ratio is

used to scale the *max_isometric_force* parameters of this generic model if it is to be used in subject specific simulations. This may be especially relevant in the simulation of gait in subjects with cerebral palsy as they are often lighter than their typically developing peers. This is confirmed in the case and control subjects recruited for this study (Chapter 3).

5 The level of agreement of simulated muscle activations with activation profiles derived from experimental EMG in typically developing adolescents and adolescents with cerebral palsy during walking

3D, multi-segment, musculo-skeletal models scaled to height, mass and muscle volume, were created for ten typically developing adolescents and ten adolescents with cerebral palsy. Each model's muscle activations were allowed to vary in order to track the subject's recorded walking pattern driven by an algorithm to minimise total muscle activation. The validity of a selection of simulated muscle activations were then determined, using a validity threshold based on intra- and inter-subject variability of activations determined from experimental electromyographic (EMG) data. Using this method, in the reduced set of nine actuators for which EMG data was available, all of the simulated muscle activations in both groups were found to be invalid. After allowing a generous optimisation of the simulated muscle activations in both amplitude and time, valid muscle activations were found in the control group for 5/9 actuators: semitendinosus, semimembranosus, biceps femoris long head, medial gastrocnemius, lateral gastrocnemius; and in the case group for only 3/9 actuators: semimembranosus, rectus femoris and medial gastrocnemius.

5.1. Introduction

The musculo-skeletal modelling software OpenSim is able to calculate muscle actuator activations that drive a model to follow a set of prescribed kinematics. In the work described in the previous chapter, the change in activation over a range of normative model strengths was used as a measure of model sensitivity. The simulations were found to be sufficiently robust to changes in actuator strength to allow bespoke model strengths

to be used. The possibility of using such computed modelling techniques in the analysis and clinical interpretation of biomechanical data is of interest to the clinician but it is important that appropriate validation studies are carried out to ensure the fidelity of the output of any such "black-box" simulations. What is the similarity between calculated muscle activation and experimental measurements of muscle action, i.e. how similar to real human muscle activations are these simulated activations?

The early development of SIMM is documented in Delp (1990) but the validation analysis carried out in this work focused on comparing simulated to experimental joint torque data rather than looking at muscle activations. The combination of less advanced computing power and computationally heavy algorithms such as Dynamic Optimisation that were available at this time made such calculations less practical and hence limited work was carried out using these techniques. Anderson & Pandy (2001) used a dynamic optimisation method with a muscle metabolic energy cost function to calculate muscle actuator activations for a model similar to gait2392 (described in Chapter 2) during a walking task in five typically developing male adults. A qualitative comparison of simulated activations to experimental EMG (normalised to maximum voluntary contractions) was used to validate the model outputs and the two datasets were generally found to be consistent.

Neptune et al. (2001) used a similar model, again based on Scott Delp's work (Delp, 1990), to investigate the contributions of the ankle plantarflexors to human gait in five typically developing male adults. They solved the static indeterminacy problem (section 2.1.3) by using a simulated annealing optimisation algorithm to minimise differences in simulated and experimental kinematics and kinetics. Muscle actuator activations were constrained to ±25% of the gait cycle timings of Perry (1992) and so the brief qualitative comparison of the resulting simulated activations gave a predictably good match. This is an important result as it demonstrates that the model can be successfully driven to follow the desired movement pattern using near normal timing of muscle activations.

Faster methods of calculating muscle activations have since become available which have led to an increased interest in these simulation techniques amongst researchers. Indeed,

the Computed Muscle Control algorithm, outlined by Thelen et al. (2003), when compared to a simulated annealing approach led to a reduction in computational time for a cycling simulation from 160 hours to 10 minutes. Validation of the resulting actuator activations is made by qualitative comparison to experimental EMG timings but as neither EMG collection nor processing methodologies are reported it is difficult to interpret these results. Some later work by Thelen & Anderson (2006) made use of a slightly modified Computed Muscle Control algorithm to simulate muscle activations during walking in ten typically developing adults using the gait2392 model and inputting experimental kinematic and kinetic data. This approach is very similar to one of the methodologies adopted in this chapter, but Thelen & Anderson (2006) validated their results principally by comparing the simulated kinematics and kinetics to the original experimental data and only gave a brief qualitative comparison of their actuator activations to EMG data published in Winter (1990).

A year later Arnold et al. (2007) used muscle actuator activations during human walking calculated from the Computed Muscle Control algorithm as input to a perturbation analysis to examine muscle contributions to knee motion during the swing phase of six typically developing children. They refer to a comparison of simulated actuator activations to experimental surface EMG for the hamstrings, rectus femoris, gastrocnemius and tibialis anterior, finding similarities in most cases, but this data is not reported in the paper and only a comparison to the EMG timings of Perry (1992) is given. They also report that one or more actuators required constraint to eliminate inappropriate excitations but do not give any further details on which actuators or how this was carried out.

Liu et al. (2008) also carried out a perturbation analysis using the gait2392 model looking at the change in muscle contributions to support and progression over a range of walking speeds in typically developing subjects. The simulated muscle activations averaged across all eight subjects were presented graphically alongside experimental surface EMG envelopes normalised to the peak EMG signal for each muscle across all walking speeds and averaged across all subjects. The authors made no comment on this comparison and described the EMG data as highly variable. Looking at their graphs (Figure 4 – Liu et al.,

2008) there is generally a good agreement in both timing and magnitude between simulated activations and EMG except: timing of simulated plantarflexion action is delayed; simulated rectus femoris activity is low during early stance; and both rectus femoris and vastus medialis simulated activity is early in swing.

Steele et al. (2010) carried out a similar approach and examined muscle contributions to support and progression during single support in crouch gait of nine subjects. Surface EMG data was collected from the medial hamstrings, biceps femoris long head, rectus femoris, gastrocnemius and tibialis anterior. Both EMG data and simulated actuator activations were normalised to the peak value of each muscle of each subject for comparison. The authors described the two data sets as exhibiting similar on-off patterns but highlighted excessive simulated rectus femoris activity during swing and reduced simulated biceps femoris activity during terminal swing (although this comment does not agree with their Figure 3 which shows a good match for biceps femoris activity and reduced semimembranosus activity in terminal swing). The authors also carried out an additional analysis looking at the sensitivity of the perturbation technique to mismatches between the simulated activations and experimental EMG. Simulated activations of ten actuators were constrained to better match the appropriate EMG and the perturbation analysis was repeated for one subject. Magnitudes of the muscle contributions to support and progression were altered but the directions stayed the same. The authors concluded that as these changes did not alter their conclusions it was therefore appropriate to have used un-constrained actuator activations in their principal analysis. This is a surprising argument as altered activations should lead to changes in the timing of muscle contributions.

Lin et al. (2011) carried out an investigation into the differences of muscle force estimates from three different methods commonly reported in the literature: Static Optimisation, Computed Muscle Control, and Neuro-Musculo-Skeletal Tracking. Using an optical motion capture system and force-plates they collected walking and running data for a single healthy adult female subject whilst simultaneously recording surface EMG data from seven lower-limb muscles. The muscle forces estimated by the three different methods

for one walking trial and one running trial were then compared using correlation coefficients. The estimated forces were also qualitatively compared to the experimental EMG data. The authors concluded that the three methods produced similar muscle force estimations and these were consistent with the sequence and timing of the EMG data. However, they also concluded that Static Optimisation possessed several advantages in relation to accuracy, robustness and efficiency (terms the authors define) when compared to the other two methods.

In response to the increased interest in using induced acceleration techniques to quantify muscle contributions during gait, Dorn et al. (2012) examined the sensitivity of these techniques to different ground contact models. They simulated the actuator activations for walking and running in fourteen typically developing adults using the gait2354 model and calculated each actuator's contribution to each of the three components of ground-reaction-force for a number of different ground contact models. Inconsistencies were found in the prediction of muscle function in the coronal plane. In addition, surface EMG was collected from the gluteus maximus, gluteus medius, medial hamstrings, vastus lateralis, medial gastrocnemius and soleus from one leg of each subject. No normalisation was carried out and actuator forces (rather that activation) were shown to be similar to EMG timings averaged across all subjects in a brief qualitative comparison.

Many musculo-skeletal gait simulation papers are published in the literature each year using software and methods similar to the Computed Muscle Control and induced acceleration techniques found in OpenSim but few make comment on the success of these simulations in terms of minimising the recruitment of residual/reserve actuators and to date none have attempted to conduct a quantitative analysis of the level of agreement between simulated and experimentally derived muscle activations. Simulation of muscle activity from generic models is adequate to elucidate our understanding of generic factors of human gait, such as muscle function, but confidence in an individual patient's simulation data from subject specific models is necessary if these techniques are to be developed further. There is an increased interest in the potential of implementing subject-specific musculo-skeletal simulations into the clinical gait analysis process and to

use them as an aid to treatment planning or as a method of virtually testing potential interventions. If this is to become a reality, then validation of these methods must be carried out.

In the work described in this chapter, the validity of the muscle actuator activations generated by OpenSim was determined by a quantitative comparison with recorded surface EMG data during human walking for ten typically developing subjects and ten subjects with cerebral palsy.

5.2. Methodology

Ten adolescents with spastic diplegic cerebral palsy and ten typically developing control subjects were recruited for the study following the methods and selection criteria described in section 2.4. In addition to the collection of muscle morphology data (Chapter 3), and the collection of walking kinematic and kinetic data (Chapter 4), EMG data was also collected for a standing pose and during walking using a Delsys Bagnoli-16 EMG system (Delsys Inc., MA, USA) as described in section 2.4.3. EMG data was also collected for a series of maximum voluntary contractions (section 2.4.4).

5.2.1. Setting up the Models

Subject mass and marker trajectories from the standing pose were used to create scaled and marker adjusted copies of the gait2392 model (section 2.2.2) for each of the twenty subjects. The strength of each model was then adjusted following a similar technique to that described in Chapter 4 but using subject specific muscle volume data. The *max_isometric_force* of each muscle actuator was multiplied by the appropriate muscle volume ratio as defined by Equation 5.1.

Equation 5.1

$$R_{m,s} = \frac{S_{m,s}}{M_{m,s}}$$

where:

$R_{m,s}$ is the volume Ratio for the m^{th} muscle for the s^{th} subject model

$S_{m,s}$ is the Subject specific muscle volume

$M_{m,s}$ is the subject scaled Model muscle actuator volume

subscripts:

m = m^{th} muscle actuator (43 muscle actuators)

s = s^{th} subject model (10 control and 10 case models)

It was not possible to measure the volumes of all 92 muscles used in the gait2392 gait model and so for muscle actuators for which subject specific values were not available, the mean volume ratio of all measured muscles was used.

5.2.2. Calculating Muscle Activations from Electromyography

Experimental surface EMG (section 2.4.3) were collected from each subject during maximum voluntary contractions and during walking for the following muscles: soleus, lateral gastrocnemius, medial gastrocnemius, tibialis anterior, rectus femoris, vastus lateralis, semimembranosus and semitendinosus. Experimental muscle activations were then calculated from the EMG using a process similar to that of Buchanan et al. (2004) – Figure 5.1.

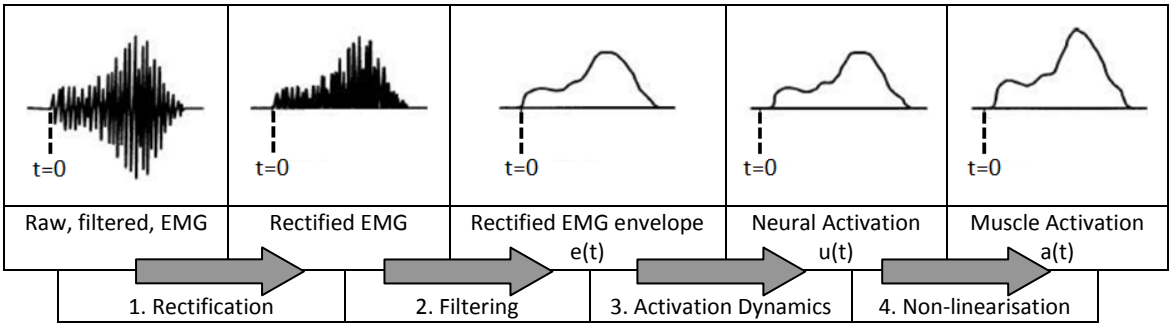

Figure 5.1 – Four step method for conversion of EMG signals to muscle activations as outlined by Buchanan et al. (2004). It is assumed that the raw EMG data has been collected after high pass filtering. Signals are then rectified and low pass filtered to produce an envelope. Normalisation to maximum voluntary contraction can be carried out at this stage. Two final processing stages then take into account activation dynamics and the non-linear relationship of muscle activation to EMG that represents the muscle twitch response mechanism.

The raw EMG signals were sampled at 1080Hz after passing through a low pass (450Hz) analogue filter to prevent aliasing. A digital band-pass filter (20-400Hz) was applied using Matlab (The Mathworks^{TM} Inc., MA, USA) to remove DC offsets and low frequency artefacts. The following additional signal processing (steps 1-4 Figure 5.1) was also performed using Matlab:

Step 1: rectification was carried out by taking the absolute value of the signal.

Step 2: the signal envelope, e(t), was calculated using a low-pass Butterworth filter (2nd order, cut-off 6Hz) with zero phase shift. Signal envelopes were then normalised to maximum voluntary contraction data.

Step 3: muscle activation dynamics can be modelled using a first order differential equation (Zajac, 1989) to convert the rectified EMG envelope e(t) to neural activation u(t). This is more conveniently done for sampled data using a second order, discretised, recursive filter (Equation 5.2) with coefficient values taken from Buchanan et al. (2004).

Equation 5.2 $$u(t) = \alpha e(t-d) - \beta_1 u(t-1) - \beta_2 u(t-2)$$

where:

$u(t)$	is neural activation
$e(t)$	is rectified EMG envelope
α, β_1, β_2	are coefficients to define the second-order dynamics
	$\alpha = 2.25$ $\beta_1 = 1$ $\beta_2 = 0.25$
d = 40ms	is the electromechanical delay

Step 4: the non-linearity between neural activation and muscle force at high stimulation frequencies that corresponds to the muscle twitch mechanism approaching tetanus is not characterised by the neural activation term u(t) and hence it is necessary to introduce a non-linearity factor. This was carried out using Equation 5.3.

Equation 5.3 $$a(t) = \frac{e^{A \cdot u(t)}}{e^{A} - 1}$$

where:

$a(t)$	is muscle activation
$u(t)$	is neural activation
A = -1	(non-linearisation curve factor)

5.2.3. Simulations and Analysis

Five gait cycles, each with three successive force-plate hits to ensure kinetic data was available over a whole gait cycle, were selected for each subject and kinematics and kinetics calculated using the Vicon Plug-in-Gait model (section 2.4.1). Following the SimTrack method described in Chapter 2, marker trajectories and ground-reaction-force data from each gait cycle were input into OpenSim, and Inverse Kinematics, Residual Reduction and both Static Optimisation and Computed Muscle Control tools were run to calculate joint kinematics and two sets of muscle actuator activations for comparison.

A number of checks were carried out to verify that each simulated gait cycle had run successfully before muscle activation validity analysis was carried out. In order to test SimTrack the recommended acceptability thresholds were adopted for this purpose despite concerns over their generosity (as discussed in section 2.2.3).

- Check 1 – first kinematics check: OpenSim Inverse Kinematics was compared to the equivalent datasets calculated using the Vicon Plug-in-Gait model to ensure appropriate joint angles were input into the Static Optimisation and Computed Muscle Control tools. Simulations were rejected for gross deviations in joint angles (>10°)

- Check 2 – second kinematics check: the resulting kinematics after the Computed Muscle Control tool was run were compared to the OpenSim Inverse Kinematics to ensure that the calculated muscle actuator activations successfully recreated the original motion. Simulations were rejected for changes in kinematics above recommended acceptability thresholds: >2° or >1cm (Table 2.5).

- Check 3 – the magnitude of residual and reserve actuators were checked against acceptability thresholds (Table 2.5, Table 2.6):

Residuals	
Forces	< 10N
Moments	< 50Nm

Reserve joint actuators (Nm/kg)	
hip flex/ext	< 0.1
hip abd/add	< 0.1
hip rotation	< 0.02
knee flex/ext	< 0.06
ankle flex/ext	< 0.19

- Check 4 – muscle activations were checked for non-physiological activations, discontinuities etc.

Muscle activation validity was carried out using a root mean square error (RMSE) analysis comparing simulated muscle activity against muscle activations calculated from experimental electromyograms (Equation 4.3).

Equation 5.4

$$E_{s,t,m} = \sqrt{\frac{\sum_{i}^{n}\left[\left(A_{i,s,t,m} - a_{i,s,t,m}\right)^2\right]}{n}}$$

where:

E is the root mean square Error of simulated muscle actuator activation to experimental muscle activation

A is simulated muscle actuator activation

a is muscle activation calculated from the experimental EMG

subscripts:

- s = s^{th} subject model (20 subject models)
- t = t^{th} gait cycle (five gait cycles)
- m = m^{th} muscle actuator (nine muscle actuators)
- i = i^{th} data-point (n data-points)

One drawback of using a root mean square error analysis as a measure of curve similarity is that large differences can be found between two identical curves differing only by a small translational shift (Figure 5.2).

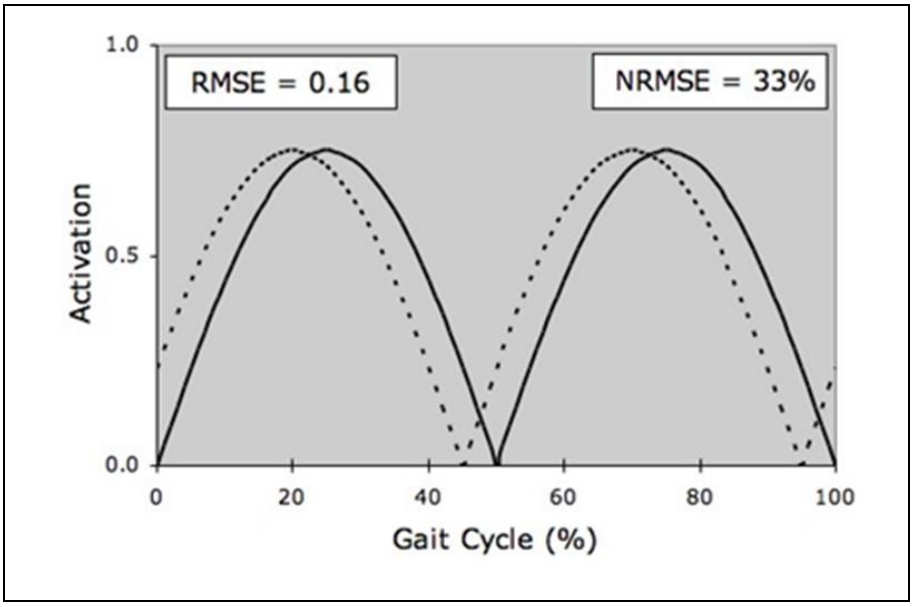

Figure 5.2 – Drawback of the root mean square error measure. A hypothetical muscle activation (solid line) is shown alongside a copy (dotted line) shifted in time by 5%. The two curves are identical apart from this small temporal shift but the root mean square error normalised to the mean activation (NRMSE) indicates a 33% difference between the activations

To overcome this problem the root mean square error was calculated within a minimisation algorithm that allowed both a time shift and gain compensation to be applied to the simulated muscle actuator activation. The time shift parameter was limited to ±0.1s based on the likelihood of mismatch between muscle model contraction dynamics and true human muscle twitch speed (Buchanan et al., 2004).

The gain parameter was limited based on the likelihood of sub-maximal maximum voluntary contractions. This was examined by Stackhouse et al. (2005) who compared the forces exerted from maximum voluntary contractions to the maximum forces generated during electrical stimulation in a group of twelve children with spastic diplegic cerebral palsy and ten typically developing age matched controls. In the quadriceps and triceps surae respectively, maximum voluntary contraction forces were found to be reduced to 70% and 90% in the control group and to 45% and 45% in the cerebral palsy group. The average of these four values (62.5%) was used as a basis to set the lower limit (0.6) of the gain compensation and the reciprocal value (1.7) was used for the upper limit. This range (0.6-1.7) was used for both groups in this analysis to allow comparison of the results.

This optimisation was implemented in Matlab (The Mathworks^{TM} Inc., MA, USA) using the least squares curve fitting algorithm (lsqcurvefit). An example can be seen in Figure 5.3.

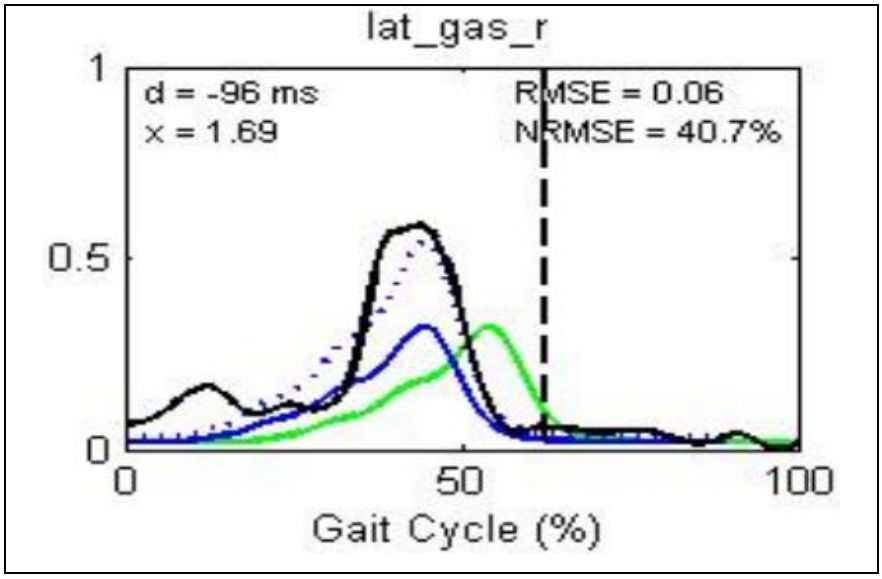

Figure 5.3 – An example comparison of simulated vs. experimental muscle activation for the right lateral gastrocnemius (lat_gas_r). The RMSE has been minimised by applying two transformations to the original simulated activation (green curve). The blue curve shows a shift in time by *d* (-96ms) and the dotted blue curve shows a subsequent increase in magnitude by *x* (1.69). The resultant RMSE (0.06) is then calculated between the adjusted simulated muscle activation (dotted blue curve) and the experimental activation (black curve) and normalised by the mean experimental muscle activation to give NRMSE=40.7%. The dashed black line marks the transition between the stance and swing phase of the gait cycle.

Once the root mean square differences between simulated and experimental muscle activations have been calculated, the validity of the simulated muscle activations can be determined by comparing these values to a validity threshold – a value of RMSE above which the two curves are deemed too dissimilar. However, choice of a suitable validity threshold is difficult due to the inherent variability seen in experimental surface electromyography of human walking (Winter & Yack, 1987). Inter-subject variation in EMG will result from physical differences between subjects such as body size/shape, and from differences in walking kinematics, but additionally will also result from the methodology of collecting surface EMG. This is due to differences: in electrode placement, in muscle morphology, in the electrical impedance of the electrode-skin contact and in the

composition/conductivity of the tissue that lies between the motor unit action potential and the electrode at the skin surface (Blok et al., 2002).

Many of these parameters will be fixed in a single individual and so intra-subject (stride-to-stride) EMG variation should be smaller than that seen between subjects, but some variability will still be present even in subjects with a very consistent walking pattern (Winter & Yack, 1987; Agostini et al., 2010). Again, this can come about from changes in the electrical impedance of the electrode-skin contact as the subject moves but also from variation in muscle motor-unit recruitment pattern as there is evidence (Hodson-Tole & Wakeling, 2007) that the generally accepted Henneman "*Size Principle"* (Henneman et al., 1965) recruitment mechanism, where smaller (usually slow) motor-units are recruited before larger (usually fast) motor-units, may not always be the case. Therefore the pattern of motor-unit recruitment in the same muscle may differ between repetitions of the same movement and hence lead to changes in the surface EMG signal as detected at the skin.

It is unreasonable that the agreement between a simulated and experimentally derived muscle activation in an individual should be closer than the inherent variability of the individual's EMG, but reasonable that this agreement should be closer than the inter-subject variation of EMG within the group. It is proposed therefore than a RMSE validity threshold range can be determined using intra-subject EMG variance and inter-subject EMG variance as upper and lower bounds respectively. As the musculo-skeletal model is not hampered by the complications of EMG electrode contact or muscle motor-unit recruitment patterns, it can be assumed that the variance in an individual's simulated muscle activations will be smaller than the intra-subject EMG variance, but to include this source of variation the lower bound will be adjusted to the sum of both (intra-subject simulated muscle activation variance + intra-subject EMG variance).

The three variances were calculated using the root mean square error between the individual trial data and the mean data across all appropriate trials (Equation 5.5).

Equation 5.5

$$V_{1,2,3_{m,s}} = \sqrt{\frac{\sum_i^n \left[\left(\bar{a}_{i,m} - a_{i,t,m,s}\right)^2\right]}{n}}$$

where: V is the Variance of: 1: intra-subject experimental activation (EMG)
2: intra-subject simulated muscle activation
3: inter-subject experimental activation (EMG)

a is the corresponding muscle activation (1, 2, 3)

subscripts:

m = m^{th} muscle actuator (nine muscle actuators)

i = i^{th} data-point (n data-points)

t = t^{th} gait cycle — 1 & 2: 5 gait cycles; 3: 50 gait cycles

s = s^{th} subject — 1 & 2: individual subjects (10xTD, 10xCP); 3: grouped subjects (TD group, CP group)

The lower bound of the RMSE validity range for each muscle for each subject was then calculated from the sum of the two intra-subject variances V_1 and V_2 (root of the sum of the squared variances – Equation 5.6) and the upper bound set as the inter-subject variance V_3

Equation 5.6

$$LB_{m,s} = \sqrt{V_{1_{m,s}}{}^2 + V_{2_{m,s}}{}^2}$$

where: LB is the Lower Bound of the RMSE validity range

subscripts:

m = m^{th} muscle (nine muscle actuators)

s = s^{th} subject (10xTD, 10xCP)

The invalidity ratio for each muscle for each subject was then calculated by dividing the RMSE of simulated muscle activation to experimental activation *E*, by the appropriate lower bound of the validity range (Equation 5.7).

Equation 5.7

$$R_{m,s} = \frac{E_{m,s}}{LB_{m,s}}$$

where:

R is the invalidity Ratio

E is the RMSE of simulated activation to experimental activation

LB is the Lower Bound of the RMSE validity range

*s*ubscripts:

m = m^{th} muscle actuator (nine muscle actuators)

s = s^{th} subject (10xTD, 10xCP)

This parameter has been termed the invalidity ratio as *R*=1 would represent simulated muscle activations matching experimental activations as closely as the variance in the individual's EMG, and *R*>1 would indicate a poorer match and hence a greater invalidity of the simulated activations. The upper bound of the RMSE validity (V_3) for each muscle in the typically developing group and the cerebral palsy group were also normalised to the corresponding lower bound to give an upper threshold limit of the invalidity ratio. Simulated muscle activations for each muscle for each subject will therefore only be considered valid if their calculated invalidity ratios are close to unity and less than this upper threshold. An invalidity ratio close to or above the upper threshold will imply that the differences between the simulated and experimental muscle activations are as large as the group variation of experimental muscle activation and hence the bespoke nature of the musculo-skeletal model has failed as an individual's muscle activations cannot be distinguished from the group.

5.2.4. Hypothesis

Previous researchers have commented on the similarity of simulated and experimentally derived muscle activations in typically developing subjects (section 5.1). It is expected therefore that the level of agreement in this group will lead to values of the invalidity ratio (R) of approximately one. However children with cerebral palsy are known to have difficulties in the selective activation of muscles during walking (section 1.2). This can lead to co-activation which generates greater overall muscular activation for the same net joint moment. Therefore, since the cost functions in both the Static Optimisation and the Computed Muscle Control algorithms are based on minimisation of total muscle excitation/activation, it is expected that invalidity ratios (R) in this group will be significantly higher.

5.3. Results

5.3.1. Data Collection

Table 5.1 gives a summary of the kinematic, kinetic and EMG data collected during walking, the EMG data collected during maximum voluntary contractions and the MRI data that was successfully collected from all ten control subjects and ten case subjects.

	Controls	Cases
Number (n)	10	10
Kinematics	10	10
Kinetics	10	10
EMG - walking	10	7 (+1 partial)
EMG - MVC	10	7 (+1 partial)
5 walking trials	7	3
4 walking trials	2	3
3 walking trials	1	3
2 walking trials	-	1
Total walking trials	46	38
Full MRI datasets	10	6
gait2392 models	10	9

Table 5.1 – Summary of data collection

Partial or no EMG data was collected from three case subjects due to a combination of tiredness, non-compliance and time constraints after the MRI data collection overran. A reduced number of walking trials were collected from three controls subjects due to inconsistencies in step length, and from seven case subjects due to a combination of obscured markers, incorrect leg hitting the force-plate and/or subject tiredness. A reduced set of muscle volumes were collected in four case subjects due to the reasons described in section 3.4.

As expected, walking kinematics amongst the control group were more consistent and closer to typically developing limits than the case group (Figure 5.4).

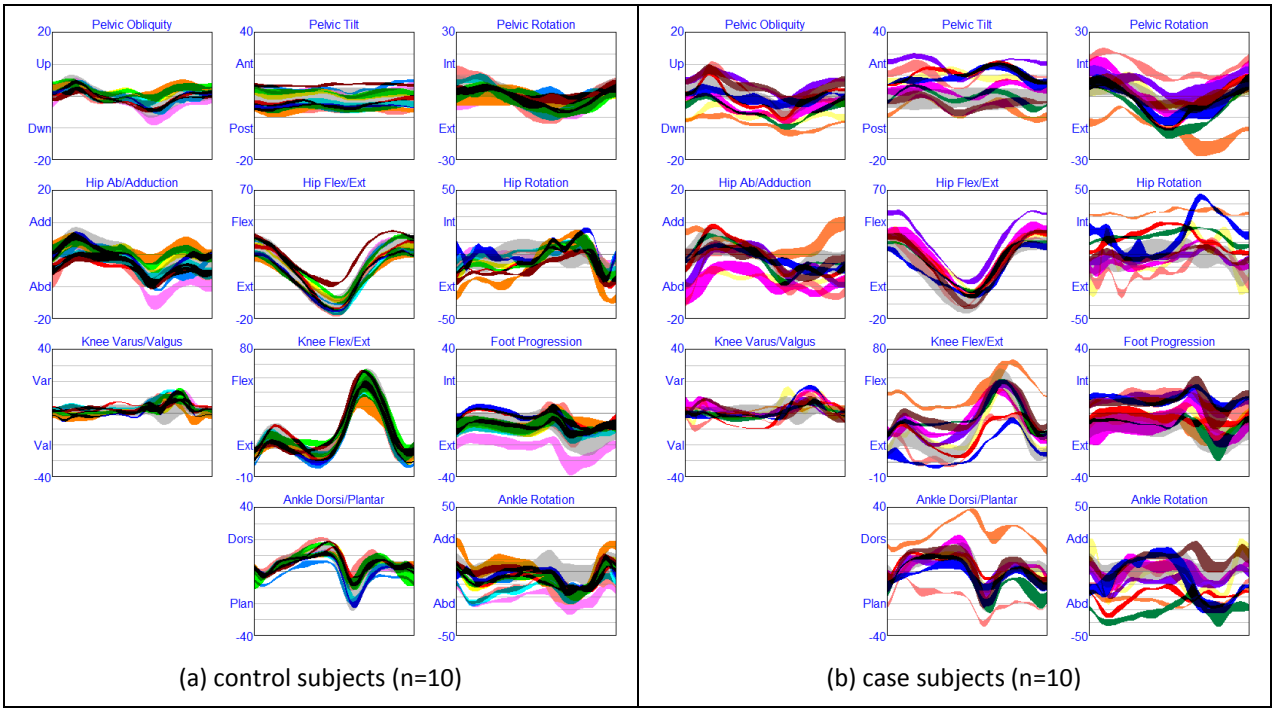

Figure 5.4 – Walking kinematics for all subjects over one gait cycle as calculated using the Conventional Gait Model. A separate colour band shows the mean joint angles (± 1SD) from all collected trials (max. 5) from each subject. The grey band shows the normal limits for typically developing adults (Guy's Hospital Gait Laboratory).

Vertical axis: joint angle (degrees), horizontal axis: gait cycle (%), Flex = flexion, Ext = extension, Ab = abduction, Add = adduction, Dors = dorsiflexion, Plan = plantarflexion, Int = internal, Ext = external, Var = varus, Val = valgus

5.3.2. Simulation and Data Quality

Muscle volume ratios for all 20 subjects can be found in Appendix G. The most strengthened actuator was the vastus intermedius in Control10 with a muscle volume ratio of 2.9, and the most weakened actuator was the biceps femoris short head in Case05 with a muscle volume ratio of 0.09. Subject scaled versions of the gait2392 OpenSim model were successfully created for all subjects except one.

The static pose adopted by Case06, which involved both right internal thigh rotation and right external foot progression (Figure 5.5) could not be replicated by the model due to restrictions in degrees of freedom. Moving the model markers to match the experimental marker positions in an unmatched pose would have led to large errors in calculated kinematics and hence in any subsequently simulated muscle activations. No simulations were therefore carried out on this subject's data.

Figure 5.5 – Standing pose for subject Case06. The combination of internal thigh rotation and external foot progression could not be replicated in the model

Inverse Kinematics, Residual Reduction and the both Static Optimisation and Computed Muscle Control tools were run on the remaining 46 control trials and 36 case trials. A number of trials failed the four kinematic, reserve/residual and muscle activation checks as described in section 5.2.3. A large number of trials failed Check 2 and so the "*OK*" rather than "*Good*" category thresholds (Table 2.5) were adopted. Full check results are summarised in Table 5.2.

	Controls		Cases	
	CMC	SO	CMC	SO
Planned number of gait cycle simulations (5 trials per subject)	50		50	
Remaining trials after collection	46		38	
Potential simulations from useable models	46		36	
Remaining trials after Check 1: OpenSim IK vs. Vicon Plug-in-Gait kinematics	46		36	
Remaining trials after Check 2: OpenSim CMC kinematics vs. OpenSim IK	45	n/a	34	n/a
Remaining trials after Check 3: Residuals/Reserves	34	46	24	24
Remaining trials after Check 4: Muscle activations	4	46	8	24
Final number of simulations with viable EMG data for validity analysis	4	46	7	20

Table 5.2 – Summary of the number of simulated gait cycle trials used in this study. Trials were eliminated following the simulation checks described in section 5.2.3.

IK = Inverse Kinematics, CMC = Computed Muscle Control, SO = Static Optimisation

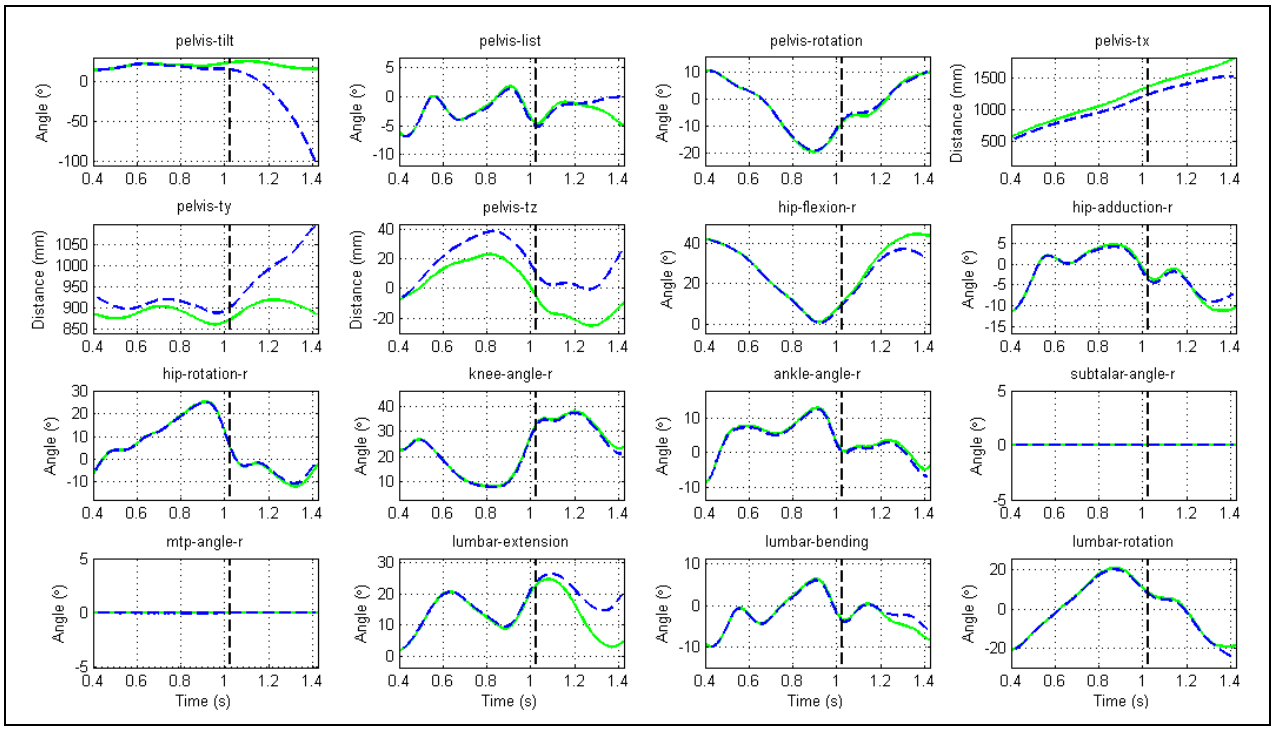

Figure 5.6 – An example trial from Case10 that failed Check 2, the kinematic matching between the kinematics as calculated by the OpenSim Inverse Kinematics tool (solid green curve) and the kinematics resulting from the muscle actuator action as calculated using the Computed Muscle Control tool (dotted blue curve). Gross deviations can be seen in pelvic tilt, hip flexion, hip adduction and in the position of the trunk (lumbar angles). The model has also undergone large global translations: upwards (pelvis-ty) by 200mm, laterally (pelvis-tz) by 20mm and posteriorly by 250mm. The dotted black line marks the transition between stance and swing phase

All trials passed Check 1 giving similar kinematic tracking to that shown in figure 4.1. In the Computed Muscle Control dataset most trials passed Check 2 despite some minor deviations in the global position of the model with many simulations showing a vertical shift upwards by 1-2cm over the course of the gait cycle. However, as the ground-reaction-force is applied to the model calcaneum segment, rather than the foot-ground contact point, a vertical translation should have no effect on the kinetics and so these trials were still acceptable. One control trial and two case trials failed Check 2 due to gross deviations in kinematic matching (Figure 5.6)

It would seem likely that the failure of these simulations is caused by some mismatch between the experimental force-plate data and recorded motion.

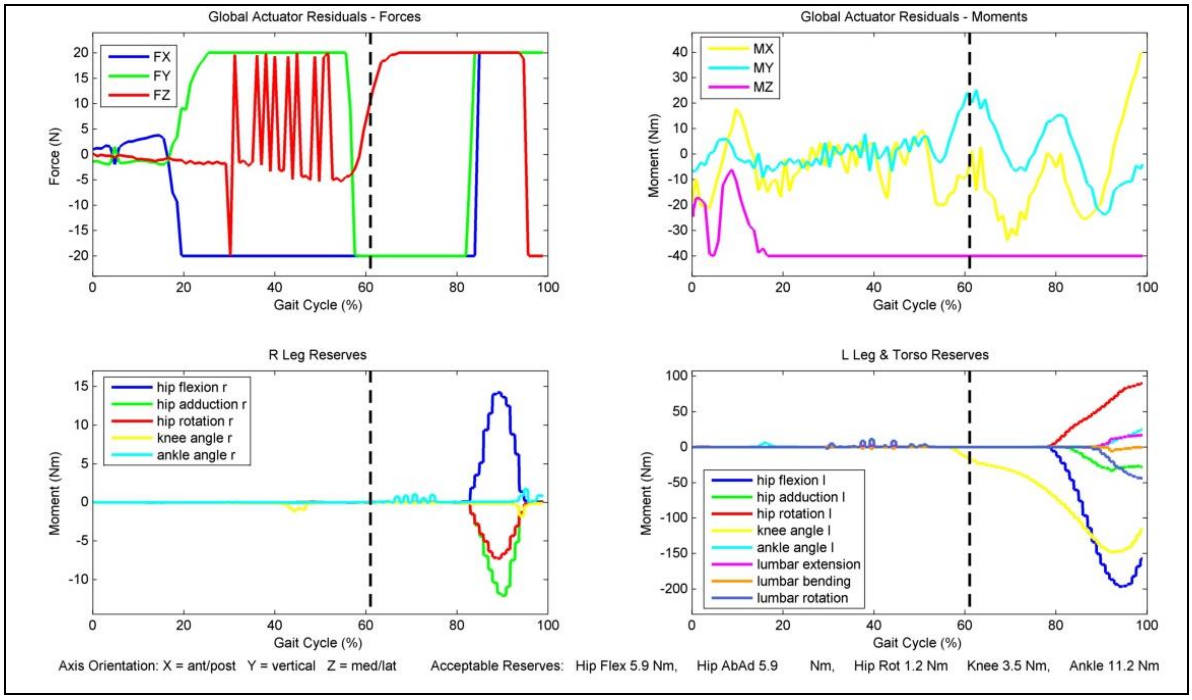

Figure 5.7 – Check 3 fail: residual/reserves. Example Computed Muscle Control residual/reserve data from Case10 trial that failed Check 2 shown in Figure 5.6. This trial also fails Check 3 as all three residual forces saturate at 20N and the residual moment about the z-axis saturates at 40Nm. Many of the joint moment reserve actuators also exceed acceptable levels. This trial was a right leg gait cycle. The vertical dotted black line marks the transition between the stance phase and swing phase.

Usually the trials that failed Check 2 also failed Check 3 (Figure 5.7) as the model applies unacceptably large residual forces/moments and reserve joint moments in an attempt to maintain kinematic tracking.

Of the remaining simulations after Check 2, a further 11 control trials and 10 case trials failed Check 3 with residual forces/moments or reserve moments above acceptable thresholds (Figure 5.8).

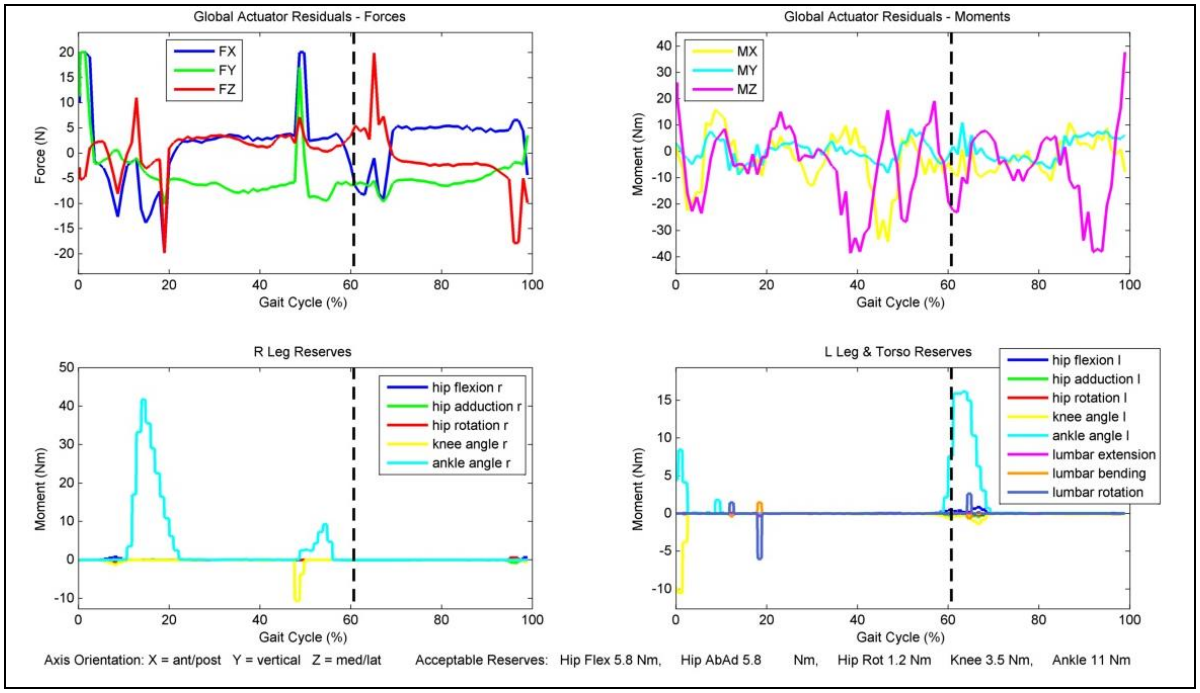

Figure 5.8 – Check 3 fail: residual/reserves. Example Computed Muscle Control residual/reserve data from Control05 that failed Check 3 – residual forces/moments and reserve moments. Excessive reserve joint torques can be seen on the bilateral ankle and knee. This trial was a right leg gait cycle. The vertical dotted black line marks the transition between the stance phase and swing phase

Of the remaining simulations after Check 3, a further 30 control trials and 16 case trials failed Check 4 with muscle actuators exhibiting unusual activity. A small number of simulations exhibited activations with non-cyclical, high magnitude end effects (Figure 5.9) which are unlikely in a cyclical walking pattern, but the vast majority of the failures were due to unexpected mid-stance tibialis anterior activity combined with high activity/saturation in swing (Figure 5.10).

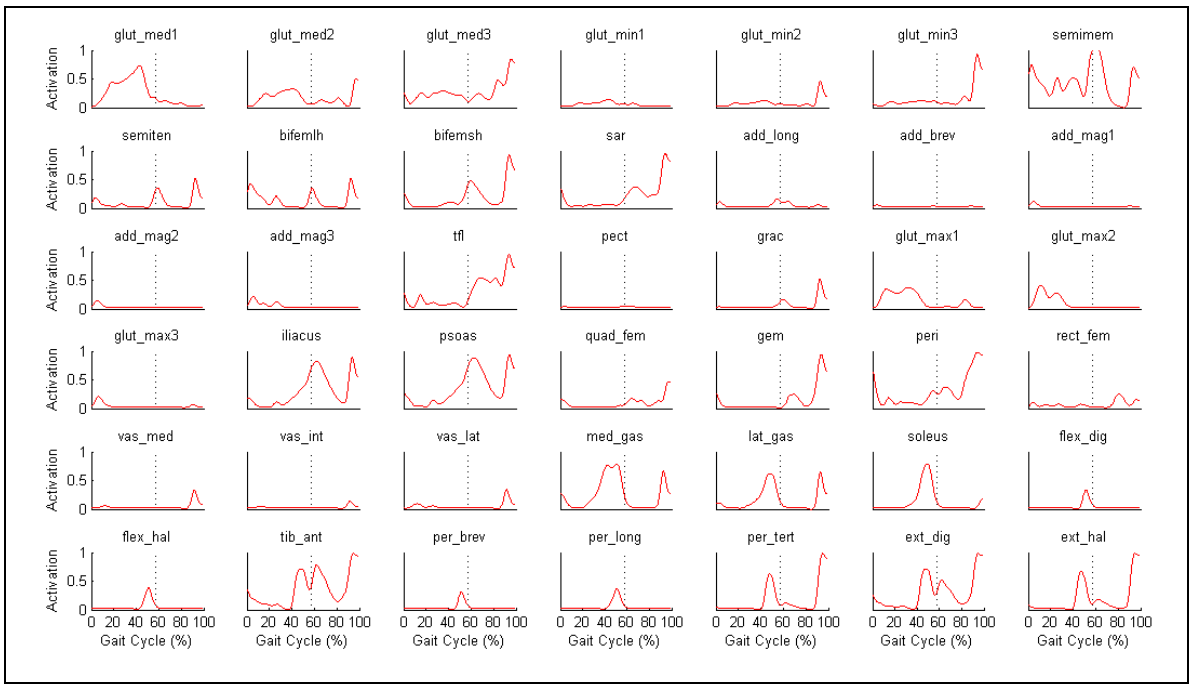

Figure 5.9 – Example Computed Muscle Control activations from Control02 that failed Check 4 due to discontinuities in muscle actuator activation. Non-cyclical, high activation, end effects can be seen on a number of actuators. This trial was a left leg gait cycle. The vertical dotted black line marks the transition between the stance phase and swing phase

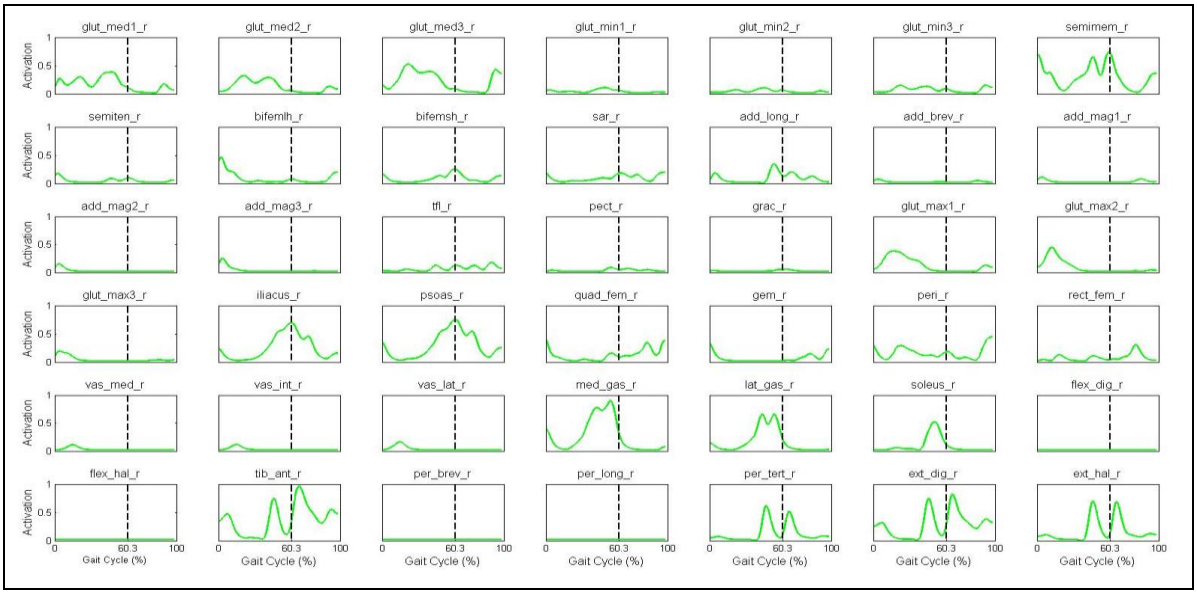

Figure 5.10 – Example Computed Muscle Control activations from Control03 that failed Check 4 due to unusual tibialis anterior activation. Neither mid-stance activation nor such high activity in swing would be expected. The vertical dotted black line marks the transition between the stance phase and swing phase

The tibialis anterior is typically quiet during mid-stance (Agostini et al., 2010; Sutherland, 2001; Winter & Yack, 1987) being active only during loading response (to control the lowering of the foot to be flat to the floor after heel strike) and during the swing phase (to lift up the foot and prevent tripping as the leg swings forward). Additionally, high activation during swing should be unnecessary as little effort is required to lift the freely hanging foot. High tibialis anterior activity/saturation has also resulted in recruitment of the lesser dorsiflexors (the toe extensors) and may also be responsible for other less obvious compensatory mechanisms.

This is the same artefact as that identified in the sensitivity analysis (section 4.3.3) where the Computed Muscle Control algorithm calculated large changes in tibialis anterior activation for small changes in muscle strength for the same movement. Whereas before it was not clear whether this effect was due a specific problem with the data of the single trial or model used in the sensitivity analysis, it now appears to be a more general problem with the SimTrack workflow. In response to this, an investigation into possible causes of instability/high activations of the tibialis anterior actuator was carried out and the results are reported in the next section 5.3.3.

In the Static Optimisation dataset all 46 control trials passed Checks 1, 3 and 4 (Check 2 was not applicable to the data output by the Static Optimisation tool). Of the 36 case trials, 12 failed Check 3 exhibiting residual forces or reserve moments above acceptable thresholds (Figure 5.11). These trials also exhibited excessive residual forces during the second run of the Residual Reduction Algorithm and so it is likely that there were some mismatches between the experimental force-plate data and recorded motion. All the remaining 24 case trials passed Check 4.

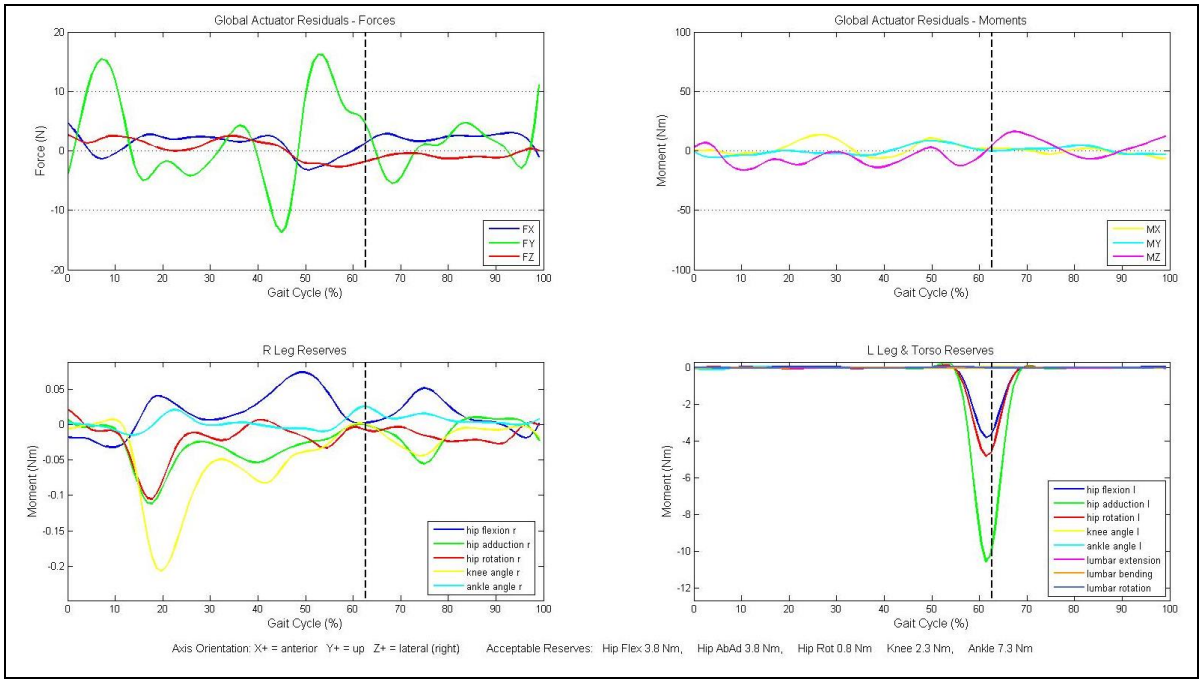

Figure 5.11 – Example Static Optimisation residual/reserve data from Case01 that failed Check 3 – residual forces/moments and reserve moments. Excessive vertical (F_y) residual forces and excessive reserve joint torques around the left hip can be seen. This trial was a right leg gait cycle. The vertical dotted black line marks the transition between the stance phase and swing phase

5.3.3. Possible Causes of High Tibialis Anterior Activation

There are a number of different mechanisms that may have been a cause of high tibialis anterior activation – these include:

a) the joint may be stiff due to antagonistic action
b) the foot segment may be inappropriately massive
c) the muscle moment-arm may be underestimated in the model
d) the strength of this muscle may be underestimated in the model
e) a problem with the Computed Muscle Control algorithm

Three of these mechanisms can be quickly disregarded:

a) the main antagonists of the tibialis anterior are the gastrocnemeii and the soleus and Figure 4.5 shows all three are inactive during swing
b) the foot mass was 1.25kg or 2.1% of bodyweight, close to the published anthropometric value of 1.5% (Winter, 2005)

c) The variation in tibialis anterior moment-arm length over one example gait cycle for the gait2392 model and for the scaled Control01 model is shown in Figure 5.12. For the 1.8m tall gait2392 model the moment-arm can be seen to range from 41-43mm which is in agreement with published adult data (Miller et al., 2015). Assuming a linear scaling factor the 1.6m tall Control01 model therefore also shows an appropriate moment-arm range (32-37mm). However, it is interesting to note a mild oscillation on the ankle joint kinematics during mid-stance – this will be examined in more detail below.

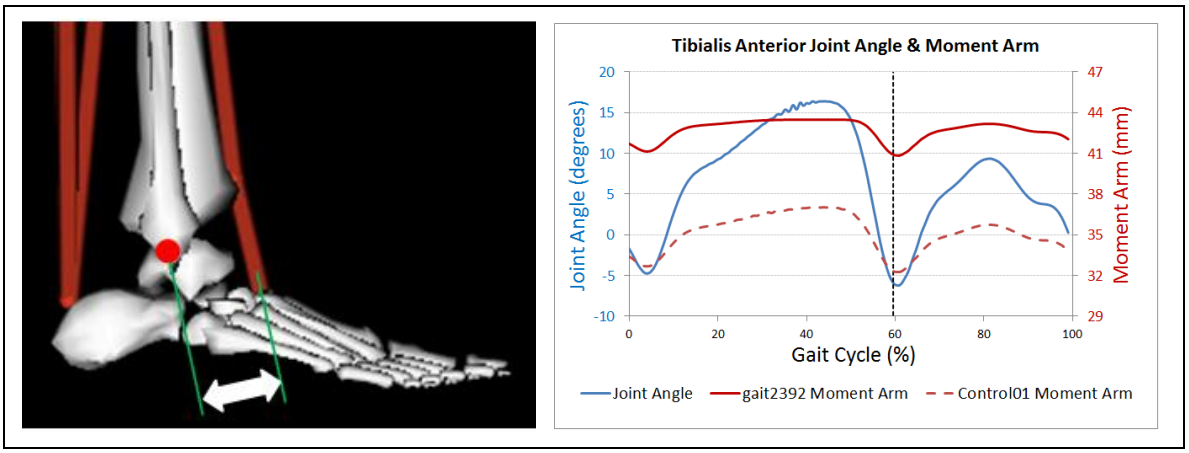

Figure 5.12 –The image shows muscle insertions for the calf muscle complex and tibialis anterior (red lines), the ankle axis of rotation (red dot) and tibialis anterior moment-arm (white arrow) of the gait2392 model. The graph shows the ankle kinematics (as output from the Computed Muscle Control tool) for one trial of Control01 as well as the moment-arm length for both the generic gait2392 model and the scaled Control01 version. The vertical dotted black line marks the transition between the stance phase and swing phase

The final two mechanisms that may have caused high tibialis anterior activation require more in-depth investigation. First it is necessary to examine the tibialis anterior muscle strength which is dependent on the muscle model (section 2.2.2). Many of the muscle parameters are the same for all muscles and so it is logical to examine the four parameters that are muscle specific: *pennation_angle*, *max_isometric_force, optimal_fiber_length* and *tendon_slack_length.*

The tibialis anterior actuator *pennation_angle* is small (5 degrees) and so this is an unlikely cause of weakness as the force exerted by the active muscle fibres will be close to the line of action of the whole musculo-tendinous unit. The *max_isometric_force* parameter is the

maximum isometric force that can be exerted by the combined active action of the muscle fibres and is proportional to muscle volume (and hence PCSA). The sensitivity models were created from the generic gait2392 model by scaling each muscle's *max_isometric_force* parameter by the appropriate volume ratio. For the baseline model (Model07) the mean volume ratio for all the muscles was 1.1 and so in general most values of *max_isometric_force* were altered only moderately. In fact only two muscles were weakened to less than 80% of their original value: biceps femoris short head (31%) and tibialis anterior (66%). This weakening is a likely cause of high tibialis anterior activation. The biceps femoris short head however, despite being more severely weakened, does not maximally activate. This is possibly because this muscle has a number of synergists available for compensation.

Increasing the *max_isometric_force* of tibialis anterior will have a direct effect on the strength of the muscle actuator and should prevent saturation. Before testing this within the model however, it will be interesting to check if the current maximum strength of this actuator is being restricted by the values of *optimal_fiber_length* and *tendon_slack_length*. In the full muscle model (section 2.2.2) the interaction of these parameters to the net muscle force is complex due to their interaction with both the active muscle contraction force and the passive forces of muscle belly and tendon stretch. However, this complexity is somewhat reduced as the Static Optimisation algorithm used in the Computed Muscle Control tool uses a simplified version of the muscle model that ignores the muscle belly passive forces (the parallel elastic element) and considers the tendon inextensible. However, even with this simplified muscle model, if the muscle fibres are operating at a different length from optimum then their active force will be restricted.

Looking at the active component of the muscle model (Figure 2.13) it can be seen that a muscle fibre operating too long or too short by half a resting fibre length will result in the maximum active force reducing to two thirds of the *max_isometric_force*. Changing the *tendon_slack_length* will change the length at which the muscle fibres operate and hence will change the operating strength of the muscle.

To investigate this interaction two more sensitivity models were created following the same protocol as described in Chapter 4 based on the control group muscle volumes. A baseline model (Model04) was scaled to the mean muscle volume of the control group (thus similar in strength to Model07) and muscle activations over the gait cycle used in the sensitivity analysis were simulated. The mean deviation of the operating fibre length of each muscle from their optimal fibre length was calculated and a second model was then created (Model04-TSL-Opt) with optimised *tendon_slack_lengths* to compensate appropriately. The simulation was re-run and muscle activations and operating muscle fibre lengths compared. In the un-optimised model, a number of actuators failed to operate at optimal length throughout the entire gait cycle, these included gluteus medius1, semimembranosus, all the adductors and tibialis anterior. These actuators therefore underwent the largest changes to their tendon slack lengths in the optimised model. In general, all corrections involved shortening of the *tendon_slack_length* to increase the operating length of the muscle fibres. This change should result in lower activation to achieve the same force as the muscle is operating at peak position on the active force curve and the tendon strain should increase for the same joint angle. The change to the tibialis anterior operating fibre length and activation can be seen in Figure 5.13.

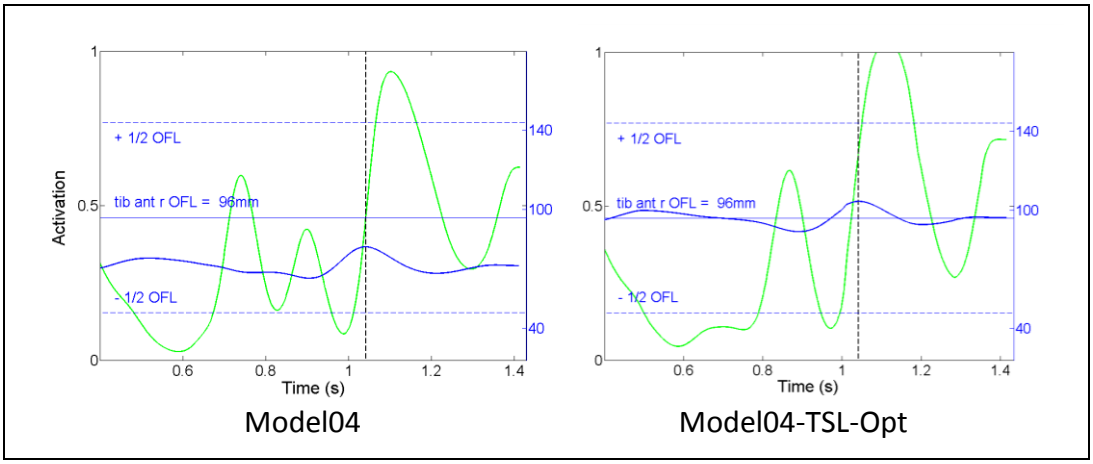

Figure 5.13 – Change in activation & operating fibre length after shortening the tendon slack length. Simulated right tibialis anterior actuator activation (green) and operating fibre length (blue) before (Model04) and after (Model04-TSL-Opt) optimising the fibre length by shortening the tendon slack length. OFL = optimum fibre length

Despite the fibre operating at optimal length the activation of the tibialis anterior in Model04-TSL-Opt has increased and, in general, most muscles increased their activation. This response of the model to changes in *tendon_slack_length* is contrary to expectations; however these results should be viewed with caution as large residual/reserve forces/moments were required to track the gait kinematics in the optimised model. A more detailed analysis of the model response to changes in both *tendon_slack_length* and *optimal_fiber_length* would therefore be warranted in future work as it would appear that simulated muscle activations are sensitive to these parameters.

Finally, the maximum isometric force parameter (*max_isometric_force*) of the tibialis anterior actuator was increased to see if the dorsiflexor insufficiency could be eliminated. Model04, as described above, was again used as the baseline model and four additional models were created (Model04-TAx2,x3,x4,x5) with the bilateral tibialis anterior actuators given 2, 3, 4 and 5 times the *max_isometric_force* of Model04. Activation of the tibialis anterior and toe extensors progressively decreased as tibialis anterior strength increased and toe extension action was finally eliminated with Model04-TAx4. However, non-cyclical "end effects" and mid-stance tibialis anterior activation remained, and there were increases in activation of both heads of the gastrocnemius (Figure 5.14).

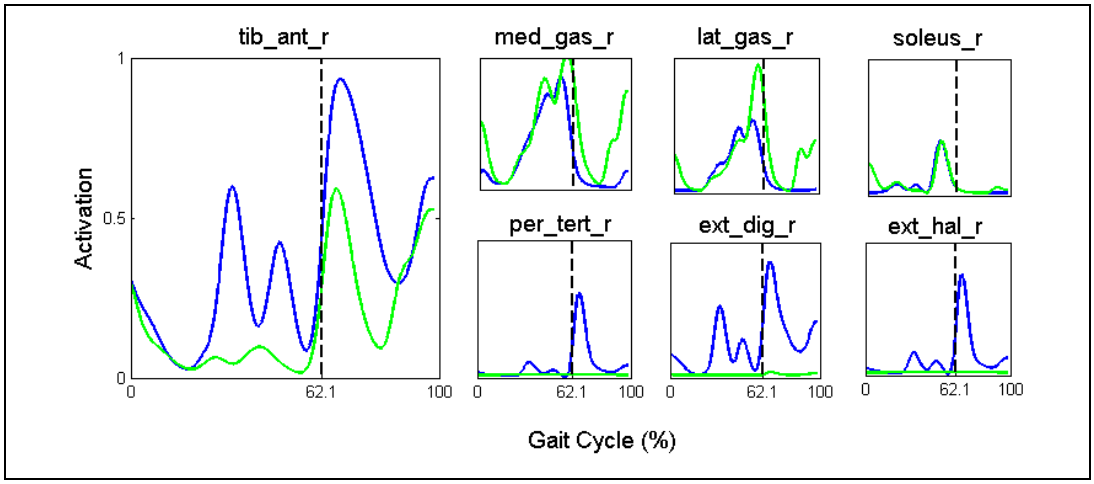

Figure 5.14 – Changes in activation after increasing tibialis anterior strength. Simulated activations of the tibialis anterior, calf muscles and toe extensors for the baseline Model04 (blue) and the most strengthened Model04-TAx5 (green).

Dorsiflexion insufficiency was eliminated therefore by an increase in the maximum isometric strength of the tibialis anterior. Making use of such a un-physiologically strong tibialis anterior muscle is not a satisfactory solution as there are consequences for the activation profiles for other muscles in the model – most notably the antagonists. Additionally, maximal calf muscle activation during normal walking of typically developing subjects is unlikely to be valid. It would appear therefore that an underestimation of muscle strength on its own is not the primary cause of high tibialis anterior activation.

The final mechanism to investigate that may have caused high tibialis anterior activation is the Computed Muscle Control algorithm. Mild oscillations on the ankle kinematics output from the algorithm were seen in Figure 5.12. If this noise was also present on the input kinematics then high muscle activations may have been necessary to cope with the subsequent high noise on the (double differentiated) desired joint accelerations. To prevent this problem occurring it is recommended that input kinematics be low pass filtered (e.g. cut off frequency 8Hz) to remove such noise from being amplified. Indeed, this was carried out and no such noise was present on kinematics generated in either of the previous SimTrack stages: Inverse Kinematics or the Residual Reduction Algorithm (Figure 5.15).

However, noise or “ringing” can clearly be seen on the output kinematics from the Computed Muscle Control algorithm. This is quite mild on the ankle angle but becomes substantially more significant in the velocity and acceleration data. This ringing is only seen at the ankle (Figure 5.16) and the timing of the highest amplitude noise region corresponds to the unexpected mid-stance tibialis anterior activation. Indeed, of the four control trials that did not exhibit mid-stance tibialis anterior activation, the corresponding ankle acceleration ringing was noticeably reduced. The second and third noise regions occur during the pre-swing and early swing phases of the gait cycle which corresponds to the increased activation/saturation of the tibialis anterior seen in many of the Computed Muscle Control simulations.

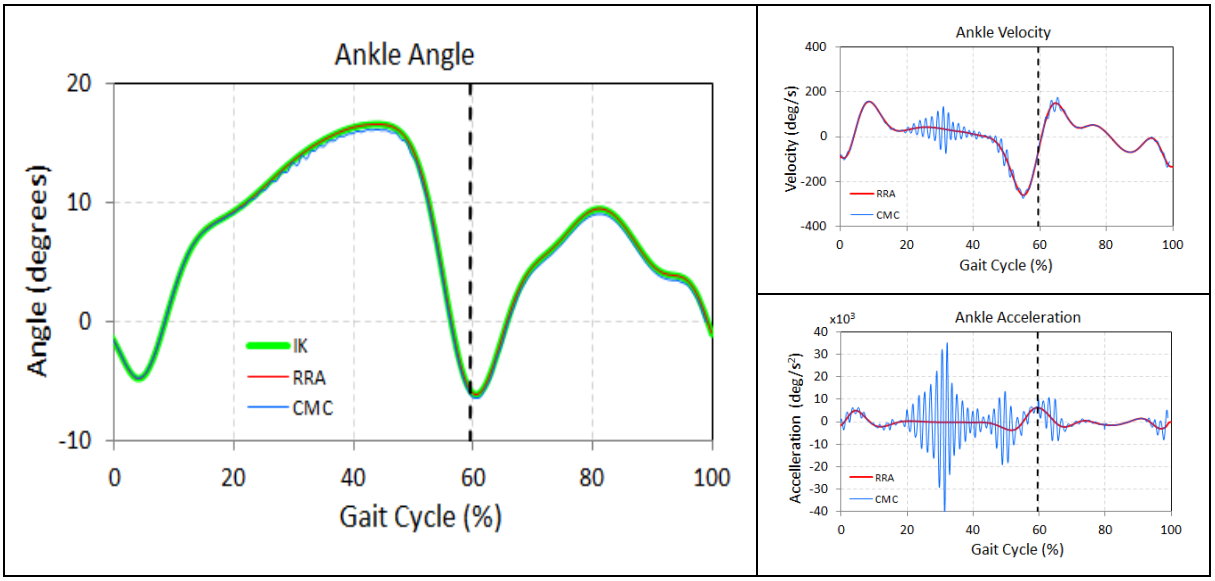

Figure 5.15 – Input and output ankle kinematics for a Control01 walking trial. No noise is visible on either the IK kinematics (input to RRA) or the RRA kinematics (input to CMC). However, mid-stance noise can be seen on the CMC output ankle angle which is greatly amplified on both the ankle velocity and acceleration.
IK – inverse kinematics RRA = residual reduction algorithm CMC = computed muscle control

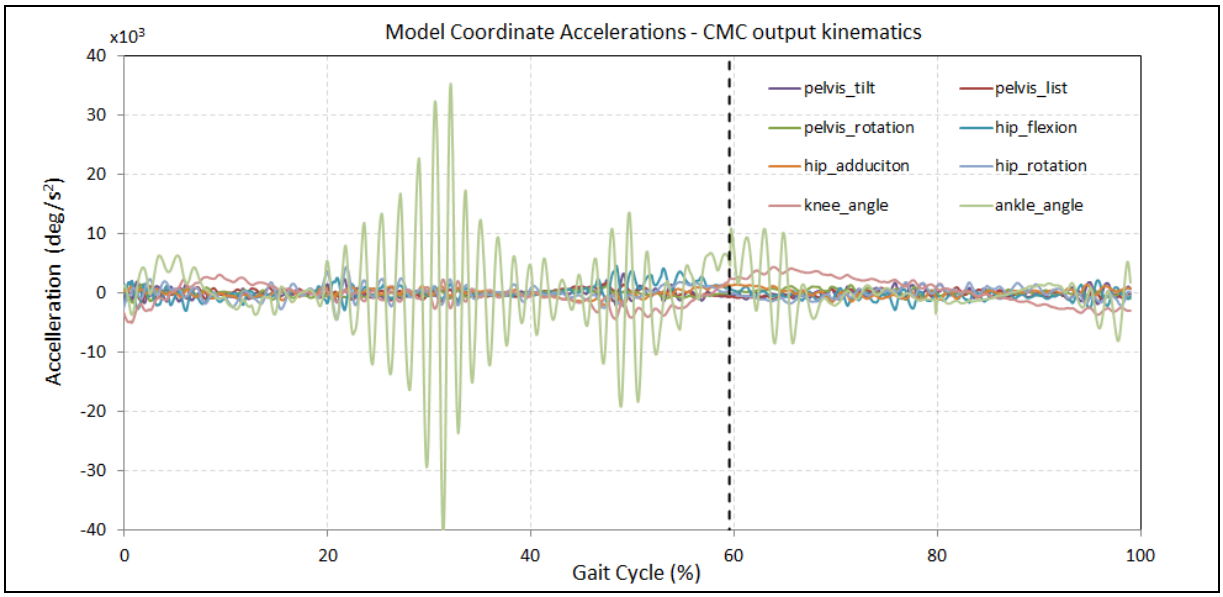

Figure 5.16 – Computed Muscle Control (CMC) output model coordinate accelerations for a Control01 walking trial. Substantial "ringing" is only seen on the ankle_angle coordinate.

It would appear therefore that this ankle coordinate ringing is the cause of both the high tibialis anterior activation in early swing and the unexpected activation in mid-stance. It has already been shown that there was no corresponding noise on the input kinematics, and additionally no noise was found on the experimental ground-reaction-force data nor on joint moments as calculated using inverse dynamics. The ringing artefact therefore appears to be being generated within the Computed Muscle Control Algorithm.

There are a number of parameters available to alter the set-up of the Computed Muscle Control algorithm but it is well known (Prentice, 2011) that ringing effects in numerical methods are sensitive to solution step-size. The *CMC_time_window* is the solution step parameter in the Computed Muscle Control algorithm and, as recommended by the OpenSim user-guide, it was set to 0.01s in these initial simulations. To investigate the effect of this parameter on ankle_angle acceleration ringing therefore, the Computed Muscle Control tool was run again on the same Control01 walking trial with three progressively smaller values of the *CMC_time_window*: 0.0075s, 0.005s and 0.001s.

It can be seen in Figure 5.17 that tibialis anterior activation is very sensitive to the choice of the time window. As the time window is reduced, the ankle angle acceleration ringing initially increases and then reduces and the tibialis anterior activation responds accordingly with increased activation during ringing periods. For this single walking trial and within this limited range of time windows tested, the optimum value of *CMC_time_window* appears to be 0.005s. However, even for this simulation, the mid-stance tibialis anterior activation has not been completely eliminated.

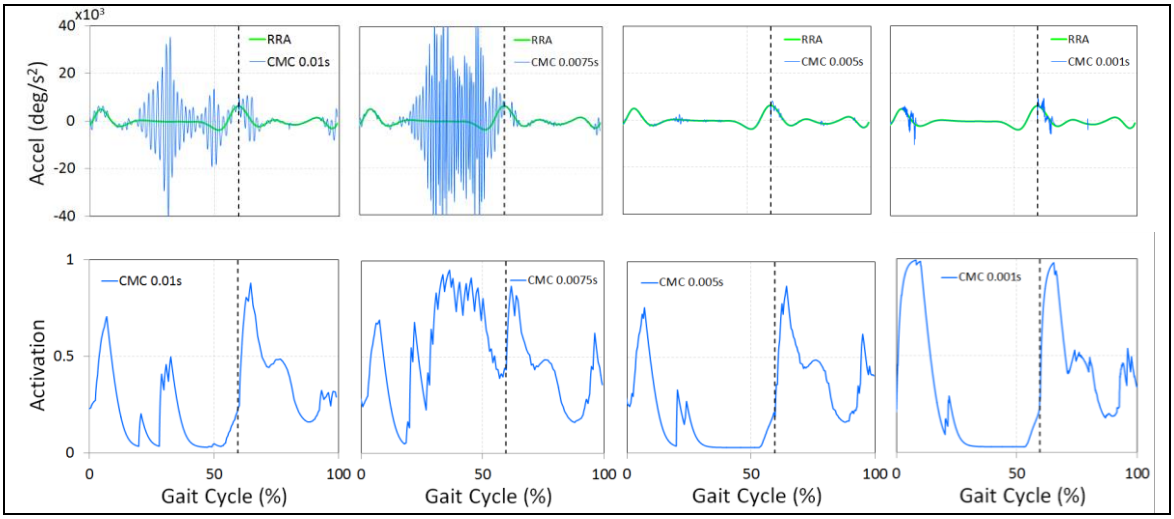

Figure 5.17 – Ankle angle accelerations (input – RRA, output – CMC) and tibialis anterior activations for a Control01 walking trial using four different values of the *CMC_time_window* parameter.
RRA = residual reduction algorithm CMC = computed muscle control

Similar tests were run on other walking trials for Control01 and on other subjects but the results were variable: ankle angle acceleration ringing was often reduced leading to reductions in mid-stance/high activation of the tibialis anterior but mid-stance activation was rarely eliminated completely; and despite improvements at the ankle, changing the *CMC_time_window* resulted in increased acceleration ringing at other model coordinates in some trials. Using the definition of Lin et al. (2011), the algorithm therefore appears to have low robustness. It is also unfortunate that there are no results on the tibialis anterior in this paper.

It would therefore appear that the low robustness, or sensitivity to changes in its input settings, of the Computed Muscle Control algorithm necessitates the use of trial specific set-up parameters. Such a task is impractical for the number of walking simulations investigated in this thesis. A number of papers (Anderson & Pandy, 2001; Lin et al., 2011) have indicated that muscle force estimates using Static Optimisation and Computed Muscle Control are practically equivalent, and therefore it seems prudent to only carry forward the Static Optimisation data into the subsequent validity analysis.

5.3.4. Validity Analysis

After all the preceding simulation data quality checks, the OpenSim muscle actuator activation validity analysis was only carried out on the Static Optimisation data, using 46/46 gait cycles from 10/10 control subjects and 20/36 gait cycles from 6/10 case subjects. Mean simulated muscle actuator activations from all these control trials and case trials are shown in Figure 5.18 and Figure 5.19 respectively.

Individual trial activations, mean experimental activations, and normal EMG timings during adult walking are shown for the EMG muscles in Figure 5.20 and Figure 5.21 for the control and case groups respectively.

Specific examples of the validity analysis for one control trial and one case trial can be seen in Figure 5.22 and Figure 5.23 respectively. Here the time shift and gain compensation optimisation can be seen for each muscle.

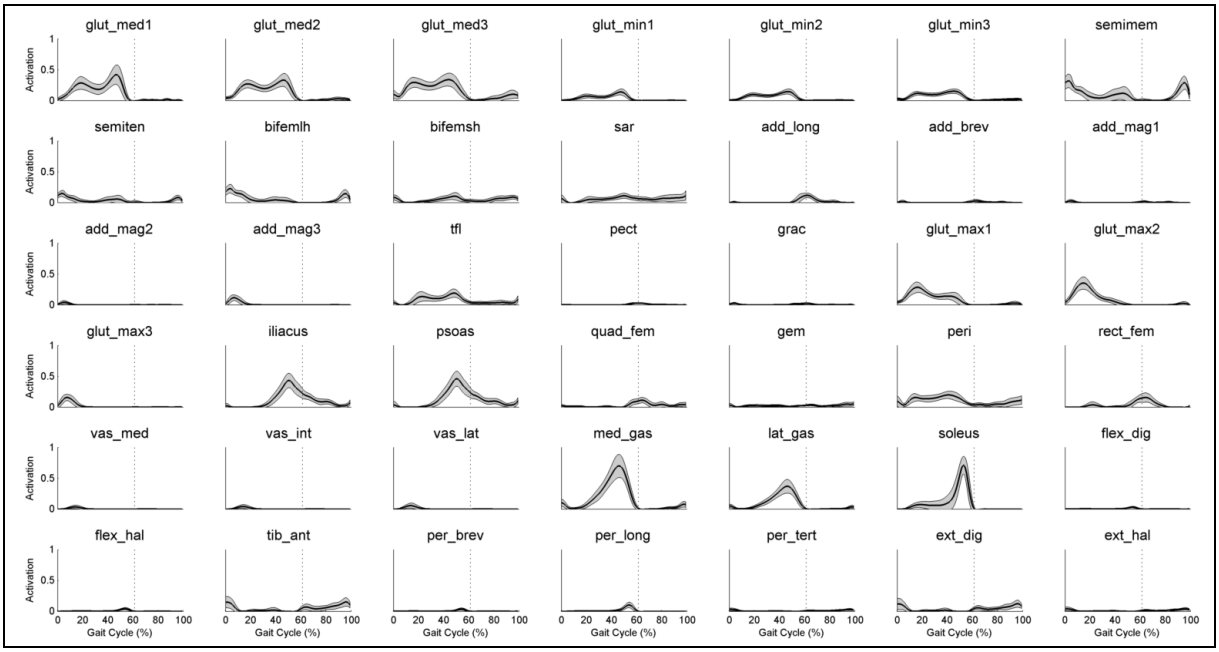

Figure 5.18 – Mean actuator activations (±1SD) from all 46 control subject gait cycle simulations. The vertical dotted black line marks the transition between the stance phase and swing phase. Trunk actuators and tib-post are omitted for graphical simplification purposes

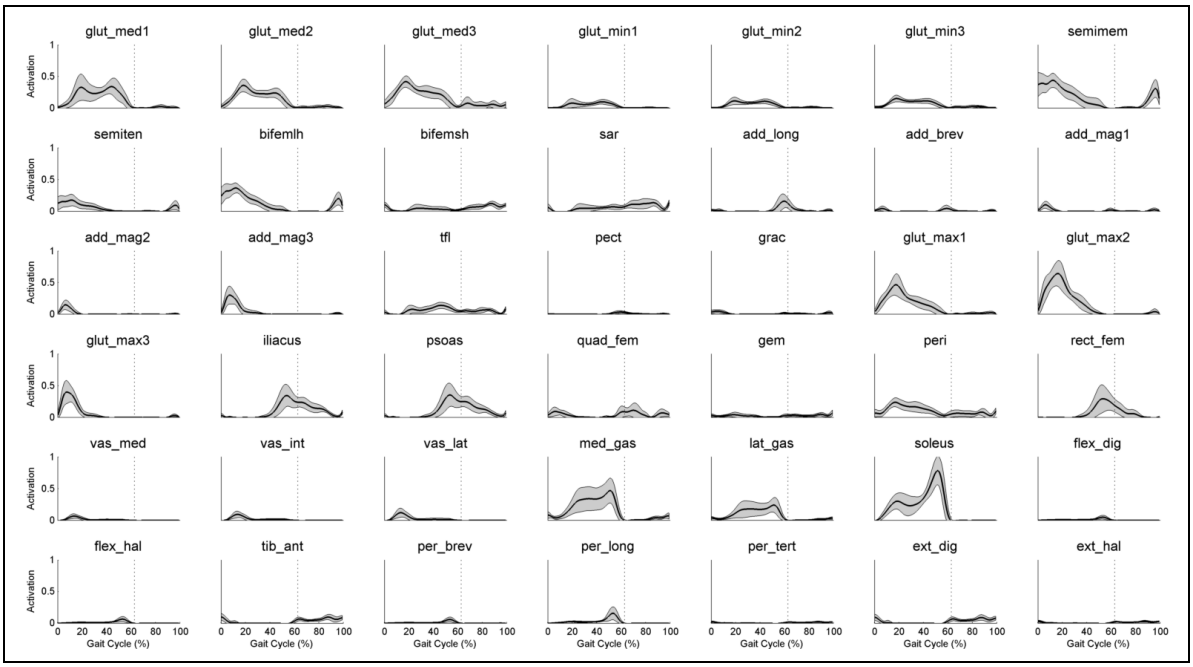

Figure 5.19 – Mean actuator activations (±1SD) from all 20 case subject gait cycle simulations. The vertical dotted black line marks the transition between the stance phase and swing phase. Trunk actuators and tib-post are omitted for graphical simplification purposes

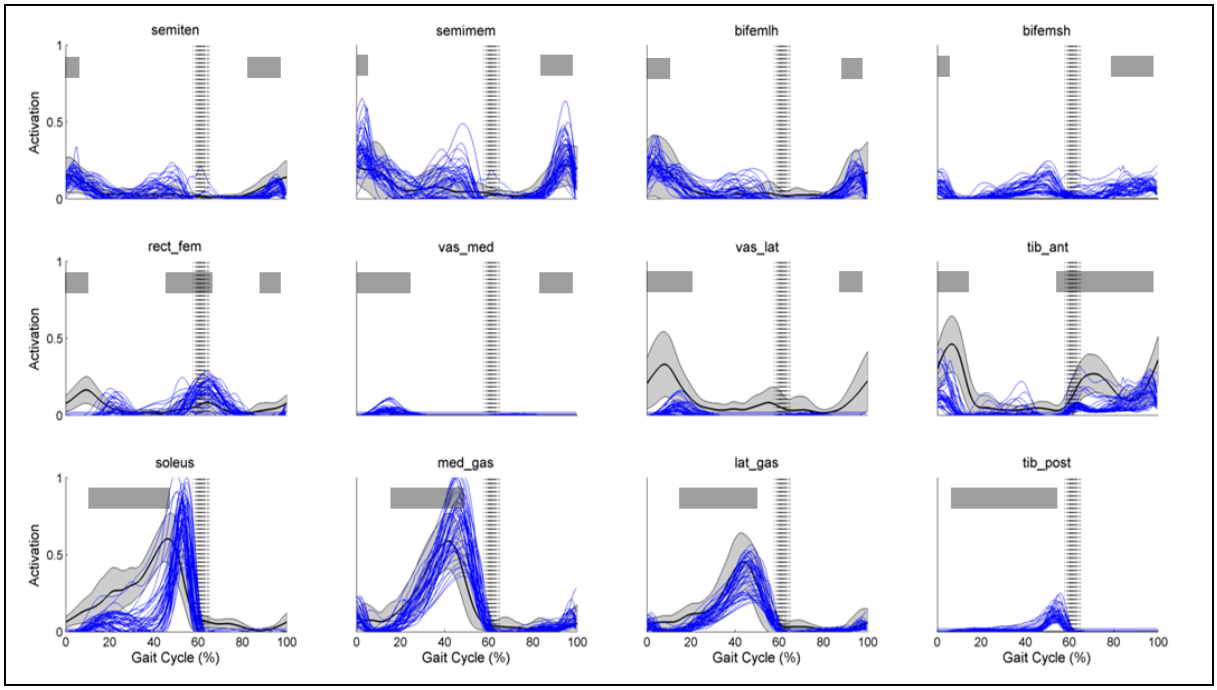

Figure 5.20 – Control subject simulated activations. Individual trial actuator activations (blue) and mean experimental muscle activation (black ±1SD) from all 46 control trials. No EMG was collected from bifemsh, vas_med or tib_post. Grey horizontal bars = normal adult EMG timings from Sutherland (2001)

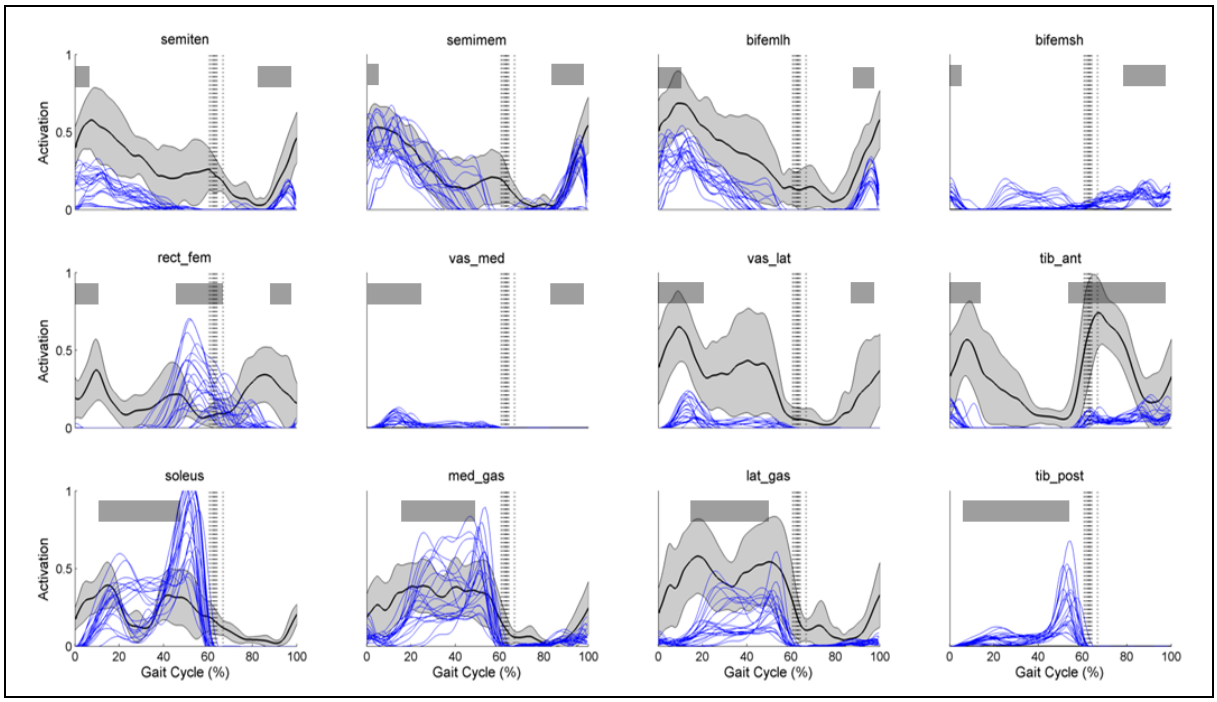

Figure 5.21 – Case subject simulated activations. Individual trial actuator activations (blue) and mean experimental muscle activation (black ±1SD) from all 20 case trials. No EMG was collected from bifemsh, vas_med or tib_post. Grey horizontal bars = normal adult EMG timings from Sutherland (2001)

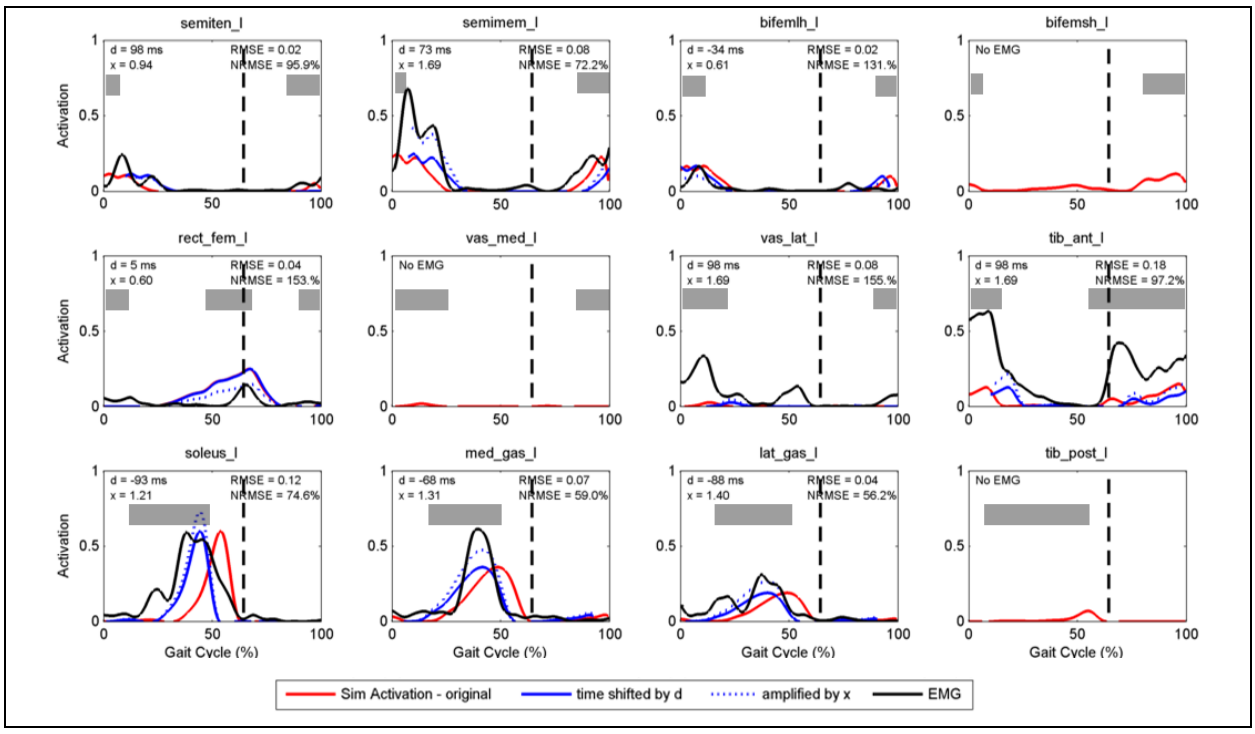

Figure 5.22 – Example validity analysis trial from Control09 for all EMG muscles (mean RMSE = 0.08 degrees)

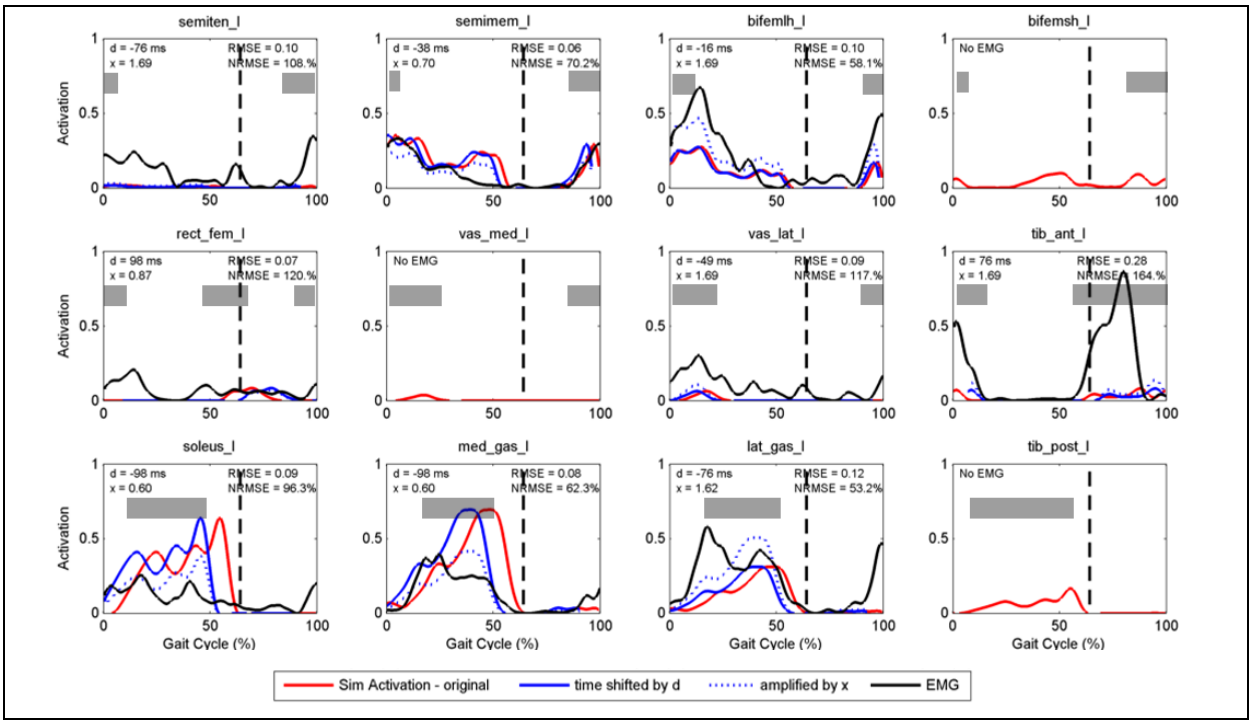

Figure 5.23 – Example validity analysis trial from Case02 for all EMG muscles (mean RMSE = 0.11 degrees)

RMSE was calculated between the adjusted simulated muscle activations (dotted blue curves) and the experimental muscle activations (black curves). Adjustment of the original simulated activations (red curves) involved a time shift by *d* (blue curves) and then a change in magnitude by *x*. The dashed black line marks the transition between the stance and swing phase of the gait cycle. Grey horizontal bars show normal adult EMG timings from Sutherland (2001)

The variances of intra-subject experimental activations (V_1), intra-subject simulated activations (V_2) and inter-subject experimental activations (V_3) were calculated using Equation 5.5. On average (across both groups) the V_1 variances were 4.3 times higher than the corresponding V_2 variances showing that there was generally higher variation in an individual's EMG than in the their simulated muscle activations. All three variances ($V_{1\text{-}3}$), lower and upper bounds of the RMSE validity range and the mean RMSE between simulated muscle actuator activations and experimental muscle activations can be seen in Figure 5.24.

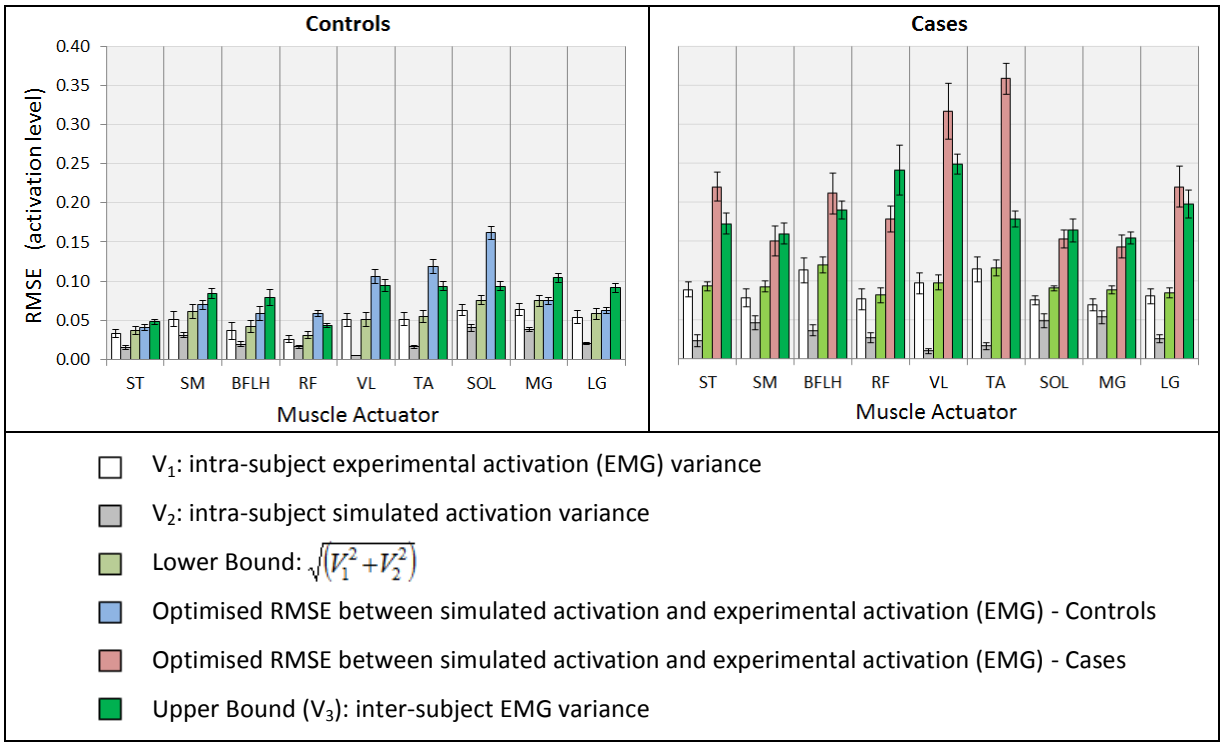

Figure 5.24 – Variance of activation data

Mean RMSE between simulated muscle actuator activations and experimental muscle activations (EMG) from all successfully simulated control (blue) and case (red) subject gait cycles. Variances ($V_{1\text{-}3}$) are also shown with the lower and upper bounds of the RMSE validity range indicated by green bars.

Error bars show ±1SE EMG = electromyography

The mean invalidity ratios were calculated using Equation 5.7 for both the un-optimised and optimised simulated activations and the results are shown in Figure 5.25.

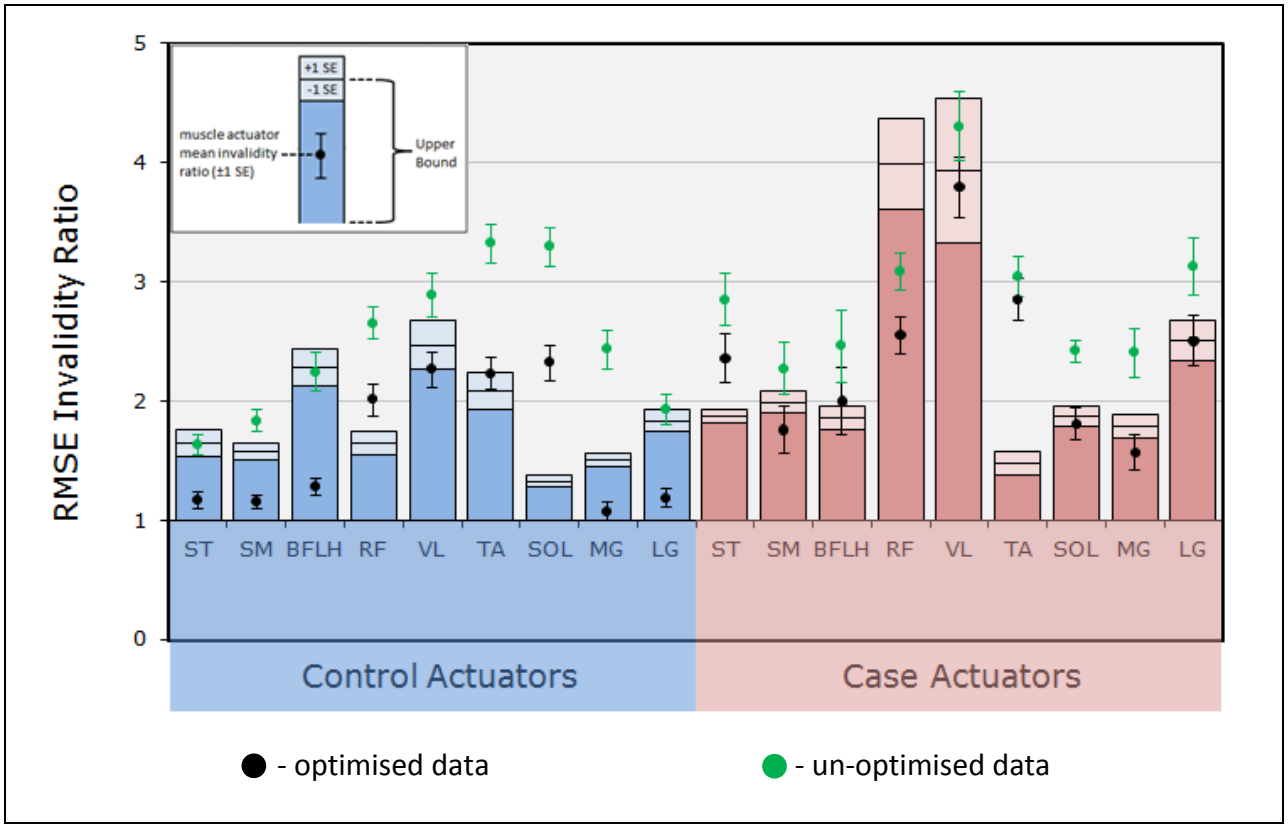

Figure 5.25 – The invalidity ratio (R)

Mean RMSE invalidity ratios for both groups from all successfully simulated gait cycles for all nine muscle actuators for which EMG data was collected.

Mean RMSE invalidity ratios are shown for both optimised (black dots) and un-optimised (green dots) data following the optimisation procedure shown in Figure 5.3. Gain compensation was set to between 0.6-1.7 and the maximum time shift was set to ±0.1s.

The underlying coloured regions (blue = control group, red = case group) show the RMSE validity range for each muscle. The block at the bottom shows the lower bound (R=1) as calculated from the sum of intra-subject experimental activation variance (V_1) and intra-subject simulated activation variance (V_2). The bar shows the upper bound as calculated from the group inter-subject experimental activation variance (V_3).

Simulated muscle activations are therefore only considered valid if the corresponding invalidity ratio lies below the upper bound (i.e. the dot appears within or below the top of the bar).

5.4. Discussion

Looking at Figure 5.18 and Figure 5.19 it can be seen that similar simulated muscle actuator activation patterns were found in both groups except for the rectus femoris and calf muscles (med_gas, lat_gas, soleus) which showed premature activity in the case group. Activations were also more consistent in the control group as can be seen from the tighter standard deviation bands.

A good agreement can be seen between the experimental muscle activations of the control group and published timings of normal adult EMG (Figure 5.20). There is also a reasonable agreement between the peak experimental activations of the case group and published timings of normal adult EMG (Figure 5.21) except for the high activation of vastus lateralis (vas_lat) in mid-stance and prolonged early stance activity of the hamstrings (semiten, semimem, bifemlh). The experimental activations of the case group also show generally prolonged activity compared to the control group – a possible indication of increased tone that would be expected in these subjects. This can also be seen in the individual case-control comparison in Figure 5.22 and Figure 5.23.

A visual comparison of simulated muscle actuator activity against the mean experimental activations (Figure 5.20 and Figure 5.21) can provide a qualitative indication of the validity of the simulated muscle activation. Looking at the differences in shape only (to mimic the time shift and gain compensations carried out in the RMSE optimisation) the least valid simulated actuator activations in the control group appear to be the rectus femoris which shows a lack of activity during loading response and the soleus with reduced activity during mid-stance. It is more difficult to make a visual assessment of the case group data due to the variability of the simulated activations but in general there is a good agreement in shape for all the muscle actuators except for the rectus femoris and late swing vastus lateralis. The semitendinosus, vastus lateralis, and tibialis anterior also show largely reduced activation amplitude compared to their experimental data.

The effects of the time shift and gain compensation optimisation can be seen in Figure 5.22 and Figure 5.23. The optimisation succeeds in closely matching many of the simulated activation curves to the experimental data. However, a poor match is found in the muscles which have low simulated activation levels due to the limit on the gain compensation.

There are a number of difficulties associated with the use of a root mean square error analysis methodology for curve comparison. Although RMSE data can be intuitive as it has the same units as the parameter of interest (in this case muscle activation) comparison of magnitudes between muscles can be misleading. This is because a finite change in activation of a very active muscle is of less interest than the same finite change in activation of a less active muscle and yet the RMSE values will be the same. One solution to this problem is to normalise the RMSE data to the mean muscle activation (either experimental or simulated) to provide a measure that takes the activation level into account and so emphasise the more significant changes in muscle activation. However, despite this advantage, this normalisation method also introduces problems. Firstly, normalised RMSE is a dimensionless parameter which makes it less intuitive to interpret and, secondly, as the case group generally shows higher levels of experimental activation than the control group, such normalisation may confound genuine differences between the groups. The alternative normalisation method used in calculating the invalidity ratio (Equation 5.7) overcomes this problem as the RMSE is normalised to the variance in experimental activation rather than the magnitude of the experimental activation, and so differences in mean activation between the groups are ignored.

Figure 5.24 shows the data variance in intra and inter-subject experimental activation (V_1 and V_3) and simulated activation (V_2) as well as the RMSE difference between the experimental and simulated data. On average the V_1 variances are 4.3 times higher than the corresponding V_2 variances showing that there was generally higher variation in an individual's EMG than in the their simulated muscle activations for both the control group and the case group. This ratio is particularly high for the vastus lateralis in both groups due

to very low values of V_2 (consistent simulated activations). Both intra and inter-subject experimental activation variance (V_1 and V_3) are higher in the case group which is to be expected in individuals with cerebral palsy (also clearly seen in Figure 5.21). The RMSE differences between simulated activations and experimental activations are higher in the case group but, due to the difficulties of interpreting RMSE data as discussed above, it is unclear whether this is due to poorer matching of simulated to experimental activations or rather due to the generally higher activity of the case muscle actuators. This should be revealed in the invalidity ratios.

An invalidity ratio of R=1 represents a RMSE deviation between an individual's simulated muscle activation and their experimental muscle activation of similar magnitude to the variance in that individual's experimental muscle activation (EMG). Using a validity range of R < Upper Bound (V_3) and looking at the un-optimised data in Figure 5.25 it can be seen that all simulated muscle activations in both groups were found to be either invalid or on the border of invalidity except for the rectus femoris in the case group. This is due to the high upper bound of this actuator as a result of a particularly high V_3 and low V_1 and V_2 (Figure 5.24). This was also the cause for a high upper bound for the vastus lateralis in the case group. However, on visual inspection of Figure 5.21, it is clear that the simulated muscle activations for the rectus femoris in the case group should also be considered invalid.

Looking at the optimised data in Figure 5.25 and using the same validity threshold, consistently invalid simulated muscle activations were generated in the control group for the rectus femoris and soleus, with vastus lateralis and tibialis anterior being on the border of invalidity. Both rectus femoris and soleus were identified from Figure 5.20 as having poor shape matches to their experimental data. Vastus lateralis and tibialis anterior score poorly due to reduced amplitude of simulated activation compared to experimental data.

In the case group consistently invalid simulated muscle activations were generated for the semitendinosus and tibialis anterior, with biceps femoris long head, vastus lateralis, soleus

and lateral gastrocnemius being on the border of invalidity. Again, three of these muscles, semitendinosus, vastus lateralis and tibialis anterior, were identified from Figure 5.20 as likely to be invalid due large deficiencies in activation amplitude compared to their experimental data. Biceps femoris long head and lateral gastrocnemius also exhibit deficiencies in activation amplitude compared to their experimental data and simulated activation of the soleus has a mismatched peak in late stance. It was expected that rectus femoris would also be calculated as invalid but, as explained above, it was not due to a high upper bound of the validity range.

5.5. Conclusions and Limitations

Musculo-skeletal models scaled to height, mass and muscle volume were created for ten typically developing adolescents and ten adolescents with cerebral palsy. Each model's muscle activations were allowed to vary in order to track the subject's recorded walking pattern and the validity of a selection of simulated muscle activations were then determined by comparison with activations derived from experimental EMG data.

A problem with simulated muscle activations as calculated by the Computed Muscle Control algorithm was observed – specifically the high activation and mid-stance activation of the tibialis anterior actuator. These unlikely muscle activations correlated with instability (acceleration "ringing") in the resulting model kinematics which was found to be very sensitive to the algorithm set-up parameters, and in particular to the time window used in the forward dynamics step.

In addition to the testing of the sensitivity of muscle activations to changes in muscle strength (Chapter 4) and as part of the investigation into the instability of the Computed Muscle Control algorithm, some preliminary tests were performed looking at the sensitivity of muscle activations to changes in tendon slack length and (as the lengths are linked) to muscle fibre length. The relationship of these muscle model parameters to the net musculo-tendinous unit force is complex and a separate investigation would be needed to fully examine the sensitivity of muscle activations to changes in each of these

parameters. However, these initial tests resulted in large changes to muscle activations and so it is likely that muscle force and activation will show high sensitivity to changes in these parameters. This is in accordance with the brief sensitivity analysis carried out by Delp in his original work on the development of SIMM (Delp, 1990). As a result of this sensitivity of the Computed Muscle Control algorithm to a number of set-up parameters, the algorithm was classified as non-robust (Lin et al., 2011) and only simulated activation data as calculated using Static Optimisation was carried forward to the validity analysis.

A good agreement between simulated and experimentally derived activations in typically developing subjects was hypothesised as previous researchers have commented on the similarity of such data (section 5.1). However, contrary to this hypothesis, using a validity threshold based on the variance of the group's experimentally derived activations, all simulated muscle activations were found to deviate from experimentally derived activation patterns. After allowing a generous optimisation in both amplitude and time, the deviation of 5/9 of the simulated muscle actuators were reduced to acceptable levels: semitendinosus, semimembranosus, biceps femoris long head, medial gastrocnemius, lateral gastrocnemius.

A poor agreement between simulated and experimentally derived activations in subjects with cerebral palsy was hypothesised as co-activation and poor selective activation associated with this group (section 1.2) are unlikely to result in activation patterns that would be predicted by algorithms based on the minimisation of total muscle activation. In agreement with this hypothesis, all of the muscle actuator activations tested in the cerebral palsy group in this study were found to deviate from experimentally derived activation patterns. After optimisation, an acceptable agreement between simulated and experimental activation was achieved for 3/9 of the simulated activations: semimembranosus, rectus femoris and medial gastrocnemius.

Only walking trials that passed the simulation checks described in section 5.2.3 were used in this analysis and so it can be assumed that the simulated muscle activations and resultant joint torques successfully recreate the experimental kinematic and kinetic data

recorded during each walk. These simulated activations therefore are an alternate solution to walking than that actually employed by the subjects. Deviation from experimental activation is likely therefore to result from a number of other factors including mechanical differences between the bespoke musculo-skeletal models and the subjects' bodies, non-physiological muscle models, and/or use of an inappropriate cost function to calculate the muscle force distribution to recreate experimental kinetic data.

In conclusion, the muscle activations (and corresponding forces) as determined by the cost function in the Static Optimisation algorithm are generally invalid in comparison to the experimentally derived activations, and so muscle contributions to support and progression in walking as could be calculated from an induced acceleration analysis using these alternate solutions to human gait are unlikely to be correct. Reliably accurate and detailed knowledge of muscle function during walking, especially the differences between normal walking and pathological walking patterns, would be an invaluable aid to both treatment decision making and to improving the efficacy of intervention. However, this type of analysis has been carried out in many studies in the literature, none of which have attempted to conduct a quantitative analysis of the level of agreement between their simulated and experimentally derived muscle activations. If musculo-skeletal modelling techniques such as these are to be adopted into routine clinical gait analysis methods then clinicians need to have confidence in the data that they produce.

There are a number of limitations in this validation technique that need to be considered. As stated in section 5.3.4, the intra-subject EMG variance (V_1) was on average 4.3 times higher (3.3 controls, 5.3 cases) than the corresponding intra-subject simulated activation variance (V_2). This is an interesting finding that raises the question of whether surface EMG has inherent features which essentially make it un-trackable (Hakanson, 2010). If true, this implies that surface EMG is not a good signal to use for the validation of simulated muscle activations.

Possible alternative methods for validation could be to track the position of musculo-tendinous junctions during walking (using portable ultrasound imaging techniques) and

compare these experimental datasets with simulated positions. Alternatively, fine-wire EMG may give more consistent signals than surface EMG as the wire electrodes are less prone to cross-talk (the detection of electrical activity from neighbouring muscles) and they do not suffer from the complications of signal transmission through soft tissue. However, as fine-wire EMG only detects very local electrical activity some variation will likely occur based on the local motor-unit recruitment strategy. In fact there is lack of consensus in the literature as to which modality is better as reliability can be affected by the intensity of contraction (Semciw et al., 2014) or the type of activity (Chapman et al., 2010; Kadaba et al., 1985).

Another limitation to this validation procedure is the inherent bias introduced by the dependence of the invalidity thresholds on the experimental and simulated muscle activations. As stated in section 5.4, both the experimental and simulated muscle activations were more consistent in the control group leading to smaller intra and inter-subject variances ($V_{1\text{-}3}$). An imbalance therefore exists between the invalidity thresholds of the two groups with the control group thresholds being lower.

6 Summary

Cerebral palsy is a condition caused by a brain injury that typically occurs during the peri-natal period. This primary injury is non-progressive but as important neurological development and growth occur after this period, progressive secondary abnormalities often result that can lead to reduced mobility and walking difficulties. Clinical gait analysis has for many years been used by clinicians working with this patient group. A subject's walking pattern can be defined by their kinematics, kinetics and spatio-temporal parameters and the deviations identified by comparison to unaffected individuals. However, these techniques are essentially a pattern recognition tool that relies on the experience of the interpreting clinician to find clinical meaning.

It has been suggested therefore that incorporating musculo-skeletal modelling methods within the gait analysis process may provide a more objective analysis of the causes of walking difficulties. For example, the energy cost or mechanical disadvantage of a deformity can be calculated, and the efficacy of potential interventions evaluated in the virtual environment as an aid to treatment decision making. However, there are currently a number of limitations to these techniques and so there is a need for evaluation and validation of such methods.

This programme of work therefore included a validity analysis of muscle activations generated using musculo-skeletal modelling simulations of human walking. Validity was assessed for both typically developing adolescents and for ambulant adolescents with cerebral palsy.

6.1. Review of Work

This programme of work set out with the following set of aims:

1. To measure and compare muscle morphology between typically developing adolescents and independently ambulant adolescents with cerebral palsy.

2. To evaluate the sensitivity of simulated muscle activations in the OpenSim model to changes in lower limb muscle volumes in typically developing adolescents during walking.

3. To evaluate the validity of simulated muscle activations in both subject groups by comparison to EMG data.

Findings of this programme of work were:

1. Muscle volumes and fibre lengths were found to be smaller in the case group with smaller volumes more prominent in the distal musculature. Physiological cross-sectional area was found to be larger in the thigh and smaller in the shank for the case group and no difference between groups was found in pennation angle. A high variation in reported muscle pennation was noted from the literature.

2. In general the model was insensitive to changes in muscle strength with only small increases in muscle activation resulting from decreases in muscle strength over a normative range. However, large increases in activation occurred in synergist and compensatory muscles when any muscle approached maximum activation.

3. All simulated muscle actuator activations that were tested were found to be invalid. After a generous optimisation process which allowed limited change to the activations in both amplitude and time, valid simulated activations were found in the control group for semitendinosus, semimembranosus, biceps femoris long

head, and both heads of the gastrocnemius; and in the case group for semimembranosus, rectus femoris and lateral gastrocnemius.

To the author's knowledge, this is the first study to carry out a quantitative validation of simulated muscle activations during walking in typically developing individuals and individuals with cerebral palsy.

6.2. Clinical Implications

Muscle volumes were found to be smaller in the cerebral palsy group in 18/19 of the muscles measured when normalised to body mass. Significant volume reductions were found in the gluteus minimus, rectus femoris, biceps femoris long head, semimembranosus, tibialis anterior and all three calf muscles. Mean percentage muscle volume deficits were 32% for the distal muscles compared to 16% for the proximal muscles. With the exception of sartorius there was a trend for larger volume deficits in the biarticular muscles compared to their monoarticular neighbours. This volume data has now been published (Noble et al., 2013) as part of a larger study of muscle morphology.

Despite finding smaller muscle volumes in the cerebral palsy group, and contrary to the accepted premise that cerebral palsy subjects have weaker muscles, muscle physiological cross-sectional areas were found to be larger in the thigh muscles (principally the quadriceps) of the case group compared to their typically developing peers. If this is a genuine finding it is possible that, due to distal weakness and poorer motor control, individuals with cerebral palsy make more use of their proximal musculature for tasks such as walking and hence alter the morphology of these muscles to make them stronger.

6.3. Methodological Findings

The increase in thigh muscle physiological cross-sectional area in the case group appears to be driven by more marked shortening of the fascicle lengths in the thigh muscles. However, this is uncertain as a poor relationship was found between fascicle lengths and

leg length and so the trend for shorter fascicle lengths in the thigh may be an artefact of the normalisation scheme. Additionally, the high variation in reported muscle pennation that exists in the literature highlights the difficulty in measuring these muscle parameters.

Muscle volume is proportional to physiological cross-sectional area which is the only muscle parameter directly proportional to the maximum tension that can be generated by a muscle. In the OpenSim gait2392 model, simulated muscle activations were shown to be insensitive to changes in muscle strength over a normative range (82-144% of the generic model strength) based on the muscle volumes of the control group. However, in the weakest sensitivity model some muscles were shown to approach maximum activation, a state where sensitivity to changes in muscle strength increased. Therefore, as the subjects in the case group were shown to have smaller and hence weaker muscles than the control subjects (40-110% of the generic model strength compared to 63-167%) then it is likely that simulations of muscle activation using models scaled to the muscle volumes of this patient group may encounter sensitivity complications caused by muscle activation saturation. This questions the suitability of using these models in the analysis of subjects with cerebral palsy.

The validity of nine simulated muscle actuator activations were evaluated by comparison to experimental activations derived from EMG data. All simulated activations were found to be invalid. Although there are many possible limitations in the musculo-skeletal modelling process that may have resulted in these discrepancies in experimentally derived versus simulated activation, the principal cause is likely to be the optimisation procedure used to overcome the static indeterminacy problem of calculating muscle forces from joint torques. This is carried out in the OpenSim Static Optimisation algorithm by minimizing the cost function $\sum(\text{activation})^2$ – Equation 2.16. As confirmed by the results of this study, this function was expected to be inappropriate for individuals with cerebral palsy due to muscle abnormalities such as spasticity and co-contraction which will work against the principles of this cost function. Based on the results of this study it would also appear that this cost function is also inappropriate for use in typically developing subjects. If musculo-skeletal modelling techniques, such as those used in this programme of work

and in the literature, are to be used in the simulation of muscle activity in individuals with neurological conditions such as cerebral palsy, then there is a need for alternative optimisations that incorporate the neurological aspects of these conditions. It may be appropriate to call such techniques neuro-musculo-skeletal modelling. However, due to the variety of cerebral injuries that exist in this group, a generic solution may not be possible. If this is the case, then alternate, hybrid solutions may be necessary that combine bespoke measurements of muscle morphology with EMG-driven simulation techniques (Lloyd & Besier, 2003; Shao et al., 2009).

As simulated muscle activations were found to be invalid, this data could not be used in any further techniques, such as induced acceleration analysis, to evaluate muscle contributions to support and progression during walking.

6.4. Conclusion

Musculo-skeletal modelling techniques were used to test the sensitivity of simulated muscle activations to changes in model muscle strength and to test the validity of simulated muscle activations against experimentally derived activations in typically developing subjects and subjects with cerebral palsy. If bespoke muscle strengths are used for this group then sensitivity is likely to be high and simulated muscle activations were shown to be invalid. There is also a lack of consensus in the literature between studies using these techniques to calculate muscle contributions in gait. Other studies have also shown variation in the output of such modelling techniques dependent on a number of factors including the number of degrees of freedom in a model and the modelling of the foot-ground interaction. Additionally, in this programme of work, the Computed Muscle Control algorithm was shown to be non-robust – specifically in relation to ankle acceleration “ringing” effects which were sensitive to the forward dynamics time window. Therefore, at present, it would be inappropriate to use these simulated muscle activations in further analyses such as induced acceleration analyses to evaluate muscle function. Further work is necessary to develop and evaluate these modelling methodologies in

order to gain confidence in the outputs of such “black box” techniques. It is hoped that these methods will then prove a valuable tool for use in the clinical setting.

6.5. Future Work

As described above, a poor relationship was found between fascicle lengths and leg length in this study suggesting that the shorter fascicle lengths found in the cerebral palsy group may have been an artefact of the normalisation scheme. It would be interesting to re-normalise the fascicle length data by muscle length, a commonly reported normalisation method, to see if the difference in fascicle length between the groups, and the more marked shortening in the thigh muscles, remains.

Simulated muscle activations in the OpenSim gait2392 model were shown to be insensitive to changes in muscle strengths over a normative range. It would also be interesting to examine the sensitivity of model outputs to changes in other muscle model parameters such as *tendon_slack_length*. Imaging data similar to that collected in this study could be used for example to determine a normative range of optimum fibre lengths and passive stiffnesses – both parameters that have direct effects on the force that a muscle can generate, and that could be altered in pathological muscle.

In this study simulated muscle activations were found to be invalid in both typically developing adolescents and adolescents with cerebral palsy. Although this may have been the result of a number of limitations in the musculo-skeletal model, i.e. incorrect bony geometry, muscle attachments, muscle moment-arms, and/or un-physiological muscle models, the principal cause is likely to be the optimisation procedure used to calculate muscle forces from joint torques. It is also likely that different cost functions will be necessary to accurately emulate muscle recruitment patterns employed by typically developing subjects and subjects with a neurological condition. Investigations examining different optimisation cost functions and the validity of the resulting simulated muscle activations would therefore be warranted.

Such studies would contribute to one part of the more general question: do we need personalised models? It is intuitive that a more personalised model will have the potential to produce more accurate data, but unless techniques are developed to speed-up/automate the conversion of imaging data to musculo-skeletal models then the heavy work load of this process currently prevents its use outside the research environment. However, work has been carried out looking at the differences in simulation outputs from bespoke verses generic models, specifically muscles' lines of action and bony geometry. More studies of this nature may provide the necessary knowledge to create quasi-bespoke models that incorporate enough elements of an individual's unique musculo-skeletal make-up to ensure accurate simulation, but few enough elements to enable them to be used practicably in a routine clinical setting.

Appendix A – Ethical Approval

NHS

National Research Ethics Service

South East London REC 1

(Formerly Guy's REC)
Governor's Hall Suite
St Thomas' Hospital
London
SE1 7EH

Telephone: 020 7188 2260
Facsimile: 020 7188 2258

06 January 2011

Dr Adam P Shortland
Consultant Clinical Scientist
One Small Step Gait Laboratory,
Guy's Hospital
St Thomas Street
London SE1 9RT

Dear Dr Shortland

Study Title: **Lower Limb Muscle Contributions to Support and Progression During Human Walking in Typically Developing Subjects and Subjects with Cerebral Palsy.**

REC reference number: **10/H0804/83**

Thank you for your letter of 22 November 2010, responding to the Committee's request for further information on the above research and submitting revised documentation.

The further information has been considered on behalf of the Committee by the Chair.

Confirmation of ethical opinion

On behalf of the Committee, I am pleased to confirm a favourable ethical opinion for the above research on the basis described in the application form, protocol and supporting documentation as revised, subject to the conditions specified below.

Ethical review of research sites

The favourable opinion applies to all NHS sites taking part in the study, subject to management permission being obtained from the NHS/HSC R&D office prior to the start of the study (see "Conditions of the favourable opinion" below).

The Committee has not yet been notified of the outcome of any site-specific assessment (SSA) for the non-NHS research site(s) taking part in this study. The favourable opinion does not therefore apply to any non-NHS site at present. I will write to you again as soon as one Research Ethics Committee has notified the outcome of a SSA. In the meantime no study procedures should be initiated at non-NHS sites.

Conditions of the favourable opinion

The favourable opinion is subject to the following conditions being met prior to the start of the study.

Management permission or approval must be obtained from each host organisation prior to the start of the study at the site concerned.

For NHS research sites only, management permission for research ("R&D approval") should be obtained from the relevant care organisation(s) in accordance with NHS research governance arrangements. Guidance on applying for NHS permission for research is available in the Integrated Research Application System or at http://www.rdforum.nhs.uk.

Where the only involvement of the NHS organisation is as a Participant Identification Centre (PIC), management permission for research is not required but the R&D office should be notified of the study and agree to the organisation's involvement. Guidance on procedures for PICs is available in IRAS. Further advice should be sought from the R&D office where necessary.

Sponsors are not required to notify the Committee of approvals from host organisations.

It is the responsibility of the sponsor to ensure that all the conditions are complied with before the start of the study or its initiation at a particular site (as applicable).

Approved documents

The final list of documents reviewed and approved by the Committee is as follows:

Document	*Version*	*Date*
Protocol	1	01 September 2010
Letter of invitation to participant	Adult v:1	01 September 2010
Letter of invitation to participant	Parent/Guardian v:1	01 September 2010
Response to Request for Further Information		22 November 2010
Participant Information Sheet: Child Control	2	18 November 2010
Participant Information Sheet: Parent/Guardian Control	2	18 November 2010
REC application	Parts A - D	10 September 2010
Participant Consent Form: Parent/Guardian Case	2	18 November 2010
Participant Consent Form: Parent/Guardian Control	2	18 November 2010
Participant Information Sheet: Child Case	2	18 November 2010
Participant Information Sheet: Parent/Guardian Case	2	18 November 2010
Referees or other scientific critique report		12 August 2010
Covering Letter		14 September 2010
Investigator CV	Dr Adam Shortland	01 September 2010
Investigator CV	Andrew Lewis	01 September 2010
Participant Information Sheet: Adult Case	2	18 November 2010
Participant Information Sheet: Adult Control	2	18 November 2010
Participant Consent Form: Adult Case	2	18 November 2010
Participant Consent Form: Adult Control	2	18 November 2010

Statement of compliance

The Committee is constituted in accordance with the Governance Arrangements for Research Ethics Committees (July 2001) and complies fully with the Standard Operating Procedures for Research Ethics Committees in the UK.

After ethical review

Now that you have completed the application process please visit the National Research Ethics Service website > After Review

You are invited to give your view of the service that you have received from the National Research Ethics Service and the application procedure. If you wish to make your views known please use the feedback form available on the website.

The attached document *"After ethical review – guidance for researchers"* gives detailed guidance on reporting requirements for studies with a favourable opinion, including:

- Notifying substantial amendments
- Adding new sites and investigators
- Progress and safety reports
- Notifying the end of the study

The NRES website also provides guidance on these topics, which is updated in the light of changes in reporting requirements or procedures.

We would also like to inform you that we consult regularly with stakeholders to improve our service. If you would like to join our Reference Group please email referencegroup@nres.npsa.nhs.uk.

10/H0804/83	**Please quote this number on all correspondence**

With the Committee's best wishes for the success of this project

Yours sincerely

Professor David Bartlett
Chair

Email: stephanie.hill@gstt.nhs.uk

Enclosures: "After ethical review – guidance for researchers" *SL- AR2 for other studies*

Copy to: *Karen Ignatian, R & D, Guy's & St Thomas' Foundation NHS Trust*

Appendix B – Example Patient Information Sheets

One Small Step Gait Laboratory
Guy's Hospital
London
SE1 9RT

Guy's and St Thomas' NHS
NHS Foundation Trust
Hospital No: 020 7188 7188
Gait Lab No: 020 7188 2476
Gait Lab Fax: 020 7188 2477
E-mail: adam.shortland@gstt.nhs.uk

PARENT/GUARDIAN INFORMATION SHEET

STUDY TITLE
Muscle Contributions to Support and Progression in Human Walking

INTRODUCTION
Your child is invited to take part in a research study. Before you decide whether or not you would like your child to take part, it is important for you to understand why the research is being done and what it will involve. Please take time to read the following information carefully and discuss it with friends, relatives and your GP if you wish. Ask us if there is anything that is not clear or if you would like more information. Take time to decide whether or not you wish your child to take part.

WHAT IS THE PURPOSE OF THIS STUDY?
In this study, we hope to learn about the differences in how the calf muscles are used by typically developing people compared with people with cerebral palsy. We think that individuals with cerebral palsy suffer from changes in their muscles, such as having smaller muscles or an increase in fat and connective tissue content, that can cause their muscles to be weaker than their typically developing peers. Changes in bone shape can also mean that muscles have to work harder than normal.

We will take measurements of your child's calf muscles and bones using ultrasound imaging and magnetic resonance imaging (MRI) as well as measuring the stiffness of their calf muscle tendons. We will also record their walking pattern using a motion capture system. This data with then be used to create a 3D computer model of your child's muscles and bones similar to the one you can see in figure 1.

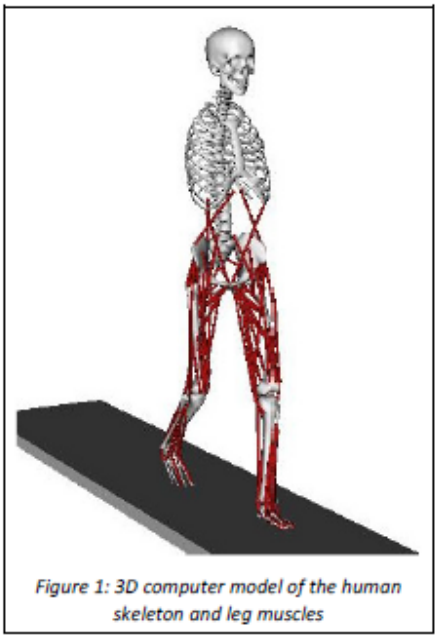

Figure 1: 3D computer model of the human skeleton and leg muscles

The computer model will be moved to match your child's walking pattern and calculations will be made to estimate which of their leg muscles are most useful for supporting their body against gravity and which are most useful for moving their body forwards as they walk.

WHY HAVE YOU BEEN CHOSEN?

Your child has cerebral palsy. We are asking 10 individuals with cerebral palsy to participate. We hope to learn more about how the muscles of individuals with cerebral palsy differ from their typically developing peers by comparing the data from typically developing subjects and subjects with cerebral palsy.

WHO DECIDES IF I WILL TAKE PART?

Any child or young adult aged between 10 and 22 years of age who has cerebral palsy may be asked to take part. It is important that they have not received any orthopaedic surgery or treatment on their lower limbs in the last 12 months. The decision to take part is up to you and your child. If you decide you would like your child to take part then you will be asked to sign a consent form on their behalf.

WHAT IS BEING ASKED OF YOU?

If you agree to allow your child to take part in the study when you come to Guy's Hospital for your child's clinical gait analysis appointment we will simply take a few extra measurements. The whole appointment will not take more than four hours. Once at the hospital we will check that you are still happy for your child to take part in the study and if so ask you to sign the consent form. There will also be a short questionnaire to fill in about your child's mobility and how easy they find it to walk.

In the first part our the study you will be accompanied by a member of the research team up to the MRI unit of the hospital. Here your child will need to remove any metal objects that they are wearing and they will be asked to lie in an MRI scanner for up to 30 minutes. This will be quite comfortable as you can see in figures 2 & 3 below and we are only scanning the legs and hips and so your child's head and arms will always be outside the scanner.

Figure 2: Required position during the scan

Figure 3: In the MRI scanner

The scanner can be quite noisy and so we will give them ear-defenders to wear. These also contain speakers so they can still talk to you and the research team or even listen to the radio.

The second part of the study will take place in the gait laboratory where we will then ask them to change into shorts and t-shirt and to lie on a couch. Here we will take measurements of their height, weight and how far they can move their hips, knees and ankles. We will place an ultrasound probe (as used to scan pregnant mothers) on the skin of their calf to obtain images of the calf muscles. We will also gently move their foot to stretch the calf muscle so we can measure the stiffness of the tendon.

Figure 4: A member of the research team wearing the plastic balls and sensors

Next, using sticky tape, we will attach small plastic balls to the skin near the ankles, knees, hips and shoulders. Our motion capture cameras will be able to see how these balls move and so we can record your child's movements in 3D. We will also stick some small sensors on their legs that can record the electrical signals of the muscles. This tells us when the body is turning muscles on and off. You can see how this will look in figure 4. Your child will then be asked to walk up and down a flat, straight, 10m walkway about ten times while we record the way they walk.

While we take the plastic balls and sensors off we will ask you both a few questions about your child's mobility, how far they can walk and if there is anything they find difficult as regards getting around and moving their body. All the tests combined should not take more than half a day.

WHAT ARE THE POSSIBLE RISKS/BENEFITS?

Ultrasound is considered a safe imaging technique. MRI is also considered safe and does not involve the use of ionising radiation. However, there are certain indirect hazards, primarily the presence of a strong magnetic field that will exert a force on magnetic materials near the scanner. Rigorous safety policies are in place to minimise these risks that meet the national and international safety guidelines for MRI. MRI has been carried out on tens of thousands of patients and volunteers at Guy's and St Thomas' Hospitals over more than 20 years without a serious adverse incident.

There are no benefits from taking part in this study.

WHAT IF YOU CHANGE YOUR MIND?

If either you or your child wish, they can withdraw from the study at any time and without giving any reason.

WHAT ABOUT CONFIDENTIALITY?
All information collected during the course of this study will be kept confidential. Any information leaving the hospital will have your and your child's personal details removed.

ARE THERE ANY COSTS?
No, you will be reimbursed for travelling expenses.

WHAT WILL HAPPEN TO THE RESULTS OF THIS STUDY?
We expect that the results of this study will be published in medical journals and presented at national and international meetings to other medical professionals.

WHO HAS REVIEWED THIS STUDY?
The research ethics committee at Guy's Hospital has reviewed this study.

WHAT SHOULD BE DONE WITH THIS INFORMATION SHEET?
Please take your time to read this information carefully and keep it for reference if you decide to allow your child to take part in this study.

WHEN YOU HAVE MADE A DECISION
If you decide that you would like your child to participate in this study then please contact Adam Shortland and he will organise an appointment for you both to come in to the One Small Step Gait Laboratory at Guy's Hospital. You will need to bring the consent form with you which should be at the back of this information pack. You should sign the consent form at the appointment and you will receive a copy for your records.

ANY QUESTIONS?
If you would like any more information about the study or have any concerns please contact: Adam Shortland, Clinical Scientist on 020 7188 2476.

One Small Step Gait Laboratory
Guy's Hospital
London
SE1 9RT

Guy's and St Thomas' NHS
NHS Foundation Trust
Hospital No: 020 7188 7188
Gait Lab No: 020 7188 2476
Gait Lab Fax: 020 7188 2477
E-mail: adam.shortland@gstt.nhs.uk

CHILD INFORMATION SHEET

WHAT WE WANT TO DO

We want to do a study to see how your muscles help you to stand and to walk.

WHAT WE WOULD LIKE YOU TO DO

We are asking if you would like to help us by taking part in our study.

WHAT WILL ACTUALLY HAPPEN?

You are already coming to the One Small Step Gait Laboratory, at Guy's Hospital in London, for an appointment. All we would like is, while you are here, for you to do a few extra things for us.

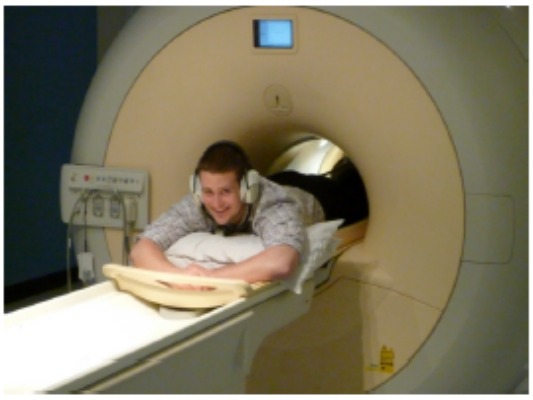

Picture 1:
What it looks like to be in the MRI scanner

The first thing we would like you to do is to have an MRI scan. This involves lying on a bed which will gently slide forwards and backwards so that you legs and hips move inside a large tube. Your head and shoulders will not go into the tube so you should be nice and comfortable. It can be a bit noisy with clicks and whirring sounds but you will get some head-phones to soften the noise and sometimes people are so comfortable that they actually fall asleep!

The machine will collect pictures of the muscles and bones in your legs and while this is happening we will ask you to stay as still as possible so that the pictures don't get blurred.

All the pictures should take about 30 minutes to collect, it doesn't hurt at all and you can even listen to music while it happens if you like (either the radio or your own music if you bring your favourite CD along). You can see what being in the MRI scanner will be like by looking at picture 1 above.

After the MRI scan, we will bring you down to the gait lab and ask you to get changed into swim wear or shorts and lie down on a bed. Here, we will move your legs around and take some measurements.

Next we will use an ultrasound machine to look at the muscles in your legs. This is done by moving a small piece of plastic over your skin that sends lots of little sound waves into your legs and creates pictures by listening to the echoes. The sound is so quiet that you won't be able to hear it and it doesn't hurt at all.

After this we will use sticky tape to stick small plastic balls around your ankles, knees, hips and shoulders. You can see how this will look by looking at picture 2 opposite. We will then ask you to walk up and down the room about ten times. Our special cameras are able to see how the balls move and so we can record the way you walk. This is the same technology that is used to make computer generated characters in films (like Gollum in The Lord of the Rings) and to record realistic movements for people in computer games. None of this will hurt at all but it might be a bit uncomfortable when we take the sticky tape off your legs. This may feel a bit like taking off a small plaster but we will do this carefully. The whole thing from start to finish will take about two hours.

Picture 2:
What is looks like to wear the motion capture balls

CAN YOU CHANGE YOUR MIND?

Yes. If you decide that you do not want to have these measurements taken then all you need to do is let your Mum, Dad, guardians or me know and then you won't have to have them done. If you decide you want to help us now but then change your mind later on, this is not a problem, you can stop joining in any time you want.

HAVE YOU GOT ANY QUESTIONS?

If you have any questions about what is happening then you can ask your Mum, Dad, or guardians or you can ask me. My name is Adam Shortland and you can contact me at the gait laboratory. All your questions will be answered and it doesn't matter if you think your questions might be silly, if you want to know anything then you just have to ask.

Appendix C – Clinical Exam Protocol

Two assessors are required to carry out a clinical examination; one to hold and move the limbs and the other to make the measurements.

The following measurements are made with the subject in supine on the examination couch:

Knee Fixed Flexion Deformity / Hyperextension

With the limb relaxed on the plinth apply pressure over the knee while simultaneously raising the heel and lifting the limb free of the surface of the plinth. Place centre of goniometer over the estimated position of the knee flexion axis. Place stationary arm of the goniometer along the thigh in line with the greater trochanter, and the moveable arm along the tibia in line with the lateral malleous. Record the angle of fixed flexion or hyperextension in the examination sheet.

Knee Flexion with Hips Flexed

With the subject in supine and the knee and hip flexed, flex the knee further until increased resistance is felt. Place centre of goniometer over the estimated position of the knee flexion axis. Place stationary arm of the goniometer along the thigh in line with the greater trochanter, and the moveable arm along the tibia in line with the lateral malleous. Note angle of knee flexion in static examination sheet.

Hip flexion

Flex the limb of interest towards the chest until there is no more available range or until the contralateral limb also starts to lift from the plinth. Assess hip flexion by placing the centre of rotation of the goniometer over the greater trochanter, the stationary arm of the goniometer parallel to the couch, and the moveable arm along the thigh in line with the lateral epicondyle. Enter measurements on static examination form. Repeat for the other lower limb.

Popliteal Angle

With the subject in supine, position the hips so that ASIS and PSIS are vertically in line. Raise one thigh to a position perpendicular to the couch and then extend the knee while palpating the ipsilateral ASIS to the point of first resistance, without allowing any rotation of the pelvis. Allow the other to rest freely. Place centre of goniometer over the estimated position of the knee flexion axis. Place stationary arm of the goniometer along the thigh in line with the greater trochanter, and the moveable arm along the tibia in line with the lateral malleous. Enter the knee flexion angle in the static examination sheet (i.e. the number degrees short of full knee extension). Repeat the procedure for the contralateral limb. Enter measurements on the static examination sheet.

Hip Abduction in Flexion

With patient in supine and hips flexed (to 90 degrees) and knees flexed, apply pressure to the medial borders of the knees to abduct the hips, whilst holding the pelvis level. Measure the angle between the vertical and each thigh with the horizontal arm of the goniometer in line with the ASIS's. Enter measurements in static examination sheet.

When the subject is small, it is acceptable to abduct both hips simultaneously. Care should be taken to keep the pelvis level.

Hip Abduction in Extension

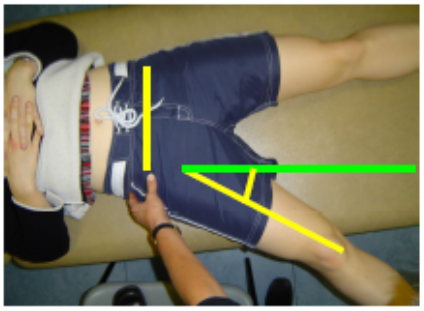

With patient in supine, palpate both ASISs to establish the coronal plane position of the pelvis. Indicate the line joining the two ASISs with one hand (thumb and index or middle finger) while abducting the hip. Stop when there is increased resistance to movement. The measurer places one arm of the goniometer in parallel to the ASIS axis indicated by the holder, with the fulcrum over the estimated hip joint centre. Measure the hip abduction angle by keeping the stationary arm aligned with the ASISs and the moveable arm along the thigh in line with the knee. Repeat procedure for contralateral limb. Enter measurements on static examination sheet.

Hip Fixed Flexion Deformity: Thomas Test

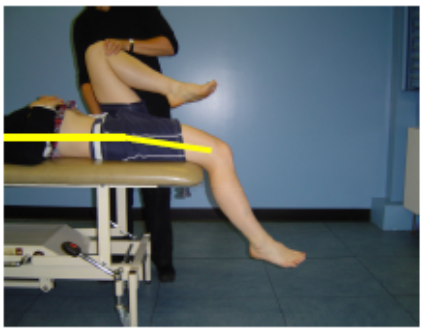

Move the patient in supine to the end of the plinth, allowing knees to flex over the end. Flex the contralateral hip so that the anterior superior iliac spine (ASIS) and the posterior superior iliac spine (PSIS) are vertically in-line avoiding rotation of the pelvis. Assess hip fixed flexion deformity by placing the centre of rotation of the goniometer over the greater trochanter, the stationary arm of the goniometer parallel to the couch, and the moveable arm along the thigh in line with the lateral epicondyle. Repeat for the other lower limb. Enter measurements on static examination form. (0° if hip in neutral, x° denoting fixed flexion deformity).

The following measurements are made with the patient in prone on the examination couch. The patient should be relaxed with their head to one side and their upper limbs adducted

Knee flexion (hip extended)

Slowly flex the knee until resistance is felt or the buttock rises (hand on the buttock). Record angle of knee flexion in static examination sheet. Repeat for other limb.

Test for quadriceps spasticity

Rapidly flex the knee. Test is positive if there is a sharp change in resistance during passive flexion. Repeat procedure for the contralateral lower limb.

Internal and external hip rotation range, and femoral anteversion

With the hip in a neutral coronal plane position, flex the knee to 90°. Stabilise the pelvis and rotate the hip by moving the shank until the end of internal and external range is felt. During this measurement, care should be taken to prevent the hip from flexing or the pelvis from moving. Place the centre of the goniometer perpendicular to the thigh so that the principal (long) axis of the thigh would pass through it. Align the stationary arm vertically and the moveable arm along the shank. Enter maximum internal and external hip rotation range in static examination sheet.

Femoral anteversion

In the same position as for hip rotation (above), rotate the hip internally and externally while palpating the most prominent part of the greater trochanter. Note the angle at which the greater trochanter is at its most prominent lateral position in the static examination sheet. Repeat procedure for contralateral limb.

Dorsiflexion Range

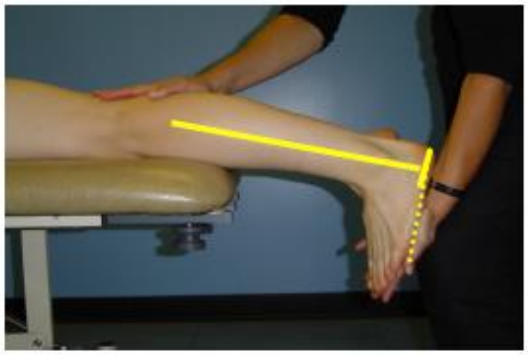

With the subject in prone and the knee flexed to 90°, move the ankle into dorsiflexion ensuring the subtalar joint remains in a neutral position. Gradually apply force to the foot to dorsiflex the ankle and wait for a few seconds until maximum dorsiflexion is achieved. Line up one arm of the goniometer parallel to the lateral border of the hindfoot and the other arm of the goniometer over the lateral malleolus pointing to the knee joint centre. Note dorsiflexion range. Maintain the dorsiflexing force on the foot and extend the knee to a as close a neutral (extended) position as possible with the foot over the end of the plinth. Repeat measurement. Enter measurements on the static examination sheet, noting degree of dorsiflexion from neutral (90°), marked DF, and degree of plantarflexion from neutral, marked PF. Repeat the procedure for contralateral lower limb.

The bimalleolar-condylar angle

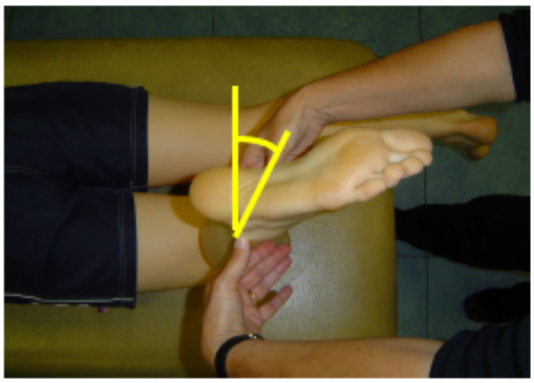

Plinth may be lowered so that the assessor can measure the angle more easily. The thigh is positioned parallel to the axis of the plinth. The knee is flexed to 90°. The holder places a finger or thumb on the most prominent points on the malleoli. The measurer places one arm of the goniometer along the axis indicated by the holder's fingers, and the other arm along the axis parallel to the end of the plinth. The bimalleolar-condylar angle is the angle between the two arms of the goniometer. Enter measurement on the static assessment form, indicating whether rotation is external or internal. Repeat for contralateral limb.

Note: avoid rotation of the shank around its long axis.

Compliance

The emotional state of the subject can affect tone and available passive range of motion. Note on the form if this is likely. Any concerns about reliability of measurements should also be noted. Where measurements are repeated, record the mean of three trials.

Appendix D – Matlab Code for the Calculation of Fibre Lengths

```
%%%%%%%%%%%%%%%%%%%%%%%%%%%%%%%%%%%%%%%%%%%%%%%%%%%%%%%%%%%%%%%%%%%%%%%%%%%%
% APLFibreLength.m
% calculates the fibre length and pennation angle from
% a 2D ultrasound image and saves to a txt file -
% Create a blank txt file with tab deliminated columns headers in the
% target directory first
% Headers are:
% ImageNumber ImageDepth(cm) MuscleThickness(mm) FibreLength(mm)
% Pennation(degs) a1 b1 a2 b2 u1 v1 u2 v2 r1 s1 r2 s2 sx sy
% explanation of a1, b1 etc given below
% A.Lewis Aug 2011

clear all
close all

% User selects Ultrasound Image
[file,path]=uigetfile('*.bmp','Select Ultrasound Image File ');
imagenumber = str2num(file(length(file)-6:length(file)-4));

% Image is loaded
USImage=imread([path,file]);
image(USImage);
% user input image depth
N = inputdlg('Enter the image depth (cm):','Image Depth');
image_depth = str2num(str2mat(N));

% User draws a line along a muscle fibre by clicking on the image
button = 'No';
while strcmp(button,'Yes') ~= 1
    close
    image(USImage);
    [Px Py Pz] = size(USImage);
    truesize([1*Px 1*Py]);
    hold on
    h=msgbox('Click two points to draw a line along the length of a
muscle fibre');
    uiwait(h);
    [u1(1),v1(1)]=ginput(1);
    plot([u1-10 u1+10],[v1 v1],'r');
    plot([u1 u1],[v1-10 v1+10],'r');
    [u2(1),v2(1)]=ginput(1);
    plot([u2-10 u2+10],[v2 v2],'r');
    plot([u2 u2],[v2-10 v2+10],'r');
    plot([u2 u1],[v2 v1],'r');

    % User marks line of action of muscle to calculate pennation angle
    h=msgbox('Now draw a line along the aponeurosis:
Deep aponeurosis: MG,LG,VL,RF
Superficial aponeurosis: SOL,VI,BFLH,BFSH,SM
Central aponeurosis: TA
Pennation is zero in VM,ST');
    uiwait(h);
    [r1(1),s1(1)]=ginput(1);
    plot([r1-10 r1+10],[s1 s1],'g');
```

```
    plot([r1 r1],[s1-10 s1+10],'g');
    [r2(1),s2(1)]=ginput(1);
    plot([r2-10 r2+10],[s2 s2],'g');
    plot([r2 r2],[s2-10 s2+10],'g');
    plot([r2 r1],[s2 s1],'g');

    % User measures the thickness of a muscle
    h=msgbox('Now draw a line to measure the thickness of the muscle
ie the perpendicular distance between superficial and deep aponeuroses');
    uiwait(h);
    [a1(1),b1(1)]=ginput(1);
    plot([a1-10 a1+10],[b1 b1],'b');
    plot([a1 a1],[b1-10 b1+10],'b');
    [a2(1),b2(1)]=ginput(1);
    plot([a2-10 a2+10],[b2 b2],'b');
    plot([a2 a2],[b2-10 b2+10],'b');
    plot([a2 a1],[b2 b1],'b');

    button = questdlg('Are you happy with this selection?');
end

%load US image depth info for various image depths
depth_info;

% convert a,b,u,v,r,s to mm in image space
a1=(a1-pixelwidthstart+1)*imagewidth/(pixelwidthend-pixelwidthstart);
b1=(b1-pixeldepthstart)*imagedepth/(pixeldepthend-pixeldepthstart);

a2=(a2-pixelwidthstart+1)*imagewidth/(pixelwidthend-pixelwidthstart);
b2=(b2-pixeldepthstart)*imagedepth/(pixeldepthend-pixeldepthstart);

u1=(u1-pixelwidthstart+1)*imagewidth/(pixelwidthend-pixelwidthstart);
v1=(v1-pixeldepthstart)*imagedepth/(pixeldepthend-pixeldepthstart);

u2=(u2-pixelwidthstart+1)*imagewidth/(pixelwidthend-pixelwidthstart);
v2=(v2-pixeldepthstart)*imagedepth/(pixeldepthend-pixeldepthstart);

r1=(r1-pixelwidthstart+1)*imagewidth/(pixelwidthend-pixelwidthstart);
s1=(s1-pixeldepthstart)*imagedepth/(pixeldepthend-pixeldepthstart);

r2=(r2-pixelwidthstart+1)*imagewidth/(pixelwidthend-pixelwidthstart);
s2=(s2-pixeldepthstart)*imagedepth/(pixeldepthend-pixeldepthstart);

% create vectors from points for pennation calc below
UV = [u2-u1,v2-v1];
RS = [r2-r1,s2-s1];

% calculate pennation angle (angle between muscle fibre and aponeurosis)
NB in radians
% a.b = ABCos(Theta) so (Theta) = acos(a.b/AB)
pennationRadians = (acos(dot(UV,RS)/(norm(UV)*norm(RS))));
if pennationRadians > (pi/2)
    pennationRadians = (pi) - pennationRadians;
end

% avoid divide by zero issues if pennation <1 deg (or (2*pi)/360 radians)
if pennationRadians < (2*pi)/360
    pennationRadians = 1;
end
```

```
% calculate muscle fibre length using trigonometry
% length = thickness / sin(pennationRadians)
thickness = ((a2-a1)^2+(b2-b1)^2)^0.5;
fibrelength = thickness /sin(pennationRadians)

% convert radians to degrees for output
pennation = (360/(2*pi))*pennationRadians

% OUTPUT RESULTS
% data columns are:
% image number
% image depth (cm)
% muscle thickness (mm)
% fibrelength (mm)
% pennation (degs)
% a1 - 1st muscle thickness point x (mm)
% b1 - 1st muscle thickness point y (mm)
% a2 - 2nd muscle thickness point x (mm)
% b2 - 2nd muscle thickness point y (mm)
% u1 - 1st fibre point x (mm)
% v1 - 1st fibre point y (mm)
% u2 - 2nd fibre point x (mm)
% v2 - 2nd fibre point y (mm)
% r1 - 1st muscle line of action point x (mm)
% s1 - 1st muscle line of action point y (mm)
% r2 - 2nd muscle line of action point x (mm)
% s2 - 2nd muscle line of action point y (mm)
% sx - pixel size x (mm)
% sy - pixel size y (mm)

% assign results to results variable
results = [imagenumber image_depth thickness fibrelength pennation a1 b1
a2 b2 u1 v1 u2 v2 r1 s1 r2 s2 sx sy];

% append data to results file
resultsfile = 'FibreLengths.txt';
fid=fopen([path,resultsfile],'a+');
fprintf(fid, '\n');
fprintf(fid, '%1.0f\t' , results(1));
fprintf(fid, '%1.0f\t' , results(2));
% write results to file
for i = 3:length(results)
    fprintf(fid, '%1.1f\t' , results(i));
end
fclose(fid);
h=msgbox('Data written to file: FibreLengths.txt');
uiwait(h);
close
```

Appendix E – MRI Safety Questionnaire

MRI Safety Questionnaire

to be completed by ANYONE entering the MAGNET ROOM

NAME:	Date of birth:	Weight:

MRI scanning uses strong magnetic fields. For your own safety and the safety of others it is **very important** that you do not go into the Magnet Room with any metal in or on your body or clothing.

Please answer the following questions carefully, and ask if anything is not clear.
All information is held in the strictest confidence.

	please circle YES or NO
1. Do you have a heart pacemaker? **(These may stop working near the MRI scanner)**	YES/NO
2. Have you ever had any surgery on your heart?	YES/NO
3. Have you ever had any surgery on your head, brain or eyes?	YES/NO
4. Have you had any surgery in the past 2 months?	YES/NO
5. Do you have any implants, wires, or other foreign bodies in your body? (e.g. clips, drug pumps, shunts, shrapnel, replacement joints, contraceptive coil)	YES/NO
6. Have you ever had any metal particles in your eyes? (e.g. from welding or metal work)	YES/NO
7. Could you be pregnant?	YES/NO
8. Do you wear dentures, a dental plate or a brace?	YES/NO
9. Have you had blackouts, epilepsy or fits in the past 2 months?	YES/NO
10. Do you have any tattoos or trans-dermal patches (skin patches)?	YES/NO
11. Are you wearing coloured contact lenses?	YES/NO
12. Are you breast feeding	YES/NO
13. Do you consent to an injection of contrast agent (dye) if required	YES/NO
14. Have you ever had an allergic reaction to contrast agent (dye) for MRI or X-ray in the past?	YES/NO
15. Have you ever had any problems with your kidneys?	YES/NO
16. Have you removed all metal objects, including coins, body-piercing jewellery, hearing aids, dentures containing metal, dental braces, cochlear implants, implanted electro-stimulator devices, artificial limbs or callipers, before entering the Magnet Room?	YES/NO
17. Is there anything else you think we should know about in relation to your MRI scan?	YES/NO

Anonymised data from your MRI scan may be used for teaching/research purposes

I have read, understood, and answered all questions

Signature:..... **Date:**.....

Checked by (MRI Authorised Person):..... **Date:**.....

Appendix F – Case Group Previous Surgery

Case01	2007	L calf lengthening & tibialis posterior recession
Case02	2007 2003/4 2002	L calf & hamstring lengthening Botulinum toxin L gastrocnemius Botulinum toxin L gastrocnemius & serial casting
Case03	2010	L calf & hamstring lengthening
Case04		None
Case05	2008 2005	Bilateral ankle serial casting, R foot correction of equino-varus deformity, R tibialis posterior, toe flexor & Achilles tendon lengthening, plantarflexor release & first metatarsal extension osteotomy Bilateral ankle serial casting
Case06	2007 2004/5	R Achilles tendon lengthening, bilateral medial/lateral hamstring lengthening & R gastrocnemius slide Botulinum toxin R hamstrings & gastrocnemius
Case07	2000 1993/4	Bilateral psoas release, rectus femoris transfer, hamstring lengthening, gastrocnemius slide & femoral de-rotation Bilateral leg & foot casting
Case08	2008 2005 2003 2002	Bilateral distal hamstring lengthening, R gastrocnemius slide & L Achilles tendon lengthening Bilateral ankle serial casting Botulinum toxin L calf - 4 courses Bilateral knee & ankle serial casting
Case09	2009 2001/2	L distal hamstring lengthening, L gastrocnemius recession & L medial displacement calcaneal osteotomy Botulinum toxin bilateral gastrocnemius
Case10	2009	R proximal femoral de-rotation, R gastrocnemius recession & L tibial exostosis excision

Appendix G – Muscle Volume Ratios

Control Subjects

	Co1	Co2	Co3	Co4	Co5	Co6	Co7	Co8	Co9	Co10
add_brev_l	1.09	0.70	1.30	1.32	1.00	1.32	1.31	1.20	2.03	2.06
add_brev_r	1.11	0.70	1.29	1.25	0.98	1.43	1.34	1.12	2.07	2.04
add_long_l	1.09	0.70	1.30	1.32	1.00	1.32	1.31	1.20	2.03	2.06
add_long_r	1.11	0.70	1.29	1.25	0.98	1.43	1.34	1.12	2.07	2.04
add_mag1_l	1.09	0.70	1.30	1.32	1.00	1.32	1.31	1.20	2.03	2.06
add_mag1_r	1.11	0.70	1.29	1.25	0.98	1.43	1.34	1.12	2.07	2.04
add_mag2_l	1.09	0.70	1.30	1.32	1.00	1.32	1.31	1.20	2.03	2.06
add_mag2_r	1.11	0.70	1.29	1.25	0.98	1.43	1.34	1.12	2.07	2.04
add_mag3_l	1.09	0.70	1.30	1.32	1.00	1.32	1.31	1.20	2.03	2.06
add_mag3_r	1.11	0.70	1.29	1.25	0.98	1.43	1.34	1.12	2.07	2.04
bifemlh_l	0.95	0.55	0.83	1.08	0.75	0.76	1.13	0.91	1.25	1.26
bifemlh_r	0.90	0.56	0.84	1.00	0.78	0.93	1.20	0.89	1.39	1.24
bifemsh_l	0.25	0.18	0.27	0.28	0.28	0.37	0.41	0.25	0.52	0.75
bifemsh_r	0.31	0.18	0.26	0.28	0.25	0.36	0.46	0.30	0.55	0.49
ercspn_l	1.02	0.63	1.10	1.24	0.93	1.18	1.29	1.07	1.67	1.67
ercspn_r	1.02	0.63	1.10	1.24	0.93	1.18	1.29	1.07	1.67	1.67
ext_dig_l	1.02	0.63	1.10	1.24	0.93	1.18	1.29	1.07	1.67	1.67
ext_dig_r	1.02	0.63	1.10	1.24	0.93	1.18	1.29	1.07	1.67	1.67
ext_hal_l	1.02	0.63	1.10	1.24	0.93	1.18	1.29	1.07	1.67	1.67
ext_hal_r	1.02	0.63	1.10	1.24	0.93	1.18	1.29	1.07	1.67	1.67
extobl_l	1.02	0.63	1.10	1.24	0.93	1.18	1.29	1.07	1.67	1.67
extobl_r	1.02	0.63	1.10	1.24	0.93	1.18	1.29	1.07	1.67	1.67
flex_dig_l	1.02	0.63	1.10	1.24	0.93	1.18	1.29	1.07	1.67	1.67
flex_dig_r	1.02	0.63	1.10	1.24	0.93	1.18	1.29	1.07	1.67	1.67
flex_hal_l	1.02	0.63	1.10	1.24	0.93	1.18	1.29	1.07	1.67	1.67
flex_hal_r	1.02	0.63	1.10	1.24	0.93	1.18	1.29	1.07	1.67	1.67
gem_l	1.02	0.63	1.10	1.24	0.93	1.18	1.29	1.07	1.67	1.67
gem_r	1.02	0.63	1.10	1.24	0.93	1.18	1.29	1.07	1.67	1.67
glut_max1_l	1.19	0.74	1.25	1.47	1.13	1.57	1.56	1.10	2.17	1.87
glut_max1_r	1.24	0.80	1.39	1.54	1.23	1.70	1.57	1.26	2.18	2.03
glut_max2_l	1.19	0.74	1.25	1.47	1.13	1.57	1.56	1.10	2.17	1.87
glut_max2_r	1.24	0.80	1.39	1.54	1.23	1.70	1.57	1.26	2.18	2.03
glut_max3_l	1.19	0.74	1.25	1.47	1.13	1.57	1.56	1.10	2.17	1.87
glut_max3_r	1.24	0.80	1.39	1.54	1.23	1.70	1.57	1.26	2.18	2.03
glut_med1_l	0.94	0.55	1.17	1.07	0.87	1.03	1.28	1.12	1.54	1.51
glut_med1_r	0.91	0.53	1.31	1.10	0.90	1.04	1.21	1.03	1.39	1.44
glut_med2_l	0.94	0.55	1.17	1.07	0.87	1.03	1.28	1.12	1.54	1.51
glut_med2_r	0.91	0.53	1.31	1.10	0.90	1.04	1.21	1.03	1.39	1.44
glut_med3_l	0.94	0.55	1.17	1.07	0.87	1.03	1.28	1.12	1.54	1.51
glut_med3_r	0.91	0.53	1.31	1.10	0.90	1.04	1.21	1.03	1.39	1.44
glut_min1_l	0.81	0.48	1.11	0.93	0.70	0.89	1.11	0.87	1.12	1.55
glut_min1_r	0.99	0.49	1.24	1.08	0.72	0.98	1.06	0.89	1.22	1.58
glut_min2_l	0.81	0.48	1.11	0.93	0.70	0.89	1.11	0.87	1.12	1.55
glut_min2_r	0.99	0.49	1.24	1.08	0.72	0.98	1.06	0.89	1.22	1.58
glut_min3_l	0.81	0.48	1.11	0.93	0.70	0.89	1.11	0.87	1.12	1.55
glut_min3_r	0.99	0.49	1.24	1.08	0.72	0.98	1.06	0.89	1.22	1.58

grac_l	1.07	0.47	0.62	0.85	0.56	0.88	0.78	0.73	1.20	1.53
grac_r	0.95	0.53	0.61	0.79	0.62	0.92	0.88	0.72	1.33	1.33
iliacus_l	1.02	0.63	1.10	1.24	0.93	1.18	1.29	1.07	1.67	1.67
iliacus_r	1.02	0.63	1.10	1.24	0.93	1.18	1.29	1.07	1.67	1.67
intobl_l	1.02	0.63	1.10	1.24	0.93	1.18	1.29	1.07	1.67	1.67
intobl_r	1.02	0.63	1.10	1.24	0.93	1.18	1.29	1.07	1.67	1.67
lat_gas_l	0.84	0.64	1.67	1.75	1.25	1.23	1.53	1.75	2.47	2.22
lat_gas_r	0.96	0.69	1.61	2.34	1.40	1.29	1.59	1.59	2.45	2.26
med_gas_l	0.90	0.62	1.20	1.35	1.15	1.27	1.30	1.44	2.14	1.63
med_gas_r	0.94	0.67	1.26	1.51	1.07	1.21	1.33	1.57	2.18	1.69
pect_l	1.02	0.63	1.10	1.24	0.93	1.18	1.29	1.07	1.67	1.67
pect_r	1.02	0.63	1.10	1.24	0.93	1.18	1.29	1.07	1.67	1.67
per_brev_l	1.02	0.63	1.10	1.24	0.93	1.18	1.29	1.07	1.67	1.67
per_brev_r	1.02	0.63	1.10	1.24	0.93	1.18	1.29	1.07	1.67	1.67
per_long_l	1.02	0.63	1.10	1.24	0.93	1.18	1.29	1.07	1.67	1.67
per_long_r	1.02	0.63	1.10	1.24	0.93	1.18	1.29	1.07	1.67	1.67
per_tert_l	1.02	0.63	1.10	1.24	0.93	1.18	1.29	1.07	1.67	1.67
per_tert_r	1.02	0.63	1.10	1.24	0.93	1.18	1.29	1.07	1.67	1.67
peri_l	1.02	0.63	1.10	1.24	0.93	1.18	1.29	1.07	1.67	1.67
peri_r	1.02	0.63	1.10	1.24	0.93	1.18	1.29	1.07	1.67	1.67
psoas_l	1.02	0.63	1.10	1.24	0.93	1.18	1.29	1.07	1.67	1.67
psoas_r	1.02	0.63	1.10	1.24	0.93	1.18	1.29	1.07	1.67	1.67
quad_fem_l	1.02	0.63	1.10	1.24	0.93	1.18	1.29	1.07	1.67	1.67
quad_fem_r	1.02	0.63	1.10	1.24	0.93	1.18	1.29	1.07	1.67	1.67
rect_fem_l	0.83	0.61	0.74	0.97	0.67	0.91	1.04	0.91	1.39	1.28
rect_fem_r	0.79	0.55	0.74	0.89	0.64	0.90	1.07	0.89	1.43	1.31
sar_l	0.93	0.50	0.97	0.98	0.77	1.22	0.94	0.62	1.64	1.46
sar_r	0.88	0.50	1.02	0.96	0.77	1.26	0.92	0.64	1.57	1.37
semimem_l	0.94	0.59	0.88	1.12	0.79	0.90	0.93	0.90	1.37	1.42
semimem_r	0.97	0.61	0.87	1.19	0.83	0.99	0.96	0.93	1.41	1.37
semiten_l	1.28	0.61	0.70	1.06	0.70	0.99	1.06	0.76	1.45	1.98
semiten_r	1.20	0.57	0.73	1.06	0.71	0.90	1.11	0.87	1.23	1.65
soleus_l	0.72	0.53	1.31	1.44	1.10	1.26	1.22	1.14	1.70	1.25
soleus_r	0.67	0.49	1.23	1.36	1.13	1.32	1.38	1.39	1.60	1.37
tfl_l	1.02	0.63	1.10	1.24	0.93	1.18	1.29	1.07	1.67	1.67
tfl_r	1.02	0.63	1.10	1.24	0.93	1.18	1.29	1.07	1.67	1.67
tib_ant_l	0.65	0.41	0.67	0.79	0.54	0.59	0.75	0.52	1.05	0.97
tib_ant_r	0.66	0.42	0.67	0.73	0.53	0.68	0.69	0.57	1.02	0.92
tib_post_l	0.90	0.55	0.83	1.17	0.70	0.92	1.25	0.85	1.06	1.16
tib_post_r	0.74	0.60	1.01	1.15	0.73	0.82	1.18	1.03	0.92	1.18
vas_int_l	1.70	0.98	1.72	1.98	1.52	1.85	2.38	1.91	2.57	2.78
vas_int_r	1.72	0.98	1.74	1.88	1.40	2.07	2.42	1.77	2.57	2.90
vas_lat_l	1.81	1.16	1.76	1.97	1.53	2.09	2.20	1.48	2.38	2.76
vas_lat_r	1.80	1.09	1.62	1.99	1.62	2.32	2.26	1.67	2.61	2.81
vas_med_l	1.74	1.13	1.75	1.58	1.56	1.77	2.03	1.45	2.52	2.50
vas_med_r	1.65	1.04	1.71	1.68	1.49	2.06	2.14	1.43	2.57	2.49
default	1.02	0.63	1.10	1.24	0.93	1.18	1.29	1.07	1.67	1.67

	Case Subjects									
	Ca1	Ca2	Ca3	Ca4	Ca5	Ca6	Ca7	Ca8	Ca9	Ca10
add_brev_l	0.44	1.38	0.72	0.52	0.51	0.83	0.53	0.55	0.90	1.16
add_brev_r	0.44	1.58	0.75	0.47	0.47	0.67	0.53	0.62	1.06	0.89
add_long_l	0.44	1.38	0.72	0.52	0.51	0.83	0.53	0.55	0.90	1.16
add_long_r	0.44	1.58	0.75	0.47	0.47	0.67	0.53	0.62	1.06	0.89
add_mag1_l	0.44	1.38	0.72	0.52	0.51	0.83	0.53	0.55	0.90	1.16
add_mag1_r	0.44	1.58	0.75	0.47	0.47	0.67	0.53	0.62	1.06	0.89
add_mag2_l	0.44	1.38	0.72	0.52	0.51	0.83	0.53	0.55	0.90	1.16
add_mag2_r	0.44	1.58	0.75	0.47	0.47	0.67	0.53	0.62	1.06	0.89
add_mag3_l	0.44	1.38	0.72	0.52	0.51	0.83	0.53	0.55	0.90	1.16
add_mag3_r	0.44	1.58	0.75	0.47	0.47	0.67	0.53	0.62	1.06	0.89
bifemlh_l	0.44	0.96	0.72	0.33	0.35	0.40	0.52	0.27	0.56	0.63
bifemlh_r	0.44	1.09	0.50	0.29	0.32	0.38	0.64	0.41	0.71	0.89
bifemsh_l	0.44	0.30	0.72	0.10	0.12	0.28	0.32	0.18	0.25	0.29
bifemsh_r	0.44	0.36	0.21	0.10	0.09	0.24	0.30	0.20	0.24	0.27
ercspn_l	0.44	1.10	0.72	0.40	0.44	0.72	0.53	0.46	0.80	0.89
ercspn_r	0.44	1.10	0.72	0.40	0.44	0.72	0.53	0.46	0.80	0.89
ext_dig_l	0.44	1.10	0.72	0.40	0.44	0.72	0.53	0.46	0.80	0.89
ext_dig_r	0.44	1.10	0.72	0.40	0.44	0.72	0.53	0.46	0.80	0.89
ext_hal_l	0.44	1.10	0.72	0.40	0.44	0.72	0.53	0.46	0.80	0.89
ext_hal_r	0.44	1.10	0.72	0.40	0.44	0.72	0.53	0.46	0.80	0.89
extobl_l	0.44	1.10	0.72	0.40	0.44	0.72	0.53	0.46	0.80	0.89
extobl_r	0.44	1.10	0.72	0.40	0.44	0.72	0.53	0.46	0.80	0.89
flex_dig_l	0.44	1.10	0.72	0.40	0.44	0.72	0.53	0.46	0.80	0.89
flex_dig_r	0.44	1.10	0.72	0.40	0.44	0.72	0.53	0.46	0.80	0.89
flex_hal_l	0.44	1.10	0.72	0.40	0.44	0.72	0.53	0.46	0.80	0.89
flex_hal_r	0.44	1.10	0.72	0.40	0.44	0.72	0.53	0.46	0.80	0.89
gem_l	0.44	1.10	0.72	0.40	0.44	0.72	0.53	0.46	0.80	0.89
gem_r	0.44	1.10	0.72	0.40	0.44	0.72	0.53	0.46	0.80	0.89
glut_max1_l	0.44	1.33	0.72	0.45	0.62	0.87	1.04	0.49	1.13	1.30
glut_max1_r	0.44	1.75	0.89	0.44	0.62	0.83	1.32	0.58	1.23	0.89
glut_max2_l	0.44	1.33	0.72	0.45	0.62	0.87	1.04	0.49	1.13	1.30
glut_max2_r	0.44	1.75	0.89	0.44	0.62	0.83	1.32	0.58	1.23	0.89
glut_max3_l	0.44	1.33	0.72	0.45	0.62	0.87	1.04	0.49	1.13	1.30
glut_max3_r	0.44	1.75	0.89	0.44	0.62	0.83	1.32	0.58	1.23	0.89
glut_med1_l	0.44	0.95	0.72	0.36	0.45	0.83	0.53	0.42	0.81	0.90
glut_med1_r	0.44	1.04	0.65	0.36	0.44	0.98	0.53	0.45	0.80	0.89
glut_med2_l	0.44	0.95	0.72	0.36	0.45	0.83	0.53	0.42	0.81	0.90
glut_med2_r	0.44	1.04	0.65	0.36	0.44	0.98	0.53	0.45	0.80	0.89
glut_med3_l	0.44	0.95	0.72	0.36	0.45	0.83	0.53	0.42	0.81	0.90
glut_med3_r	0.44	1.04	0.65	0.36	0.44	0.98	0.53	0.45	0.80	0.89
glut_min1_l	0.44	0.73	0.72	0.23	0.41	0.65	0.53	0.27	0.52	0.73
glut_min1_r	0.44	0.89	0.57	0.27	0.42	0.76	0.53	0.39	0.75	0.89
glut_min2_l	0.44	0.73	0.72	0.23	0.41	0.65	0.53	0.27	0.52	0.73
glut_min2_r	0.44	0.89	0.57	0.27	0.42	0.76	0.53	0.39	0.75	0.89
glut_min3_l	0.44	0.73	0.72	0.23	0.41	0.65	0.53	0.27	0.52	0.73
glut_min3_r	0.44	0.89	0.57	0.27	0.42	0.76	0.53	0.39	0.75	0.89
grac_l	0.44	0.41	0.72	0.32	0.35	0.42	0.53	0.16	0.51	0.84
grac_r	0.44	1.04	0.56	0.34	0.32	0.28	0.53	0.27	0.73	0.89
iliacus_l	0.44	1.10	0.72	0.40	0.44	0.72	0.53	0.46	0.80	0.89

iliacus_r	0.44	1.10	0.72	0.40	0.44	0.72	0.53	0.46	0.80	0.89
intobl_l	0.44	1.10	0.72	0.40	0.44	0.72	0.53	0.46	0.80	0.89
intobl_r	0.44	1.10	0.72	0.40	0.44	0.72	0.53	0.46	0.80	0.89
lat_gas_l	0.39	0.97	0.72	0.42	0.55	0.72	0.60	0.38	0.58	1.02
lat_gas_r	0.58	1.60	0.80	0.43	0.46	0.50	0.53	0.43	0.80	0.74
med_gas_l	0.30	0.98	0.72	0.43	0.57	0.75	0.47	0.46	0.46	0.92
med_gas_r	0.41	1.43	0.67	0.34	0.36	0.54	0.53	0.51	0.55	0.68
pect_l	0.44	1.10	0.72	0.40	0.44	0.72	0.53	0.46	0.80	0.89
pect_r	0.44	1.10	0.72	0.40	0.44	0.72	0.53	0.46	0.80	0.89
per_brev_l	0.44	1.10	0.72	0.40	0.44	0.72	0.53	0.46	0.80	0.89
per_brev_r	0.44	1.10	0.72	0.40	0.44	0.72	0.53	0.46	0.80	0.89
per_long_l	0.44	1.10	0.72	0.40	0.44	0.72	0.53	0.46	0.80	0.89
per_long_r	0.44	1.10	0.72	0.40	0.44	0.72	0.53	0.46	0.80	0.89
per_tert_l	0.44	1.10	0.72	0.40	0.44	0.72	0.53	0.46	0.80	0.89
per_tert_r	0.44	1.10	0.72	0.40	0.44	0.72	0.53	0.46	0.80	0.89
peri_l	0.44	1.10	0.72	0.40	0.44	0.72	0.53	0.46	0.80	0.89
peri_r	0.44	1.10	0.72	0.40	0.44	0.72	0.53	0.46	0.80	0.89
psoas_l	0.44	1.10	0.72	0.40	0.44	0.72	0.53	0.46	0.80	0.89
psoas_r	0.44	1.10	0.72	0.40	0.44	0.72	0.53	0.46	0.80	0.89
quad_fem_l	0.44	1.10	0.72	0.40	0.44	0.72	0.53	0.46	0.80	0.89
quad_fem_r	0.44	1.10	0.72	0.40	0.44	0.72	0.53	0.46	0.80	0.89
rect_fem_l	0.44	1.00	0.72	0.34	0.32	0.57	0.34	0.32	0.62	0.67
rect_fem_r	0.44	1.16	0.49	0.30	0.29	0.42	0.53	0.35	0.69	0.89
sar_l	0.44	0.88	0.72	0.26	0.37	0.81	0.53	0.41	1.00	0.83
sar_r	0.44	0.90	0.57	0.30	0.31	0.65	0.53	0.43	0.95	0.99
semimem_l	0.44	1.07	0.72	0.36	0.31	0.45	0.54	0.29	0.45	0.67
semimem_r	0.44	1.35	0.53	0.29	0.32	0.33	0.52	0.37	0.72	0.60
semiten_l	0.44	0.14	0.72	0.36	0.39	0.27	0.29	0.34	0.44	0.91
semiten_r	0.44	1.15	0.63	0.38	0.35	0.27	0.30	0.28	0.69	0.91
soleus_l	0.51	0.72	0.72	0.52	0.48	0.68	0.53	0.29	0.55	0.89
soleus_r	0.64	1.19	0.77	0.45	0.28	0.62	0.53	0.49	0.65	0.66
tfl_l	0.44	1.10	0.72	0.40	0.44	0.72	0.53	0.46	0.80	0.89
tfl_r	0.44	1.10	0.72	0.40	0.44	0.72	0.53	0.46	0.80	0.89
tib_ant_l	0.27	0.54	0.72	0.18	0.26	0.45	0.29	0.21	0.35	0.37
tib_ant_r	0.27	0.65	0.37	0.18	0.23	0.34	0.53	0.24	0.34	0.38
tib_post_l	0.57	0.99	0.72	0.42	0.68	1.15	0.53	0.51	0.76	0.99
tib_post_r	0.49	0.71	0.76	0.53	0.45	0.88	0.53	0.55	0.83	0.86
vas_int_l	0.44	2.00	0.72	0.78	0.77	1.44	0.53	0.97	1.39	2.04
vas_int_r	0.44	1.79	1.31	0.75	0.65	1.35	0.53	1.01	1.59	0.89
vas_lat_l	0.44	1.59	0.72	0.72	0.85	1.77	0.53	0.77	1.35	1.89
vas_lat_r	0.44	2.05	1.41	0.72	0.76	1.59	0.53	0.89	1.59	0.89
vas_med_l	0.44	1.45	0.72	0.60	0.63	1.36	0.53	0.77	1.26	1.79
vas_med_r	0.44	1.69	1.16	0.53	0.53	1.13	0.53	0.79	1.42	0.89
default	0.44	1.10	0.72	0.40	0.44	0.72	0.53	0.46	0.80	0.89

References

Agostini, V., Nascimbeni, A., Gaffuri, A., Imazio, P., Benedetti, M., & Knaflitz, M. (2010). Normative EMG activation patterns of school-age children during gait. *Gait & Posture*, *32*(3), 285–9. doi:10.1016/j.gaitpost.2010.06.024

Albright, L. (2009a). Basal Ganglia Injury and Resulting Movement Disorders. In J. Gage, M. Schwartz, S. Koop, & T. Novacheck (Eds.), *The Indentification & Treatment of gait problems in cerebral palsy* (2nd ed., pp. 99–106). London: Mac Keith Press.

Albright, L. (2009b). *Neurosurgical Treatment of Dystonia*. (J. Gage, M. Schwartz, S. Koop, & T. Novacheck, Eds.) (2nd ed., pp. 429–38). London: Mac Keith Press.

Anderson, F. C., Goldberg, S. R., & Pandy, M. G. (2004). Contributions of muscle forces and toe-off kinematics to peak knee flexion during the swing phase of normal gait: an induced position analysis. *Journal of Biomechanics*, *37*, 731–737. doi:10.1016/j.jbiomech.2003.09.018

Anderson, F. C., & Pandy, M. G. (1999). A Dynamic Optimization Solution for Vertical Jumping in Three Dimensions. *Computer methods in biomechanics and biomedical engineering*, *2*(3), 201–231. doi:10.1080/10255849908907988

Anderson, F. C., & Pandy, M. G. (2001). Static and dynamic optimization solutions for gait are practically equivalent. *Journal of biomechanics*, *34*(2), 153–61.

Anderson, F. C., & Pandy, M. G. (2003). Individual muscle contributions to support in normal walking. *Gait & posture*, *17*, 159–169.

Arnold, A. A., Anderson, F. C., Pandy, M. G., & Delp, S. L. (2005). Muscular contributions to hip and knee extension during the single limb stance phase of normal gait: a framework for investigating the causes of crouch gait. *Journal of biomechanics*, *38*(11), 2181–9. doi:10.1016/j.jbiomech.2004.09.036

Arnold, A. S., Blemker, S. S., & Delp, S. L. (2001). Evaluation of a Deformable Musculoskeletal Model for Estimating Muscle–Tendon Lengths During Crouch Gait. *Annals of Biomedical Engineering*, *29*(3), 263–274. doi:10.1114/1.1355277

Arnold, A. S., & Delp, S. L. (2005). Computer modeling of gait abnormalities in cerebral palsy: application to treatment planning. *Theoretical Issues in Ergonomics Science*, *6*(3-4), 305–312. doi:10.1080/14639220412331329636

Arnold, A. S., Thelen, D. G., Schwartz, M. H., Anderson, F. C., & Delp, S. L. (2007). Muscular coordination of knee motion during the terminal-swing phase of normal gait. *Journal of biomechanics*, *40*(15), 3314–24. doi:10.1016/j.jbiomech.2007.05.006

Arnold, E. M., Ward, S. R., Lieber, R. L., & Delp, S. L. (2010). A model of the lower limb for analysis of human movement. *Annals of biomedical engineering*, *38*(2), 269–79. doi:10.1007/s10439-009-9852-5

Baker, R. (2006). Gait analysis methods in rehabilitation. *Journal of neuroengineering and rehabilitation*, *3*, 4. doi:10.1186/1743-0003-3-4

Baker, R. (2007). The history of gait analysis before the advent of modern computers. *Gait & posture*, *26*(3), 331–42. doi:10.1016/j.gaitpost.2006.10.014

Baker, R., McGinley, J. L., Schwartz, M. H., Beynon, S., Rozumalski, A., Graham, H. K., & Tirosh, O. (2009). The gait profile score and movement analysis profile. *Gait & posture*, *30*(3), 265–9. doi:10.1016/j.gaitpost.2009.05.020

Barber, L., Barrett, R., & Lichtwark, G. (2011). Passive muscle mechanical properties of the medial gastrocnemius in young adults with spastic cerebral palsy. *Journal of biomechanics*, *44*(13), 2496–500. doi:10.1016/j.jbiomech.2011.06.008

Barber, L., Hastings-Ison, T., Baker, R., Barrett, R., & Lichtwark, G. (2011). Medial gastrocnemius muscle volume and fascicle length in children aged 2 to 5 years with cerebral palsy. *Developmental medicine and child neurology*, *53*(6), 543–8. doi:10.1111/j.1469-8749.2011.03913.x

Benjamini, Y., Drai, D., Elmer, G., Kafkafi, N., & Golani, I. (2001). Controlling the false discovery rate in behavior genetics research. *Behavioural brain research*, *125*(1-2), 279–84.

Blazevich, A., Gill, N., & Zhou, S. (2006). Intra- and intermuscular variation in human quadriceps femoris architecture assessed in vivo. *Journal of anatomy*, *209*(3), 289–310. doi:10.1111/j.1469-7580.2006.00619.x

Blok, J., Stegeman, D., & van Oosterom, A. (2002). Three-Layer Volume Conductor Model and Software Package for Applications in Surface Electromyography. *Annals of Biomedical Engineering*, *30*(4), 566–577. doi:10.1114/1.1475345

Booth, C. M., Cortina-Borja, M. J., & Theologis, T. N. (2001). Collagen accumulation in muscles of children with cerebral palsy and correlation with severity of spasticity. *Developmental medicine and child neurology*, *43*(5), 314–20.

Brown, J. K., Rodda, J., Walsh, E. G., & Wright, G. W. (1991). Neurophysiology of lower-limb function in hemiplegic children. *Developmental medicine and child neurology*, *33*(12), 1037–47.

Buchanan, T. S., Lloyd, D. G., Manal, K., & Besier, T. F. (2004). Neuromusculoskeletal modeling: estimation of muscle forces and joint moments and movements from measurements of neural command. *Journal of applied biomechanics*, *20*(4), 367–95.

Castle, M. E., Reyman, T., & Schneider, M. (1979). Pathology of spastic muscle in cerebral palsy. *Clinical orthopaedics and related research*, (142), 223–32.

Chapman, A. R., Vicenzino, B., Blanch, P., Knox, J. J., & Hodges, P. W. (2010). Intramuscular fine-wire electromyography during cycling: repeatability, normalisation and a comparison to surface electromyography. *Journal of electromyography and kinesiology : official journal of the International Society of Electrophysiological Kinesiology*, *20*(1), 108–17. doi:10.1016/j.jelekin.2008.11.013

Chen, G. (2006). Induced acceleration contributions to locomotion dynamics are not physically well defined. *Gait & posture*, *23*(1), 37–44. doi:10.1016/j.gaitpost.2004.11.016

Correa, T, Baker, R., Graham, H., & Pandy, M. (2011). Accuracy of generic musculoskeletal models in predicting the functional roles of muscles in human gait. *Journal of biomechanics*, *44*(11), 2096–105. doi:10.1016/j.jbiomech.2011.05.023

Correa, T, Schache, A., Graham, H., Baker, R., Thomason, P., & Pandy, M. (2012). Potential of lower-limb muscles to accelerate the body during cerebral palsy gait. *Gait & posture*, *36*(2), 194–200.

Correa, T, & Pandy, M. (2011). A mass-length scaling law for modeling muscle strength in the lower limb. *Journal of biomechanics*, *44*(16), 2782–9. doi:10.1016/j.jbiomech.2011.08.024

Crowninshield, R., & Brand, R. (1981). A physiologically based criterion of muscle force prediction in locomotion. *Journal of biomechanics*, *14*(11), 793–801.

Damiano, D. L., Dodd, K., & Taylor, N. F. (2002). Should we be testing and training muscle strength in cerebral palsy? *Developmental medicine and child neurology*, *44*(1), 68–72.

Damiano, D. L., Kelly, L. E., & Vaughn, C. L. (1995). Effects of quadriceps femoris muscle strengthening on crouch gait in children with spastic diplegia. *Physical therapy*, *75*(8), 658–67; discussion 668–71.

Darrah, J., Fan, J., Chen, L., Nunweiler, J., & Watkins, B. (1997). Review of the effects of progressive resisted muscle strengthening in children with cerebral palsy: a clinical consensus exercise. *Pediatric Phyical Therapy*, *9*, 12–7.

Davis, R. B., Ounpuu, S., Tyburski, D., & Gage, J. R. (1991). A gait analysis data collection and reduction technique. *Human Movement Science*, *10*, 575–587.

Davy, D. T., & Audu, M. L. (1987). A dynamic optimization technique for predicting muscle forces in the swing phase of gait. *Journal of biomechanics*, *20*(2), 187–201.

Day, S. M., Strauss, D. J., Vachon, P. J., Rosenbloom, L., Shavelle, R. M., & Wu, Y. W. (2007). Growth patterns in a population of children and adolescents with cerebral palsy. *Developmental medicine and child neurology*, *49*(3), 167–71. doi:10.1111/j.1469-8749.2007.00167.x

Delp, S. (1990). Surgery simulation: a computer graphics system to analyze and design musculoskeletal reconstructions of the lower limb, PhD Thesis, Stanford University.

Delp, S., Anderson, F., Arnold, A., Loan, P., Habib, A., John, C., … Thelen, D. (2007). OpenSim: open-source software to create and analyze dynamic simulations of movement. *IEEE transactions on bio-medical engineering*, *54*(11), 1940–50. doi:10.1109/TBME.2007.901024

Delp, S., & Loan, J. (1995). A graphics-based software system to develop and analyze models of musculoskeletal structures. *Computers in biology and medicine*, *25*(1), 21–34.

Delp, S., Loan, J., Hoy, M., Zajac, F., Topp, E., & Rosen, J. (1990). An interactive graphics-based model of the lower extremity to study orthopaedic surgical procedures. *IEEE transactions on bio-medical engineering*, *37*(8), 757–67. doi:10.1109/10.102791

Dorn, T. (2008). Gait Extract Toolbox for Matlab, Version 1.5. Retrieved November 26, 2009, from http://www.mathworks.com/matlabcentral/fileexchange/authors/31722

Dorn, T., Lin, Y., & Pandy, M. (2012). Estimates of muscle function in human gait depend on how foot-ground contact is modelled. *Computer methods in biomechanics and biomedical engineering*, *15*(6), 657–68. doi:10.1080/10255842.2011.554413

Du Plessis, A. (2009). Mechanisms and Manifestations of Neonatal Brain Injury. In J. Gage, M. Schwartz, S. Koop, & T. Novacheck (Eds.), *The Indentification & Treatment of gait problems in cerebral palsy* (2nd ed., pp. 67–88). London: Mac Keith Press.

Dutta, C., Hadley, E. C., & Lexell, J. (1997). Sarcopenia and physical performance in old age: overview. *Muscle & nerve. Supplement*, *5*, S5–9.

Elder, G. C. B., Kirk, J., Stewart, G., Cook, K., Weir, D., Marshall, A., & Leahey, L. (2003). Contributing factors to muscle weakness in children with cerebral palsy. *Developmental medicine and child neurology*, *45*(8), 542–50.

Erdemir, A., McLean, S., Herzog, W., & van den Bogert, A. J. (2007). Model-based estimation of muscle forces exerted during movements. *Clinical biomechanics*, *22*(2), 131–54. doi:10.1016/j.clinbiomech.2006.09.005

Fowler, E. G., & Goldberg, E. J. (2009). The effect of lower extremity selective voluntary motor control on interjoint coordination during gait in children with spastic diplegic cerebral palsy. *Gait & posture*, *29*(1), 102–7. doi:10.1016/j.gaitpost.2008.07.007

Friederich, J., & Brand, R. (1990). Muscle fiber architecture in the human lower limb. *Journal of biomechanics*, *23*(1), 91–5.

Fry, N. (2008). Musculoskeletal deformity in spastic cerebral palsy, PhD Thesis, King's College London.

Fry, N. R., Gough, M., McNee, A. E., & Shortland, A. P. (2007). Changes in the volume and length of the medial gastrocnemius after surgical recession in children with spastic diplegic cerebral palsy. *Journal of pediatric orthopedics*, *27*(7), 769–74. doi:10.1097/BPO.0b013e3181558943

Fukunaga, T., Roy, R. R., Shellock, F. G., Hodgson, J. A., Day, M. K., Lee, P. L., … Edgerton, V. R. (1992). Physiological cross-sectional area of human leg muscles based on magnetic resonance imaging. *Journal of orthopaedic research*, *10*(6), 928–34. doi:10.1002/jor.1100100623

Gage, J., & Schwartz, M. (2009a). Consequences of Brain Injury on Musculoskeletal Development. In J. Gage, M. Schwartz, S. Koop, & T. Novacheck (Eds.), *The Indentification & Treatment of gait problems in cerebral palsy* (2nd ed., pp. 107–29). London: Mac Keith Press.

Gage, J., & Schwartz, M. (2009b). Normal Gait. In J. Gage, M. Schwartz, S. Koop, & T. Novacheck (Eds.), *The Indentification & Treatment of gait problems in cerebral palsy* (2nd ed., pp. 31–64). London: Mac Keith Press.

Gage, J., Schwartz, M., Koop, S., & Novacheck, T. (Eds.). (2009). *The Indentification & Treatment of gait problems in cerebral palsy* (2nd ed.). London: Mac Keith Press.

Goldberg, S. R., Anderson, F. C., Pandy, M. G., & Delp, S. L. (2004). Muscles that influence knee flexion velocity in double support: implications for stiff-knee gait. *Journal of biomechanics*, *37*(8), 1189–96. doi:10.1016/j.jbiomech.2003.12.005

Gormley, M. E. (2001). Treatment of neuromuscular and musculoskeletal problems in cerebral palsy. *Pediatric rehabilitation*, *4*(1), 5–16.

Gough, M., & Shortland, A. P. (2012). Could muscle deformity in children with spastic cerebral palsy be related to an impairment of muscle growth and altered adaptation? *Developmental medicine and child neurology*, *54*(6), 495–9. doi:10.1111/j.1469-8749.2012.04229.x

Hakanson, K. (2010). *Surface EMG recordings of muscle activation – a simulation of the effects of fat thickness and muscle morphology*. MSc Thesis - King's College London.

Haney, N. (1998). Muscle Strengthening in Children with Cerebral Palsy. *Physical & Occupational Therapy In Pediatrics*, *18*(3), 149–157. doi:10.1300/J006v18n03_11

Hardt, D. E. (1978). Determining Muscle Forces in the Leg During Normal Human Walking—An Application and Evaluation of Optimization Methods. *Journal of Biomechanical Engineering*, *100*(2), 72. doi:10.1115/1.3426195

Henneman, E., Somjen, G., & Carpenter, D. (1965). Functional significance of cell size in spinal motoneurons. *Journal of Neurophysiology*, *28*, 560–80.

Hicks, J., Arnold, A., Anderson, F., Schwartz, M., & Delp, S. (2007). The effect of excessive tibial torsion on the capacity of muscles to extend the hip and knee during single-limb stance. *Gait & posture*, *26*(4), 546–52. doi:10.1016/j.gaitpost.2006.12.003

Hicks, J., Schwartz, M., Arnold, A., & Delp, S. (2008). Crouched postures reduce the capacity of muscles to extend the hip and knee during the single-limb stance phase of gait. *Journal of biomechanics*, *41*(5), 960–7. doi:10.1016/j.jbiomech.2008.01.002

Higginson, J. S., Zajac, F. E., Neptune, R. R., Kautz, S. A., Burgar, C. G., & Delp, S. L. (2006). Effect of equinus foot placement and intrinsic muscle response on knee extension during stance. *Gait & posture*, *23*(1), 32–6. doi:10.1016/j.gaitpost.2004.11.011

Hodson-Tole, E. F., & Wakeling, J. M. (2007). Variations in motor unit recruitment patterns occur within and between muscles in the running rat (Rattus norvegicus). *The Journal of experimental biology*, *210*(Pt 13), 2333–45. doi:10.1242/jeb.004457

Hof, A. L., & Otten, E. (2005). Assessment of two-dimensional induced accelerations from measured kinematic and kinetic data. *Gait & posture*, *22*(3), 182–8. doi:10.1016/j.gaitpost.2004.08.007

Hoy, M. G., Zajac, F. E., & Gordon, M. E. (1990). A musculoskeletal model of the human lower extremity: the effect of muscle, tendon, and moment arm on the moment-angle relationship of musculotendon actuators at the hip, knee, and ankle. *Journal of biomechanics*, *23*(2), 157–69.

Jaspers, E., Verhaegen, A., Geens, F., Van Campenhout, A., Desloovere, K., & Molenaers, G. (2013). Lower limb functioning and its impact on quality of life in ambulatory children with cerebral palsy. *European journal of paediatric neurology*, 1–7. doi:10.1016/j.ejpn.2013.04.006

John, C. T., Seth, A., Schwartz, M. H., & Delp, S. L. (2012). Contributions of muscles to mediolateral ground reaction force over a range of walking speeds. *Journal of biomechanics*, *45*(14), 2438–43. doi:10.1016/j.jbiomech.2012.06.037

Johnson, D. L., Miller, F., Subramanian, P., & Modlesky, C. M. (2009). Adipose tissue infiltration of skeletal muscle in children with cerebral palsy. *The Journal of pediatrics*, *154*(5), 715–20. doi:10.1016/j.jpeds.2008.10.046

Jones, M. W., Morgan, E., Shelton, J. E., & Thorogood, C. (2007). Cerebral palsy: introduction and diagnosis (part I). *Journal of pediatric health care*, *21*(3), 146–52. doi:10.1016/j.pedhc.2006.06.007

Jonkers, I., Stewart, C., & Spaepen, A. (2003). The study of muscle action during single support and swing phase of gait: clinical relevance of forward simulation techniques. *Gait & posture*, *17*(2), 97–105.

Kadaba, M. P., Ramakrishnan, H. K., & Wootten, M. E. (1990). Measurement of lower extremity kinematics during level walking. *Journal of orthopaedic research*, *8*(3), 383–92. doi:10.1002/jor.1100080310

Kadaba, M. P., Ramakrishnan, H. K., Wootten, M. E., Gainey, J., Gorton, G., & Cochran, G. V. (1989). Repeatability of kinematic, kinetic, and electromyographic data in normal adult gait. *Journal of orthopaedic research : official publication of the Orthopaedic Research Society*, *7*(6), 849–60. doi:10.1002/jor.1100070611

Kadaba, M. P., Wootten, M. E., Gainey, J., & Cochran, G. V. (1985). Repeatability of phasic muscle activity: performance of surface and intramuscular wire electrodes in gait analysis. *Journal of orthopaedic research : official publication of the Orthopaedic Research Society*, *3*(3), 350–9. doi:10.1002/jor.1100030312

Kepple, T. M., Siegel, K. L., & Stanhope, S. J. (1997). Relative contributions of the lower extremity joint moments to forward progression and suport during gait. *Gait & Posture*, *6*, 1–8.

Koman, L. A., Mooney, J. F., Smith, B., Goodman, A., & Mulvaney, T. (1993). Management of cerebral palsy with botulinum-A toxin: preliminary investigation. *Journal of pediatric orthopedics*, *13*(4), 489–95.

Krach, L. (2009). Treatment of Spasticity with Inthrathecal Baclofen. In J. Gage, M. Schwartz, S. Koop, & T. Novacheck (Eds.), *The Indentification & Treatment of gait problems in cerebral palsy* (2nd ed., pp. 383–96). London: Mac Keith Press.

Lampe, R., Grassl, S., Mitternacht, J., Gerdesmeyer, L., & Gradinger, R. (2006). MRT-measurements of muscle volumes of the lower extremities of youths with spastic hemiplegia caused by cerebral palsy. *Brain & development*, *28*(8), 500–6. doi:10.1016/j.braindev.2006.02.009

Lieber, R., & Fridén, J. (2000). Functional and clinical significance of skeletal muscle architecture. *Muscle & nerve*, *23*(11), 1647–66.

Lieber, R., Runesson, E., Einarsson, F., & Fridén, J. (2003). Inferior mechanical properties of spastic muscle bundles due to hypertrophic but compromised extracellular matrix material. *Muscle & nerve*, *28*(4), 464–71. doi:10.1002/mus.10446

Lin, Y.-C., Dorn, T. W., Schache, a. G., & Pandy, M. G. (2011). Comparison of different methods for estimating muscle forces in human movement. *Proceedings of the Institution of Mechanical Engineers, Part H: Journal of Engineering in Medicine*, *226*(2), 103–112. doi:10.1177/0954411911429401

Liu, M. Q., Anderson, F. C., Pandy, M. G., & Delp, S. L. (2006). Muscles that support the body also modulate forward progression during walking. *Journal of biomechanics*, *39*(14), 2623–30. doi:10.1016/j.jbiomech.2005.08.017

Liu, M. Q., Anderson, F. C., Schwartz, M. H., & Delp, S. L. (2008). Muscle contributions to support and progression over a range of walking speeds. *Journal of biomechanics*, *41*(15), 3243–52. doi:10.1016/j.jbiomech.2008.07.031

Lloyd, D. G., & Besier, T. F. (2003). An EMG-driven musculoskeletal model to estimate muscle forces and knee joint moments in vivo. *Journal of biomechanics*, *36*(6), 765–76. doi:10.1016/S0021-9290(03)00010-1

Malaiya, R., McNee, A. E., Fry, N. R., Eve, L. C., Gough, M., & Shortland, A. P. (2007). The morphology of the medial gastrocnemius in typically developing children and children with spastic hemiplegic cerebral palsy. *Journal of electromyography and kinesiology*, *17*(6), 657–63. doi:10.1016/j.jelekin.2007.02.009

Martin, D. C., Medri, M. K., Chow, R. S., Oxorn, V., Leekam, R. N., Agur, a M., & McKee, N. H. (2001). Comparing human skeletal muscle architectural parameters of cadavers with in vivo ultrasonographic measurements. *Journal of anatomy*, *199*(Pt 4), 429–34.

Miller, S. C., Korff, T., Waugh, C., Fath, F., & Blazevich, A. J. (2015). Tibialis anterior moment arm: effects of measurement errors and assumptions. *Medicine and science in sports and exercise*, *47*(2), 428–39. doi:10.1249/MSS.0000000000000399

Modenese, L., Phillips, A. T. M., & Bull, A. M. J. (2011). An open source lower limb model: Hip joint validation. *Journal of biomechanics*, *44*(12), 2185–93. doi:10.1016/j.jbiomech.2011.06.019

Mohagheghi, a a, Khan, T., Meadows, T. H., Giannikas, K., Baltzopoulos, V., & Maganaris, C. N. (2008). In vivo gastrocnemius muscle fascicle length in children with and without diplegic cerebral palsy. *Developmental medicine and child neurology*, *50*(1), 44–50. doi:10.1111/j.1469-8749.2007.02008.x

Molenaers, G., & Desloovere, K. (2009). Pharmacologic Treatment with Botulinum Toxin. In J. Gage, M. Schwartz, S. Koop, & T. Novacheck (Eds.), *The Indentification & Treatment of gait problems in cerebral palsy* (2nd ed., pp. 363–80). London: Mac Keith Press.

Murr, S., & Walt, K. (2009). Physical Therapy. In J. Gage, M. Schwartz, S. Koop, & T. Novacheck (Eds.), *The Indentification & Treatment of gait problems in cerebral palsy* (2nd ed., pp. 315–26).

Mutch, L., Alberman, E., Hagberg, B., Kodama, K., & Perat, M. (1992). Cerebral palsy epidemiology: where are we now and where are we going? *Developmental Medicine & Child Neurology*, *24*(6), 547–51.

Neptune, R., Kautz, S., & Zajac, F. (2001). Contributions of the individual ankle plantar flexors to support, forward progression and swing initiation during walking. *Journal of biomechanics*, *34*(11), 1387–98.

Neptune, R., Zajac, F., & Kautz, S. (2004a). Muscle force redistributes segmental power for body progression during walking. *Gait & posture*, *19*(2), 194–205. doi:10.1016/S0966-6362(03)00062-6

Neptune, R., Zajac, F., & Kautz, S. (2004b). Muscle mechanical work requirements during normal walking: the energetic cost of raising the body's center-of-mass is significant. *Journal of biomechanics*, *37*(6), 817–25. doi:10.1016/j.jbiomech.2003.11.001

Noble, J. J., Fry, N. R., Lewis, A. P., Keevil, S. F., Gough, M., & Shortland, A. P. (2013). Lower limb muscle volumes in bilateral spastic cerebral palsy. *Brain & development*, *d*. doi:10.1016/j.braindev.2013.05.008

Noorkoiv, M., Stavnsbo, A., Aagaard, P., & Blazevich, A. J. (2010). In vivo assessment of muscle fascicle length by extended field-of-view ultrasonography. *Journal of applied physiology*, *109*(6), 1974–9. doi:10.1152/japplphysiol.00657.2010

Novacheck, T., Kroll, G., Gent, G., Rozumalski, A., Beattie, C., & Schwartz, M. (2009). Orthoses. In J. Gage, M. Schwartz, S. Koop, & T. Novacheck (Eds.), *The Indentification & Treatment of gait problems in cerebral palsy* (2nd ed., pp. 327–48). London: Mac Keith Press.

Novacheck, T., Stout, J., & Tervo, R. (2000). Reliability and validity of the Gillette Functional Assessment Questionnaire as an outcome measure in children with walking disabilities. *Journal of pediatric orthopedics*, *20*(1), 75–81.

Oberhofer, K., Stott, N., Mithraratne, K., & Anderson, I. (2010). Subject-specific modelling of lower limb muscles in children with cerebral palsy. *Clinical biomechanics*, *25*(1), 88–94. doi:10.1016/j.clinbiomech.2009.09.007

Ostensjø, S., Carlberg, E. B., & Vøllestad, N. K. (2004). Motor impairments in young children with cerebral palsy: relationship to gross motor function and everyday activities. *Developmental medicine and child neurology*, *46*(9), 580–9.

Palisano, R., Rosenbaum, P., Walter, S., Russell, D., Wood, E., & Galuppi, B. (1997). Development and reliability of a system to classify gross motor function in children with cerebral palsy. *Developmental medicine and child neurology*, *39*(4), 214–23.

Peacock, W. (2009). The Pathophysiology of Spasticity. In J. Gage, M. Schwartz, S. Koop, & T. Novacheck (Eds.), *The Indentification & Treatment of gait problems in cerebral palsy* (2nd ed., pp. 89–98). London: Mac Keith Press.

Potvin, J. R., & Brown, S. H. M. (2004). Less is more: high pass filtering, to remove up to 99% of the surface EMG signal power, improves EMG-based biceps brachii muscle force estimates. *Journal of electromyography and kinesiology*, *14*(3), 389–99. doi:10.1016/j.jelekin.2003.10.005

Prentice, J. S. C. (2011). Stepsize Selection in Explicit Runge-Kutta Methods for Moderately Stiff Problems. *Applied Mathematics*, *02*(06), 711–717. doi:10.4236/am.2011.26094

Purslow, P. (2008). The Extracellular Matrix of Skeletal and Cardiac Muscle. In P. Fratzl (Ed.), *Collagen - Structure and Mechanics* (pp. 325–57). Springer US.

Rauch, A., Cieza, A., & Stucki, G. (2008). How to apply the International Classification of Functioning, Disability and Health (ICF) for rehabilitation management in clinical practice. *European journal of physical and rehabilitation medicine*, *44*(3), 329–42.

Read, H. S., Hazlewood, M. E., Hillman, S. J., Prescott, R. J., & Robb, J. E. (2003). Edinburgh visual gait score for use in cerebral palsy. *Journal of pediatric orthopedics*, *23*(3), 296–301.

Rosset, A., Spadola, L., & Ratib, O. (2004). OsiriX: an open-source software for navigating in multidimensional DICOM images. *Journal of digital imaging*, *17*(3), 205–16. doi:10.1007/s10278-004-1014-6

Russell, D. J., Rosenbaum, P., Avery, L., & Lane, M. (2002). *Gross Motor Function Measure (GMFM-66 & GMFM-88). User's Manual*. London: Mac Keith Press.

Sangeux, M., Wolfe, R., & Graham, H. K. (2013). One side or two? *Developmental medicine and child neurology*, *55*(9), 786–7. doi:10.1111/dmcn.12230

Scheys, L., Desloovere, K., Spaepen, A., Suetens, P., & Jonkers, I. (2011). Calculating gait kinematics using MR-based kinematic models. *Gait & posture*, *33*(2), 158–64. doi:10.1016/j.gaitpost.2010.11.003

Scheys, L., Jonkers, I., Schutyser, F., Pans, S., Spaepen, A., & Suetens, P. (2005). Image based methods to generate subject-specific musculoskeletal models for gait analysis. *International Congress Series*, *1281*, 62–67. doi:10.1016/j.ics.2005.03.076

Scheys, L., Loeckx, D., Spaepen, A., Suetens, P., & Jonkers, I. (2008a). Atlas-based non-rigid image registration to automatically define line-of-action muscle models: a validation study. *Journal of biomechanics*, *42*(5), 565–72. doi:10.1016/j.jbiomech.2008.12.014

Scheys, L., Spaepen, A., Suetens, P., & Jonkers, I. (2008b). Calculated moment-arm and muscle-tendon lengths during gait differ substantially using MR based versus rescaled generic lower-limb musculoskeletal models. *Gait & posture*, *28*(4), 640–8. doi:10.1016/j.gaitpost.2008.04.010

Scheys, L., Van Campenhout, A., Spaepen, A., Suetens, P., & Jonkers, I. (2008c). Personalized MR-based musculoskeletal models compared to rescaled generic models in the presence of increased femoral anteversion: effect on hip moment arm lengths. *Gait & posture*, *28*(3), 358–65. doi:10.1016/j.gaitpost.2008.05.002

Schutte, L. M., Narayanan, U., Stout, J. L., Selber, P., Gage, J. R., & Schwartz, M. H. (2000). An index for quantifying deviations from normal gait. *Gait & posture*, *11*(1), 25–31.

Schutte, L., Rodgers, M., Zajac, F., & Glaser, R. (1993). Improving the Efficacy of Electrical Stimulation- Induced Leg Cycle Ergometry : An Analysis Based on a Dynamic Musculoskeletal Model. *IEEE Transactions on Rehabilitation Engineering*, *1*(2), 109–125.

Schwartz, M. H., & Rozumalski, A. (2008). The Gait Deviation Index: a new comprehensive index of gait pathology. *Gait & posture*, *28*(3), 351–7. doi:10.1016/j.gaitpost.2008.05.001

SCPE. (2000). Surveillance of cerebral palsy in Europe: a collaboration of cerebral palsy surveys and registers. *Developmental Medicine & Child Neurology*, *42*(12), 816–824. doi:10.1111/j.1469-8749.2000.tb00695.x

Semciw, A. I., Neate, R., & Pizzari, T. (2014). A comparison of surface and fine wire EMG recordings of gluteus medius during selected maximum isometric voluntary contractions of the hip. *Journal of electromyography and kinesiology : official journal of the International Society of Electrophysiological Kinesiology*, *24*(6), 835–40. doi:10.1016/j.jelekin.2014.08.015

Shao, Q., Bassett, D. N., Manal, K., & Buchanan, T. S. (2009). An EMG-driven model to estimate muscle forces and joint moments in stroke patients. *Computers in biology and medicine*, *39*(12), 1083–8. doi:10.1016/j.compbiomed.2009.09.002

Shortland, A. (2009). Muscle deficits in cerebral palsy and early loss of mobility: can we learn something from our elders? *Developmental medicine and child neurology*, *51 Suppl 4*, 59–63. doi:10.1111/j.1469-8749.2009.03434.x

Shortland, A., Harris, C., Gough, M., & Robinson, R. (2002). Architecture of the medial gastrocnemius in children with spastic diplegia. *Developmental medicine and child neurology*, *44*(3), 158–63.

Siegel, K. L., Kepple, T. M., & Stanhope, S. J. (2006). Using induced accelerations to understand knee stability during gait of individuals with muscle weakness. *Gait & posture*, *23*(4), 435–40. doi:10.1016/j.gaitpost.2005.05.007

Smith, L. R., Lee, K. S., Ward, S. R., Chambers, H. G., & Lieber, R. L. (2011). Hamstring contractures in children with spastic cerebral palsy result from a stiffer extracellular matrix and increased in vivo sarcomere length. *The Journal of physiology*, *589*(Pt 10), 2625–39. doi:10.1113/jphysiol.2010.203364

Spector, S., Gardiner, P., Zernicke, R., Roy, R. R., & Edgerton, V. (1980). Muscle architecture and force-velocity characteristics of cat soleus and medial gastrocnemius: implications for motor control. *Journal of neurophysiology*, *44*(5), 951–60.

Stackhouse, S. K., Binder-Macleod, S. A., & Lee, S. C. K. (2005). Voluntary muscle activation, contractile properties, and fatigability in children with and without cerebral palsy. *Muscle & nerve*, *31*(5), 594–601. doi:10.1002/mus.20302

Steele, K. M., Seth, A., Hicks, J. L., Schwartz, M. S., & Delp, S. L. (2010). Muscle contributions to support and progression during single-limb stance in crouch gait. *Journal of biomechanics*, *43*(11), 2099–105. doi:10.1016/j.jbiomech.2010.04.003

Stewart, C, Postans, N., Schwartz, M. H., Rozumalski, a, & Roberts, a P. (2008). An investigation of the action of the hamstring muscles during standing in crouch using functional electrical stimulation (FES). *Gait & posture*, *28*(3), 372–7. doi:10.1016/j.gaitpost.2008.05.007

Stewart, Caroline, Postans, N., Schwartz, M. H., Rozumalski, A., & Roberts, A. (2007). An exploration of the function of the triceps surae during normal gait using functional electrical stimulation. *Gait & posture*, *26*(4), 482–8. doi:10.1016/j.gaitpost.2006.12.001

Strauss, D., Ojdana, K., Shavelle, R., & Rosenbloom, L. (2004). Decline in function and life expectancy of older persons with cerebral palsy. *NeuroRehabilitation*, *19*(1), 69–78.

Sutherland, D. H. (2001). The evolution of clinical gait analysis part l: kinesiological EMG. *Gait & posture*, *14*(1), 61–70.

Sutherland, D. H. (2002). The evolution of clinical gait analysis. Part II kinematics. *Gait & posture*, *16*(2), 159–79.

Tammik, K., Matlep, M., Ereline, J., Gapeyeva, H., & Pääsuke, M. (2008). Quadriceps femoris muscle voluntary force and relaxation capacity in children with spastic diplegic cerebral palsy. *Pediatric exercise science*, *20*(1), 18–28.

Tanner, J. M., & Whitehouse, R. H. (1976). Clinical longitudinal standards for height, weight, height velocity, weight velocity, and stages of puberty. *Archives of disease in childhood*, *51*(3), 170–9.

Thelen, D. G. (2003). Adjustment of Muscle Mechanics Model Parameters to Simulate Dynamic Contractions in Older Adults. *Journal of Biomechanical Engineering*, *125*(1), 70. doi:10.1115/1.1531112

Thelen, D. G., & Anderson, F. C. (2006). Using computed muscle control to generate forward dynamic simulations of human walking from experimental data. *Journal of biomechanics*, *39*(6), 1107–15. doi:10.1016/j.jbiomech.2005.02.010

Thelen, D. G., Anderson, F. C., & Delp, S. L. (2003). Generating dynamic simulations of movement using computed muscle control. *Journal of Biomechanics*, *36*(3), 321–328. doi:10.1016/S0021-9290(02)00432-3

Tortora, G., & Derrickson, B. (2007). *Introduction to the Human Body - the essentials of anatomy and physiology* (7th ed.). New York: Wiley & Sons, Inc.

Trost, J., Dunn, M., Krach, L., Langerak, N., Novacheck, T., & Schwartz, M. (2009). Treatment of Spasticity with Selective Dorsal Rhizotomy. In J. Gage, M. Schwartz, S. Koop, & T. Novacheck (Eds.), *The Indentification & Treatment of gait problems in cerebral palsy* (2nd ed., pp. 397–428). London: Mac Keith Press.

Van der Krogt, M. M., Delp, S. L., & Schwartz, M. H. (2012). How robust is human gait to muscle weakness? *Gait & posture*, *36*(1), 113–9. doi:10.1016/j.gaitpost.2012.01.017

Ward, S., Eng, C., Smallwood, L., & Lieber, R. (2008). Are current measurements of lower extremity muscle architecture accurate? *Clinical orthopaedics and related research*, *467*(4), 1074–82. doi:10.1007/s11999-008-0594-8

Wearing, S. C., Urry, S. R., & Smeathers, J. E. (2000). The effect of visual targeting on ground reaction force and temporospatial parameters of gait. *Clinical biomechanics (Bristol, Avon)*, *15*(8), 583–91.

WHO. (2001). International Classification of Functioning, Disability and Health, World Health Organisation, Geneva.

Wickiewicz, T. L., Roy, R. R., Powell, P. L., & Edgerton, V. R. (1983). Muscle architecture of the human lower limb. *Clinical orthopaedics and related research*, (179), 275–83.

Wiley, M. E., & Damiano, D. L. (1998). Lower-extremity strength profiles in spastic cerebral palsy. *Developmental medicine and child neurology*, *40*(2), 100–7.

Winter, D. (1990). *Biomechanics and Motor Control of Human Movement* (1st ed.). New York: Wiley & Sons, Inc.

Winter, D. (2005). *Biomechanics and Motor Control of Human Movement* (3rd ed.). New York: Wiley & Sons, Inc.

Winter, D., & Yack, H. (1987). EMG profiles during normal human walking: stride-to-stride and inter-subject variability. *Electroencephalography and clinical neurophysiology*, *67*(5), 402–11.

Wren, T. A. L., Rethlefsen, S., & Kay, R. M. (2005). Prevalence of specific gait abnormalities in children with cerebral palsy: influence of cerebral palsy subtype, age, and previous surgery. *Journal of pediatric orthopedics*, *25*(1), 79–83.

Xiao, M., & Higginson, J. S. (2008). Muscle function may depend on model selection in forward simulation of normal walking. *Journal of biomechanics*, *41*(15), 3236–42. doi:10.1016/j.jbiomech.2008.08.008

Yamaguchi, G. T., & Zajac, F. E. (1989). A planar model of the knee joint to characterize the knee extensor mechanism. *Journal of biomechanics*, *22*(1), 1–10.

Zajac, F. (1989). Muscle and tendon: properties, models, scaling, and application to biomechanics and motor control. *Critical reviews in biomedical engineering*, *17*(4), 359–411.

Zajac, F., Neptune, R., & Kautz, S. (2003). Biomechanics and muscle coordination of human walking: part II: lessons from dynamical simulations and clinical implications. *Gait & posture*, *17*(1), 1–17.